

Naučnom veću Instituta za fiziku u Beogradu

Beograd, 03. juli 2019. godine

Predmet: Molba za pokretanje postupka za sticanje zvanja naučni saradnik

S obzirom da ispunjavam kriterijume propisane od strane Ministarstva prosvete, nauke i tehnološkog razvoja za sticanje naučnog zvanja naučni saradnik, kao i kriterijume propisane Pravilnikom o sticanju naučnih zvanja u Institutu za fiziku, molim Naučno veće Instituta za fiziku u Beogradu da pokrene postupak za moj izbor u navedeno zvanje.

U prilogu dostavljam:

1. Mišljenje rukovodioca projekta sa predlogom članova komisije
2. Stručnu biografiju
3. Pregled naučne aktivnosti
4. Elemente za kvalitativnu analizu naučnog rada
5. Elemente za kvantitativnu analizu naučnog rada
6. Spisak objavljenih naučnih radova
7. Podatke o citiranosti
8. Skeniranu doktorsku diplomu sa sertifikatom, uz dokaz o nostrifikaciji
9. Primerak doktorske disertacije
10. Kopije objavljenih radova i doktorske diplome

Sa Poštovanjem,



Dr Milena M. Filipović

Naučnom veću Instituta za fiziku u Beogradu

Predmet: Mišljenje rukovodioca projekta za izbor Dr Milene Filipović u zvanje naučni saradnik

Pošto ispunjava sve uslove predviđene Pravilnikom za izbore u naučno-istraživačka zvanja, saglasna sam sa pokretanjem postupka za izbor Dr Milene M. Filipović u zvanje naučni saradnik. Stoga molim Naučno veće Instituta za Fiziku u Beogradu da pokrene odgovarajući postupak.

Predlog članova komisije za pisanje izveštaja:

1. Dr Dimitrije Stepanenko, viši naučni saradnik, Institut za fiziku u Beogradu
2. Dr Zorana Dohčević-Mitrović, naučni savetnik, Institut za fiziku u Beogradu
3. Dr Božidar Nikolić, vanredni profesor, Fizički fakultet Univerziteta u Beogradu

Beograd, 03. juli 2019. godine



Dr Zorana Dohčević-Mitrović

naučni savetnik

STRUČNA BIOGRAFIJA

Milena (Milorad) Filipović je rođena 19. juna 1980. godine u Beogradu, gde je završila osnovnu školu Ujedinjene nacije i XIII beogradsku gimnaziju, a zatim je upisala Fizički fakultet Univerziteta u Beogradu, smer Teorijska i eksperimentalna fizika, gde je diplomirala 2007. godine. Iste godine je upisala Master studije fizike na Univerzitetu Illinois u Čikagu koje je završila 2009. godine. Na Univerzitetu Illinois, Milena je radila kao asistent u nastavi, gde je držala vežbe iz kurseva: Uvod u fiziku, Elektricitet i magnetizam, Astronomija i univerzum.

Od 2010. do 2015. godine Milena je boravila na doktorskim studijama i post doktorskom usavršavanju u Nemačkoj, na Univerzitetu u Konstanci, gde je bila zaposlena kao naučni saradnik u istraživačkoj grupi za kvantni transport. Milena se bavila naučnim radom u okviru Integrisane Istraživačke Grupe Kolaborativnog Centra 767 "Kontrolisani nanosistemi: Interakcija i povezivanje na makronivou". Bila je asistent u nastavi na predmetima: Kvantna teorija polja u fizici čvrstog stanja, Napredna kvantna mehanika i elektrodinamika. Mentor doktorskih studija bio joj je Prof. Dr Wolfgang Belzig. Milena je odbranila doktorsku disertaciju iz teorijske fizike kondenzovanog stanja, pod nazivom "Quantum Transport Through Molecular Magnets" u julu 2015. godine. Sa svojim mentorom Milena je nastavila saradnju do aprila 2018. godine.

PREGLED NAUČNE AKTIVNOSTI

Tokom svog rada Milena je teorijski izučavala vremenski zavisni elektronski i spinski transport kroz molekulske orbitale povezanu sa dva metalna kontakta i spregnutu sa molekularnim magnetom putem izmenske interakcije. Spin molekula je tretiran kao klasična varijabla koja precesira oko spoljašnjeg konstantnog magnetnog polja Larmorovom frekvencijom. Koristeći Keldysh-ov formalizam za Green-ove funkcije u neravnoteži izvedeni su izrazi za električnu i spinsku struju. Sprega između elektronskog spina i dinamike magnetizacije molekula vodi do neelastičnih procesa tunelovanja, koji doprinose spinskim strujama. Neelastične spinske struje izazivaju torziju molekularnog spina usled prenosa spinskog angularnog momenta između spinski polarizovane struje i molekularnog spina, koja je kompenzovana spoljašnjim faktorima. Ova povratna akcija uključuje doprinos Gilbertovom prigušenju i promeni frekvencije precesionog kretanja molekularnog spina. Koeficijent Gilbertovog prigušenja može da se kontroliše putem napona ili spoljašnjeg magnetnog polja i njegova zavisnost od širine molekularnog nivoa nije monotona.

Sledeće, Milena je izučavala elektronski i spinski transport dodajući vremenski zavisne elektrohemijske potencijale u metalne kontakte koji su povezani sa molekularnom orbitalom. Koristeći Keldysh-ov formalizam za neravnotežne Green-ove funkcije Milena je računala električnu i spinsku struju linearno u odnosu na vremenski zavisne potencijale. Oscilatorni elektrohemijski potencijali omogućavaju da se detektuje Larmorova frekvencija putem merenja provodnosti ako je frekvencija naizmjenične struje jednaka

Larmorovoj frekvenciji. U režimu niske frekvencije naizmjenične struje sistem se ponaša kao klasično električno kolo, koje se sastoji od paralelno vezane dve redne kombinacije, otpornika i induktora, i otpornika i kondenzatora. Štaviše, pokazalo se da sistem može da se koristi za generisanje jednosmerne struje, koja se može kontrolisati promenom pravca magnetizacije molekula i relativnih faza između Larmorove precesije i naizmjeničnog napona.

Na kraju, Milena je izučavala neravnotežni šum električne struje, spinskih struja i molekulske spinske torzije u odsustvu vremenski zavisnih elektrohemijskih potencijala, koristeći Keldysh-ov formalizam neravnotežnih Green-ovih funkcija. Slično kao kod Fano efekta, uočena su udubljenja kod šuma električne struje zbog prisustva neelastičnih procesa tunelovanja koji uključuju promenu energije transportnih elektrona u vrednosti jedne Larmorove frekvencije. Ovim procesima upravlja precesija molekularnog spina i oni vode do kvantne interferencije između korelisanih struja. Napon i precesija molekularnog spina upravljaju komponentama šuma molekularne spinske torzije. Elastični i neelastični procesi tunelovanja spinskih čestica, koje prati promena energije za jednu ili dve Larmorove frekvencije daju doprinos komponentama šuma spinske torzije koje povezuju torzije u istom pravcu u precesionoj ravni. Korelacije ortogonalnih komponenti spinske torzije u precesionoj ravni su povezane sa Gilbertovim prigušenjem.

ELEMENTI ZA KVALITATIVNU ANALIZU NAUČNOG RADA

1. Kvalitet naučnih rezultata

1.1 Značaj naučnih rezultata

Milena Filipović se bavi teorijskim istraživanjima kvantnog elektronskog i spinskog transporta kroz nanosisteme. Njena uža specijalnost je kvantni transport kroz sisteme koji sadrže molekularne magnete. Teorijski izučava vremenski zavisni transport elektrona i spina primenjujući Keldysh-ov formalizam neravnotežnih Green-ovih funkcija. U tom kontekstu tokom svog rada razvila je koncept generalizovanog formalizma odziva.

Milena je publikovala 3 rada u vrhunskom međunarodnom časopisu kao prvi autor. Bila je učesnik brojnih međunarodnih konferencija i letnjih škola gde je predstavila svoj rad.

1.2 Parametri kvaliteta časopisa

Milena Filipović je publikovala 3 rada u vrhunskom međunarodnom časopisu *Physical Review B* [IF 3.813 (2017)], kategorije M21.

1.3 Podaci o citiranosti

Prema podacima sa baze *Google Scholar*, radovi Milene Filipović su citirani 13 puta, od čega 10 puta izuzimajući autocitate. Prema bazi *Web of Science*, radovi Milene Filipović su citirani 10 puta, a prema podacima sa baze *Scopus*, radovi kandidatkinje su citirani 11 puta.

1.4 Međunarodna saradnja

Međunarodne aktivnosti Dr Milene Filipović obuhvataju:

- Saradnju sa teorijskom grupom za kvantni transport čiji je rukovodilac Prof. Dr Wolfgang Belzig na Univerzitetu u Konstanci, Nemačka
- Saradnju sa odsekom za fiziku Univerziteta Iinois u Čikagu, Sjedinjene Američke Države

2. Normiranje broja koautorskih radova, patenata i tehničkih rešenja

Budući da 1 objavljeni rad kandidatkinje ima 4 koautora, on nakon normiranja donosi 6.7 M-bodova, a ostali radovi se računaju sa punom težinom jer imaju po 2 koautora.

3. Učešće u projektima, potprojektima i projektnim zadacima

Kandidatkinja je učestvovala na sledećim projektima:

- Collaborative Research Center SFB 767 "Controlled Nanosystems: Interactions and Interfacing to the Macroscale", Project C03: *Time-dependent transport in correlated electron nanostructures*, 01/2008-12/2019
- Collaborative Research Center SFB 767 "Controlled Nanosystems: Interactions and Interfacing to the Macroscale", Project C08: *Controlling quantum systems by electrical current*, 2008-2011
- Project *UltraPhase* of Prof. Dr. Alfred Leitenstorfer, ERC Advanced Grant-Condensed matter physics, 04/2012-03/2017

4. Uticaj naučnih rezultata

Uticaj naučnih rezultata Milene Filipović se ogleda u broju citata koji su navedeni u odeljku 1.3. Spisak radova koji citiraju radove kandidatkinje nalazi se u prilogu.

5. Konkretni doprinosi kandidatkinje u realizaciji radova u naučnim centrima u zemlji i inostranstvu

Milena Filipović je sve svoje istraživačke aktivnosti realizovala na Univerzitetu u Konstanci u Nemačkoj, u grupi za kvantni transport, čiji je rukovodilac Prof. Dr Wolfgang Belzig. Kandidatkinja je dala ključni doprinos objavljenim radovima i u svim radovima je prvi autor. Njen doprinos se ogleda u izradi proračuna, dobijanju, interpretaciji i prezentaciji rezultata, pisanju radova i komunikaciji sa urednicima i recenzentima časopisa.

ELEMENTI ZA KVANTITATIVNU ANALIZU NAUČNOG RADA

OSTVARENI M-BODOVI PO KATEGORIJAMA PUBLIKACIJA

Kategorija	M-bodova po publikaciji	Broj publikacija	Ukupno M-bodova
M21	pun broj bodova 8	2	16
M21	normirani 6.7	1	6.7
M32	1.5	1	1.5
M34	0.5	3	1.5
M70	6	1	6

Poređenje ostvarenog broja M-bodova sa minimalnim uslovima potrebnim za izbor u zvanje naučni saradnik:

	Potrebno	Ostvareno
Ukupno	16	31.7
M10+M20+M31+M32+M33+M41+M42	10	24.2
M11+M12+M21+M22+M23	6	22.7

Budući da je Mileni Filipović ovo prvi izbor u naučno zvanje, ona ima 3 rada (M21), jedno predavanje na međunarodnoj konferenciji DPG Spring Meeting u Berlinu (M32), 3 saopštenja sa međunarodnog skupa (M34) i odbranjenu doktorsku disertaciju (M70).

SPISAK RADOVA DR MILENE FILIPOVIĆ

SPISAK OBJAVLJENIH RADOVA U VRHUNSKOM MEĐUNARODNOM ČASOPISU (M21):

1. Spin transport and tunable Gilbert damping in a single-molecule magnet junction
Milena Filipović, Cecilia Holmqvist, Federica Haupt and Wolfgang Belzig
Phys. Rev. B **87**, 045426 (2013); **88**, 119901(E) (2013)
2. Photon-assisted electronic and spin transport in a junction containing precessing molecular spin
Milena Filipović and Wolfgang Belzig
Phys. Rev. B **93**, 075402 (2016)
3. Shot noise of charge and spin transport in a junction with a precessing molecular spin
Milena Filipović and Wolfgang Belzig
Phys. Rev. B **97**, 115441 (2018)

PREDAVANJE PO POZIVU SA MEĐUNARODNOG SKUPA ŠTAMPANO U IZVODU (M32):

03/2012 *Tunable Gilbert Damping in a Single Molecule Magnet* (talk)
Deutsche Physikalische Gesellschaft (DPG) Spring Meeting, Berlin,
Germany

SAOPŠTENJA SA MEĐUNARODNOG SKUPA ŠTAMPANA U IZVODU (M34):

- 09/2015 *Quantum Transport Through Molecular Magnets* (poster)
The 19th Symposium on Condensed Matter Physics, SFKM 2015,
Belgrade, Serbia
- 02/2013 *Spin Transport and Tunable Gilbert Damping in a Single-Molecule Magnet Junction* (poster)
Trends in Nanoscience 2013, Kloster Irsee, Germany
- 03/2011 *Time-dependent Transport Through a Molecular Level Coupled to a Nanomagnet* (poster)
Deutsche Physikalische Gesellschaft (DPG) Spring Meeting,
Dresden, Germany

ODBRANJENA DOKTORSKA DISERTACIJA (M70):

1. Doktorska disertacija: "Kvantni Transport Kroz Molekularne Magnete"
(naslov originala: "Quantum Transport Through Molecular Magnets")

Milena Filipović

Doktorska disertacija (2015), Univerzitet u Konstanci, Nemačka

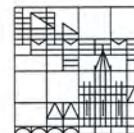
Mentor: Prof. Dr Wolfgang Belzig

Doktorska disertacija Milene Filipović se u elektronskoj formi može naći na sajtu:

1. Nacionalne biblioteke Nemačke:
<https://d-nb.info/1098136519/34>
2. KOPS Univerziteta u Konstanci:
<http://kops.uni-konstanz.de/handle/123456789/31978>



Universität
Konstanz



Sonderforschungsbereich 767
IRTG nano

sfb767@uni-konstanz.de
www.uni-konstanz.de/sfb767

Certificate of Training in the IRTG Nano

This certifies that

Dr. Milena Filipović

has obtained her PhD in the framework of the Integrated Research Training Group of the Collaborative Research Center 767

"Controlled Nanosystems: Interaction and Interfacing to the Macroscale".

She was a member from 10/2009 until 07/2015. The Departments of Physics and Chemistry of the University of Konstanz maintain the training program together in collaboration with the Academic Staff Development Unit of the University of Konstanz.

Besides the research project in the field of nanosciences conducted by Dr. Filipović, the training program encompassed

- Participation in a topical discussion group
- Participation and/or organization of crash courses
- Organization of mini symposia
- Participation in scientific summer or winter schools
- Course lectures
- Training in transferable skills
- Mutual knowledge transfer of theoretical or experimental methods
- Scientific talks at an international conference and mini symposia
- Publication(s) as main author in a refereed journal

The board of the SFB 767 congratulates and wishes Dr. Filipović a further successful career.

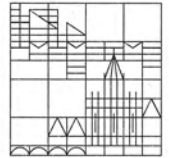
Konstanz, July 29, 2015

The Spokesperson of the SFB 767

Prof. Dr. Wolfgang Belzig

The Spokesperson of the IRTG Nano

Prof. Dr. Elke Scheer



23.07.2015

Dear Ms Filipović,

I would like to congratulate you upon the successful completion of your degree at the University of Konstanz. You may be very proud of your achievements.

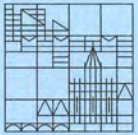
Providing high-quality education to its students is one of the most important tasks for the University of Konstanz. We carefully select our professors and pay great attention to the conception and quality of our study programmes. This is why I am certain that you have received excellent training for your future career and will make your way in the world.

When you leave the University of Konstanz now, I hope you will fondly remember your student days and like to come back later –be it for further studies, training, alumni meetings, our Dies academicus or another event.

I wish you every success and all the best for the future.

Yours sincerely

Ulrich Rüdiger



Die Universität Konstanz verleiht

Frau Milena FILIPOVIĆ

geboren am 19. Juni 1980 in Belgrad, Serbien

aufgrund der mit „sehr gut“ bewerteten Dissertation

“Quantum Transport Through
Molecular Magnets”

und einer mündlichen Prüfung über die Spezialgebiete
aus den Fachrichtungen

Kondensierte Materie: Elektronische Struktur,
elektrische, magnetische und optische Eigenschaften
Optik

Kondensierte Materie: Struktur,
mechanische und thermische Eigenschaften

den akademischen Grad

DOKTOR DER NATURWISSENSCHAFTEN (Dr.rer.nat.)

mit dem Gesamturteil

„magna cum laude“ (sehr gut)

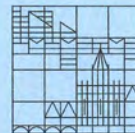
Konstanz, den 23. Juli 2015

Der Rektor

Professor Dr. Dr. h.c. Ulrich Rüdiger

Fachbereich Physik
Der Fachbereichssprecher

Professor Dr. Thomas Dekorsy



The University of Konstanz confers on

Ms Milena FILIPOVIĆ

born on 19 June 1980 in Belgrade, Serbia

on the basis of her dissertation

**“Quantum Transport Through
Molecular Magnets”**

assessed with the grade very good

and an oral examination on special fields from the subjects

**Condensed Matter: Electronic Structure,
Electrical, Magnetic and Optical Properties
Optics**

**Condensed Matter: Structure,
Mechanical and Thermal Properties**

the degree of

DOCTOR OF NATURAL SCIENCES (Dr.rer.nat.)

with the overall grade

magna cum laude (very good)

Konstanz, 23 July 2015

The Rector

Department of Physics
The Head of Department

Professor Dr. Dr. h.c. Ulrich Rüdiger

Professor Dr. Thomas Dekorsy



Република Србија
МИНИСТАРСТВО ПРОСВЕТЕ,
НАУКЕ И ТЕХНОЛОШКОГ РАЗВОЈА

Број: 612-01-00414/2019-06

Датум: 21.05.2019. године

Немањина 22-26

Београд

јк

На основу члана 130. став 1, 131. став 1 и 4, члана 133. став 4. Закона о високом образовању („Службени гласник РС”, бр. 88/17, 27/18 – др. закон и 73/18), члана 136. став 1. Закона о општем управном поступку („Службени гласник РС”, бр. 18/16) и члана 23. став 2. Закона о државној управи („Службени гласник РС”, бр. 79/05, 101/07, 95/10, 99/14, 47/18, 30/18 – др. закон) и члана 51. став 2, Закона о националном оквиру квалификација Републике Србије (Сл. гласник РС 27/18), решавајући по захтеву Милене Филиповић из Београда, Република Србија, за признавање високошколске исправе издате у СР Немачкој, ради запошљавања, министар просвете, науке и технолошког развоја доноси

РЕШЕЊЕ

1. Диплома коју је 23.07.2015. године издао Универзитет у Констанци (Universitat Konstanz/The University of Konstanz), Констанц, СР Немачка, на име Милена Филиповић, рођена 19.06.1980. године у Београду, о завршеним докторским академским студијама, студијски програм: Физичке науке, докторска дисертација: „Квантни транспорт кроз молекуларне магнете“, звање/квалификација: Doctor of Natural Sciences (Dr.reg.nat) / Доктор природних наука, Доктор наука – физичке науке (на основу превода овлашћеног судског тумача за енглески језик), **признаје се** као диплома докторских академских студија трећег степена високог образовања (180 ЕСПБ), у оквиру образовно-научног поља: Природно-математичке науке, научна, односно стручна област: Физичке науке, ради запошљавања.
2. Ово решење омогућава имаоцу општи приступ тржишту рада у Републици Србији, али га не ослобађа од испуњавања посебних услова за бављење професијама које су регулисане законом или другим прописом.
3. Превод звања/квалификације из тачке 1. диспозитива овог решења које је са оригиналне стране јавне исправе превео овлашћени судски тумач за енглески језик, не представља стручни, академски, научни односно уметнички назив који у складу са чланом 12. ставом 1. тачка 9. Закона о високом образовању, утврђује Национални савет за високо образовање.

Образложење

Овом министарству обратила се Милена Филиповић из Београда, Република Србија, захтевом од 05.03.2019. године за признавање дипломе Универзитета у Констанци (Universitat Konstanz/The University of Konstanz), Констанц, СР Немачка, докторске академске студије високог образовања, студијски програм: Физичке науке, докторска дисертација: „Квантни транспорт кроз молекуларне магнете“ звање/квалификација: Doctor of Natural Sciences (Dr.reg.nat) / Доктор природних наука, Доктор наука – физичке науке, ради запошљавања.

Уз захтев, подносилац захтева доставио је:

- 1) оверену копију дипломе коју је 23.07.2015. године издао Универзитет у Констанци (Universitat Konstanz/The University of Konstanz), Констанц, СР Немачка, студијски програм: Физичке науке, звање/квалификација: Doctor of Natural Sciences (Dr.rer.nat) / Доктор природних наука, Доктор наука – физичке науке;
- 2) оверени превод дипломе на српски језик;
- 3) примерак докторске дисертације;
- 4) апстракт рада на енглеском језику;
- 5) оверену копију сертификата о похађаном програму студија на енглеском језику;
- 6) листу објављених радова;
- 7) копију претходно стечене квалификације са документацијом;
- 8) радну биографију;
- 9) пријавни формулар;
- 10) доказ о уплати таксе за професионално признавање.

Одредбом члана 136. став 1. Закона о општем управном поступку прописано је да се решењем одлучује о праву, обавези или правном интересу странке.

Одредбом члана 23. став 2. Закона о државној управи прописано је да Министар представља Министарство, доноси прописе и решења у управним и другим појединачним стварима и одлучује о другим питањима из делокруга Министарства.

Одредбом члана 130. став 1. Закона о високом образовању, прописано је да признавање стране високошколске исправе јесте поступак којим се имаоцу те исправе утврђује право на наставак образовања, односно на запошљавање. Поступак признавања стране високошколске исправе спроводи се у складу са одредбама овог закона, ако међународним уговором није предвиђено другачије.

Одредбом члана 131. став 1. Закон о високом образовању, прописано је да се вредновање страног студијског програма врши на основу врсте и нивоа постигнутих компетенција стечених завршетком студијског програма, узимајући у обзир систем образовања у земљи у којој је високошколска исправа стечена, услове уписа, права која проистичу из стране високошколске исправе у земљи у којој је стечена и друге релевантне чињенице, без разматрања формалних обележја и структуре студијског програма. Ставом 3. истог члана Закона о високом образовању прописано је да вредновање страног студијског програма ради запошљавања врши Национални центар за признавање страних високошколских исправа (у даљем тексту: ENIC/NARIC центар), као унутрашња организациона јединица Министарства.

Одредбом члана 131. став 4. Закона о високом образовању, прописано је да за потребе давања стручног мишљења у поступку првог вредновања страног студијског програма ради запошљавања, министар образује комисију од најмање три рецензента са листе Конференције универзитета, односно Конференције академија и високих школа.

Одредбом члана 133. став 4. Закона о високом образовању прописано је да Министар доноси решење о професионалном признавању у року од 90 дана од дана пријема уредног захтева.

Именована комисија је извршила прво вредновање страног студијског програма и дала предлог да се диплома Универзитета у Констанци (Universitat Konstanz/The University of Konstanz), Констанц, СР Немачка, призна као диплома докторских академских студија трећег степена високог образовања (180 ЕСПБ), у оквиру образовно-научног поља: Природно-математичке науке, научна односно стручна област: Физичке науке.

Одредбом члана 51. став 2, Закона о националном оквиру квалификација, прописано је да поступци за професионално признавање стране високошколске исправе, односно за вредновање страног студијског програма ради запошљавања који су започети до почетка ENIC/NARIC центра у складу са овим законом, окончаће се по тим прописима.

Имајући у виду одредбе члана 51. став 2. Закона о НОКС-у, као и чињеницу да је захтев за признавање стране високошколске исправе поднет пре почетка рада ENIC/NARIC центра, као организационе јединице Агенције за квалификације, то су у конкретном случају примењени напред наведени чланови Закона о високом образовању.

Такса за решење по захтеву, по тарифном броју 172. тачка 3. подтачка 4а) Закона о републичким административним таксама ("Службени гласник РС", бр. 43/03, 51/03-испр., 61/05, 101/05-др.закон, 5/09, 54/09, 50/11, 70/11- усклађени дин.изн., 55/12- усклађени дин.изн., 93/12, 47/13 - усклађени дин.изн, 65/13-др.закон, 57/14- усклађени дин.изн, 45/15- усклађени дин.изн,

83/15, 112/15, 50/16- усклађени дин.изн., 61/17- усклађени дин.изн., 113/17, 3/18, 50/18 и 95/18),
плаћена је и поништена.

Сходно претходно наведеном, донета је одлука као у диспозитиву решења.

Упутство о правном средству: Ово решење је коначно у управном поступку и против истог може се покренути управни спор. Тужба се подноси Управном суду у року од 30 дана од дана пријема овог решења.

Решење доставити:

- Милена Филиповић, ул.Кестенова бр. 5, 11000 Београд;
- Архиви.



Verhandlungen



der Deutschen Physikalischen Gesellschaft e.V.

Berlin 2012 – wissenschaftliches Programm

**Bereiche | Tage |
Auswahl | Suche |
Aktualisierungen |
Downloads | Hilfe**

**TT: Fachverband
Tiefe
Temperaturen**

TT 44: Transport:

Nanoelectronics III - Molecular Electronics 2

TT 44.3: Vortrag

**Donnerstag, 29. März
2012, 15:30–15:45, BH
334**

Auswahlstatus für diesen Beitrag:

gemäß den Sitzungseinstellungen



**Spin transport and tunable
Gilbert damping in a single-
molecule magnet** — •MILENA

FILIPOVIC¹, FEDERICA HAUPT²,

CECILIA HOLMQVIST¹, and

WOLFGANG BELZIG¹ —

¹Fachbereich Physik, Universität
Konstanz, D-78457 Konstanz,

Germany — ²Institut für Theorie
der Statistischen Physik, RWTH
Aachen, D-52056 Aachen,
Germany

We study spin transport through a molecular level coupled to two leads and a single-molecule magnet in a magnetic field. The molecular spin is treated as a classical variable and, due to the external magnetic field, precesses around the field axis. Expressions for charge and spin currents are derived by means of the Keldysh nonequilibrium Green's function technique in linear response. The exchange coupling between the electronic spins and the magnetization dynamics of the molecule creates inelastic tunneling processes which contribute to the spin currents. The inelastic spin currents, in turn, generate a spin

transfer torque [1,2] acting on the molecular spin. This back-action includes one component that gives a contribution to the Gilbert damping and one component that changes the precession frequency. The Gilbert damping coefficient, α , can be controlled by changing the bias and gate voltages, and has a non-monotonic dependence on the tunneling rates. We compare our results to the Gilbert damping coefficient calculated in Ref. [3] in the small precession frequency regime $\hbar\omega \ll k_B T$.

Y. Tserkovnyak et al., Rev. Mod. Phys. 77, 1375 (2005).

C. Holmqvist et al., Phys. Rev. B 83, 104521 (2011).

N. Bode et al.,
arXiv:1110.4270v1 (2011).

TT 44: Transport: Nanoelectronics III - Molecular Electronics 2

Time: Thursday 15:00–17:15

Location: BH 334

TT 44.1 Thu 15:00 BH 334

Charge transport in single molecule junctions with graphene leads — ●IVAN PSHENICHNYUK, SUSANNE LEITHERER, PEDRO B. COTO, and MICHAEL THOSS — Friedrich-Alexander-Universität Erlangen-Nürnberg, Germany

High electron mobility, mechanical rigidity and optical transparency make graphene a promising candidate as material for electrodes in nanoelectronic devices. In this work, we investigate charge transport in single molecule junctions with graphene leads. The methodology used is based on a combination of first-principles electronic structure calculations to characterize the molecule-graphene junctions and the Landauer transport formalism. Considering different examples for molecular bridges between graphene electrodes, in particular pentacene-based molecules as well as polyene chains, we analyze the transmission probability and the current-voltage characteristics.

TT 44.2 Thu 15:15 BH 334

Thermopower of biphenyl-based single-molecule junctions — ●MARIUS BÜRKLE¹, LINDA A. ZOTTI², JANNE K. VILJAS³, THOMAS WANDLOWSKI⁴, MARCEL MAYOR⁵, GERD SCHÖN¹, and FABIAN PAULY¹ — ¹Institut für Theoretische Festkörperphysik and DFG Center for Functional Nanostructures, Karlsruhe Institute of Technology, Karlsruhe, Germany — ²Departamento de Física Teórica de la Materia Condensada, Universidad Autónoma de Madrid, Madrid, Spain — ³Low Temperature Laboratory, Aalto University, Aalto, Finland — ⁴Department of Chemistry and Biochemistry, University of Bern, Bern, Switzerland — ⁵Department of Chemistry, University of Basel, Basel, Switzerland

Employing ab initio electronic structure calculations combined with non-equilibrium Green's function techniques we study the dependence of the thermopower on the degree of π -conjugation in biphenyl-based single molecule gold junctions. We control the degree of π -conjugation by changing the torsion angle φ between the two phenyl rings by means of alkyl side chains connected to the molecules. We find that the absolute value of the thermopower decreases weakly as $\cos^2 \varphi$. We show that the observed $\cos^2 \varphi$ dependence is robust with respect to different anchoring groups and binding positions. The anchoring group determines the sign of the thermopower. Sulfur and amine give rise to $Q > 0$ and cyano to $Q < 0$ respectively. Different binding positions on the contrary lead to variations of the absolute values of the thermopower. The observed ab initio results are found to be described well by means of a π -electron tight binding model.

TT 44.3 Thu 15:30 BH 334

Spin transport and tunable Gilbert damping in a single-molecule magnet — ●MILENA FILIPOVIC¹, FEDERICA HAUPT², CECILIA HOLMQVIST¹, and WOLFGANG BELZIG¹ — ¹Fachbereich Physik, Universität Konstanz, D-78457 Konstanz, Germany — ²Institut für Theorie der Statistischen Physik, RWTH Aachen, D-52056 Aachen, Germany

We study spin transport through a molecular level coupled to two leads and a single-molecule magnet in a magnetic field. The molecular spin is treated as a classical variable and, due to the external magnetic field, precesses around the field axis. Expressions for charge and spin currents are derived by means of the Keldysh nonequilibrium Green's function technique in linear response. The exchange coupling between the electronic spins and the magnetization dynamics of the molecule creates inelastic tunneling processes which contribute to the spin currents. The inelastic spin currents, in turn, generate a spin transfer torque [1,2] acting on the molecular spin. This back-action includes one component that gives a contribution to the Gilbert damping and one component that changes the precession frequency. The Gilbert damping coefficient, α , can be controlled by changing the bias and gate voltages, and has a non-monotonic dependence on the tunneling rates. We compare our results to the Gilbert damping coefficient calculated in Ref. [3] in the small precession frequency regime $\hbar\omega \ll k_B T$.
[1] Y. Tserkovnyak et al., Rev. Mod. Phys. 77, 1375 (2005).
[2] C. Holmqvist et al., Phys. Rev. B 83, 104521 (2011).
[3] N. Bode et al., arXiv:1110.4270v1 (2011).

TT 44.4 Thu 15:45 BH 334

THz torsional vibrations in biphenyl-based molecular junctions:

transient oscillations and resonance — ●MATTHIAS HINREINER¹, DMITRY RYNDYK¹, DENIS USVYAT², THOMAS MERZ², MARTIN SCHÜTZ², and KLAUS RICHTER¹ — ¹Institute for Theoretical Physics, University of Regensburg, Regensburg, Germany — ²Institute for Physical and Theoretical Chemistry, University of Regensburg, Regensburg, Germany

We investigate the torsional vibrations in biphenyl-based molecular junctions and transport properties in presence of an external THz field.

Ab-initio calculations with external electric fields show that the torsional angle ϕ of 4,4'-dithiol-biphenyl demonstrates only very tiny response. However, if functional groups are added to the molecule to induce a dipole moment in each of the rings, an external field can change ϕ . Two examples of such molecules are 3,3'-difluoride-4,4'-dithiol-biphenyl and 2,2'-dithiol-5,5'-bipyridine. As the conductivity of biphenyl-based molecules is proportional to $\cos^2(\phi)$, we show that the current through these molecules drops if the external THz field frequency gets in resonance to the torsional vibration mode.

15 min. break.

TT 44.5 Thu 16:15 BH 334

Electron transport through helical, biimidazole-based structures — ●THOMAS BRUMME, RAFAEL GUTIÉRREZ, and GIANAURELIO CUNIBERTI — Institute for Materials Science and Max Bergmann Center of Biomaterials, TU Dresden, Germany

Molecular electronics and spintronics provide a promising strategy to overcome limitations of semiconductor-based technologies by implementing electronic functionalities at the molecular scale. However, in order to create single molecule spintronics devices one needs to understand the spin-dependent transport through the molecular system, its dependence on different molecular properties and possible mechanisms to change the magnetization of the molecule. Molecular systems with screw symmetry like DNA are especially interesting for spintronics applications since the transport through these systems can be spin selective [1]. We investigate the electronic structure of a molecular helix formed by silver atoms and biimidazole units ($[Ag(NO_3)(H_2biim)]_n$, [2, 3]). First-principles calculations reveal that several molecular orbitals possess screw symmetry and are completely delocalized along the helix. Based on this results we explore the possibility of spin-selective electron transport through this molecular helix.

[1] B. Göhler et al., Science **331**, 894 (2011)[2] C.A. Hester et al., Polyhedron **16**, 2893 (1997)[3] M. Sowwan et al., Journal of Nanomaterials **2010** (2010)

TT 44.6 Thu 16:30 BH 334

Spin selective transport through helical molecular systems — ●RAFAEL GUTIERREZ¹, ELENA DIAZ², RON NAAMAN³, and GIANAURELIO CUNIBERTI¹ — ¹Institute for Materials Science, Dresden University of Technology, 01062 Dresden, Germany — ²GISC, Departamento de Física de Materiales, Universidad Complutense, E-28040 Madrid, Spain — ³Department of Chemical Physics, Weizmann Institute, 76100 Rehovot, Israel

Highly spin selective transport of electrons through a helically shaped electrostatic potential is demonstrated in the frame of a minimal model approach. The effect is significant even in the case of weak spin-orbit coupling. Two main factors determine the selectivity, an unconventional Rashba-like spin-orbit interaction, reflecting the helical symmetry of the system, and a weakly dispersive electronic band of the helical system. The weak electronic coupling, associated with the small dispersion, leads to a low mobility of the charges in the system and allows even weak spin-orbit interactions to be effective. The results are expected to be generic for chiral molecular systems displaying low spin-orbit coupling and low conductivity.

TT 44.7 Thu 16:45 BH 334

Quantum Interference Effects in Single-Molecule Junctions — ●STEFAN BALLMANN¹, RAINER HÄRTLE², PEDRO BRANA-COTO², MICHAEL THOSS², and HEIKO B. WEBER¹ — ¹Lehrstuhl für Angewandte Physik, Universität Erlangen-Nürnberg, Germany — ²Institut für Theoretische Festkörperphysik, Universität Erlangen-Nürnberg, Germany

We analyze quantum interference effects in single-molecule junctions

Verhandlungen



der Deutschen Physikalischen Gesellschaft e.V.

Dresden 2011 – wissenschaftliches Programm

**Bereiche | Tage |
Auswahl | Suche |
Aktualisierungen |
Downloads | Hilfe**

**TT: Fachverband
Tiefe
Temperaturen**

TT 38: Poster Session

Transport

TT 38.27: Poster

**Mittwoch, 16. März 2011,
14:00–18:00, P3**

Auswahlstatus für diesen Beitrag:

gemäß den Sitzungseinstellungen



Time-dependent transport through a molecular level coupled to a nanomagnet —

•MILENA FILIPOVIC, FEDERICA HAUPT,
and WOLFGANG BELZIG —

University of Konstanz, Konstanz,
Germany

We study the transport through a single level quantum dot coupled to two leads in the presence of a magnetic field. The magnetic field is coupled to the quantum

dot and the leads are treated as noninteracting. We use the Keldysh nonequilibrium Green function technique to derive and analyze the properties of the spin-dependent tunneling current and its linear response to the applied time-dependent magnetic field. We further analyze the transport through the single level quantum dot coupled to a precessing molecular nanomagnet.

[1] V. Brosco *et al.*, Phys. Rev. B **82**, 041309(R) (2010).

TT 38.21 Wed 14:00 P3

Probing of coherence in molecular and CNT transport —

•BIRGIT KIESSIG^{1,2}, RALPH KRUPKE³, REGINA HOFFMANN², DOMINIK STÖFFLER², KAI GRUBE¹, ROLAND SCHÄFER¹, and HILBERT VON LÖHNESEN^{1,2} — ¹Karlsruher Institut für Technologie, Institut für Festkörperphysik, 76021 Karlsruhe — ²Karlsruher Institut für Technologie, Physikalisches Institut, 76128 Karlsruhe — ³Karlsruher Institut für Technologie, Institut für Nanotechnologie, 76021 Karlsruhe

The advancing miniaturisation of electronic circuits has increased the scientific interest in transport properties of single molecules as the smallest available building blocks. Other promising candidates for ultrasmall electronic devices are carbon nanotubes (CNTs), which at the same time are already today far easier to handle than molecules.

We aim to probe a very special characteristic of transport through nanoscale devices, namely coherence. Its occurrence in a single electronic building block leads to divergence of the behaviour of a combination of several such devices from the classical expectation.

Molecular transport measurements require the fabrication of conductive electrodes spaced only a few nm apart. To achieve such we chose a feedback controlled electromigration procedure for the preparation of our samples, which we investigated in detail.

Furthermore we also prepared and measured appropriate samples for coherence probing of transport through CNTs.

TT 38.22 Wed 14:00 P3

Inelastic transport through octane molecules and a single level model with light —

•THOMAS HELLMUTH¹, FABIAN PAULY¹, and GERD SCHÖN^{1,2} — ¹Institut für Theoretische Festkörperphysik, Karlsruhe Institut of Technology (KIT) — ²Institut für Nanotechnologie, Karlsruhe Institut of Technology (KIT)

We study the transport and vibrational modes of single-molecule junctions containing octanediamine and octanedithiol. For this we use a scheme based on density functional theory. We compare our results to experiments and map the calculated vibrational modes to the measured IETS [1]. We show the substantially different behavior for the different terminal groups, namely the pulling of gold chains for dithiols, while they are absent for the diamines. In addition to these studies, we explore the inelastic rectification current of a light irradiated single level contact.

[1] Y. Kim, T. Hellmuth, F. Pauly, and E. Scheer (in preparation)

TT 38.23 Wed 14:00 P3

Ab-initio description of transport through biphenyl-based molecular junctions —

•MARIUS BÜRCKLE¹, FABIAN PAULY¹, and GERD SCHÖN^{1,2} — ¹Institut für Theoretische Festkörperphysik, Karlsruhe Institute of Technology — ²Institut für Nanotechnologie, Karlsruhe Institute of Technology

Biphenyl molecules serve as prototype systems for transport through single molecule junctions. In combination with experiments, we study the electric and thermoelectric transport properties by means of density functional theory. We explore the effects of molecular conformation and anchoring groups on the electric transport in biphenyl dithiols, dinitriles, and diamines [1,2,3]. In addition, we show that they have also a strong influence on the thermoelectric properties. Namely, increasing torsion angle generally decreases the thermopower and, through doping via the anchoring groups, HOMO transport for dithiol and diamine linked molecules changes to LUMO transport for dinitriles.

[1] A. Mishchenko, D. Vonlanthen, V. Meded, M. Bürkle, C. Li, I. V. Pobelov, A. Bagrets, J. K. Viljas, F. Pauly, F. Evers, M. Mayor, and T. Wandlowski Nano Lett. **10**, 156 (2010)

[2] A. Mishchenko, L. A. Zotti, D. Vonlanthen, M. Bürkle, F. Pauly, J. C. Cuevas, M. Mayor, and T. Wandlowski J. Am. Chem. Soc. (2010), accepted

[3] L. Venkataraman, J. E. Klare, C. Nuckolls, M. S. Hybertsen and M. L. Steigerwald, Nature **442**, 904-907 (2006).

TT 38.24 Wed 14:00 P3

Optical Control of Single-Molecule Conductance —

•YAROSLAV ZELINSKYI^{1,2} and VOLKHARD MAY² — ¹Bogolyubov Institute for theoretical physics, National Academy of Science of Ukraine, 14-b Metrologichna str. UA-03680, Kiev, Ukraine — ²Institut für Physik, Humboldt Universität zu Berlin, Newtonstraße 15, D-12489, Berlin, Germany

A kinetic model is established for current formation through a single molecule embedded in between two metallic electrodes and irradiated by an external laser pulse. Focusing on the particular case of a molecule which can be moved in its excited electronic state if it became singly charged, an analytical expression for the steady-state current is presented. A detailed analysis of the current-voltage as well as conductance-voltage characteristics at the different wavelength of the applied laser light is carried out. Based on such computations a photo-switching effect between molecular states of low and height conductivity can be proposed. In the case of weak molecule-lead coupling a voltage region showing negative differential resistance is found. Its suppression due to laser pulse excitation is indicated.

TT 38.25 Wed 14:00 P3

Electrical Characterization of Short DNA Fragments —

•MATTHIAS WIESER¹, SHOU-PENG LIU², SAMUEL WEISBROD², ZHUO TANG², ANDREAS MARX², ELKE SCHEER², and ARTUR ERBE¹ — ¹Helmholtz-Zentrum Dresden-Rossendorf e.V., D-01328 Dresden — ²Universität Konstanz, D-78457 Konstanz

The electrical transport properties of DNA molecules are important for future molecular electronics applications. We characterized the electrical conductance of single DNA fragments in ambient condition and in buffer solution using a Mechanically Controllable Break Junction (MCBJ) setup which allows us binding molecules between two gold electrodes. We analyzed the electrical conductance of double stranded DNA and G-quadruplex molecules. G-quadruplex molecules consist of four guanine bases arranged in the shape of a square and a cation in the center. The electrical characterization is done by investigating the I-V curves characteristics of the molecules in different conditions.

TT 38.26 Wed 14:00 P3

Electronic transport through switchable molecules —

•BERND BRIECHLE¹, NIKOLA TRESKA¹, DIMA SYSOIEV², JANNIC WOLF², YOUNGSANG KIM¹, JOHANNES BONEBERG¹, THOMAS HUHN², ULRICH GROTH², ULRICH STEINER², ARTUR ERBE³, and ELKE SCHEER¹ — ¹Department of Physics, University of Konstanz, Germany — ²Department of Chemistry, University of Konstanz, Germany — ³Forschungszentrum Dresden-Rossendorf, Dresden, Germany

We investigate transport properties of molecules in liquid solvent at room temperature. For that purpose we use lithographically fabricated Mechanically Controllable Break Junctions (MCBJs) to generate atomic-size contacts and atomically sharp tips to contact the molecules. We study molecular switches for which reversible switching from an opened to a closed conjugated backbone via light irradiation is expected. The molecular switches feature thiol- or nitrogen-based endgroups for a strong bond to the metal. Analysis is based on statistics of conductance traces recorded during opening and closing the junction, and on current-voltage characteristics taken at constant electrode distance. It has been shown that the latter can be described by a simple transport model involving a single broadened molecular orbital. Fitting the experimental current-voltage characteristics to this model, we can extract the strength of the molecule-metal bond as well as the energy of the molecular orbital next to the Fermi level. This analysis enables us to determine promising combinations of metal and molecule endgroup for stable and reproducible contacting which is a crucial requirement for our transport studies.

TT 38.27 Wed 14:00 P3

Time-dependent transport through a molecular level coupled to a nanomagnet —

•MILENA FILIPOVIC, FEDERICA HAUPT, and WOLFGANG BELZIG — University of Konstanz, Konstanz, Germany

We study the transport through a single level quantum dot coupled to two leads in the presence of a magnetic field. The magnetic field is coupled to the quantum dot and the leads are treated as noninteracting. We use the Keldysh nonequilibrium Green function technique to derive and analyze the properties of the spin-dependent tunneling current and its linear response to the applied time-dependent magnetic field. We further analyze the transport through the single level quantum dot coupled to a precessing molecular nanomagnet.

TT 38.28 Wed 14:00 P3

Quantum Interference and Dephasing Due to Vibronic Coupling in a Single-Molecule Junction —

•MICHAEL BUTZIN, RAINER HÄRTLE, and MICHAEL THOSS — Theoretische Festkörperphysik, Friedrich-Alexander-Universität Erlangen-Nürnberg, Staudtstr. 7/B2, D-91058 Erlangen, Germany

Poster contributions
Poster Session 1
Mon Febr 25, 14:00-16:30

- P-01** *Search for stimulated emission and absorption of photons in ferromagnetic point contacts caused by inverse spin pumping* [Y. G. Naidyuk](#), O. P. Balkashin, V. V. Fisun, I. K. Yanson, A. Kadigrobov, R. I. Shekhter, M. Jonson, V. Neu, M. Seifert, S. Andersson and V. Korenivski
- P-03** *Entangled photons from the polariton vacuum in a switchable optical cavity* [A. Auer](#) and G. Burkard
- P-05** *Quantum limit of nuclear spin polarization in semiconductor quantum dots* [J. Hildmann](#), E. Kavousanaki, H. Ribeiro, and G. Burkard
- P-07** *Enhanced THz transmission through a single plasmonic nano slot antenna* J. Flock, T. Rybka, [T. Dekorsy](#)
- P-09** *Generation of a broadband acoustic frequency comb in the 100 GHz-range* [M. Grossmann](#), O. Ristow, M. Hettich, C. He, R. Waitz, P. Scheel, A. Bruchhausen, M. Schubert
- P-11** *Spin transport and tunable Gilbert damping in a single-molecule magnet junction* [M. Filipovic](#), C. Holmqvist, F. Haupt, and W. Belzig
- P-13** *Keratin 8/18 Networks and their Interplay with Plectin* [I. Martin](#), S. Nafeey, T. Paust, M. Beil, H. Herrmann, O. Marti
- P-15** *Control of Magnetic Domain Walls by Thermal Gradients* [M. Stärk](#), J. Boneberg, M. Fonin, E. Scheer
- P-17** *Spin injection from a normal metal into a mesoscopic superconductor* [M. J. Wolf](#), F. Hübner, S. Kolenda, H. v. Löhneysen, and D. Beckmann
- P-19** *Cellular powerplants: Energy production via integration of cells and nanoelectrode arrays* J.P. Spatz, [A. Rustom](#), H. Bading, P. Bengtson, T. Schimmel, S. Walheim
- P-21** *Colloidal Quantum Dots for Quantum Optic Applications* [J. Haase](#), C. Negele, A. Budweg, S. Mecking, D. V. Seletskiy, and A. Leitenstorfer
- P-23** *Charge transport in TiO₂ films and nanowires used for hybrid solar* [J. Kalb](#), J. Reindl, T. Pfadler, J. Weickert, J. Dorman, and L. Schmidt-Mende
- P-25** *Synthetic organelles as complex compartments with nano-defined bioorthogonal functionalities for defined bioconjugation – steps towards nano-factories* A. Schreiber, M. C. Huber, [S. Schiller](#)
- P-27** *Temperature and magnetic field dependence of the Kondo resonance in the weak coupling regime* Y.-H. Zhang, S. Kahle, T. Herden, C. Stroh, M. Mayor, U. Schlickum, [M. Ternes](#), P. Wahl, K. Kern

Poster Session 2
Wed Febr 27, 14:00-16:30

- P-02** *Spin-polarized Shapiro steps and assisted tunneling in a superconducting point contact coupled to magnetization dynamics* [C. Holmqvist](#), W. Belzig, and M. Fogelström
- P-04** *Switchable molecular wires: chemical gating and solvent dependency of quantum yields* [J. Wolf](#), A. Fedoseev, U. Groth, and T. Huhn
- P-06** *Investigation of ultrathin sandwiched molecular layers by coherent acoustic phonon spectroscopy* M. Hettich, K. Jacob, O. Ristow, J. Mayer, C. He, M. Schubert, A. Bruchhausen, V. Gusev, and [T. Dekorsy](#)
- P-08** *The new point of view of therapeutic effect of interaction between the viruses and nanoparticles* [V. Lozovski](#), V. Lysenko, V. Piantnytsia, M. Spivak
- P-10** *Magneto-optical effect in magnetoplasmonic systems with nanostructures surfaces* Yu. Demidenko, [V. Lozovski](#), D. Makarov, and O. Schmidt
- P-12** *Competition between intermolecular interactions and substrate-molecule interactions for Co-Phthalocyanine molecules deposited on Graphene/Ir(111)* [S. Bouvron](#), P. Erler, E. Cavar, M. Fonin
- P-14** *Magnetization reversal of self-assembled antidot arrays on the nanoscale* [F. Häring](#), [U. Wiedwald](#), P. Ziemann, J. Graefe, E. Goering, G. Schütz, A. Wallucks, K. Lebecki, U. Nowak
- P-16** *Coupling properties in "1-3" multiferroic composites* [D. Bueno-Baques](#), V. Corral-Flores, N. A. Morales-Carrillo, C. A. Gallardo-Vega and R. Ziolo
- P-18** *NiFe₂O₄-BaTiO₃ Core-Shell Type Nanostructures* [V. Corral-Flores](#), G. Hurtado-López, D. Bueno-Baqués
- P-20** *Nonadiabatic switching of a photonic band structure by sub-cycle activation of ultrastrong light matter interaction* [M. Porer](#), J.-M. Ménard, R. Degl'Innocenti, S. Zanotto, G. Biasiol, L. Sorba, A. Tredicucci, A. Pashkin, A. Leitenstorfer, R. Huber
- P-22** *Magneto resistance measurements on monatomic platinum contacts* [F. Strigl](#), C. Espy, M. Bückle, and E. Scheer
- P-24** *Injection molding of monolithic micro/nano channels without post bonding process* [Doo-Sun Choi](#), Yeong-Eun Yoo
- P-26** *Coded self-organization of nanoparticles and mechanism of non-classical crystallization* A. Schreiber, H. Cölfen, [T. A. Pham](#), A. Ziegler, [S. Schiller](#)
- P-28** *Probing mechanical properties of the BN -nanomesh by combined STM and AFM measurements at low temperatures* [T. Herden](#), M. Ternes, and K. Kern

The 19th Symposium on Condensed Matter Physics (SFKM2015) 7-11 September 2015, Belgrade, Serbia

Conference Program

Monday, 7 September 2015, Main hall, 2nd floor

8:30-9:00 **Conference Opening**

Superconductivity – Frontiers

Session Chairs: Christoph Bruder, Marco Aprili, Zoran Radović and Mihajlo Vanević

9:00-9:45	Ivan Božović	The Origin of High-Tc Superconductivity in Cuprates
9:45-10:10	Čedomir Petrović	Superconducting and Normal States in Iron Chalcogenides
10:10-10:35	Emil S. Božin	Evolution of Orthogonally Inequivalent States in Cuprates - Atomic Structure Footprints
Coffee Break		
10:50-11:15	Dragana Popović	Quantum Criticality and Far-from-Equilibrium Dynamics in Strongly Correlated (Quasi-) Two-Dimensional Electron Systems
11:15-11:40	Stevan Nadj-Perge	Majorana Fermions in Ferromagnetic Atomic Chains on a Superconductor
11:40-12:05	Milorad Milošević	Emergent Phenomena in Multigap Superconductors
12:05-12:30	Nenad Lazarević	Raman Scattering in Iron-Based Superconductors and Related Materials

- Poster 17:** Oscillator Strengths in an Off-Center Spherically Confined Hydrogen Atom
Vladan Pavlović
- Poster 18:** Density Functional Theory Study of Li and Ti-Intercalated Graphene
Jelena Pešić
- Poster 19:** Fano Resonances in the Conductance of Graphene Nanoribbons with Side Gates
Marko D. Petrović
- Poster 20:** Electro-acoustic Analogy of an Open, Minimum Volume, Photoacoustic Cell
Marica Popović
- Poster 21:** Charge Density Wave in CeTe₃ – A Scanning Tunneling Microscopy Study
Uroš Ralević
- Poster 22:** Conference Attendance Patterns
Jelena Smiljanić
- Poster 23:** Specifics in Optical Properties of Molecular Crystalline Nanofilms
Igor J. Šetrajić
- Poster 24:** Electrical and Mechanical Properties of CVD Graphene Studied by Scanning Probe Microscopy
Borislav Vasić
- Poster 25:** Collective Modes of Dipolar Fermi Gas from Collisionless to Hydrodynamic Regime
Vladimir Veljić
- Poster 26:** Faraday Waves in Dipolar Bose-Einstein Condensates
Dušan Vudragović
- Poster 27:** Simulations of Optical Properties of III-Nitride Quantum Dots and Nanowires
Nenad Vukmirović

Post-deadline Posters (Tuesday Evening)

- Poster 28:** Enhanced Performance of Organic Solar Cells with the Addition of Molecular Mo₆S_{9-x}I_x Nanowires and Factors Determining it
Nevena Čelić
- Poster 29:** Quantum Transport Through Molecular Magnets
Milena Filipović



Milena Filipovic

Unknown affiliation

	All	Since 2014
Citations	13	13
h-index	2	2
i10-index	0	0

TITLE	CITED BY	YEAR
<p>Spin transport and tunable Gilbert damping in a single-molecule magnet junction M Filipović, C Holmqvist, F Haupt, W Belzig Physical Review B 87 (4), 045426</p>	9	2013
<p>Photon-assisted electronic and spin transport in a junction containing precessing molecular spin M Filipović, W Belzig Physical Review B 93 (7), 075402</p>	3	2016
<p>Shot noise of charge and spin transport in a junction with a precessing molecular spin M Filipović, W Belzig Physical Review B 97 (11), 115441</p>	1	2018
<p>Photon-assisted electronic and spin transport through a precessing single-molecule magnet M Filipović, W Belzig</p>		2014
<p>Erratum: Spin transport and tunable Gilbert damping in a single-molecule magnet junction [Phys. Rev. B 87, 045426 (2013)] M Filipović, C Holmqvist, F Haupt, W Belzig Physical Review B 88 (11), 119901</p>		2013

Spin transport and tunable Gilbert damping in a single-molecule magnet junction

Search within citing articles

Time-dependent spin and transport properties of a single-molecule magnet in a tunnel junction

H Hammar, J Fransson - *Physical Review B*, 2016 - APS

In single-molecule magnets, the exchange between a localized spin moment and the electronic background provides a suitable laboratory for studies of dynamical aspects of both local spin and transport properties. Here we address the time evolution of a localized ...

☆  Cited by 13 [Related articles](#) [All 5 versions](#)

Transient spin dynamics in a single-molecule magnet

H Hammar, J Fransson - *Physical Review B*, 2017 - APS

We explore the limitations and validity of semiclassically formulated spin equations of motion. Using a single-molecule magnet as a test model, we employ three qualitatively different approximation schemes. From a microscopic model, we derive a generalized spin ...

☆  Cited by 7 [Related articles](#) [All 6 versions](#)

Dynamical exchange and phase induced switching of a localized molecular spin

H Hammar, J Fransson - *Physical Review B*, 2018 - APS

We address the dynamics of a localized molecular spin under the influence of external voltage pulses using a generalized spin equation of motion which incorporates anisotropic fields, nonequilibrium conditions, and nonadiabatic dynamics. We predict a recurring 4π ...

☆  Cited by 3 [Related articles](#) [All 5 versions](#)

Photon-assisted electronic and spin transport in a junction containing precessing molecular spin

M Filipović, W Belzig - *Physical Review B*, 2016 - APS

We study the ac charge and-spin transport through an orbital of a magnetic molecule with spin precessing in a constant magnetic field. We assume that the source and drain contacts have time-dependent chemical potentials. We employ the Keldysh nonequilibrium Green's ...

☆  Cited by 3 [Related articles](#) [All 6 versions](#)

Spin resonance transport properties of a single Au atom in S–Au–S junction and Au–Au–Au junction

F Wang, G Li - *Chinese Physics B*, 2016 - iopscience.iop.org

The spin transport properties of S–Au–S junction and Au–Au–Au junction between Au nanowires are investigated with density functional theory and the non-equilibrium Green's function. We mainly focus on the spin resonance transport properties of the center Au atom ...

☆  Cited by 1 [Related articles](#) [All 4 versions](#)

Dynamics of Magnetic Molecules under Electrical Control

H Hammar - 2019 - diva-portal.org

This thesis theoretically studies the dynamics of molecular magnets under electrical control. Molecular magnets are nanoscale magnets that can, eg, consist of single-molecules or singleatoms. In these magnets, the electronically mediated exchange and transport can be ...

☆  [Related articles](#) 

Non-equilibrium dynamics of a single spin in a tunnel junction

H Hammar - 2014 - diva-portal.org

Electronic devices and circuits are getting smaller and smaller and more effective and has for many years followed the prediction of Moore's law [1]. Conventional electronic devices as silicon integrated circuits are now entering a level where quantum effects starts to come into ...

☆  [Related articles](#) 

Quantum Transport Through Molecular Magnets

M Filipovic - 2015 - kops.uni-konstanz.de

In this thesis we theoretically study time-dependent electronic and spin transport through a molecular orbital connected to two Fermi leads, and coupled to a molecular magnet via exchange interaction. The molecular spin is considered as a classical variable and is ...

☆  [Related articles](#) [All 2 versions](#) 

Dinámica de un dímero magnético

L Pérez-Fuentes - 2014 - dadun.unav.edu

De igual manera, autorizo al Departamento de Física y Matemática Aplicada de la Universidad de Navarra, la distribución de esta memoria y, si procede, de la "fe de erratas" correspondiente por cualquier medio, sin perjuicio de los derechos de propiedad intelectual que me ...

☆  [Related articles](#) [All 2 versions](#) 

Photon-assisted electronic and spin transport in a junction containing precessing molecular spin

Search within citing articles

Spin-resolved dynamical conductance of a correlated large-spin magnetic molecule

A Płomińska, M Misiorny, I Weymann - *Physical Review B*, 2017 - APS

The finite-frequency transport properties of a large-spin molecule attached to ferromagnetic contacts are studied theoretically in the Kondo regime. The focus is on the behavior of the dynamical conductance in the linear response regime, which is determined by using the ...

☆  Cited by 5 [Related articles](#) [All 7 versions](#)

On the Choi–Lam analogue of Hilbert's 1888 theorem for symmetric forms

C Goel, S Kuhlmann, B Reznick - *Linear Algebra and its Applications*, 2016 - Elsevier

A famous theorem of Hilbert from 1888 states that for given n and d , every positive semidefinite (psd) real form of degree $2d$ in n variables is a sum of squares (sos) of real forms if and only if $n=2$ or $d=1$ or $(n, 2d)=(3, 4)$. In 1976, Choi and Lam proved the ...

☆  Cited by 3 [Related articles](#) [All 10 versions](#)

Shot noise of charge and spin transport in a junction with a precessing molecular spin

M Filipović, W Belzig - *Physical Review B*, 2018 - APS

Magnetic molecules and nanomagnets can be used to influence the electronic transport in mesoscopic junction. In a magnetic field, the precessional motion leads to resonances in the dc- and ac-transport properties of a nanocontact, in which the electrons are coupled to the ...

☆  Cited by 1 [Related articles](#) [All 6 versions](#)

Shot noise of charge and spin transport in a junction with a precessing molecular spin

Search within citing articles

Thermodynamics and spin mapping of quantum excitations in a Heisenberg spin heptamer

A Roxburgh, JT Haraldsen - *Physical Review B*, 2018 - APS

In this study, we examine the thermodynamics and spin dynamics of spin-1/2 and spin-3/2 heptamers. Through an exact diagonalization of the isotropic Heisenberg Hamiltonian, we find the closed-form, analytical representations for thermodynamic properties, spin ...

☆  Cited by 1 [Related articles](#) [All 5 versions](#)

Search

Tools ▾ Searches and alerts ▾ Search History Marked List

Results: 4
(in your subscription)

View the articles authored by:
Filipovic, Milena

For: AUTHOR: Filipovic, Milena
[...More](#)

Refine Results

Search within results for...

Publication Years

- 2018 (1)
- 2016 (1)
- 2013 (2)

[more options / values...](#)

Refine

Web of Science Categories

- MATERIALS SCIENCE MULTIDISCIPLINARY (4)
- PHYSICS APPLIED (4)
- PHYSICS CONDENSED MATTER (4)

[more options / values...](#)

Refine

Document Types

- ARTICLE (3)
- CORRECTION (1)

Sort by: **Date** ▾ Times Cited Usage Count Relevance More ▾

◀ 1 of 1 ▶

Select Page

1. **Shot noise of charge and spin transport in a junction with a precessing molecular spin**

By: Filipovic, Milena; Belzig, Wolfgang

PHYSICAL REVIEW B Volume: 97 Issue: 11 Article Number: 115441 Published: MAR 26 2018

2. **Photon-assisted electronic and spin transport in a junction containing precessing molecular spin**

By: Filipovic, Milena; Belzig, Wolfgang

PHYSICAL REVIEW B Volume: 93 Issue: 7 Article Number: 075402 Published: FEB 1 2016

3. **Spin transport and tunable Gilbert damping in a single-molecule magnet junction (vol 87, 045426, 2013)**

By: Filipovic, Milena; Holmqvist, Cecilia; Haupt, Federica; et al.

PHYSICAL REVIEW B Volume: 88 Issue: 11 Article Number: 119901 Published: SEP 5 2013

4. **Spin transport and tunable Gilbert damping in a single-molecule magnet junction**

By: Filipovic, Milena; Holmqvist, Cecilia; Haupt, Federica; et al.

PHYSICAL REVIEW B Volume: 87 Issue: 4 Article Number: 045426 Published: JAN 28 2013

Select Page

Sort by: **Date** ▾ Times Cited Usage Count Relevance More ▾

◀ 1 of 1 ▶

Show:

Times Cited: 1
(from Web of Science Core Collection)

Usage Count ▾

Times Cited: 2
(from Web of Science Core Collection)

Usage Count ▾

Times Cited: 0
(from Web of Science Core Collection)

Usage Count ▾

Times Cited: 7
(from Web of Science Core Collection)

Usage Count ▾

Author details

[Print](#) [Email](#)

Filipović, Milena

[Follow this Author](#)

h-index: Ⓢ

[View *h*-graph](#)

2

Is this you? [Claim profile](#)

[View potential author matches](#)

Universität Konstanz, Konstanz, Germany

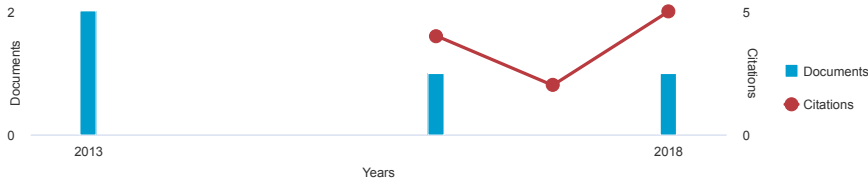
Author ID: 55572942900 ⓘ

Other name formats:

Subject area:

[Materials Science](#) [Physics and Astronomy](#)

Document and citation trends:



Documents by author

4

[Analyze author output](#)

Total citations

11 by 8 documents

[View citation overview](#)

[Get citation alerts](#) [+ Add to ORCID](#) [Edit author profile](#)

[4 Documents](#) [Cited by 8 documents](#) [3 co-authors](#) [Author history](#) [Topics](#)

[View in search results format](#)

Sort on: [Date \(newest\)](#)

[Export all](#) [Add all to list](#) [Set document alert](#) [Set document feed](#)

Document title	Authors	Year	Source	Cited by
----------------	---------	------	--------	----------

Shot noise of charge and spin transport in a junction with a precessing molecular spin	Filipović, M., Belzig, W.	2018	Physical Review B 97(11),115441	1
--	---------------------------	------	---------------------------------	---

[View abstract](#) [KOBSON](#) [View at Publisher](#) [Related documents](#)

Photon-assisted electronic and spin transport in a junction containing precessing molecular spin	Filipović, M., Belzig, W.	2016	Physical Review B 93(7),075402	2
--	---------------------------	------	--------------------------------	---

[View abstract](#) [KOBSON](#) [View at Publisher](#) [Related documents](#)

Erratum: Spin transport and tunable Gilbert damping in a single-molecule magnet junction (Physical Review B (2013) 87 (045426) DOI:10.1103/PhysRevB.87. 045426)	Filipović, M., Holmqvist, C., Haupt, F., Belzig, W.	2013	Physical Review B - Condensed Matter and Materials Physics 88(11),119901	2
---	---	------	--	---

[KOBSON](#) [View at Publisher](#)

Spin transport and tunable Gilbert damping in a single-molecule magnet junction	Filipović, M., Holmqvist, C., Haupt, F., Belzig, W.	2013	Physical Review B - Condensed Matter and Materials Physics 87(4),045426	6
---	---	------	---	---

[View abstract](#) [KOBSON](#) [View at Publisher](#) [Related documents](#)

Display: [20](#) results per page

Author details

[Print](#) [Email](#)

Filipović, Milena

[Follow this Author](#)

h-index: 2

[View *h*-graph](#)

Is this you? [Claim profile](#)

[View potential author matches](#)

Universität Konstanz, Konstanz, Germany

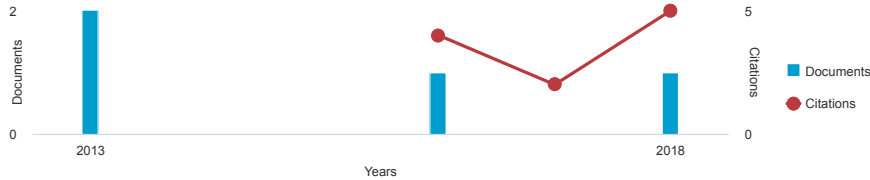
Author ID: 55572942900

Other name formats:

Subject area:

[Materials Science](#) [Physics and Astronomy](#)

Document and citation trends:



Documents by author

4

[Analyze author output](#)

Total citations

11 by 8 documents

[View citation overview](#)

[Get citation alerts](#) [Add to ORCID](#) [Edit author profile](#)

[4 Documents](#) [Cited by 8 documents](#) [3 co-authors](#) [Author history](#) [Topics](#)

[View in search results format](#)

Sort on: [Date \(newest\)](#)

[Export all](#) [Add all to list](#) [Set citation alert](#)

Document title	Authors	Year	Source	Cited by
Thermodynamics and spin mapping of quantum excitations in a Heisenberg spin heptamer	Roxburgh, A., Haraldsen, J.T.	2018	Physical Review B 98(21),214434	1
View abstract KOBSON View at Publisher Related documents				
Dynamical exchange and phase induced switching of a localized molecular spin	Hammar, H., Fransson, J.	2018	Physical Review B 98(17),174438	2
View abstract KOBSON View at Publisher Related documents				
Shot noise of charge and spin transport in a junction with a precessing molecular spin	Filipović, M., Belzig, W.	2018	Physical Review B 97(11),115441	1
View abstract KOBSON View at Publisher Related documents				
Transient spin dynamics in a single-molecule magnet	Hammar, H., Fransson, J.	2017	Physical Review B 96(21),214401	4
View abstract KOBSON View at Publisher Related documents				
Spin-resolved dynamical conductance of a correlated large-spin magnetic molecule	Płomińska, A., Misiorny, M., Weymann, I.	2017	Physical Review B 95(15),155446	5
View abstract KOBSON View at Publisher Related documents				

Document title	Authors	Year	Source	Cited by
Time-dependent spin and transport properties of a single-molecule magnet in a tunnel junction	Hammar, H., Fransson, J.	2016	Physical Review B 94(5),054311	9
View abstract  View at Publisher Related documents				
Spin resonance transport properties of a single Au atom in S-Au-S junction and Au-Au-Au junction	Wang, F., Li, G.	2016	Chinese Physics B 25(7),077304	1
View abstract  View at Publisher Related documents				
Photon-assisted electronic and spin transport in a junction containing precessing molecular spin	Filipović, M., Belzig, W.	2016	Physical Review B 93(7),075402	2
View abstract  View at Publisher Related documents				

Display: results per page

1

[^ Top of page](#)

The data displayed above is compiled exclusively from documents indexed in the Scopus database. To request corrections to any inaccuracies or provide any further feedback, please use the Author Feedback Wizard .

Spin transport and tunable Gilbert damping in a single-molecule magnet junction

Milena Filipović,¹ Cecilia Holmqvist,¹ Federica Haupt,² and Wolfgang Belzig¹

¹*Fachbereich Physik, Universität Konstanz, D-78457 Konstanz, Germany*

²*Institut für Theorie der Statistischen Physik, RWTH Aachen, D-52056 Aachen, Germany*

(Received 15 November 2012; published 28 January 2013)

We study time-dependent electronic and spin transport through an electronic level connected to two leads and coupled with a single-molecule magnet via exchange interaction. The molecular spin is treated as a classical variable and precesses around an external magnetic field. We derive expressions for charge and spin currents by means of the Keldysh nonequilibrium Green's functions technique in linear order with respect to the time-dependent magnetic field created by this precession. The coupling between the electronic spins and the magnetization dynamics of the molecule creates inelastic tunneling processes which contribute to the spin currents. The inelastic spin currents, in turn, generate a spin-transfer torque acting on the molecular spin. This back-action includes a contribution to the Gilbert damping and a modification of the precession frequency. The Gilbert damping coefficient can be controlled by the bias and gate voltages or via the external magnetic field and has a nonmonotonic dependence on the tunneling rates.

DOI: [10.1103/PhysRevB.87.045426](https://doi.org/10.1103/PhysRevB.87.045426)

PACS number(s): 73.23.-b, 75.76.+j, 85.65.+h, 85.75.-d

I. INTRODUCTION

Single-molecule magnets (SMMs) are quantum magnets, i.e., mesoscopic quantum objects with a permanent magnetization. They are typically formed by paramagnetic ions stabilized by surrounding organic ligands.¹ SMMs show both classical properties such as magnetization hysteresis² and quantum properties such as spin tunneling,³ coherence,⁴ and quantum phase interference.^{2,5} They have recently been in the center of interest^{2,6,7} in view of their possible applications as information storage⁸ and processing devices.⁹

Currently, a goal in the field of nanophysics is to control and manipulate individual quantum systems, in particular, individual spins.^{10,11} Some theoretical works have investigated electronic transport through a molecular magnet contacted to leads.^{12–19} In this case, the transport properties are modified due to the exchange interaction between the itinerant electrons and the SMM,²⁰ making it possible to read out the spin state of the molecule using transport currents. Conversely, the spin dynamics and hence the state of an SMM can also be controlled by transport currents. Efficient control of the molecule's spin state can be achieved by coupling to ferromagnetic contacts as well.²¹

Experiments have addressed the electronic transport properties through magnetic molecules such as Mn₁₂ and Fe₈,^{22,23} which have been intensively studied as they are promising candidates for memory devices.²⁴ Various phenomena such as large conductance gaps,²⁵ switching behavior,²⁶ negative differential conductance, dependence of the transport on magnetic fields and Coulomb blockades have been experimentally observed.^{22,23,27,28} Experimental techniques, including, for instance, scanning tunneling microscopy (STM),^{22,23,29–31} break junctions,³² and three-terminal devices,^{22,23,27} have been employed to measure electronic transport through an SMM. Scanning tunneling spectroscopy and STM experiments show that quantum properties of SMMs are preserved when deposited on substrates.²⁹ The Kondo effect in SMMs with magnetic anisotropy has been investigated both theoretically¹⁴ and experimentally.^{33,34} It has been suggested³⁵ and experi-

mentally verified³⁶ that a spin-polarized tip can be used to control the magnetic state of a single Mn atom.

In some limits, the large spin S of an SMM can be treated as a classical magnetic moment. In that case, the spin dynamics is described by the Landau-Lifshitz-Gilbert (LLG) equation that incorporates effects of external magnetic fields as well as torques originating from damping phenomena.^{37,38} In tunnel junctions with magnetic particles, LLG equations have been derived using perturbative couplings^{39,40} and the nonequilibrium Born-Oppenheimer approximation.¹⁶ Current-induced magnetization switching is driven by a generated spin-transfer torque (STT)^{41–44} as a back-action effect of the electronic spin transport on the magnetic particle.^{16,45–47} A spin-polarized STM (Ref. 36) has been used to experimentally study STTs in relation to a molecular magnetization.⁴⁸ This experimental achievement opens new possibilities for data storage technology and applications using current-induced STTs.

The goal of this paper is to study the interplay between electronic spin currents and the spin dynamics of an SMM. We focus on the spin-transport properties of a tunnel junction through which transport occurs via a single electronic energy level in the presence of an SMM. The electronic level may belong to a neighboring quantum dot (QD) or it may be an orbital related to the SMM itself. The electronic level and the molecular spin are coupled via exchange interaction, allowing for interaction between the spins of the itinerant electrons tunneling through the electronic level and the spin dynamics of the SMM. We use a semiclassical approach in which the magnetization of the SMM is treated as a classical spin whose dynamics is controlled by an external magnetic field, while for the electronic spin and charge transport we use instead a quantum description. The magnetic field is assumed to be constant, leading to a precessional motion of the spin around the magnetic field axis. The electronic level is subjected both to the effects of the molecular spin and the external magnetic field, generating a Zeeman split of the level. The spin precession makes additional channels available for transport, which leads to the possibility of precession-assisted inelastic tunneling. During a tunnel event, spin-angular momentum

may be transferred between the inelastic spin currents and the molecular spin, leading to an STT that may be used to manipulate the spin of the SMM. This torque includes the so-called *Gilbert damping*, which is a phenomenologically introduced damping term of the LLG equation,³⁸ and a term corresponding to a modification of the precession frequency. We show that the STT and hence the SMM's spin dynamics can be controlled by the external magnetic field, the bias voltage across the junction, and the gate voltage acting on the electronic level.

The paper is organized as follows: We introduce our model and formalism based on the Keldysh nonequilibrium Green's functions technique^{49–51} in Sec. II, where we derive expressions for the charge and spin currents in linear order with respect to a time-dependent magnetic field and analyze the spin-transport properties at zero temperature. In Sec. III we replace the general magnetic field of Sec. II by an SMM whose spin precesses in an external constant magnetic field, calculate the STT components related to the Gilbert damping, and the modification of the precession frequency, and analyze the effects of the external magnetic field as well as the bias and gate voltages on the spin dynamics. Conclusions are given in Sec. IV.

II. CURRENT RESPONSE TO A TIME-DEPENDENT MAGNETIC FIELD

A. Model and formalism

For the sake of clarity, we start by considering a junction consisting of a noninteracting single-level QD coupled with two normal, metallic leads in the presence of an external, time-dependent magnetic field (see Fig. 1). The leads are assumed to be noninteracting and unaffected by the external field. The total Hamiltonian describing the junction is given by $\hat{H}(t) = \hat{H}_{L,R} + \hat{H}_T + \hat{H}_D(t)$. The Hamiltonian of the free electrons in the leads reads $\hat{H}_{L,R} = \sum_{k,\sigma,\xi \in \{L,R\}} \epsilon_{k\sigma\xi} \hat{c}_{k\sigma\xi}^\dagger \hat{c}_{k\sigma\xi}$, where ξ denotes the left (*L*) or right (*R*) lead, whereas the tunnel coupling between the QD and the leads can be written as $\hat{H}_T = \sum_{k,\sigma,\xi \in L,R} [V_{k\sigma\xi} \hat{c}_{k\sigma\xi}^\dagger \hat{d}_\sigma + V_{k\sigma\xi}^* \hat{d}_\sigma^\dagger \hat{c}_{k\sigma\xi}]$. The tunnel matrix element is given by $V_{k\sigma\xi}$. The operators $\hat{c}_{k\sigma\xi}^\dagger$ ($\hat{c}_{k\sigma\xi}$) and \hat{d}_σ^\dagger (\hat{d}_σ) are the creation (annihilation) operators of the electrons in the leads and the QD, respectively. The subscript $\sigma = \uparrow, \downarrow$ denotes the spin-up or spin-down state of the electrons. The electronic level ϵ_0 of the QD is influenced by an external

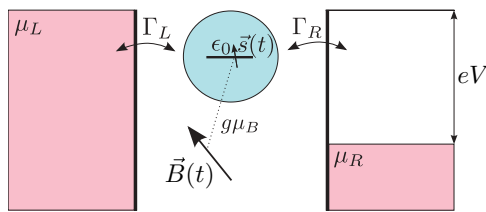


FIG. 1. (Color online) A quantum dot with a single electronic level ϵ_0 coupled to two metallic leads with chemical potentials μ_L and μ_R in the presence of an external time-dependent magnetic field $\vec{B}(t)$. The spin-transport properties of the junction are determined by the bias voltage $eV = \mu_L - \mu_R$, the position of the level ϵ_0 , the tunnel rates Γ_L and Γ_R , and the magnetic field.

magnetic field $\vec{B}(t)$ consisting of a constant part \vec{B}^c and a time-dependent part $\vec{B}'(t)$. The Hamiltonian of the QD describing the interaction between the electronic spin \hat{s} and the magnetic field is then given by $\hat{H}_D(t) = \hat{H}_D^c + \hat{H}'(t)$, where the constant and time-dependent parts are $\hat{H}_D^c = \sum_\sigma \epsilon_0 \hat{d}_\sigma^\dagger \hat{d}_\sigma + g\mu_B \hat{s} \vec{B}^c$ and $\hat{H}'(t) = g\mu_B \hat{s} \vec{B}'(t)$. The proportionality factor g is the gyromagnetic ratio of the electron and μ_B is the Bohr magneton.

The average charge and spin currents from the left lead to the electronic level are given by

$$I_{L\nu}(t) = q_\nu \left\langle \frac{d}{dt} \hat{N}_{L\nu} \right\rangle = q_\nu \frac{i}{\hbar} \langle [\hat{H}, \hat{N}_{L\nu}] \rangle, \quad (1)$$

where $\hat{N}_{L\nu} = \sum_{k,\sigma,\sigma'} \hat{c}_{k\sigma L}^\dagger (\hat{\sigma}_\nu)_{\sigma\sigma'} \hat{c}_{k\sigma' L}$ is the charge and spin occupation number operator of the left contact. The index $\nu = 0$ corresponds to the charge current, while $\nu = x, y, z$ indicates the different components of the spin-polarized current. The current coefficients q_ν are then $q_0 = -e$ and $q_{\nu \neq 0} = \hbar/2$. In addition, it is useful to define the vector $\hat{\sigma}_\nu = (\hat{1}, \hat{\sigma})$, where $\hat{1}$ is the identity operator and $\hat{\sigma}$ consists of the Pauli operators with matrix elements $(\hat{\sigma})_{\sigma\sigma'}$. Using the Keldysh nonequilibrium Green's functions technique, the currents can then be obtained as^{50,51}

$$I_{L\nu}(t) = -\frac{2q_\nu}{\hbar} \text{Re} \int dt' \text{Tr} \left\{ \hat{\sigma}_\nu [\hat{G}^r(t, t') \hat{\Sigma}_L^<(t', t) + \hat{G}^<(t, t') \hat{\Sigma}_L^a(t', t)] \right\}, \quad (2)$$

where $\hat{G}^{r,a,<}$ are the retarded, advanced, and lesser Green's functions of the electrons in the QD with the matrix elements $G_{\sigma\sigma'}^{r,a}(t, t') = \mp i \theta(\pm t \mp t') \langle \{\hat{d}_\sigma(t), \hat{d}_{\sigma'}^\dagger(t')\} \rangle$ and $G_{\sigma\sigma'}^<(t, t') = i \langle \hat{d}_{\sigma'}^\dagger(t') \hat{d}_\sigma(t) \rangle$, while $\hat{\Sigma}_L^{a,<}(t, t')$ are self-energies from the coupling between the QD and the left lead. Their matrix elements are given by $[\Sigma_L^{r,a,<}(t, t')]_{\sigma\sigma'} = \sum_k V_{k\sigma L} g_{kL}^{r,a,<}(t, t') V_{k\sigma' L}^*$. The Green's functions $g_{kL}^{r,a,<}(t, t')$ are the retarded, advanced, and lesser Green's functions of the free electrons in the left lead. The retarded Green's functions \hat{G}_0^r of the electrons in the QD, in the presence of the constant magnetic field \vec{B}^c , are found using the equation of motion technique,⁵² while the lesser Green's functions $\hat{G}_0^<$ are obtained from the Keldysh equation $\hat{G}_0^< = \hat{G}_0^r \hat{\Sigma}^< \hat{G}_0^a$, where multiplication implies internal time integrations.⁵¹ The time-dependent part of the magnetic field can be expressed as $\vec{B}'(t) = \sum_\omega (\vec{B}_\omega e^{-i\omega t} + \vec{B}_\omega^* e^{i\omega t})$, where \vec{B}_ω is a complex amplitude. This magnetic field acts as a time-dependent perturbation that can be expressed as $\hat{H}'(t) = \sum_\omega (\hat{H}_\omega e^{-i\omega t} + \hat{H}_\omega^\dagger e^{i\omega t})$, where \hat{H}_ω is an operator in the electronic spin space and its matrix representation in the basis of eigenstates of \hat{s}_z is given by

$$\hat{H}_\omega = \frac{g\mu_B}{2} \begin{pmatrix} B_{\omega z} & B_{\omega x} - i B_{\omega y} \\ B_{\omega x} + i B_{\omega y} & -B_{\omega z} \end{pmatrix}. \quad (3)$$

Applying Dyson's expansion, analytic continuation rules, and the Keldysh equation,⁵¹ one obtains a first-order approximation of the Green's functions describing the electrons in the QD that can be written as

$$\begin{aligned} \hat{G}^r &\approx \hat{G}_0^r + \hat{G}_0^r \hat{H}' \hat{G}_0^r, \\ \hat{G}^< &\approx \hat{G}_0^r \hat{\Sigma}^< \hat{G}_0^a + \hat{G}_0^r \hat{H}' \hat{G}_0^r \hat{\Sigma}^< \hat{G}_0^a + \hat{G}_0^r \hat{\Sigma}^< \hat{G}_0^a \hat{H}' \hat{G}_0^a. \end{aligned} \quad (4)$$

The expression for the currents in this linear approximation is given by

$$I_{Lv}(t) = \frac{2q_v}{\hbar} \text{Re Tr} \{ \hat{\sigma}_v [\hat{G}_0^r \hat{\Sigma}_L^< + \hat{G}_0^< \hat{\Sigma}_L^a + \hat{G}_0^r \hat{H}' \hat{G}_0^r \hat{\Sigma}_L^< + \hat{G}_0^r \hat{H}' \hat{G}_0^< \hat{\Sigma}_L^a + \hat{G}_0^< \hat{H}' \hat{G}_0^a \hat{\Sigma}_L^a] \}. \quad (5)$$

Equation (5) is then Fourier transformed in the wide-band limit, in which the level width function, $\Gamma(\epsilon) = -2 \text{Im}\{\Sigma^r(\epsilon)\}$, is constant, $\text{Re}\{\Sigma^r(\epsilon)\} = 0$, and one can hence write the retarded self-energy originating from the dot-lead coupling as $\Sigma^{r,a}(\epsilon) = \mp i\Gamma/2$. From this transformation, one obtains

$$I_{Lv}(t) = I_{Lv}^{\text{dc}} + \sum_{\omega} [I_{Lv}(\omega) e^{-i\omega t} + I_{Lv}^*(\omega) e^{i\omega t}]. \quad (6)$$

Using units in which $\hbar = 1$, the dc part of the currents⁵¹ I_{Lv}^{dc} and the time-independent complex components $I_{Lv}(\omega)$ are given by

$$I_{Lv}^{\text{dc}} = q_v \int \frac{d\epsilon}{\pi} \frac{\Gamma_L \Gamma_R}{\Gamma} [f_L(\epsilon) - f_R(\epsilon)] \text{Tr Im} \{ \hat{\sigma}_v \hat{G}_0^r(\epsilon) \} \quad (7)$$

and

$$I_{Lv}(\omega) = -iq_v \int \frac{d\epsilon}{2\pi} \frac{\Gamma_L \Gamma_R}{\Gamma} \left\{ [f_L(\epsilon) - f_R(\epsilon)] \times \text{Tr} \{ \hat{\sigma}_v [\hat{G}_0^r(\epsilon - \omega) \hat{H}_\omega \hat{G}_0^r(\epsilon) + 2i \text{Im} \{ \hat{G}_0^r(\epsilon) \} \hat{H}_\omega \hat{G}_0^a(\epsilon + \omega)] \} + \sum_{\xi=L,R} \frac{\Gamma_\xi}{\Gamma_R} [f_L(\epsilon + \omega) - f_\xi(\epsilon)] \times \text{Tr} [\hat{\sigma}_v \hat{G}_0^r(\epsilon) \hat{H}_\omega \hat{G}_0^a(\epsilon + \omega)] \right\}. \quad (8)$$

In the above expressions, $f_\xi(\epsilon) = [e^{(\epsilon - \mu_\xi)/k_B T} + 1]^{-1}$ is the Fermi distribution of the electrons in lead ξ , where k_B is the Boltzmann constant. The retarded Green's function $\hat{G}_0^r(\epsilon)$ is given by $\hat{G}_0^r(\epsilon) = [\epsilon - \epsilon_0 - \Sigma^r(\epsilon) - (1/2)g\mu_B \hat{\sigma} \vec{B}^c]^{-1}$.¹⁶

The linear response of the spin current with respect to the applied time-dependent magnetic field can be expressed in terms of complex spin-current susceptibilities defined as

$$\chi_{vj}^L(\omega) = \frac{\partial I_{Lv}(\omega)}{\partial B_{\omega j}}, \quad j = x, y, z. \quad (9)$$

The complex components $I_{Lv}(\omega)$ are conversely given by $I_{Lv}(\omega) = \sum_j \chi_{vj}^L(\omega) B_{\omega j}$. By taking into account that $\partial \hat{H}_\omega / \partial B_{\omega j} = (1/2)g\mu_B \hat{\sigma}_j$ and using Eq. (8), the current susceptibilities can be written as

$$\chi_{vj}^L(\omega) = -i \frac{q_v g \mu_B}{\hbar} \int \frac{d\epsilon}{4\pi} \frac{\Gamma_L \Gamma_R}{\Gamma} \left\{ [f_L(\epsilon) - f_R(\epsilon)] \times \text{Tr} \{ \hat{\sigma}_v [\hat{G}_0^r(\epsilon - \omega) \hat{\sigma}_j \hat{G}_0^r(\epsilon) + 2i \text{Im} \{ \hat{G}_0^r(\epsilon) \} \hat{\sigma}_j \hat{G}_0^a(\epsilon + \omega)] \} + \sum_{\xi} \frac{\Gamma_\xi}{\Gamma_R} [f_\xi(\epsilon + \omega) - f_L(\epsilon)] \times \text{Tr} [\hat{\sigma}_v \hat{G}_0^r(\epsilon) \hat{\sigma}_j \hat{G}_0^a(\epsilon + \omega)] \right\}. \quad (10)$$

The components obey $\chi_{vj}^L(-\omega) = \chi_{vj}^{L*}(\omega)$. In other words, they satisfy the Kramers-Kronig relations⁵³ that can be written in a compact form as

$$\chi_{vj}^L(\omega) = \frac{1}{i\pi} P \int_{-\infty}^{\infty} \frac{\chi_{vj}^L(\xi)}{\xi - \omega} d\xi, \quad (11)$$

with P denoting the principal value.

For any $i, j, k = x, y, z$ such that $j \neq k$ and $j, k \neq i$, where i indicates the direction of the constant part of the magnetic field $\vec{B}^c = B^c \vec{e}_i$, the complex current susceptibilities satisfy the relations

$$\chi_{jj}^L(\omega) = \chi_{kk}^L(\omega) \quad (12)$$

$$\text{and } \chi_{jk}^L(\omega) = -\chi_{kj}^L(\omega), \quad (13)$$

in addition to Eq. (11). The other nonzero components are $\chi_{0i}^L(\omega)$ and $\chi_{ii}^L(\omega)$. In the absence of a constant magnetic field, the only nonvanishing components obey $\chi_{xx}^L(\omega) = \chi_{yy}^L(\omega) = \chi_{zz}^L(\omega)$.

Finally, the average value of the electronic spin in the QD reads $\vec{s}(t) = \langle \vec{s}(t) \rangle = (1/2) \sum_{\sigma\sigma'} \vec{\sigma}_{\sigma\sigma'} \langle \hat{d}_\sigma^\dagger(t) \hat{d}_{\sigma'}(t) \rangle = -(i/2) \sum_{\sigma\sigma'} \vec{\sigma}_{\sigma\sigma'} \hat{G}_{\sigma'\sigma}^<(t, t)$ and the complex spin susceptibilities are defined as

$$\chi_{ij}^s(\omega) = \frac{\partial s_i(\omega)}{\partial B_{\omega j}}. \quad (14)$$

They represent the linear responses of the electronic spin components to the applied time-dependent magnetic field and satisfy the relations similar to Eqs. (11)–(13) given above.

B. Analysis of the spin and current responses

We start by analyzing the transport properties of the junction at zero temperature in response to the external time-dependent magnetic field $\vec{B}(t)$. The constant component of the magnetic field \vec{B}^c generates a Zeeman split of the QD level ϵ_0 , resulting in the levels $\epsilon_{\uparrow, \downarrow}$, where $\epsilon_{\uparrow, \downarrow} = \epsilon_0 \pm g\mu_B B^c/2$ in this section. The time-dependent periodic component of the magnetic field $\vec{B}'(t)$ then creates additional states, i.e., sidebands, at energies $\epsilon_{\uparrow} \pm \omega$ and $\epsilon_{\downarrow} \pm \omega$ (see Fig. 2). These Zeeman levels and sidebands contribute to the elastic transport properties of the junction when their energies lie inside the bias-voltage window of $eV = \mu_L - \mu_R$.

However, energy levels outside the bias-voltage window may also contribute to the electronic transport due to inelastic tunnel processes generated by the time-dependent magnetic field. In these inelastic processes, an electron transmitted from the left lead to the QD can change its energy by ω and either tunnel back to the left lead or out into the right lead. If this perturbation is small, as is assumed in this paper where we consider first-order corrections, the transport properties are still dominated by the elastic, energy-conserving tunnel processes that are associated with the Zeeman levels.

The energy levels of the QD determine transport properties such as the spin-current susceptibilities and the spin susceptibilities, which are shown in Fig. 3. The imaginary and real parts of the susceptibilities are plotted as functions of the frequency ω in Figs. 3(a) and 3(c). In this case, the position of the unperturbed level ϵ_0 is symmetric with respect to the Fermi

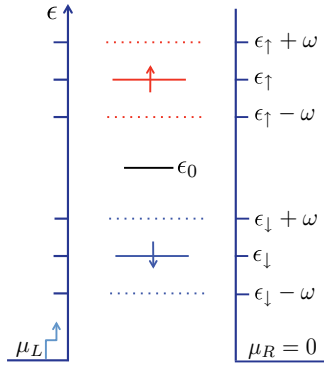


FIG. 2. (Color online) Sketch of the electronic energy levels of the QD in the presence of a time-dependent magnetic field. In a static magnetic field, the electronic level ϵ_0 (solid black line) splits into the Zeeman levels $\epsilon_{\uparrow,\downarrow}$ (solid red and blue lines). If the magnetic field in addition to the static component also includes a time-dependent part with a characteristic frequency ω , additional levels appear at energies $\epsilon_{\uparrow} \pm \omega$ (dotted red lines) and $\epsilon_{\downarrow} \pm \omega$ (dotted blue lines). Hence, there are six channels available for transport.

surfaces of the leads and a peak or step in the spin-current and spin susceptibilities appears at a value of ω , for which an energy level is aligned with one of the lead Fermi surfaces. In Figs. 3(b) and 3(d), the susceptibilities are instead plotted as functions of the bias voltage, eV . Here, each peak or step in the susceptibilities corresponds to a change in the number of available transport channels. The bias voltage is applied in such a way that the energy of the Fermi surface of the right lead is fixed at $\mu_R = 0$ while the energy of the left lead's Fermi surface is varied according to $\mu_L = eV$.

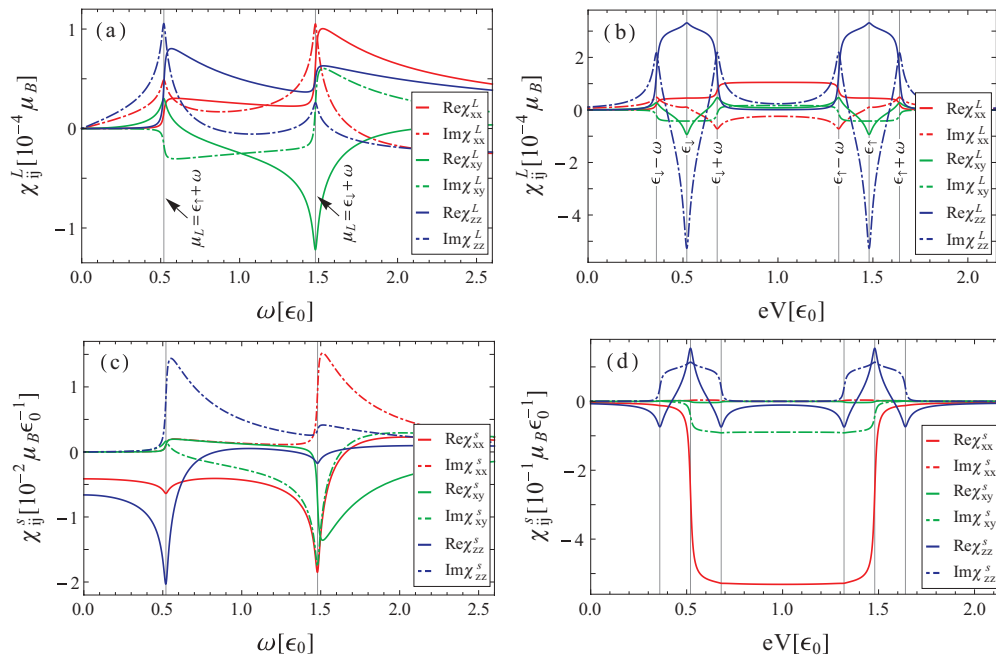


FIG. 3. (Color online) (a) Frequency and (b) bias-voltage dependence of the spin-current susceptibilities. (c) Frequency and (d) bias-voltage dependence of the spin susceptibilities. In (a) and (c), the chemical potential of the left lead is $\mu_L = 2\epsilon_0$, while in (b) and (d) the frequency is set to $\omega = 0.16\epsilon_0$. All plots are obtained at zero temperature with $\vec{B}^c = B^c \vec{e}_z$, and the other parameters set to $\mu_R = 0$, $\epsilon_{\uparrow} = 1.48\epsilon_0$, $\epsilon_{\downarrow} = 0.52\epsilon_0$, $\Gamma = 0.02\epsilon_0$, and $\Gamma_L = \Gamma_R = 0.01\epsilon_0$.

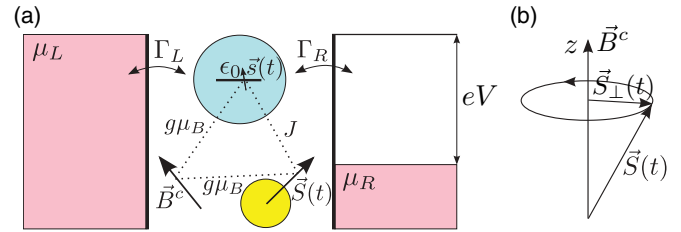


FIG. 4. (Color online) (a) Resonant tunneling in the presence of an SMM and an external, constant magnetic field. The electronic level of Fig. 1 is now coupled with the spin of an SMM via exchange interaction with the coupling constant J . The dynamics of the SMM's spin \vec{S} is controlled by the external magnetic field \vec{B}^c that also affects the electronic level. (b) Precessional motion of the SMM's spin in a constant magnetic field \vec{B}^c applied along the z axis.

III. SPIN-TRANSFER TORQUE AND MOLECULAR SPIN DYNAMICS

A. Model with a precessing molecular spin

Now we apply the formalism of the previous section to the case of resonant tunneling through a QD in the presence of a constant external magnetic field and an SMM [see Fig. 4(a)]. An SMM with a spin S lives in a $(2S + 1)$ -dimensional Hilbert space. We assume that the spin S of the SMM is large and neglecting the quantum fluctuations, one can treat it as a classical vector whose end point moves on a sphere of radius S . In the presence of a constant magnetic field $\vec{B}^c = B^c \vec{e}_z$, the molecular spin precesses around the field axis according to $\vec{S}(t) = S_{\perp} \cos(\omega_L t) \vec{e}_x + S_{\perp} \sin(\omega_L t) \vec{e}_y + S_z \vec{e}_z$, where S_{\perp} is the projection of \vec{S} onto the xy plane, $\omega_L = g\mu_B B^c$ is the Larmor precession frequency, and S_z is the projection of the

spin on the z axis [see Fig. 4(b)]. The spins of the electrons in the electronic level are coupled to the spin of the SMM via the exchange interaction J . The contribution of the external magnetic field and the precessional motion of the SMM's spin create an effective time-dependent magnetic field acting on the electronic level.

The Hamiltonian of the system is now given by $\hat{H}(t) = \hat{H}_{L,R} + \hat{H}_T + \hat{H}_D(t) + \hat{H}_S$, where the Hamiltonians $\hat{H}_{L,R}$ and \hat{H}_T are the same as in Sec. II. The Hamiltonian $\hat{H}_S = g\mu_B \vec{S} \vec{B}^c$ represents the interaction of the molecular spin \vec{S} with the magnetic field \vec{B}^c and consequently does not affect the electronic transport through the junction but instead contributes to the spin dynamics of the SMM. The Hamiltonian of the QD in this case is given by $\hat{H}_D(t) = \hat{H}_D^c + \hat{H}'(t)$. Here, $\hat{H}_D^c = \sum_{\sigma} \epsilon_0 \hat{d}_{\sigma}^{\dagger} \hat{d}_{\sigma} + g\mu_B \hat{s} \vec{B}_{\text{eff}}^c$ is the Hamiltonian of the electrons in the QD in the presence of the constant part of the effective magnetic field, given by $\vec{B}_{\text{eff}}^c = [B^c + \frac{J}{g\mu_B} S_z] \vec{e}_z$. The second term of the QD Hamiltonian, $\hat{H}'(t) = g\mu_B \hat{s} \vec{B}'_{\text{eff}}(t)$, represents the interaction between the electronic spins of the QD, \hat{s} , and the time-dependent part of the effective magnetic field, given by $\vec{B}'_{\text{eff}}(t) = \frac{JS_{\perp}}{g\mu_B} [\cos(\omega_L t) \vec{e}_x + \sin(\omega_L t) \vec{e}_y]$. The time-dependent effective magnetic field can be rewritten as $\vec{B}'_{\text{eff}}(t) = \vec{B}_{\omega_L} e^{-i\omega_L t} + \vec{B}_{\omega_L}^* e^{i\omega_L t}$, where \vec{B}_{ω_L} consists of the complex amplitudes $B_{\omega_L x} = JS_{\perp}/2g\mu_B$, $B_{\omega_L y} = iJS_{\perp}/2g\mu_B$, and $B_{\omega_L z} = 0$. The time-dependent perturbation can then be expressed as $\hat{H}'(t) = \hat{H}_{\omega_L} e^{-i\omega_L t} + \hat{H}_{\omega_L}^{\dagger} e^{i\omega_L t}$, where \hat{H}_{ω_L} is an operator that can be written, using Eq. (3) and the above expressions for $B_{\omega_L i}$, as

$$\hat{H}_{\omega_L} = \frac{JS_{\perp}}{2} \begin{pmatrix} 0 & 1 \\ 0 & 0 \end{pmatrix}. \quad (15)$$

The time-dependent part of the effective magnetic field creates inelastic tunnel processes that contribute to the currents. The in-plane components of the inelastic spin current fulfill

$$\begin{aligned} I_{Lx}(\omega_L) &= -iI_{Ly}(\omega_L) \\ &= \frac{JS_{\perp}}{2g\mu_B} [\chi_{xx}^L(\omega_L) + i\chi_{xy}^L(\omega_L)], \end{aligned} \quad (16)$$

where \vec{B}^c is replaced by \vec{B}_{eff}^c . The z component vanishes to lowest order in $H'(t)$.⁵⁴ Therefore, the inelastic spin current has a polarization that precesses in the xy plane. The inelastic spin-current components, in turn, exert an STT (Refs. 41–44) on the molecular spin given by

$$\vec{T}(t) = \vec{T}_L(t) + \vec{T}_R(t), \quad (17)$$

thus contributing to the dynamics of the molecular spin through

$$\dot{\vec{S}}(t) = g\mu_B \vec{B}^c \times \vec{S}(t) + \vec{T}(t). \quad (18)$$

Using expressions (6), (8), and (15), the torque of Eq. (17) can be calculated in terms of the Green's functions $\hat{G}_0^r(\epsilon)$ and $\hat{G}_0^a(\epsilon)$ as

$$\begin{aligned} T_i(t) &= \frac{JS_{\perp}}{2} \int \frac{d\epsilon}{2\pi} \sum_{\xi\lambda} \frac{\Gamma_{\xi} \Gamma_{\lambda}}{\Gamma} [f_{\xi}(\epsilon + \omega_L) - f_{\lambda}(\epsilon)] \\ &\quad \times \text{Im}\{(\hat{\sigma}_i)_{\downarrow\uparrow} G_{0,\uparrow\uparrow}^r(\epsilon) G_{0,\downarrow\downarrow}^a(\epsilon + \omega_L) e^{-i\omega_L t}\}, \end{aligned} \quad (19)$$

with $\lambda = L, R$. Here $(\hat{\sigma}_i)_{\downarrow\uparrow}$, $G_{0,\uparrow\uparrow}^r(\epsilon)$, and $G_{0,\downarrow\downarrow}^a(\epsilon)$ are matrix elements of $\hat{\sigma}_i$, $\hat{G}_0^r(\epsilon)$ and $\hat{G}_0^a(\epsilon)$ with respect to the basis of eigenstates of \hat{s}_z . This STT can be rewritten in terms of the SMM's spin vector as

$$\vec{T}(t) = \frac{\alpha}{S} \dot{\vec{S}}(t) \times \vec{S}(t) + \beta \dot{\vec{S}}(t) + \gamma \vec{S}(t). \quad (20)$$

The first term in this back-action gives a contribution to the Gilbert damping, characterized by the Gilbert damping coefficient α . The second term acts as an effective constant magnetic field and changes the precession frequency of the spin \vec{S} with the corresponding coefficient β . The third term cancels the z component of the Gilbert damping term, thus restricting the STT to the xy plane. The coefficient of the third term γ is related to α by $\gamma/\alpha = \omega_L S_{\perp}^2 / SS_z$. Expressing the coefficients α and β in terms of the current susceptibilities $\chi_{xx}^{\xi}(\omega_L)$ and $\chi_{xy}^{\xi}(\omega_L)$ results in

$$\alpha = \frac{JS_z}{g\mu_B \omega_L S} \sum_{\xi} [\text{Re}\{\chi_{xx}^{\xi}(\omega_L)\} - \text{Im}\{\chi_{xy}^{\xi}(\omega_L)\}], \quad (21)$$

$$\beta = -\frac{J}{g\mu_B \omega_L} \sum_{\xi} [\text{Im}\{\chi_{xx}^{\xi}(\omega_L)\} + \text{Re}\{\chi_{xy}^{\xi}(\omega_L)\}]. \quad (22)$$

By inserting the explicit expressions for $G_{0,\uparrow\uparrow}^r(\epsilon)$ and $G_{0,\downarrow\downarrow}^a(\epsilon + \omega_L)$, one obtains

$$\begin{aligned} \alpha &= \frac{1}{\omega_L S} \int \frac{d\epsilon}{8\pi} \sum_{\xi\lambda} \Gamma_{\xi} \Gamma_{\lambda} [f_{\xi}(\epsilon + \omega_L) - f_{\lambda}(\epsilon)] \\ &\quad \times \frac{\omega_L^2 - (\epsilon_{\uparrow} - \epsilon_{\downarrow})^2}{\left[\left(\frac{\Gamma}{2}\right)^2 + (\epsilon - \epsilon_{\uparrow})^2\right] \left[\left(\frac{\Gamma}{2}\right)^2 + (\epsilon - \epsilon_{\downarrow} + \omega_L)^2\right]}, \quad (23) \\ \beta &= \frac{J}{\omega_L \Gamma} \int \frac{d\epsilon}{4\pi} \sum_{\xi\lambda} \Gamma_{\xi} \Gamma_{\lambda} [f_{\xi}(\epsilon + \omega_L) - f_{\lambda}(\epsilon)] \\ &\quad \times \frac{\left(\frac{\Gamma}{2}\right)^2 + (\epsilon - \epsilon_{\uparrow})(\epsilon - \epsilon_{\downarrow} + \omega_L)}{\left[\left(\frac{\Gamma}{2}\right)^2 + (\epsilon - \epsilon_{\uparrow})^2\right] \left[\left(\frac{\Gamma}{2}\right)^2 + (\epsilon - \epsilon_{\downarrow} + \omega_L)^2\right]}, \quad (24) \end{aligned}$$

where $\epsilon_{\uparrow,\downarrow} = \epsilon_0 \pm g\mu_B B_{\text{eff}}^c/2 = \epsilon_0 \pm (\omega_L + JS_z)/2$ are the energies of the Zeeman levels in this section. In the small precession frequency regime, $\omega_L \ll k_B T$, $\gamma \rightarrow 0$ and in the limit of $S_z/S \rightarrow 1$ the expression for the coefficient α is in agreement with Ref. 16.

B. Analysis of the spin-transfer torque

In the case of resonant tunneling in the presence of a molecular spin precessing in a constant external magnetic field, one also needs to take the exchange of spin-angular momentum between the molecular spin and the electronic spins into account in addition to the effects of the external magnetic field. Due to the precessional motion of the molecular spin, an electron in the QD absorbing (emitting) an energy ω_L also undergoes a spin flip from spin up (down) to spin down (up), as indicated by the arrows in Fig. 5. As a result, the levels at energies $\epsilon_{\uparrow,\downarrow} \mp \omega_L$ are forbidden and hence do not contribute to the transport processes. Consequently, there are only four transport channels, which are located at energies $\epsilon_{\uparrow,\downarrow} \pm \omega_L$. Also in this case, there are elastic and inelastic tunnel processes. Some of the possible inelastic tunnel processes are shown in Fig. 6. These restrictions on the inelastic tunnel processes are also

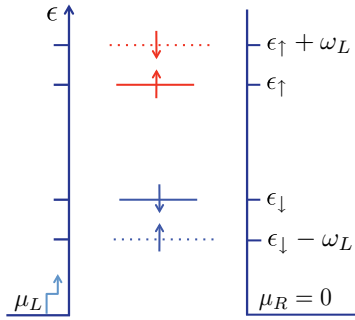


FIG. 5. (Color online) Sketch of the electronic energy levels of the QD in the presence of a molecular spin precessing with the frequency ω_L around an external, constant magnetic field. The corresponding Zeeman levels are $\epsilon_{\uparrow,\downarrow}$. The precessional motion of the molecular spin results in absorption (emission) of energy corresponding to a spin flip from spin up (down) to spin down (up). Hence, there are only four channels available for transport.

visible in Fig. 3(b), which identically corresponds to the case of the presence of a precessing molecular spin with $\omega_L = 0.16\epsilon_0$ and $JS_z = 0.8\epsilon_0$. Namely, from Eq. (16), which is equivalent to $\text{Re}\{I_{Lx}(\omega_L)\} = \text{Im}\{I_{Ly}(\omega_L)\} = \frac{JS_{\perp}}{2g\mu_B} [\text{Re}\{\chi_{xx}^L(\omega_L)\} - \text{Im}\{\chi_{xy}^L(\omega_L)\}]$ and $\text{Im}\{I_{Lx}(\omega_L)\} = -\text{Re}\{I_{Ly}(\omega_L)\} = \frac{JS_{\perp}}{2g\mu_B} [\text{Im}\{\chi_{xx}^L(\omega_L)\} + \text{Re}\{\chi_{xy}^L(\omega_L)\}]$, and from the symmetries of the susceptibilities displayed in Fig. 3(b), it follows that there are no spin currents at $eV = \epsilon_{\uparrow,\downarrow} \mp \omega_L$.

As was mentioned, the spin currents generate an STT acting on the molecular spin. A necessary condition for the existence of an STT, and hence finite values of the coefficients α and β in Eqs. (23) and (24), is that $\vec{I}_L(t) \neq -\vec{I}_R(t)$ [see Eq. (17)]. This condition is met by the spin currents generated, e.g., by the inelastic tunnel processes shown in Figs. 6(b) and 6(c). These tunnel processes occur when an electron can tunnel into the

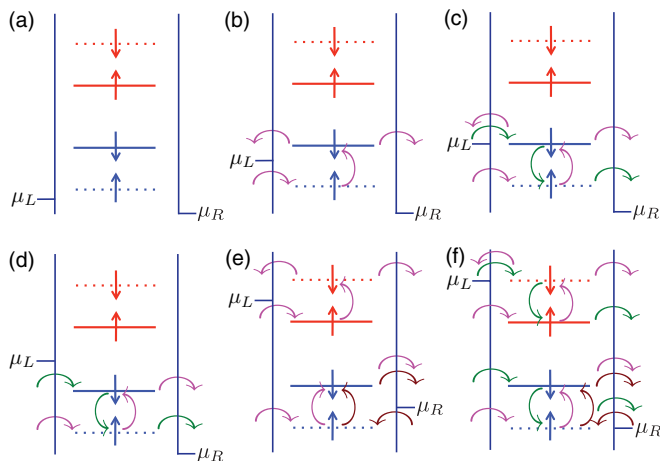


FIG. 6. (Color online) Sketch of the inelastic spin-tunneling processes in the QD in the presence of the precessing molecular spin in the field $\vec{B}^c = B^c \vec{e}_z$ for different positions of the energy levels with respect to the chemical potentials of the leads, μ_L and μ_R . Only transitions between levels with the same color (blue or red) are allowed. Different colored curved arrows (magenta, brown, or green) represent different processes.

QD, undergo a spin flip, and then tunnel off the QD into either lead. From these tunnel processes it is implied that the Gilbert damping coefficient α and the coefficient β can be controlled by the applied bias or gate voltage as well as by the external magnetic field. If a pair of QD energy levels, coupled via spin-flip processes, lie within the bias-voltage window, the spin currents instead fulfill $\vec{I}_L(t) = \vec{I}_R(t)$, leading to a vanishing STT [see Fig. 6(d)]. In Figs. 6(e) and 6(f) the position of the energy levels of the QD are symmetric with respect to the Fermi levels of the leads, μ_L and μ_R . When the QD level with energy $\epsilon_{\uparrow} + \omega_L$ is aligned with μ_L , this simultaneously corresponds to the energy level $\epsilon_{\downarrow} - \omega_L$ being aligned with μ_R [see Fig. 6(f)]. As a result, a spin-down electron can now tunnel from the left lead into the level $\epsilon_{\uparrow} + \omega_L$, while a spin-up electron in the level $\epsilon_{\downarrow} - \omega_L$ can tunnel into the right lead. These additional processes enhance the STT compared to that of the case 6(e).

The two spin-torque coefficients α and β exhibit a non-monotonic dependence on the tunneling rates Γ , as can be seen in Figs. 7–9. For $\Gamma \rightarrow 0$, it is obvious that $\alpha, \beta \rightarrow 0$. In the weak coupling limit $\Gamma \ll \omega_L$, the coefficients α and β are finite if the Fermi surface energy of the lead ξ , μ_{ξ} fulfills either of the conditions

$$\epsilon_{\downarrow} - \omega_L \leq \mu_{\xi} \leq \epsilon_{\downarrow} \quad (25)$$

$$\text{or } \epsilon_{\uparrow} \leq \mu_{\xi} \leq \epsilon_{\uparrow} + \omega_L \quad (26)$$

in such a way that each condition is satisfied by the Fermi energy of maximum one lead. These conditions are relaxed for larger tunnel couplings as a consequence of the broadening of the QD energy levels, which is also responsible for the initial enhancement of α and β with increasing Γ . Notice, however, that α and β are eventually suppressed for $\Gamma \gg \omega_L$, when the QD energy levels are significantly broadened and overlap so that spin-flip processes are equally probable in each direction and there is no net effect on the molecular spin. Physically, this suppression of the STT can be understood by noticing that for $\Gamma \gg \omega_L$ a current-carrying electron perceives the molecular spin as almost static due to its slow precession compared to the electronic tunneling rates and hence the exchange of angular momenta is reduced. With increasing tunneling rates, the coefficient β becomes negative before it drops to zero, causing the torque $\beta \dot{\vec{S}}$ to oppose the rotational motion of the spin \vec{S} .

In Fig. 7, the Gilbert damping coefficient α and the coefficient β are plotted as functions of the applied bias voltage at zero temperature. We analyze the case of the smallest value of Γ (red lines), assuming that $\omega_L > 0$. For small eV , all QD energy levels lie outside the bias-voltage window and there is no spin transport [see Fig. 6(a)]. Hence $\alpha, \beta \rightarrow 0$. At $eV = \epsilon_{\downarrow} - \omega_L$ the tunnel processes in Fig. 6(b) come into play, leading to a finite STT and the coefficient α increases while the coefficient β has a local minimum. In the voltage region specified by Eq. (25) for μ_L , the coefficient α approaches a constant value while the coefficient β increases. By increasing the bias voltage to $eV = \epsilon_{\downarrow}$ the tunnel processes in Fig. 6(c) occur, leading to a decrease of α and a local maximum of β . For $\epsilon_{\downarrow} < eV < \epsilon_{\uparrow}$, the coefficients $\alpha, \beta \rightarrow 0$ [see Fig. 6(d)]. In the voltage region specified by Eq. (26) for μ_L , α approaches the same constant value mentioned above while β decreases

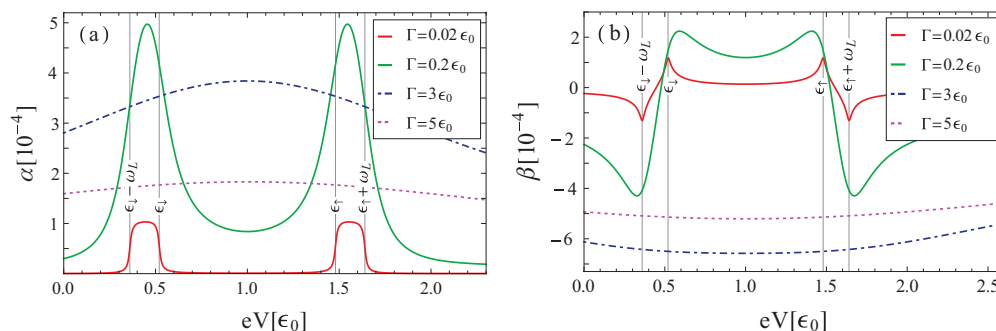


FIG. 7. (Color online) (a) Gilbert damping coefficient α and (b) coefficient β as functions of the applied bias voltage $eV = \mu_L - \mu_R$, with $\mu_R = 0$, for different tunneling rates Γ at zero temperature. Other parameters are $\Gamma_L = \Gamma_R = \Gamma/2$, $\epsilon_\uparrow = 1.48\epsilon_0$, $\epsilon_\downarrow = 0.52\epsilon_0$, $S = 100$, $J = 0.01\epsilon_0$, $JS_z = 0.8\epsilon_0$, and $\omega_L = 0.16\epsilon_0$. In the case of the smallest value of Γ (red lines), α approaches a constant value when μ_L lies within the energy range specified by Eqs. (25) and (26). The coefficient β has one local minimum and one local maximum for the same energy range.

between a local maximum at $eV = \epsilon_\uparrow$ and a local minimum at $eV = \epsilon_\uparrow + \omega_L$, which have the same values as previously mentioned extrema. With further increase of eV , all QD energy levels lie within the bias-voltage window and the STT consequently vanishes.

Figure 8 shows the spin-torque coefficients α and β as functions of the position of the electronic level ϵ_0 . An STT acting on the molecular spin occurs if the electronic level ϵ_0 is positioned in such a way that the inequalities (25) and (26) may be satisfied by some values of eV , ϵ_B , and ω_L . Again, we analyze the case of the smallest value of Γ (red curve). For the particular choice of parameters in Fig. 8, there are four regions in which the inequalities (25) and (26) are satisfied. Within these regions, α approaches a constant value while β has a local maximum as well as a local minimum. These local extrema occur when one of the Fermi surfaces is aligned with one of the energy levels of the QD. For other values of ϵ_0 , both α and β vanish.

The coefficients α and β are plotted as functions of the precession frequency ω_L in Fig. 9. Here, $\epsilon_0 = eV/2$ and therefore the positions of the energy levels of the QD are symmetric with respect to the Fermi levels of the leads, μ_L and μ_R . Once more, we focus first on the case of the smallest value of Γ (indicated by the red curve). The energies of all

four levels of the QD depend on ω_L , i.e., \vec{B}^c . For $\omega_L > 0$, when the magnitude of the external magnetic field is large enough, the tunnel processes in Fig. 6(f) take place due to the above-mentioned symmetries. These tunnel processes lead to a finite STT, a maximum for the Gilbert damping coefficient α , and a negative minimum value for the β coefficient. As ω_L increases, the inequalities of Eqs. (25) and (26) are satisfied and the tunnel processes shown in Fig. 6(e) may occur. Hence, there is a contribution to the STT, but as is shown in Eq. (23), the Gilbert damping decreases with increasing precession frequency. At larger values of ω_L , resulting in $\epsilon_\uparrow = \mu_L$, the Gilbert damping coefficient drops to zero, while the coefficient β has a maximum value. For even larger value of ω_L , the conditions (25) and (26) are no longer fulfilled and both coefficients vanish. It is energetically unfavorable to flip the spin of an electron against the direction of the effective constant magnetic field \vec{B}_{eff}^c . As a consequence, as ω_L increases, more energy is needed to flip the electronic spin to the direction opposite that of the field. This causes α to decrease with increasing ω_L . Additionally, the larger the ratio ω_L/Γ , the less probable it is that spin-angular momentum will be exchanged between the molecular spin and the itinerant electrons. For $\omega_L = 0$, the molecular spin is static, i.e., $\dot{\vec{S}} = 0$. In this case $\vec{T}(t) = \vec{0}$. According to Eq. (23),

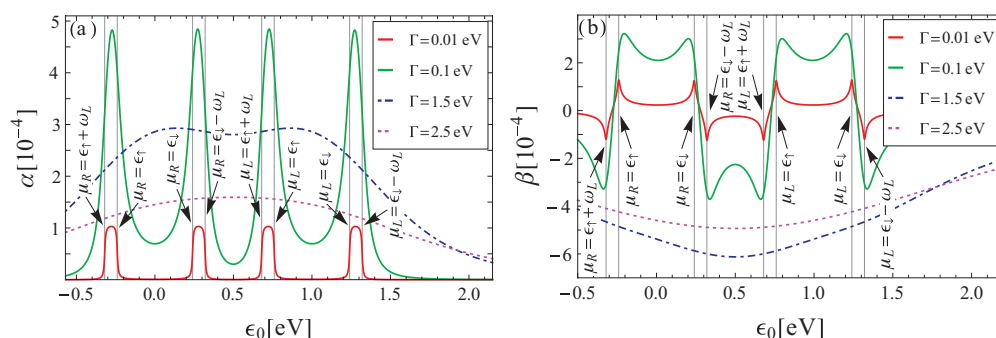


FIG. 8. (Color online) (a) Gilbert damping coefficient α and (b) coefficient β as functions of the position of the electronic level ϵ_0 for different tunneling rates Γ at zero temperature. The applied bias voltage is $eV = \mu_L - \mu_R$, with $\mu_R = 0$. Other parameters are $\Gamma_L = \Gamma_R = \Gamma/2$, $\epsilon_\uparrow - \epsilon_0 = 0.24eV$, $S = 100$, $J = 0.005eV$, $JS_z = 0.4eV$ and $\omega_L = 0.08eV$. In the case of the smallest value of Γ (red lines), there are four regions in which the Gilbert damping and the change of the precession frequency occur. In each of these regions ϵ_0 satisfies the inequalities (25) and (26), and α approaches a constant value, while β has one local maximum and one local minimum.

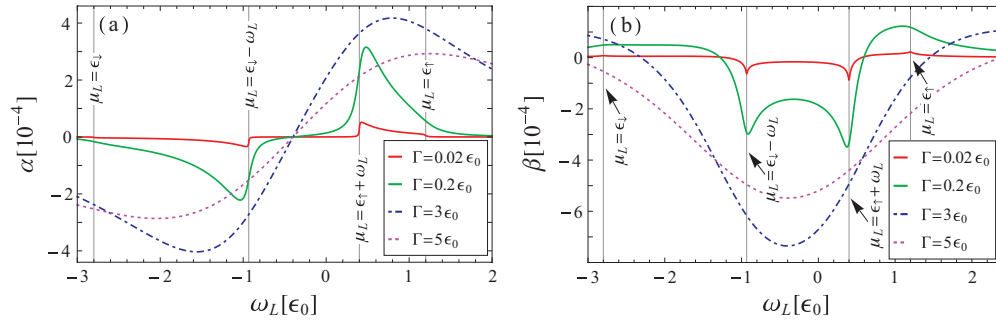


FIG. 9. (Color online) (a) Gilbert damping coefficient α and (b) coefficient β as functions of the precession frequency $\omega_L = g\mu_B B^c$ of the spin \vec{S} of the SMM, with $\vec{B}^c = B^c \hat{e}_z$, for different tunneling rates Γ at zero temperature. The applied bias voltage is $eV = \mu_L - \mu_R = 2\epsilon_0$, with $\mu_R = 0$. The other parameters are the same as in Fig. 7. In the case of the smallest Γ (red lines), the coefficient α is positive for $\epsilon_\uparrow \leq eV \leq \epsilon_\uparrow + \omega_L$, $\omega_L > 0$ and negative for $\epsilon_\downarrow \leq eV \leq \epsilon_\downarrow - \omega_L$, $\omega_L < 0$. The coefficient β has two local maxima and two local minima corresponding to the resonance of μ_L with energy of the levels in the QD.

the coefficient α drops to zero for values $\omega_L = \pm(\epsilon_\uparrow - \epsilon_\downarrow)$, i.e., for values $|\omega_L|$ equal to the Zeeman splitting energy. At $\omega_L = -(\epsilon_\uparrow - \epsilon_\downarrow) = -0.4\epsilon_0$, the level $\epsilon_\downarrow - \omega_L$ is aligned with the Zeeman level ϵ_\uparrow , while the level $\epsilon_\uparrow + \omega_L$ is aligned with the Zeeman level ϵ_\downarrow . Therefore there are only two channels available for electronic transport. At this point, the Gilbert damping vanishes while the coefficient β reaches an extremum value for large values of Γ . With further decrease of ω_L , the relative position of the spin-up levels ϵ_\uparrow and $\epsilon_\downarrow - \omega_L$ is reversed, as well as the relative position of the spin-down levels ϵ_\downarrow and $\epsilon_\uparrow + \omega_L$. In this case, the transfer of spin-angular momenta occurs in such a way that the coefficient α takes negative values and hence the molecular spin \vec{S} becomes unstable. For $\omega_L < 0$ and $\Gamma \ll |\omega_L|$ (red lines), at the value of ω_L for which $\mu_L = \epsilon_\downarrow - \omega_L$, the coefficient α has a negative minimum value while the coefficient β has a negative local minimum. The coefficient α then increases with a further decrease of ω_L as long as $\epsilon_\downarrow \leq \mu_L \leq \epsilon_\downarrow - \omega_L$. At the value of ω_L for which $\mu_L = \epsilon_\downarrow$, α drops to zero while β has a small local maximum. According to Eq. (23), the Gilbert damping also does not occur for $\omega_L = \epsilon_\uparrow - \epsilon_\downarrow$, which is realized if \vec{S} is perpendicular to \vec{B}^c .

IV. CONCLUSIONS

In this paper we have first theoretically studied time-dependent charge and spin transport through a small junction consisting of a single-level quantum dot coupled to two non-interacting metallic leads in the presence of a time-dependent magnetic field. We used the Keldysh nonequilibrium Green's functions method to derive the charge and spin currents in linear order with respect to the time-dependent component of the magnetic field with a characteristic frequency ω .

We then focused on the case of a single electronic level coupled via exchange interaction to an effective magnetic field created by the precessional motion of an SMM's spin in a constant magnetic field. The inelastic tunneling processes that contribute to the spin currents produce an STT that acts on the molecular spin. The STT consists of a Gilbert damping component, characterized by the coefficient α , as well as a component, characterized by the coefficient β , that acts as an additional effective constant magnetic field and changes the precession frequency ω_L of the molecular spin. Both α and β depend on ω_L and show a nonmonotonic dependence on the tunneling rates Γ . In the weak coupling limit $\Gamma \ll \omega_L$, α can be switched on and off as a function of bias and gate voltages. The coefficient β correspondingly has a local extremum. For $\Gamma \rightarrow 0$, both α and β vanish. Taking into account that spin transport can be controlled by the bias and gate voltages, as well as by external magnetic fields, our results might be useful in spintronic applications using SMMs. Besides a spin-polarized STM, it may be possible to detect and manipulate the spin state of an SMM in a ferromagnetic resonance experiment^{56–59} and thus extract information about the effects of the current-induced STT on the SMM. Our study could be complemented with a quantum description of an SMM in a single-molecule magnet junction and its coherent properties, as these render the SMM suitable for quantum information storage.

ACKNOWLEDGMENTS

We gratefully acknowledge discussions with Mihajlo Vanević and Christian Wickles. This work was supported by Deutsche Forschungsgemeinschaft through SFB 767. We are thankful for partial financial support by an ERC Advanced Grant, project *UltraPhase* of Alfred Leitenstorfer.

¹G. Christou, D. Gatteschi, D. Hendrickson, and R. Sessoli, *MRS Bull.* **25**, 66 (2000).

²W. Wernsdorfer and R. Sessoli, *Science* **284**, 133 (1999).

³J. R. Friedman, M. P. Sarachik, J. Tejada, and R. Ziolo, *Phys. Rev. Lett.* **76**, 3830 (1996); L. Thomas, F. Lioni, R. Ballou,

D. Gatteschi, R. Sessoli, and B. Barbara, *Nature (London)* **383**, 145 (1996); C. Sangregorio, T. Ohm, C. Paulsen, R. Sessoli, and D. Gatteschi, *Phys. Rev. Lett.* **78**, 4645 (1997); W. Wernsdorfer, M. Murugesu, and G. Christou, *ibid.* **96**, 057208 (2006).

- ⁴A. Ardavan, O. Rival, J. J. L. Morton, S. J. Blundell, A. M. Tyryshkin, G. A. Timco, and R. E. P. Winpenny, *Phys. Rev. Lett.* **98**, 057201 (2007); S. Carretta, P. Santini, G. Amoretti, T. Guidi, J. R. D. Copley, Y. Qiu, R. Caciuffo, G. A. Timco, and R. E. P. Winpenny, *ibid.* **98**, 167401 (2007); S. Bertaina, S. Gambarelli, T. Mitra, B. Tsukerblat, A. Muller, and B. Barbara, *Nature (London)* **453**, 203 (2008).
- ⁵A. Garg, *Europhys. Lett.* **22**, 205 (1993); W. Wernsdorfer, N. E. Chakov, and G. Christou, *Phys. Rev. Lett.* **95**, 037203 (2005).
- ⁶R. Sessoli, D. Gatteschi, A. Caneschi, and M. A. Novak, *Nature (London)* **365**, 141 (1993).
- ⁷D. Gatteschi, R. Sessoli, and J. Villain, *Molecular Nanomagnets* (Oxford University Press, New York, 2006).
- ⁸C. Timm and M. Di Ventura, *Phys. Rev. B* **86**, 104427 (2012).
- ⁹D. D. Awschalom, M. E. Flatte, and N. Samarth, *Spintronics* (Scientific American, New York, 2002), pp. 67–73.
- ¹⁰D. D. Awschalom, D. Loss, and N. Samarth, *Semiconductor Spintronics and Quantum Computation* (Springer, Berlin, 2002).
- ¹¹L. Bogani and W. Wernsdorfer, *Nature Mater.* **7**, 189 (2008).
- ¹²G.-H. Kim and T.-S. Kim, *Phys. Rev. Lett.* **92**, 137203 (2004).
- ¹³M. N. Leuenberger and E. R. Mucciolo, *Phys. Rev. Lett.* **97**, 126601 (2006).
- ¹⁴C. Romeike, M. R. Wegewijs, W. Hofstetter, and H. Schoeller, *Phys. Rev. Lett.* **96**, 196601 (2006); **97**, 206601 (2006).
- ¹⁵S. Teber, C. Holmqvist, and M. Fogelström, *Phys. Rev. B* **81**, 174503 (2010); C. Holmqvist, S. Teber, and M. Fogelström, *ibid.* **83**, 104521 (2011); C. Holmqvist, W. Belzig, and M. Fogelström, *ibid.* **86**, 054519 (2012).
- ¹⁶N. Bode, L. Arrachea, G. S. Lozano, T. S. Nunner, and F. von Oppen, *Phys. Rev. B* **85**, 115440 (2012).
- ¹⁷J.-X. Zhu, Z. Nussinov, A. Shnirman, and A. V. Balatsky, *Phys. Rev. Lett.* **92**, 107001 (2004); Z. Nussinov, A. Shnirman, D. P. Arovas, A. V. Balatsky, and J.-X. Zhu, *Phys. Rev. B* **71**, 214520 (2005); J. Michelsen, V. S. Shumeiko, and G. Wendin, *ibid.* **77**, 184506 (2008).
- ¹⁸K. Mosshammer, G. Kiesslich, and T. Brandes, *Phys. Rev. B* **86**, 165447 (2012).
- ¹⁹C. Timm, *Phys. Rev. B* **76**, 014421 (2007).
- ²⁰C. Timm and F. Elste, *Phys. Rev. B* **73**, 235304 (2006).
- ²¹F. Elste and C. Timm, *Phys. Rev. B* **73**, 235305 (2006).
- ²²H. B. Heersche, Z. de Groot, J. A. Folk, H. S. J. van der Zant, C. Romeike, M. R. Wegewijs, L. Zobbi, D. Barreca, E. Tondello, and A. Cornia, *Phys. Rev. Lett.* **96**, 206801 (2006).
- ²³M.-H. Jo, J. E. Grose, K. Baheti, M. M. Deshmukh, J. J. Sokol, E. M. Rumberger, D. N. Hendrickson, J. R. Long, H. Park, and D. C. Ralph, *Nano Lett.* **6**, 2014 (2006).
- ²⁴M. N. Leuenberger and D. Loss, *Nature (London)* **410**, 789 (2001).
- ²⁵S. Voss, M. Fonin, U. Rüdiger, M. Burgert, and U. Groth, *Appl. Phys. Lett.* **90**, 133104 (2007).
- ²⁶B. Y. Choi, S. J. Kahng, S. Kim, H. Kim, H. W. Kim, Y. J. Song, J. Ihm, and Y. Kuk, *Phys. Rev. Lett.* **96**, 156106 (2006); E. Lörtscher, J. W. Ciszek, J. Tour, and H. Riel, *Small* **2**, 973 (2006); C. Benesch, M. F. Rode, M. Cizek, R. Härtle, O. Rubio-Pons, M. Thoss, and A. L. Sobolewski, *J. Phys. Chem. C* **113**, 10315 (2009).
- ²⁷A. S. Zyazin, J. W. G. van den Berg, E. A. Osorio, H. S. J. van der Zant, N. P. Konstantinidis, M. Leijnse, M. R. Wegewijs, F. May, W. Hofstetter, C. Danieli, and A. Cornia, *Nano Lett.* **10**, 3307 (2010).
- ²⁸N. Roch, R. Vincent, F. Elste, W. Harneit, W. Wernsdorfer, C. Timm, and F. Balestro, *Phys. Rev. B* **83**, 081407(R) (2011).
- ²⁹S. Kahle, Z. Deng, N. Malinowski, C. Tonnoir, A. Forment-Aliaga, N. Thontasen, G. Rinke, D. Le, V. Turkowski, T. S. Rahman, S. Rauschenbach, M. Ternes, and K. Kern, *Nano Lett.* **12**, 518 (2012).
- ³⁰C. Hirjibehedin, C.-Y. Lin, A. Otte, M. Ternes, C. P. Lutz, B. A. Jones, and A. J. Heinrich, *Science* **317**, 1199 (2007).
- ³¹L. Zhou, J. Wiebe, S. Lounis, E. Vedmedenko, F. Meier, S. Blügel, P. H. Dederichs, and R. Wiesendanger, *Nat. Phys.* **6**, 187 (2010).
- ³²M. A. Reed, C. Zhou, C. J. Muller, T. P. Burgin, and J. M. Tour, *Science* **278**, 252 (1997); R. Smit, Y. Noat, C. Untiedt, N. Lang, M. van Hemert, and J. van Ruitenbeek, *Nature (London)* **419**, 906 (2002); C. A. Martin, J. M. van Ruitenbeek, and H. S. J. van de Zandt, *Nanotechnology* **21**, 265201 (2010).
- ³³A. F. Otte, M. Ternes, K. von Bergmann, S. Loth, H. Brune, C. P. Lutz, C. F. Hirjibehedin, and A. J. Heinrich, *Nat. Phys.* **4**, 847 (2008).
- ³⁴J. Parks, A. Champagne, T. Costi, W. Shum, A. Pasupathy, E. Neuscamman, S. Flores-Torres, P. Cornaglia, A. Aligia, C. Balseiro, G.-L. Chan, H. Abrunña, and D. Ralph, *Science* **328**, 1370 (2010).
- ³⁵F. Delgado, J. J. Palacios, and J. Fernández-Rossier, *Phys. Rev. Lett.* **104**, 026601 (2010).
- ³⁶S. Loth, K. von Bergmann, M. Ternes, A. F. Otte, C. P. Lutz, and A. J. Heinrich, *Nat. Phys.* **6**, 340 (2010).
- ³⁷L. Landau and E. M. Lifshitz, *Phys. Z. Sowjetunion* **8**, 153 (1935).
- ³⁸T. L. Gilbert, *Phys. Rev.* **100**, 1243 (1955); T. Gilbert, *IEEE Trans. Magn.* **40**, 3443 (2004).
- ³⁹J. Fransson, *Phys. Rev. B* **77**, 205316 (2008).
- ⁴⁰C. López-Monís, C. Emary, G. Kiesslich, G. Platero, and T. Brandes, *Phys. Rev. B* **85**, 045301 (2012).
- ⁴¹J. C. Slonczewski, *J. Magn. Magn. Mater.* **159**, L1 (1996).
- ⁴²L. Berger, *Phys. Rev. B* **54**, 9353 (1996).
- ⁴³Y. Tserkovnyak, A. Brataas, G. E. W. Bauer, and B. I. Halperin, *Rev. Mod. Phys.* **77**, 1375 (2005).
- ⁴⁴D. C. Ralph and M. D. Stiles, *J. Magn. Magn. Mater.* **320**, 1190 (2008).
- ⁴⁵J. C. Slonczewski, *Phys. Rev. B* **71**, 024411 (2005); J. Xiao, G. E. W. Bauer, and A. Brataas, *ibid.* **77**, 224419 (2008).
- ⁴⁶J. C. Sankey, Y.-T. Cui, J. Z. Sun, J. C. Slonczewski, R. A. Buhrman, and D. C. Ralph, *Nat. Phys.* **4**, 67 (2008).
- ⁴⁷A. L. Chudnovskiy, J. Swiebodzinski, and A. Kamenev, *Phys. Rev. Lett.* **101**, 066601 (2008).
- ⁴⁸S. Krause, G. Berbil-Bautista, G. Herzog, M. Bode, and R. Wiesendanger, *Science* **317**, 1537 (2007); S. Krause, G. Herzog, A. Schlenhoff, A. Sonntag, and R. Wiesendanger, *Phys. Rev. Lett.* **107**, 186601 (2011).
- ⁴⁹N. S. Wingreen, A.-P. Jauho, and Y. Meir, *Phys. Rev. B* **48**, 8487 (1993).
- ⁵⁰A.-P. Jauho, N. S. Wingreen, and Y. Meir, *Phys. Rev. B* **50**, 5528 (1994).
- ⁵¹A.-P. Jauho and H. Haug, *Quantum Kinetics in Transport and Optics of Semiconductors* (Springer, Berlin, 1998).
- ⁵²H. Bruus and K. Flensberg, *Many-Body Quantum Theory in Condensed Matter Physics* (Oxford University Press, Oxford, UK, 2004).
- ⁵³L. D. Landau and E. M. Lifshitz, *Statistical Physics, Part I*, Course of Theoretical Physics Vol. 5 (Pergamon Press, Oxford, 1980).
- ⁵⁴However, z -polarized dc spin currents appear in second-order approximations.⁵⁵

- ⁵⁵B. Wang, J. Wang, and H. Guo, *Phys. Rev. B* **67**, 092408 (2003).
- ⁵⁶M. V. Costache, M. Sladkov, S. M. Watts, C. H. van der Wal, and B. J. van Wees, *Phys. Rev. Lett.* **97**, 216603 (2006).
- ⁵⁷C. Bell, S. Milikisyants, M. Huber, and J. Aarts, *Phys. Rev. Lett.* **100**, 047002 (2008).
- ⁵⁸M. Harder, Z. X. Cao, Y. S. Gui, X. L. Fan, and C.-M. Hu, *Phys. Rev. B* **84**, 054423 (2011).
- ⁵⁹K. Ando, S. Takahashi, J. Ieda, H. Kurebayashi, T. Trypiniotis, C. H. W. Barnes, S. Maekawa, and E. Saitoh, *Nature Mater.* **10**, 655 (2011).

Erratum: Spin transport and tunable Gilbert damping in a single-molecule magnet junction [Phys. Rev. B **87**, 045426 (2013)]

Milena Filipović, Cecilia Holmqvist, Federica Haupt, and Wolfgang Belzig
(Received 22 July 2013; published 5 September 2013)

DOI: [10.1103/PhysRevB.88.119901](https://doi.org/10.1103/PhysRevB.88.119901) PACS number(s): 73.23.-b, 75.76.+j, 85.65.+h, 85.75.-d, 99.10.Cd

In this Erratum, we correct errors in the original paper which were mainly due to inconsistencies in the definitions of Fourier transformations. These changes do not affect our conclusions. For the correct version, please see the revised paper.

In the original paper, we assume spin-independent tunneling so that, in Sec. II, p. 2, the correct tunnel matrix element in \hat{H}_T should read $V_{k\xi}$. In the fourth line after Eq. (2), “ r ” should be added in the superscript of the self-energies, which are diagonal matrices in the electronic spin space with respect to the basis of eigenstates of \hat{S}_z , and their correct matrix elements should be $\Sigma_L^{r,a,<}(t,t') = \sum_k V_{kL} g_{kL}^{r,a,<}(t,t') V_{kL}^*$. The correct forms of Eqs. (5), (17), (19), (21), and (24) should be multiplied by -1 . The difference $f_L(\epsilon + \omega) - f_\xi(\epsilon)$ should be replaced by $f_\xi(\epsilon - \omega) - f_L(\epsilon)$ in Eq. (8). The correct form of Eq. (22) should contain a factor $+$ instead of the factor $-$ on the right-hand side. The multiplicative factor in Eq. (23) $\omega_L^2 - (\epsilon_\uparrow - \epsilon_\downarrow)^2$ should be replaced with $J^2 S_z^2$. Additionally, in the correct form of Eqs. (8) and (10), $\epsilon + \omega$ should be replaced with $\epsilon - \omega$ and vice versa, and in Eqs. (19), (23), and (24), $\epsilon + \omega_L$ should be replaced with $\epsilon - \omega_L$. The correct expressions of Eqs. (5), (8), (10), (17), (19), and (21)–(24) should read

$$I_{L\nu}(t) = -\frac{2q_\nu}{\hbar} \text{Re Tr} \{ \hat{\sigma}_\nu [\hat{G}_0^r \hat{\Sigma}_L^< + \hat{G}_0^< \hat{\Sigma}_L^a + \hat{G}_0^r \hat{H}' \hat{G}_0^r \hat{\Sigma}_L^< + \hat{G}_0^r \hat{H}' \hat{G}_0^< \hat{\Sigma}_L^a + \hat{G}_0^< \hat{H}' \hat{G}_0^a \hat{\Sigma}_L^a] \}, \quad (5)$$

$$I_{L\nu}(\omega) = -iq_\nu \int \frac{d\epsilon}{2\pi} \frac{\Gamma_L \Gamma_R}{\Gamma} \left\{ [f_L(\epsilon) - f_R(\epsilon)] \text{Tr} \{ \hat{\sigma}_\nu [\hat{G}_0^r(\epsilon + \omega) \hat{H}_\omega \hat{G}_0^r(\epsilon) + 2i \text{Im} \{ \hat{G}_0^r(\epsilon) \} \hat{H}_\omega \hat{G}_0^a(\epsilon - \omega)] \} \right. \\ \left. + \sum_{\xi=L,R} \frac{\Gamma_\xi}{\Gamma_R} [f_\xi(\epsilon - \omega) - f_L(\epsilon)] \text{Tr} \{ \hat{\sigma}_\nu \hat{G}_0^r(\epsilon) \hat{H}_\omega \hat{G}_0^a(\epsilon - \omega) \} \right\}, \quad (8)$$

$$\chi_{\nu j}^L(\omega) = -iq_\nu g \mu_B \int \frac{d\epsilon}{4\pi} \frac{\Gamma_L \Gamma_R}{\Gamma} \left\{ [f_L(\epsilon) - f_R(\epsilon)] \text{Tr} \{ \hat{\sigma}_\nu [\hat{G}_0^r(\epsilon + \omega) \hat{\sigma}_j \hat{G}_0^r(\epsilon) + 2i \text{Im} \{ \hat{G}_0^r(\epsilon) \} \hat{\sigma}_j \hat{G}_0^a(\epsilon - \omega)] \} \right. \\ \left. + \sum_{\xi} \frac{\Gamma_\xi}{\Gamma_R} [f_\xi(\epsilon - \omega) - f_L(\epsilon)] \text{Tr} \{ \hat{\sigma}_\nu \hat{G}_0^r(\epsilon) \hat{\sigma}_j \hat{G}_0^a(\epsilon - \omega) \} \right\}, \quad (10)$$

$$\vec{T}(t) = -[\vec{I}_L(t) + \vec{I}_R(t)], \quad (17)$$

$$T_i(t) = -\frac{JS_\perp}{2} \int \frac{d\epsilon}{2\pi} \sum_{\xi\lambda} \frac{\Gamma_\xi \Gamma_\lambda}{\Gamma} [f_\xi(\epsilon - \omega_L) - f_\lambda(\epsilon)] \text{Im} \{ (\hat{\sigma}_i)_{\uparrow\downarrow} G_{0,\uparrow}^r(\epsilon) G_{0,\downarrow}^a(\epsilon - \omega_L) e^{-i\omega t} \}, \quad (19)$$

$$\alpha = -\frac{JS_z}{g\mu_B \omega_L S} \sum_{\xi} [\text{Re} \{ \chi_{xx}^\xi(\omega_L) \} - \text{Im} \{ \chi_{xy}^\xi(\omega_L) \}], \quad (21)$$

$$\beta = \frac{J}{g\mu_B \omega_L} \sum_{\xi} [\text{Im} \{ \chi_{xx}^\xi(\omega_L) \} + \text{Re} \{ \chi_{xy}^\xi(\omega_L) \}], \quad (22)$$

$$\alpha = \frac{1}{\omega_L S} \int \frac{d\epsilon}{8\pi} \sum_{\xi\lambda} \Gamma_\xi \Gamma_\lambda [f_\xi(\epsilon - \omega_L) - f_\lambda(\epsilon)] \frac{J^2 S_z^2}{\left[\left(\frac{\Gamma}{2} \right)^2 + (\epsilon - \epsilon_\uparrow)^2 \right] \left[\left(\frac{\Gamma}{2} \right)^2 + (\epsilon - \epsilon_\downarrow - \omega_L)^2 \right]}, \quad (23)$$

$$\beta = -\frac{J}{\omega_L \Gamma} \int \frac{d\epsilon}{4\pi} \sum_{\xi\lambda} \Gamma_\xi \Gamma_\lambda [f_\xi(\epsilon - \omega_L) - f_\lambda(\epsilon)] \frac{\left(\frac{\Gamma}{2} \right)^2 + (\epsilon - \epsilon_\uparrow)(\epsilon - \epsilon_\downarrow - \omega_L)}{\left[\left(\frac{\Gamma}{2} \right)^2 + (\epsilon - \epsilon_\uparrow)^2 \right] \left[\left(\frac{\Gamma}{2} \right)^2 + (\epsilon - \epsilon_\downarrow - \omega_L)^2 \right]}. \quad (24)$$

As a consequence of these changes, the energy levels of the quantum dot (QD) in the presence of a precessing molecular spin should be changed to ϵ_\uparrow , $\epsilon_\uparrow - \omega_L$, $\epsilon_\downarrow + \omega_L$, and ϵ_\downarrow . Figures 3 and 5–9 should be replaced with the correct figures given in this Erratum (and in the revised paper). The magnitude scale of the spin-current susceptibilities should be corrected as $10^{-3} \mu_B$ in Fig. 3(a) and $10^{-2} \mu_B$ in Fig. 3(b). In the line before Eq. (16), p. 5, “inelastic” should be removed, and in the line before Eq. (23), $G_{0,\downarrow}^a(\epsilon + \omega_L)$ should be corrected as $G_{0,\downarrow}^a(\epsilon - \omega_L)$.

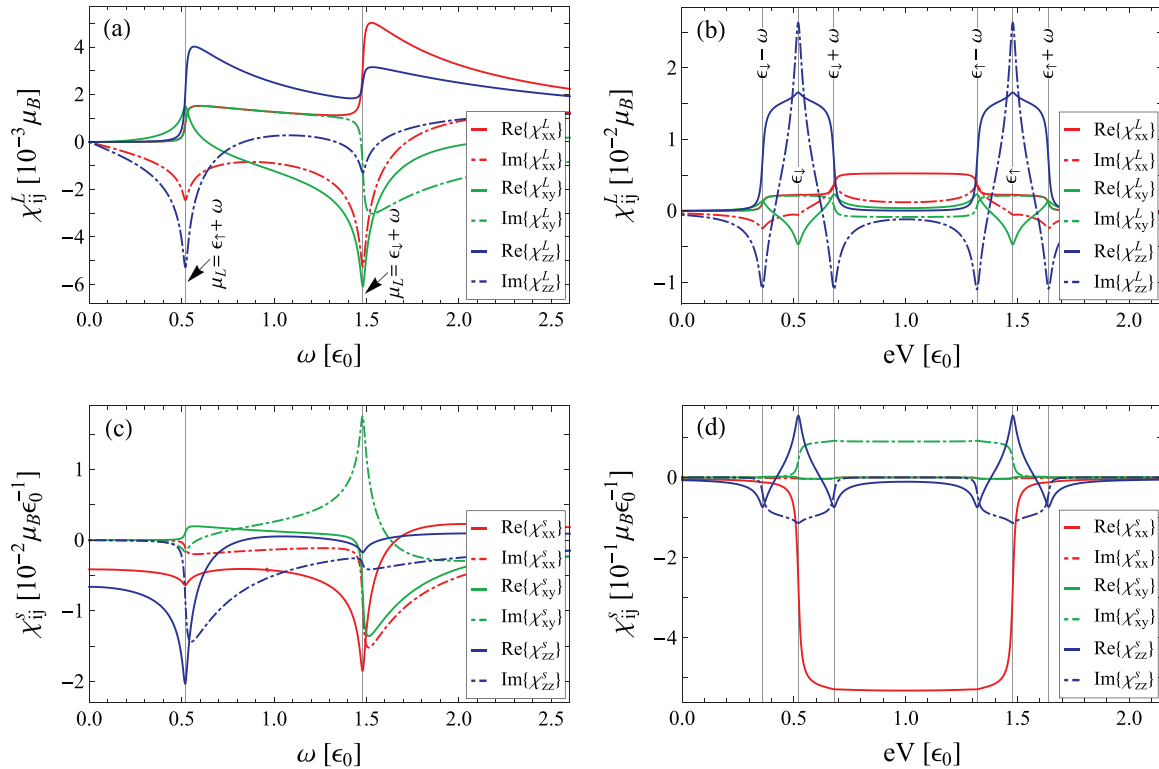


FIG. 3. (Color online) (a) Frequency and (b) bias-voltage dependence of the spin-current susceptibilities. (c) Frequency and (d) bias-voltage dependence of the spin susceptibilities. In (a) and (c), the chemical potential of the left lead is $\mu_L = 2\epsilon_0$, whereas, in (b) and (d), the frequency is set to $\omega = 0.16\epsilon_0$. All plots are obtained at zero temperature with $\vec{B}^c = B^c \vec{e}_z$ and the other parameters set to $\mu_R = 0$, $\epsilon_\uparrow = 1.48\epsilon_0$, $\epsilon_\downarrow = 0.52\epsilon_0$, $\Gamma = 0.02\epsilon_0$, and $\Gamma_L = \Gamma_R = 0.01\epsilon_0$.

In the first paragraph of Sec. III B, in the second sentence, “absorbing (emitting)” should be replaced with “emitting (absorbing).” In the same paragraph, $\epsilon_{\uparrow,\downarrow} \pm \omega_L$ should be replaced with $\epsilon_{\uparrow,\downarrow} \mp \omega_L$, and vice versa. In the caption for Fig. 5, “absorption (emission)” should be replaced with “emission (absorption).” In the remaining part of the same subsection, except in the last paragraph that we separately analyze, $\epsilon_\uparrow + \omega_L$ should be replaced with ϵ_\uparrow , ϵ_\uparrow should be replaced with $\epsilon_\uparrow - \omega_L$, ϵ_\downarrow should be replaced with $\epsilon_\downarrow + \omega_L$, and $\epsilon_\downarrow - \omega_L$ should be replaced with ϵ_\downarrow . Therefore, the correct expressions for Eqs. (25) and (26) read

$$\epsilon_\downarrow \leq \mu_\xi \leq \epsilon_\downarrow + \omega_L, \tag{25}$$

or

$$\epsilon_\uparrow - \omega_L \leq \mu_\xi \leq \epsilon_\uparrow, \tag{26}$$

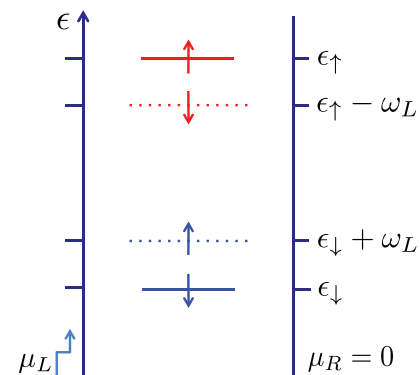


FIG. 5. (Color online) Sketch of the electronic energy levels of the QD in the presence of a molecular spin precessing with the frequency ω_L around an external constant magnetic field. The corresponding Zeeman levels are $\epsilon_{\uparrow,\downarrow}$. The precessional motion of the molecular spin results in emission (absorption) of energy corresponding to a spin flip from spin up (down) to spin down (up). Hence, there are only four channels available for transport.

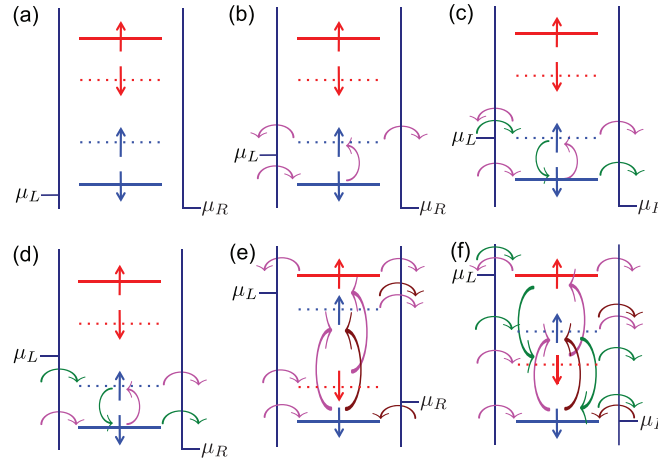


FIG. 6. (Color online) Sketch of the inelastic spin-tunneling processes in the QD in the presence of the precessing molecular spin in the field $\vec{B}^c = B^c \vec{e}_z$ for different positions of the energy levels with respect to the chemical potentials of the leads μ_L and μ_R . Only transitions between levels with the same color (blue or red) are allowed. Different colored curved arrows (magenta, brown, or green) represent different processes.

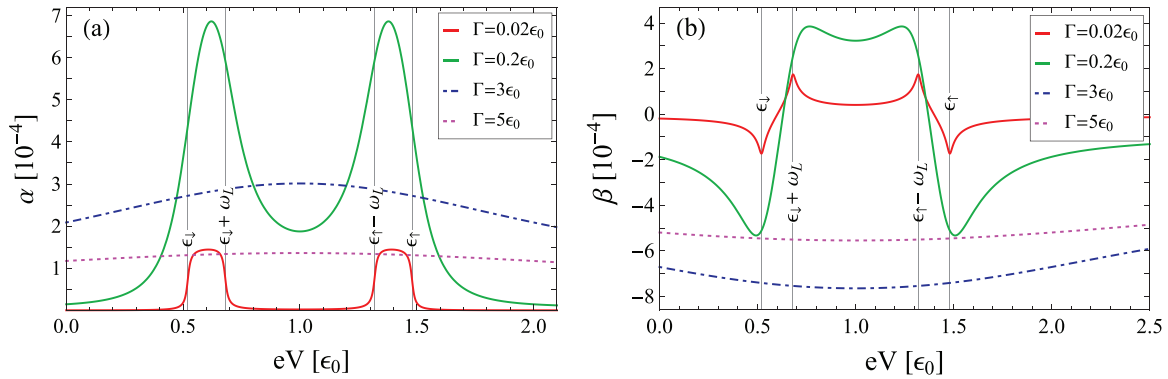


FIG. 7. (Color online) (a) Gilbert damping coefficient α and (b) coefficient β as functions of the applied bias voltage $eV = \mu_L - \mu_R$ with $\mu_R = 0$ for different tunneling rates Γ at zero temperature. Other parameters are $\Gamma_L = \Gamma_R = \Gamma/2$, $\epsilon_\uparrow = 1.48\epsilon_0$, $\epsilon_\downarrow = 0.52\epsilon_0$, $S = 100$, $J = 0.01\epsilon_0$, $JS_z = 0.8\epsilon_0$, and $\omega_L = 0.16\epsilon_0$. In the case of the smallest value of Γ (red lines), α approaches a constant value when μ_L lies within the energy range specified by Eqs. (25) and (26). The coefficient β has one local minimum and one local maximum for the same energy range.

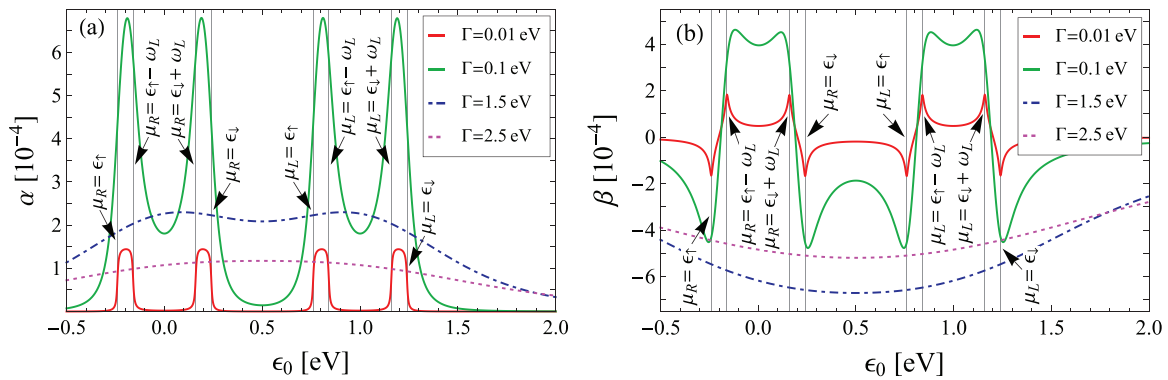


FIG. 8. (Color online) (a) Gilbert damping coefficient α and (b) coefficient β as functions of the position of the electronic level ϵ_0 for different tunneling rates Γ at zero temperature. The applied bias voltage is $eV = \mu_L - \mu_R$ with $\mu_R = 0$. Other parameters are $\Gamma_L = \Gamma_R = \Gamma/2$, $\epsilon_\uparrow - \epsilon_0 = 0.24$ eV, $S = 100$, $J = 0.005$ eV, $JS_z = 0.4$ eV, and $\omega_L = 0.08$ eV. In the case of the smallest value of Γ (red lines), there are four regions in which the Gilbert damping and the change in the precession frequency occur. In each of these regions, ϵ_0 satisfies the inequalities (25) and (26), and α approaches a constant value, whereas, β has one local maximum and one local minimum.

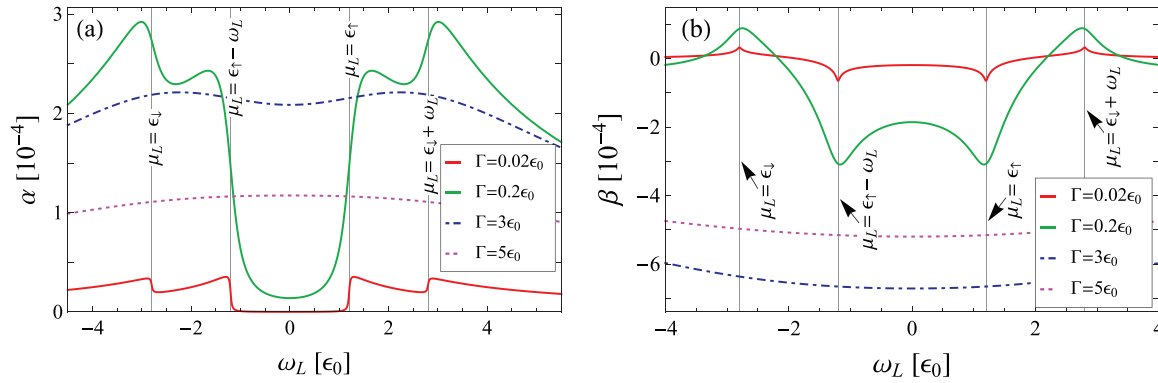


FIG. 9. (Color online) (a) Gilbert damping coefficient α and (b) coefficient β as functions of the precession frequency $\omega_L = g\mu_B B^c$ of the spin \vec{S} of the single-molecule magnet with $\vec{B}^c = B^c \vec{e}_z$ for different tunneling rates Γ at zero temperature. The applied bias voltage is $eV = \mu_L - \mu_R = 2\epsilon_0$ with $\mu_R = 0$. The other parameters are the same as in Fig. 7. In the case of the smallest Γ (red lines), the coefficient α has a step increase towards a local maximum, whereas, the coefficient β has a local maximum or minimum at a value of ω_L corresponding to a resonance of μ_L with one of the levels in the QD.

giving the conditions for the spin-transfer torque (STT) to occur. Also, in the second paragraph of this subsection, in the sentence before last, “spin-down” should be replaced with “spin-up” and vice versa.

In the paragraph before last in Sec. III, there is a typographical error in the second sentence, and ϵ_B should be replaced with ϵ_0 .

The last part of Sec. III, beginning with “At larger values of ω_L , resulting in,” p. 7, should be replaced with “At larger values of ω_L , resulting in $\epsilon_\downarrow + \omega_L = \mu_L$, the Gilbert damping coefficient has a step increase towards a local maximum, whereas, the coefficient β has a local maximum as a consequence of the enhancement of the STT due to additional spin-flip processes occurring in this case. For even larger values of ω_L , the conditions (25) and (26) are no longer fulfilled, and both coefficients vanish. It is energetically unfavorable to flip the spin of an electron against the antiparallel direction of the effective constant magnetic field \vec{B}_{eff}^c . Hence, as ω_L increases, more energy is needed to flip the electronic spin to the direction of the field. This causes α to decrease with increasing ω_L . Additionally, the larger the ratio ω_L/Γ , the less probable it is that spin-angular momentum will be exchanged between the molecular spin and the itinerant electrons. For $\omega_L = 0$, the molecular spin is static, i.e., $\dot{\vec{S}} = 0$. In this case, $\vec{T}(t) = \vec{0}$. The coefficient α then drops to zero, whereas, the coefficient β reaches a negative local maximum which is close to 0. Both α and β reach an extremum value for large values of Γ at this point. For $\omega_L < 0$ and $\Gamma \ll |\omega_L|$ (red lines), at the value of ω_L for which $\mu_L = \epsilon_\uparrow - \omega_L$, the coefficient α has a step increase towards a local maximum, whereas, the coefficient β has a negative local minimum. The coefficient α then decreases with a further decrease in ω_L as long as $\epsilon_\downarrow \leq \mu_L \leq \epsilon_\uparrow - \omega_L$. At the value of ω_L for which $\mu_L = \epsilon_\downarrow$, α has another step increase towards a local maximum, whereas, β has a maximum value. According to Eq. (23), the Gilbert damping also does not occur if \vec{S} is perpendicular to \vec{B}^c . In this case, $\beta \lesssim 0$, and the only nonzero torque component $\beta \dot{\vec{S}}(t)$ acts in the opposite direction than the molecular spin’s rotational motion. In the caption for Fig. 9, the two last sentences should be replaced with the one given in this Erratum.

Photon-assisted electronic and spin transport in a junction containing precessing molecular spin

Milena Filipović and Wolfgang Belzig

Fachbereich Physik, Universität Konstanz, D-78457 Konstanz, Germany

(Received 12 December 2014; published 1 February 2016)

We study the ac charge and -spin transport through an orbital of a magnetic molecule with spin precessing in a constant magnetic field. We assume that the source and drain contacts have time-dependent chemical potentials. We employ the Keldysh nonequilibrium Green's functions method to calculate the spin and charge currents to linear order in the time-dependent potentials. The molecular and electronic spins are coupled via exchange interaction. The time-dependent molecular spin drives inelastic transitions between the molecular quasienergy levels, resulting in a rich structure in the transport characteristics. The time-dependent voltages allow us to reveal the internal precession time scale (the Larmor frequency) by a dc conductance measurement if the ac frequency matches the Larmor frequency. In the low-ac-frequency limit the junction resembles a classical electric circuit. Furthermore, we show that the setup can be used to generate dc-spin currents, which are controlled by the molecular magnetization direction and the relative phases between the Larmor precession and the ac voltage.

DOI: [10.1103/PhysRevB.93.075402](https://doi.org/10.1103/PhysRevB.93.075402)**I. INTRODUCTION**

Since the early 1970s, the potential use of molecules as components of electronic circuitry was proposed [1], thereby introducing the field of molecular electronics. Since then, the goal of the field has been to create high-speed processing molecular devices with miniature size [2,3]. In that respect, it is important to investigate the properties of transport through single molecules in the presence of external fields [4–8]. Single-molecule magnets are a class of molecular magnets with a large spin, strong magnetic anisotropy, and slow magnetization relaxation at low temperatures [9]. Due to both classical [10] and quantum [10–13] characteristics of single-molecule magnets, their application in molecular electronics became a topic of intense research, considering their potential usage in creation of memory devices [14]. Several experiments have already achieved transport through single-molecule magnets [15–17].

Time-dependent transport through molecular junctions has been theoretically studied using different techniques, such as nonequilibrium Green's functions technique [18–22], time-dependent density functional theory [23–27], reduced density matrix approach [28], etc. Time-dependent periodic fields in electrical contacts cause photon-assisted tunneling [4,29–31], a phenomenon based on the fact that by applying an external harmonic field with frequency Ω to the contact, the conduction electrons interact with the ac field and, consequently, participate in the inelastic tunneling processes by absorbing or emitting an amount of energy $n\hbar\Omega$, where $n = \pm 1, \pm 2, \dots$. Theoretically, photon-assisted tunneling through atoms and molecules was investigated in numerous works [4,32–37]. Some experimental studies addressed photon-assisted tunneling through atomic-sized [38–40] and molecular [41,42] junctions in the presence of laser fields. Time-dependent electric control of the state of quantum spins of atoms has also been investigated [43]. In junctions with time-dependent ac bias, the presence of displacement currents is inevitable due to the charge accumulation in the scattering region [44,45]. This problem can be solved either implicitly by including the Coulomb interaction in the Hamiltonian of the system [46,47] or explicitly by adding the displacement current to the

conduction current [45,48], thus providing the conservation of the total ac current.

Spin transport through magnetic nanostructures can be used to manipulate the state of the magnetization via spin-transfer torques (STTs) [49,50]. The concept of STT is based on the transfer of spin angular momenta from the conduction electrons to a local magnetization in the scattering region, generating a torque as a back-action of the spin transport, and thus changing the state of the magnetic nanostructure [49–52]. Hence, current-induced magnetization reversal has become an active topic in recent years [53–59]. The measurement and control of the magnetization of single-molecule magnets employing spin transport may bring important applications in spintronics.

In this work we theoretically study the charge and spin transport through a single electronic energy level in the presence of a molecular spin in a constant magnetic field. The electronic level may be an orbital of the molecule or it may belong to a nearby quantum dot. The molecular spin, treated as a classical magnetic moment, exhibits Larmor precession around the magnetic field axis. The Zeeman field and interaction of the orbital with the precessing molecular spin result in four quasienergy levels in the quantum dot, obtained using the Floquet theorem [60–63]. The system is then connected to electric contacts subject to oscillating electric potentials, considered as a perturbation. The oscillating chemical potentials induce photon-assisted charge and spin tunneling. A photon-assisted STT is exerted on the molecular spin by the photon-assisted spin currents. This torque is not included in the dynamics of the molecular spin, since the molecular spin precession is assumed to be kept steady by external means, thus compensating the STT. The precessing molecular spin in turn pumps spin currents into the leads, acting as an external rotating exchange field. Some of our main results are as follows:

- (1) In the limit of low ac frequency, the junction can be mapped onto a classical electric circuit modeling the inductive-like or capacitive-like response.
- (2) The real and imaginary components of the dynamic conductance, associated with the resonant position of the chemical potentials with molecular quasienergy levels, are

both enhanced around the ac frequency matching the Larmor frequency, allowing the detection of the internal precession time scale (see Fig. 4).

(3) The setup can be employed to generate and control dc spin currents by tuning the molecular precession angle and the relative phases between the ac voltage and Larmor precession if the ac frequency matches the Larmor frequency.

A part of this article is a complement to Ref. [64], representing the solution for the Gilbert damping coefficient [65], nonperturbative in the coupling to the molecular magnet, in the absence of time-varying voltage. The other corresponding STT coefficients and an arising nonzero z component of the STT are obtained as well.

The article is organized in the following way: We describe the model setup of the system in Sec. II. The theoretical formalism based on the Keldysh nonequilibrium Green's functions technique [18–20] is introduced in Sec. III. Here we derive expressions for spin and charge currents in linear order with respect to ac harmonic potentials in the leads. In Sec. IV we obtain and analyze the dynamic conductance of the charge current using the current partitioning scheme developed by Wang *et al.* [48]. This section is followed by Sec. V in which we analyze spin transport and STT under dc-bias voltage and in the presence of oscillating chemical potentials. We finally conclude in Sec. VI.

II. MODEL SETUP

We consider a junction consisting of a single spin-degenerate molecular orbital of a molecular magnet with a precessing spin in a constant magnetic field along z axis, $\vec{B} = B\vec{e}_z$, coupled to two normal metallic leads. We assume the spin of the molecular magnet is large and neglecting the quantum fluctuations treat it as a classical vector \vec{S} , with constant length $S = |\vec{S}|$. The magnetic field does not affect the electric contacts, which are assumed to be noninteracting. An external ac harmonic potential $V_{ac}^{\xi}(t) = v_{ac}^{\xi}\cos(\Omega t + \phi_{\xi})$ is applied to each lead $\xi = L, R$, modulating the single electron energy as $\epsilon_{k\xi}(t) = \epsilon_{k\xi} + eV_{ac}^{\xi}(t)$, with $\epsilon_{k\xi}$ being the single-particle energy of an electron with the wave number k , in the absence of the time-varying voltage (see Fig. 1). Since we

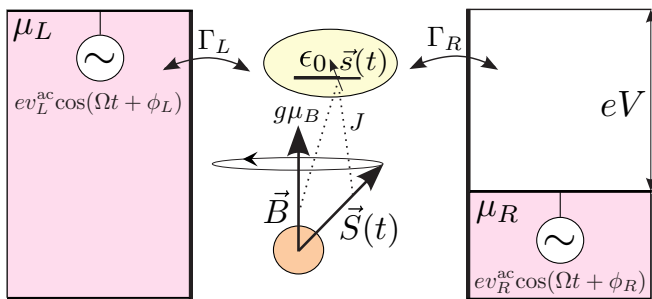


FIG. 1. Photon-assisted tunneling through a single molecular level with energy ϵ_0 coupled to the spin $\vec{S}(t)$ of a molecular magnet via exchange interaction with the coupling constant J in the presence of a constant magnetic field \vec{B} . External ac potentials $V_{ac}^{\xi}(t) = v_{ac}^{\xi}\cos(\Omega t + \phi_{\xi})$ are applied to the leads $\xi = L, R$ with chemical potentials μ_{ξ} and tunnel rates Γ_{ξ} .

want to unravel the quantum effects induced by the tunneling electrons and the ac harmonic potentials, we consider a well coupled molecular orbital and treat it as noninteracting by disregarding the intraorbital Coulomb interactions between the electrons.

The junction is described by the Hamiltonian $\hat{H}(t) = \hat{H}_L(t) + \hat{H}_R(t) + \hat{H}_T + \hat{H}_{MO}(t) + \hat{H}_S$. Here $\hat{H}_{\xi}(t) = \sum_{k,\sigma} \epsilon_{k\xi}(t) \hat{c}_{k\sigma\xi}^{\dagger} \hat{c}_{k\sigma\xi}$ is the Hamiltonian of lead $\xi = L, R$. The subscript $\sigma = \uparrow, \downarrow = 1, 2 = \pm 1$ denotes the spin-up or spin-down state of the electrons. The tunneling Hamiltonian $\hat{H}_T = \sum_{k,\sigma,\xi} [V_{k\xi} \hat{c}_{k\sigma\xi}^{\dagger} \hat{d}_{\sigma} + V_{k\xi}^* \hat{d}_{\sigma}^{\dagger} \hat{c}_{k\sigma\xi}]$ introduces the spin-independent tunnel coupling between the molecular orbital and the leads, with matrix element $V_{k\xi}$. The operators $\hat{c}_{k\sigma\xi}^{\dagger} (\hat{c}_{k\sigma\xi})$ and $\hat{d}_{\sigma}^{\dagger} (\hat{d}_{\sigma})$ represent the creation (annihilation) operators of the electrons in the leads and the molecular orbital. The next term in the Hamiltonian of the system is given by $\hat{H}_{MO}(t) = \sum_{\sigma} \epsilon_0 \hat{d}_{\sigma}^{\dagger} \hat{d}_{\sigma} + (g\mu_B/\hbar) \hat{s} \vec{B} + J \vec{s} \vec{S}(t)$. Here, the first term describes the noninteracting molecular orbital with energy ϵ_0 . The second term represents the electronic spin in the molecular orbital, $\hat{s} = (\hbar/2) \sum_{\sigma\sigma'} (\hat{\sigma})_{\sigma\sigma'} \hat{d}_{\sigma}^{\dagger} \hat{d}_{\sigma'}$, in the presence of the external constant magnetic field \vec{B} , and the third term expresses the exchange interaction between the electronic spin and the molecular spin $\vec{S}(t)$. Here $\hat{\sigma} = (\hat{\sigma}_x, \hat{\sigma}_y, \hat{\sigma}_z)^T$ represents the vector of the Pauli matrices. The proportionality factors g and μ_B are the gyromagnetic ratio of the electron and the Bohr magneton, respectively, while J is the exchange coupling constant between the molecular and electronic spins.

Presuming, for simplicity, that the molecular spin g factor equals that of a free electron, the term $\hat{H}_S = g\mu_B \vec{S} \vec{B}$ represents the energy of the classical molecular spin S in the magnetic field \vec{B} . Accordingly, the field \vec{B} exerts a torque on the spin \vec{S} leading to its precession around the field axis with Larmor frequency $\omega_L = g\mu_B B/\hbar$. To compensate for the dissipation of magnetic energy due to the interaction with conduction electrons, we assume that the molecular spin is kept precessing by external means (e.g., rf fields) [66]. Hence, we keep the tilt angle θ between \vec{B} and \vec{S} fixed and determined by the initial conditions. The dynamics of the molecular spin is then given by $\vec{S}(t) = S_{\perp} \cos(\omega_L t) \vec{e}_x + S_{\perp} \sin(\omega_L t) \vec{e}_y + S_z \vec{e}_z$, where S_{\perp} is the magnitude of the instantaneous projection of $\vec{S}(t)$ onto the $x - y$ plane, given by $S_{\perp} = S \sin(\theta)$, while the projection of the molecular spin on the z axis equals $S_z = S \cos(\theta)$. The precessing spin $\vec{S}(t)$ pumps spin currents into the system, but the effects of spin currents onto the molecular spin dynamics are compensated by the above-mentioned external sources.

III. THEORETICAL FORMALISM

The ensemble and quantum average charge and spin currents from the lead ξ to the molecular orbital are given by

$$I_{\xi\nu}(t) = q_{\nu} \left\langle \frac{d}{dt} \hat{N}_{\xi\nu} \right\rangle = q_{\nu} \frac{i}{\hbar} \langle [\hat{H}, \hat{N}_{\xi\nu}] \rangle, \quad (1)$$

with $\hat{N}_{\xi\nu} = \sum_{k,\sigma,\sigma'} \hat{c}_{k\sigma\xi}^{\dagger} (\sigma_{\nu})_{\sigma\sigma'} \hat{c}_{k\sigma\xi}$ representing the charge and spin occupation number operator of the contact ξ . The index ν takes values $\nu = 0$ for the charge and $\nu = 1, 2, 3$

for the components x, y, z of the spin-polarized current. The prefactors q_v correspond to the electronic charge $q_0 = -e$ and spin $q_{v \neq 0} = \hbar/2$. Employing the Keldysh nonequilibrium Green's functions technique, the currents can be calculated in units in which $\hbar = e = 1$ as [19,20]

$$I_{\xi v}(t) = -2q_v \text{Re} \int dt' \text{Tr} \left\{ \hat{\sigma}_v \left[\hat{G}^r(t, t') \hat{\Sigma}_{\xi}^<(t', t) + \hat{G}^<(t, t') \hat{\Sigma}_{\xi}^a(t', t) \right] \right\}, \quad (2)$$

where $\hat{\sigma}_0 = \hat{1}$ is the identity operator, while $\hat{\sigma}_{v \neq 0}$ are the Pauli matrices. In Eq. (2), $\hat{\Sigma}_{\xi}^{r, a, <}(t, t')$ are the retarded, advanced, and lesser self-energies from the tunnel coupling between the molecular orbital and the lead ξ , while $\hat{G}^{r, a, <}(t, t')$ are the corresponding Green's functions of the electrons in the molecular orbital. The matrices of the self-energies are diagonal in the electronic spin space with respect to the basis of eigenstates of \hat{s}_z , and their nonzero entries are given by $\Sigma_{\xi}^{r, a, <}(t, t') = \sum_k V_{k\xi} g_{k\xi}^{r, a, <}(t, t') V_{k\xi}^*$, where $g_{k\xi}^{r, a, <}(t, t')$ are the retarded, advanced, and lesser Green's functions of the electrons in contact ξ . The matrix elements of the Green's functions $\hat{G}^{r, a, <}(t, t')$ are given by $G_{\sigma\sigma'}^{r, a, <}(t, t') = \mp i \theta(\pm t \mp t') \langle \{ \hat{d}_{\sigma}(t), \hat{d}_{\sigma'}^{\dagger}(t') \} \rangle$ and $G_{\sigma\sigma'}^<(t, t') = i \langle \hat{d}_{\sigma}^{\dagger}(t') \hat{d}_{\sigma}(t) \rangle$, where $\{ \cdot, \cdot \}$ denotes the anticommutator. The self-energies of lead ξ can be expressed as [18–20]

$$\Sigma_{\xi}^<(t, t') = i \int \frac{d\epsilon}{2\pi} e^{-i\epsilon(t-t') + i\varphi_{\xi}(t, t')} f_{\xi}(\epsilon) \Gamma_{\xi}(\epsilon), \quad (3)$$

$$\Sigma_{\xi}^r(t, t') = -i \theta(t - t') \int \frac{d\epsilon}{2\pi} e^{-i\epsilon(t-t') + i\varphi_{\xi}(t, t')} \Gamma_{\xi}(\epsilon). \quad (4)$$

Here we introduced the Faraday phases $\varphi_{\xi}(t, t') = e \int_{t'}^{t'} dt'' V_{k\xi}^{\text{ac}}(t'')$. From its definition, it follows that $\Sigma_{\xi}^a(t, t') = [\Sigma_{\xi}^r(t', t)]^*$. Furthermore, $f_{\xi}(\epsilon) = [e^{(\epsilon - \mu_{\xi})/k_B T} + 1]^{-1}$ is the Fermi-Dirac distribution of the electrons in the lead ξ , with k_B the Boltzmann constant and T the temperature, while $\Gamma_{\xi}(\epsilon) = 2\pi \sum_k |V_{k\xi}|^2 \delta(\epsilon - \epsilon_{k\xi})$ is the tunnel coupling to the lead ξ . Using the self-energies defined above, and applying the double Fourier transformations in Eq. (2), in the wide-band limit, in which Γ_{ξ} is energy independent, one obtains

$$I_{\xi v}(t) = 2q_v \Gamma_{\xi} \text{Im} \int \frac{d\epsilon}{2\pi} \int \frac{d\epsilon'}{2\pi} e^{-i(\epsilon - \epsilon')t} \times \sum_{m, n} J_m \left(\frac{v_{\xi}^{\text{ac}}}{\Omega} \right) J_n \left(\frac{v_{\xi}^{\text{ac}}}{\Omega} \right) e^{i(m-n)\phi_{\xi}} \times \text{Tr} \left\{ \hat{\sigma}_v \left[f_{\xi}(\epsilon'_m) \hat{G}^r(\epsilon, \epsilon'_{mn}) + \frac{1}{2} \hat{G}^<(\epsilon, \epsilon'_{mn}) \right] \right\}, \quad (5)$$

with the abbreviations $\epsilon_m = \epsilon - m\Omega$ and $\epsilon_{mn} = \epsilon - (m - n)\Omega$. The generating function $\exp[ia \sin(\Omega t + \phi)] = \sum_m J_m(a) \exp[im(\Omega t + \phi)]$ was used in Eq. (5), where J_m is the Bessel function of the first kind of order m .

The matrix components of the retarded Green's function of the electrons in the molecular orbital, in the absence of the ac harmonic potentials in the leads, can be obtained exactly by applying Dyson's expansion and analytic continuation rules [20]. Their double Fourier transforms are written

as [67]

$$\mathcal{G}_{\sigma\sigma}^r(\epsilon, \epsilon') = \frac{2\pi \delta(\epsilon - \epsilon') G_{\sigma\sigma}^{0r}(\epsilon)}{1 - \gamma^2 G_{\sigma\sigma}^{0r}(\epsilon) G_{-\sigma-\sigma}^{0r}(\epsilon)}, \quad (6)$$

$$\mathcal{G}_{\sigma-\sigma}^r(\epsilon, \epsilon') = \frac{2\pi \gamma \delta(\epsilon - \epsilon') G_{\sigma\sigma}^{0r}(\epsilon) G_{-\sigma-\sigma}^{0r}(\epsilon)}{1 - \gamma^2 G_{\sigma\sigma}^{0r}(\epsilon) G_{-\sigma-\sigma}^{0r}(\epsilon)}, \quad (7)$$

with $\gamma = JS \sin(\theta)/2$ and $\epsilon_{\sigma} = \epsilon - \sigma \omega_L$. The matrix elements of the corresponding lesser Green's function are obtained using the Fourier transformed Keldysh equation $\hat{G}^<(\epsilon, \epsilon') = \int d\epsilon'' \hat{G}^r(\epsilon, \epsilon'') \hat{\Sigma}_0^<(\epsilon'') \hat{G}^a(\epsilon'', \epsilon')/2\pi$ [20]. Here $\hat{G}^a(\epsilon, \epsilon') = [\hat{G}^r(\epsilon', \epsilon)]^{\dagger}$ and $\Sigma_0^<(\epsilon) = i \sum_{\xi} \Gamma_{\xi} f_{\xi}(\epsilon)$ is the lesser self-energy originating from the orbital-lead coupling in the absence of harmonic potentials in the leads. The retarded Green's functions \hat{G}^{0r} of the electrons in the molecular orbital, in the presence of the static component of the molecular spin and the constant magnetic field \vec{B} , are found using the equation of motion technique [68] and, Fourier transformed, read $\hat{G}^{0r}(\epsilon) = [\epsilon - \epsilon_0 - \Sigma_0^r(\epsilon) - \hat{\sigma}_z (g\mu_B B + JS_z)/2]^{-1}$ [59,67], where $\Sigma_0^r(\epsilon) = -i\Gamma/2$ and $\Gamma = \sum_{\xi} \Gamma_{\xi}$.

For a weak ac field $v_{\xi}^{\text{ac}} \ll \Omega$, the retarded and lesser Green's functions of the electrons in the molecular orbital can be obtained by applying Dyson's expansion, analytic continuation rules, and the Keldysh equation [20]. Keeping only terms linear in $v_{\xi}^{\text{ac}}/\Omega$ they read

$$\hat{G}^r(\epsilon, \epsilon') \approx \hat{G}^r(\epsilon, \epsilon'), \quad (8)$$

$$\hat{G}^<(\epsilon, \epsilon') \approx \hat{G}^<(\epsilon, \epsilon') + i \sum_{\xi, n=\pm 1} n \Gamma_{\xi} \frac{v_{\xi}^{\text{ac}}}{\Omega} e^{in\phi_{\xi}} \int \frac{d\epsilon''}{4\pi} \times [f_{\xi}(\epsilon''_n) - f_{\xi}(\epsilon'')] \hat{G}^r(\epsilon, \epsilon''_n) \hat{G}^a(\epsilon'', \epsilon'). \quad (9)$$

In the rest of the paper we will stay in this limit.

The particle current contains the following contributions:

$$I_{\xi v}(t) = I_{\xi v}^{\omega_L}(t) + I_{\xi v}^{\Omega}(t). \quad (10)$$

The first component represents the transport in the absence of ac voltages in the leads. It has a static and a time-dependent contribution, which are both created by the precession of the molecular spin. This precession-induced current reads

$$I_{\xi v}^{\omega_L}(t) = 2q_v \Gamma_{\xi} \text{Im} \left\{ \int \frac{d\epsilon}{2\pi} \int \frac{d\epsilon'}{2\pi} e^{-i(\epsilon - \epsilon')t} \times \text{Tr} \left\{ \hat{\sigma}_v \left[\frac{1}{2} \hat{G}^<(\epsilon, \epsilon') + f_{\xi}(\epsilon') \hat{G}^r(\epsilon, \epsilon') \right] \right\} \right\}. \quad (11)$$

In the limit $\gamma^2 \rightarrow 0$, Eq. (11) reduces to the result obtained previously [64]. The second term of Eq. (10) is induced when an ac voltage is applied to lead ξ and can be expressed in linear order with respect to $v_{\xi}^{\text{ac}}/\Omega$ using Eqs. (5), (8), and (9) as

$$I_{\xi v}^{\Omega}(t) = q_v \sum_{\zeta, n=\pm 1} n \Gamma_{\xi} \Gamma_{\zeta} \frac{v_{\xi}^{\text{ac}}}{\Omega} \text{Re} \int \frac{d\epsilon}{2\pi} \int \frac{d\epsilon'}{2\pi} e^{-i(\epsilon - \epsilon')t + in\phi_{\zeta}} \times \left\{ \int \frac{d\epsilon''}{4\pi} \{ [f_{\zeta}(\epsilon''_n) - f_{\zeta}(\epsilon'')] \text{Tr} [\hat{\sigma}_v \hat{G}^r(\epsilon, \epsilon''_n) \hat{G}^a(\epsilon'', \epsilon')] \} \right. \\ \left. - \frac{i}{\Gamma_{\zeta}} \delta_{\xi\zeta} [f_{\zeta}(\epsilon'_n) - f_{\zeta}(\epsilon')] \text{Tr} [\hat{\sigma}_v \hat{G}^r(\epsilon, \epsilon'_n)] \right\}. \quad (12)$$

These expressions for the currents constitute the main results of the article. They allow us to calculate the dynamic charge conductance and spin transport properties of our molecular contact. Note that spin currents are more conveniently discussed in terms of the spin-transfer torque exerted by the inelastic spin currents onto the spin of the molecule, given by [49–52]

$$\vec{T}(t) = \vec{T}^{\omega_L}(t) + \vec{T}^{\Omega}(t) = -[\vec{I}_L(t) + \vec{I}_R(t)]. \quad (13)$$

Hence, in the remainder of the article we will concentrate on the ac charge conductance and the dc spin-transfer torque.

IV. CHARGE TRANSPORT

A. Dynamic charge conductance

The time-dependent particle charge current from the lead ξ to the molecular orbital is induced by the ac harmonic potentials in the leads and can be written as

$$I_{\xi 0}^{\Omega}(t) = \text{Re} \left\{ \sum_{\zeta} G_{\xi\zeta}^c(\Omega) v_{\zeta}^{\text{ac}} e^{-i(\Omega t + \phi_{\zeta})} \right\}, \quad (14)$$

where $G_{\xi\zeta}^c(\Omega)$ is the conductance between leads ξ and ζ .

In order to determine the dynamic conductance under ac bias-voltage conditions, one also needs to take into account the contribution from the displacement current. Coulomb interaction leads to screening of the charge accumulation in the quantum dot given by $I^d(t) = \frac{dQ(t)}{dt} = -e \text{Im} \left\{ \frac{d}{dt} [\text{Tr} \hat{G}^<(t, t)] \right\}$. According to the Kirchhoff's current law, $I^d(t) + \sum_{\xi} I_{\xi 0}^{\Omega}(t) = 0$. The following expression defines the total conductance of charge current, $G_{\xi\zeta}^d$:

$$I_{\xi 0}^{\Omega, \text{tot}}(t) = \text{Re} \left\{ \sum_{\zeta} G_{\xi\zeta}^d(\Omega) v_{\zeta}^{\text{ac}} e^{-i(\Omega t + \phi_{\zeta})} \right\}, \quad (15)$$

while the displacement conductance G_{ζ}^d is given by

$$I^d(t) = \text{Re} \left\{ \sum_{\zeta} G_{\zeta}^d(\Omega) v_{\zeta}^{\text{ac}} e^{-i(\Omega t + \phi_{\zeta})} \right\}. \quad (16)$$

The conservation of the total charge current and gauge invariance with respect to the shift of the chemical potentials lead to $\sum_{\xi} G_{\xi\zeta}^c = 0$ and $\sum_{\zeta} G_{\xi\zeta}^c = 0$ [45]. These equations are satisfied by partitioning the displacement current into each lead [48], $I_{\xi 0}^{\Omega, \text{tot}} = I_{\xi 0}^{\Omega} + A_{\xi} I^d$, or, equivalently, $G_{\xi\zeta}^d = G_{\xi\zeta}^c + A_{\xi} G_{\zeta}^d$, in such a way that the sum of the partitioning factors A_{ξ} obeys $\sum_{\xi} A_{\xi} = 1$. Using the sum rules given above one obtains the expression for the dynamic conductance [45,48],

$$G_{\xi\zeta}^d = G_{\xi\zeta}^c - G_{\zeta}^d \frac{\sum_{\lambda} G_{\xi\lambda}^c}{\sum_{\lambda} G_{\lambda}^d}, \quad (17)$$

where $A_{\xi} = -(\sum_{\lambda} G_{\xi\lambda}^c)/(\sum_{\lambda} G_{\lambda}^d)$, $G_{\zeta}^d = -\sum_{\xi} G_{\xi\zeta}^c$, and $G(\Omega) = G_{LL}(\Omega) = G_{RR}(\Omega) = -G_{LR}(\Omega) = -G_{RL}(\Omega)$. The first term of Eq. (17) represents the dynamic response of the charge current, while the second term is the internal response to the applied external ac perturbation due to screening by Coulomb interaction. Note that the dynamic conductance

consists of a real dissipative component G_R and an imaginary nondissipative component G_I , indicating the difference in phase between the current and the voltage. Due to the total current conservation, the two terms in Eq. (17) should behave in a way that a minimum (maximum) of $G_{\xi\zeta}^c(\Omega)$ corresponds to a maximum (minimum) of $G_{\zeta}^d(\Omega)$ for both real and imaginary parts.

B. Density of states in the quantum dot

Since the dynamic conductance is an experimentally directly accessible quantity, we hope that a measurement can help to reveal the internal time scales of the coupling between the molecular and electronic spins in the transport. We begin by analyzing the density of states available for electron transport in the quantum dot,

$$\rho(\epsilon) = -\frac{1}{\pi} \sum_{\sigma=\pm 1} \text{Im} \left\{ \frac{G_{\sigma\sigma}^{0r}(\epsilon)}{1 - \gamma^2 G_{\sigma\sigma}^{0r}(\epsilon) G_{-\sigma-\sigma}^{0r}(\epsilon_{\sigma})} \right\}. \quad (18)$$

There are four resonant transmission channels. They are positioned at quasienergy levels $\epsilon_1 = \epsilon_{\downarrow} = \epsilon_0 - (\omega_L + JS)/2$ (spin-down), $\epsilon_2 = \epsilon_{\uparrow} + \omega_L = \epsilon_0 + (\omega_L - JS)/2$ (spin-up), $\epsilon_3 = \epsilon_{\uparrow} - \omega_L = \epsilon_0 - (\omega_L - JS)/2$ (spin-down) and $\epsilon_4 = \epsilon_{\downarrow} + \omega_L = \epsilon_0 + (\omega_L + JS)/2$ (spin-up).

The Hamiltonian of the molecular orbital is a periodic function of time $\hat{H}_{\text{MO}}(t) = \hat{H}_{\text{MO}}(t + \tau)$, with period $\tau = 2\pi/\omega_L$. Its Fourier expansion is given by $\hat{H}_{\text{MO}}(t) = \sum_n \hat{H}_{\text{MO}}^{(n)} e^{in\omega_L t}$. Applying the Floquet theorem, one can obtain the Floquet quasienergy ϵ_{α} corresponding to the Floquet state $|\psi_{\alpha}(t)\rangle$ in the Schrödinger equation,

$$\hat{\mathcal{H}}_{\text{MO}}(t) |\psi_{\alpha}(t)\rangle = \epsilon_{\alpha} |\psi_{\alpha}(t)\rangle, \quad (19)$$

where $\hat{\mathcal{H}}_{\text{MO}}(t) = \hat{H}_{\text{MO}}(t) - i\partial_t$ [60–63]. The Floquet Hamiltonian matrix is block diagonal, with matrix elements given by $\langle \alpha; n | \hat{\mathcal{H}}_{\text{MO}} | \beta; m \rangle = [\hat{H}_{\text{MO}}^{(n-m)}]_{\alpha\beta} + n\omega_L \delta_{\alpha\beta} \delta_{nm}$ [61], where $|\alpha; n\rangle$ describes the Floquet states, while α denotes the electron spin states. For restricted Floquet quasienergies to the frequency interval $[0, \omega_L)$ a block is given by

$$\begin{pmatrix} \lambda_1 - \omega_L & JS_{\perp}/2 \\ JS_{\perp}/2 & \lambda_2 \end{pmatrix}, \quad (20)$$

with $\lambda_{1,2} = \epsilon_0 \pm (\omega_L + JS_{\perp})/2$. The corresponding Floquet quasienergies are eigenenergies of the matrix (20), equal to ϵ_1 and ϵ_3 . The precessing component of the molecular spin couples states with quasienergies ϵ_1 and ϵ_3 to states with quasienergies ϵ_2 and ϵ_4 , which differ in energy by an energy quantum ω_L . Namely, due to the periodic motion of the molecular spin, an electron can absorb or emit an energy ω_L , accompanied with a spin flip. Spin-flip processes due to rotating magnetic field were analyzed in some works [64,67]. A similar mechanism was discussed in a recent work for a nanomechanical spin valve, in which inelastic spin-flip processes are assisted by molecular vibrations [69].

C. Analysis of dynamic conductance

Now we analyze the charge conductance in response to the ac voltages. The suppression of dc conductance of charge current due to photon-assisted processes in the presence of an

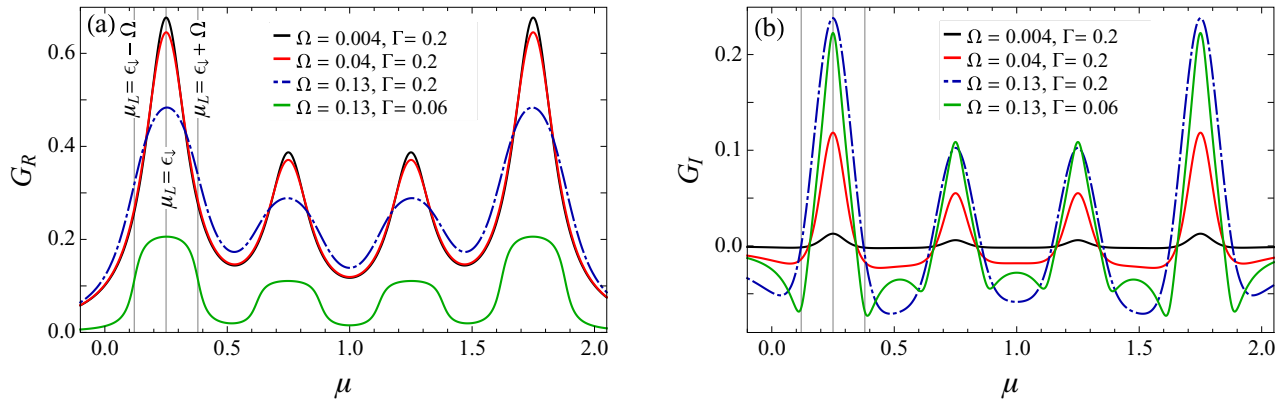


FIG. 2. (a) Real part G_R and (b) imaginary part G_I of the dynamic conductance as functions of the chemical potential μ , with $\mu = \mu_L = \mu_R$. The plots are obtained for different ac frequencies Ω and tunneling rates Γ at zero temperature, with $\Gamma_L = \Gamma_R = \Gamma/2$, and $\vec{B} = B\vec{e}_z$. All energies are given in the units of ϵ_0 . The other parameters are set to: $\omega_L = 0.5$, $J = 0.01$, $S = 100$, $\theta = 1.25$, $\gamma \approx 0.474$. The molecular quasienergy levels are positioned at: $\epsilon_1 = 0.25$, $\epsilon_2 = 0.75$, $\epsilon_3 = 1.25$, and $\epsilon_4 = 1.75$. The conductance components G_R and G_I are given in the units of conductance quantum e^2/h .

ac gate voltage, or a rotating magnetic field, was discussed in Ref. [63]. Here we consider ac conductance in a double-driving experiment, where we first induce molecular spin precession at Larmor frequency ω_L and then turn on the oscillating fields with frequency Ω in the leads. Assuming equal chemical potentials of the leads $\mu_L = \mu_R = \mu$, we analyze the dynamic conductance $G(\Omega)$ at zero temperature. Since we work in the wide-band limit, this symmetry simplifies the partitioning

factors to $A_\xi = \Gamma_\xi/\Gamma$. Hence, Eq. (17) can be transformed into

$$G_{\xi\xi}(\Omega) = \frac{e^2}{h} \int d\epsilon T_{\xi\xi}(\epsilon, \Omega) \frac{f_\zeta(\epsilon - \Omega) - f_\zeta(\epsilon)}{\Omega}. \quad (21)$$

Here $T_{\xi\xi}(\epsilon, \Omega)$ is the effective transmission function that can be expressed as $T(\epsilon, \Omega) = T_{LL}(\epsilon, \Omega) = T_{RR}(\epsilon, \Omega) = -T_{LR}(\epsilon, \Omega) = -T_{RL}(\epsilon, \Omega)$, which reads

$$T(\epsilon, \Omega) = \frac{\Gamma_L \Gamma_R}{\Gamma} (\Gamma - i\Omega) \sum_{\sigma=\pm 1} \frac{G_{\sigma\sigma}^{0r}(\epsilon) G_{\sigma\sigma}^{0a}(\epsilon - \Omega) [1 + \gamma^2 G_{-\sigma-\sigma}^{0r}(\epsilon_\sigma) G_{-\sigma-\sigma}^{0a}(\epsilon_\sigma - \Omega)]}{[1 - \gamma^2 G_{\sigma\sigma}^{0a}(\epsilon - \Omega) G_{-\sigma-\sigma}^{0a}(\epsilon_\sigma - \Omega)] [1 - \gamma^2 G_{\sigma\sigma}^{0r}(\epsilon) G_{-\sigma-\sigma}^{0r}(\epsilon_\sigma)]}. \quad (22)$$

The real part G_R and imaginary part G_I of the dynamic conductance versus chemical potential μ are plotted in Figs. 2(a) and 2(b). Both G_R and G_I achieve their maximum at $\mu_\zeta = \epsilon_i$, where the resonance peaks are positioned. In accordance with Eq. (21) the electrons in lead $\zeta = L, R$, with energies $\mu_\zeta - \Omega \leq \epsilon \leq \mu_\zeta$, can participate in the transport processes by absorbing a photon of energy Ω . For $\Omega \rightarrow 0$ the dynamic conductance reduces to dc conductance, $G_{\xi\xi}(\Omega \rightarrow 0) = e^2 T_{\xi\xi}(\mu_\zeta, \Omega \rightarrow 0)/h$, and reaches its maximum at resonances given by the Floquet quasienergies [63]. The imaginary part of the dynamic conductance G_I approaches zero for $\Omega \rightarrow 0$ [black line in Fig. 2(b)]. The considerable contribution of the displacement current to the total current is reflected in the decrease of G_R , and the increase of G_I near resonances with increasing Ω , as the displacement current opposes the change of the particle charge current under ac bias [red and blue dot-dashed lines in Figs. 2(a) and 2(b)]. For a small value of both Γ and Ω , G_R show sharp resonant peaks. However, with the increase of Ω , each of the peaks in G_R broadens [green line in Fig. 2(a)]. It approaches a constant value around the corresponding resonant level, with the width equal to 2Ω , since the inequality

$$|\epsilon_i - \mu_\zeta| \leq \Omega \quad (23)$$

is the condition for the inelastic photon-assisted tunneling to occur.

D. Frequency dependence of the ac conductance and equivalent circuit

The behavior of the ac conductance in the low-ac-frequency regime can be understood using a classical circuit theory [70]. Namely, at small ac frequencies $\Omega \ll \Gamma$, the molecular magnet junction behaves as a parallel combination of two serial connections: one of a resistor and an inductor and the other of a resistor and a capacitor, i.e., as a classical electric circuit (see Fig. 3). Depending on the phase difference between the voltage and the current, the circuit shows inductive-like (positive phase difference) or capacitive-like (negative phase difference) responses to the applied ac voltage. Thus, the dynamic conductance can be expanded up to the second order in Ω in the small-ac-frequency limit as

$$G(\Omega) = G(0) + G'(0)\Omega + \frac{1}{2}G''(0)\Omega^2 + O(\Omega^3) \\ \approx \frac{1}{R_1} + i\left(\frac{L}{R_1^2} - C\right)\Omega + \left(R_2C^2 - \frac{L^2}{R_1^3}\right)\Omega^2, \quad (24)$$

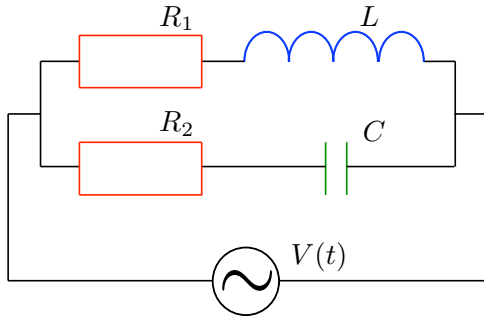


FIG. 3. The equivalent classical circuit of the molecular magnet junction in the low-ac-frequency regime. It is composed of two serial combinations: one of a resistor and an inductor and the other of a resistor and a capacitor connected in parallel and driven by a source of ac voltage $V(t)$. The resistances are denoted by R_1 and R_2 ; L is the inductance and C is the capacitance of the circuit elements.

where R_1 , R_2 , L , and C denote the resistances, inductance, and capacitance of the circuit. In our further analysis we will assume that $R_1 = R_2 = R$. The first term of Eq. (24) represents the dc conductance $G(0) = 1/R$. The second, imaginary term, linear in Ω , is iG_I in the low-ac-frequency limit.

Depending on the sign of $L/R^2 - C$, the linear response is inductive-like ($G_I > 0$) while G_R decreases or capacitive-like ($G_I < 0$) while G_R increases with the increase of Ω . For $C = L/R^2$ the system behaves like a resistor with $G = G(0)$. The nondissipative component G_I shows inductive-like behavior for

$$|\epsilon_i - \mu_\zeta| < \frac{\Gamma}{2}, \quad (25)$$

as we have observed in Fig. 2(b) (red line), and capacitive-like or resistive behavior otherwise.

The behavior of the dynamic conductance components G_R and G_I as functions of the ac frequency Ω for $\mu = \epsilon_3$ and $\mu = 0.1\epsilon_0$, with two values of Γ at zero temperature is presented in Fig. 4. The real part G_R is an even, while the imaginary part G_I

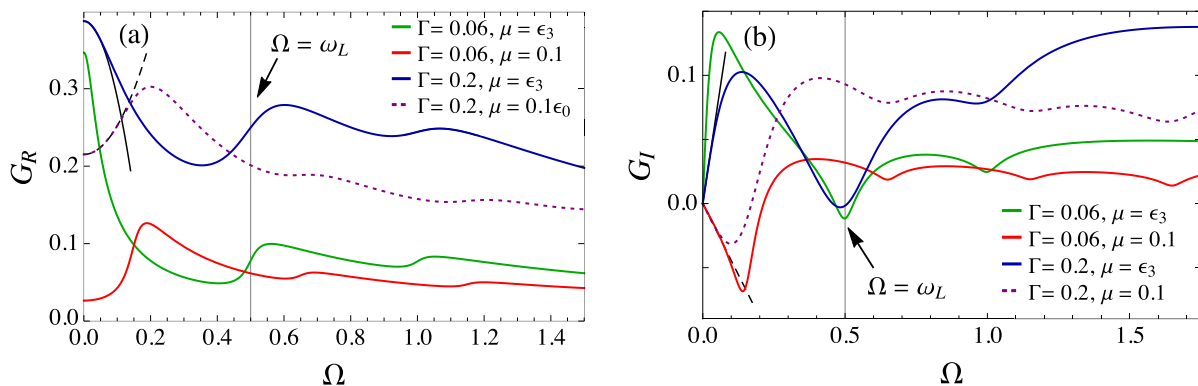


FIG. 4. (a) Real part G_R and (b) imaginary part G_I of the dynamic conductance as functions of the ac frequency Ω . The plots are obtained for two different tunneling rates Γ and chemical potentials μ , with $\mu = \mu_L = \mu_R$ and $\vec{B} = B\vec{e}_z$, at zero temperature. All energies are given in the units of ϵ_0 . The other parameters are set to: $\Gamma_L = \Gamma_R = \Gamma/2$, $S = 100$, $J = 0.01$, $\omega_L = 0.5$, $\theta = 1.25$, $\gamma \approx 0.474$. The molecular quasienergy levels lie at: $\epsilon_1 = 0.25$, $\epsilon_2 = 0.75$, $\epsilon_3 = 1.25$, and $\epsilon_4 = 1.75$. In the resonant case $\mu = \epsilon_3$, the response of the system is inductive-like in the low-ac-frequency limit ($G_I > 0$), and G_R and G_I are both enhanced around $\Omega = \omega_L$, after going to a local minimum, as the channel with quasienergy ϵ_4 becomes available for photon-assisted tunneling, i.e., $\mu + \Omega = \epsilon_4$. The conductance components G_R and G_I are given in the units of e^2/h .

is an odd function of Ω . In the low-ac-frequency regime $\Omega \ll \Gamma$, G_R is a quadratic function, while G_I is a linear function of ac frequency (solid and dashed black lines in Fig. 4). By fitting parameters of these functions and using Eq. (24), one obtains circuit parameters R , L , and C , confirming that in this limit the ac conductance of the system resembles the previously described classical circuit model. The circuit parameters can be calculated in terms of the dynamic conductance according to Eq. (24). Note that they depend on the relative position of the Fermi energy of the leads with respect to the molecular quasienergy levels.

Near the four resonances we expect the system to be highly transmissive and therefore to conduct well. This is confirmed by Figs. 2 and 4. Namely the imaginary conductance component $G_I > 0$ around resonances and is a positive linear function of Ω in the low-ac-frequency limit [see Fig. 4(b), black solid line]. This implies that the behavior of the system is inductive-like, since the displacement current tends to reduce the charge current, as electrons reside awhile in the quantum dot, causing the delay in phase between the voltage and the current. Accordingly, the real component G_R decreases quadratically from initial value $G(0)$ upon switching on the ac frequency Ω [black solid line in Fig. 4(a)]. However, the off-resonance behavior is capacitive-like, resulting from intraorbital Coulomb interactions, included via displacement current [48]. Hence, in the low-ac-frequency limit $G_I(\Omega)$ is negative and decreases linearly with the increase of Ω for Fermi energies of the leads which are far from the resonant energies ϵ_i [black dashed line in Fig. 4(b)]. In this case $G_R(\Omega)$ increases quadratically with Ω [black dashed line in Fig. 4(a)]. Obviously, the molecular magnet junction behaves as a classical circuit only in the low-ac-frequency regime.

For higher ac frequencies Ω we use Eq. (21) to analyze the behavior of G_R and G_I , where the dynamic response of the system remains predominantly inductive-like for $\mu = \epsilon_\uparrow - \omega_L = \epsilon_3$. With further increase of Ω , the ac conductance $G(\Omega)$ vanishes asymptotically. Upon turning on the ac frequency, while the system is on resonance $\mu = \epsilon_\uparrow - \omega_L$, the imaginary

component G_I increases quickly from 0 to a local maximum and then decreases to its minimum value around $\Omega = \omega_L$ [green and blue lines in Fig. 4(b)]. The real part G_R decreases to a local minimum and then has a steplike increase towards a local maximum around $\Omega = \omega_L$ [green and blue lines in Fig. 4(a)]. This behavior of the dynamic conductance can be understood as follows. For $\mu = \epsilon_\uparrow - \omega_L$, at $\Omega = \omega_L$, besides the resonant level with quasienergy $\epsilon_\uparrow - \omega_L$, the upper level with quasienergy ϵ_\uparrow becomes available for photon-assisted electron transport. It is then distanced by the energy Ω from the chemical potential μ . Consequently, an electron with Fermi energy equal to $\epsilon_\uparrow - \omega_L$ can absorb a photon of energy $\Omega = \omega_L$ in the lead ζ and tunnel into the level with quasienergy ϵ_\uparrow . This leads to an enhancement of the response functions G_R and G_I , after going to a local minimum, with features corresponding to photon-assisted tunneling processes. Each steplike increase of G_R and the corresponding dip of G_I in Fig. 4 are determined by the difference between the quasienergy levels ϵ_i and the chemical potential μ , viz. $|\epsilon_i - \mu| = \Omega$. Thus, for $\mu = \epsilon_3$ and the set of parameters given in Fig. 4, they are positioned around $\Omega/\epsilon_0 = 0.5$ and $\Omega/\epsilon_0 = 1$. For the larger tunnel couplings each steplike increase in G_R is broadened due to the level broadening Γ . We notice that the enhancement of the dynamic conductance is higher around $\Omega = \omega_L$ than around the subsequent frequency $\Omega/\epsilon_0 = 1$. This is due to the fact that the frequency has to traverse one resonant peak in G_R , or dip in G_I , to reach the second one. We need to mention that the off-diagonal conductances $G_{\xi\zeta} = -G$, where $\xi \neq \zeta$, and hence have a behavior that opposes that of the diagonal ones.

In the spirit of the scattering matrix formalism, the dynamic conductance of our molecular magnet junction, in the low-ac-frequency regime, can be expanded as [71]

$$G_{\xi\zeta}(\Omega) = G_{\xi\zeta}(0) - i\Omega E_{\xi\zeta} + \Omega^2 K_{\xi\zeta} + O(\Omega^3), \quad (26)$$

where $G_{\xi\zeta}(0)$ is the dc conductance. The quantity $E_{\xi\zeta} = -\text{Im}\{\partial G_{\xi\zeta}(0)/\partial\Omega\}$ is called the emittance [71]. It contains the contribution from the displacement current and the partial density of states that characterize the scattering process [46,72,73]. The partial density of states can be calculated

using the scattering matrix, and can be understood as density of states due to electrons injected from lead ζ , and leaving through lead ξ [46,72,73]. The emittance $E_{\xi\zeta}$ measures the dynamic response of the system to an external oscillating ac field and, depending on its sign, the response is capacitive-like or inductive-like [71]. The matrix element of the third term, $K_{\xi\zeta} = \text{Re}\{\partial^2 G_{\xi\zeta}(0)/\partial\Omega^2\}/2$, represents the correction to the real part of the dynamic conductance and describes the dynamic dissipation in the low-ac-frequency regime [71]. Both $E_{\xi\zeta}$ and $K_{\xi\zeta}$ obey the sum rules, since the total current conservation and gauge invariance conditions have to be satisfied [45]. According to Eq. (26), their diagonal elements $E = E_{\xi\xi}$ and $K = K_{\xi\xi}$ can be approximated as $E \approx -G_I/\Omega$ and $K \approx [G_R - G(0)]/\Omega^2$ in the low frequency limit [71]. Based on the analyzed G_R and G_I the behavior of E and K can be examined. Around all resonances $\mu = \epsilon_i$ the emittance $E < 0$ (inductive-like response) and $K < 0$ since $G_R < G(0)$, while off resonance $E > 0$ (capacitive-like response) and $K > 0$ (see Figs. 2 and 4).

E. Effects of the molecular magnetization direction on the ac conductance

Now we analyze the ac conductance components G_R and G_I as functions of the tilt angle θ of the molecular spin \vec{S} from the external field \vec{B} , plotted in Figs. 5(a) and 5(b). For $\theta = 1.25$, the peaks of both G_R and G_I in Figs. 2(a) and 2(b) at $\mu = \epsilon_{\uparrow,\downarrow} \mp \omega_L$ are much lower than those at $\mu = \epsilon_{\uparrow,\downarrow}$, implying that the molecular magnet junction is less transmissive at the upper two mentioned resonances. This can be qualitatively understood by looking at Fig. 5. The behavior of the conductance components near the resonances for $\mu = \epsilon_\uparrow - \omega_L$ (solid lines in Fig. 5) and $\mu = \epsilon_\uparrow$ (dot-dashed lines in Fig. 5) depends on the direction of \vec{S} with respect to the external magnetic field \vec{B} . For $\theta = 0$ the molecular spin \vec{S} is static and the only two levels available for electron transport are Zeeman levels $\epsilon_1 = \epsilon_\downarrow$ and $\epsilon_4 = \epsilon_\uparrow$. In this case, when the system is at the resonance $\mu = \epsilon_\uparrow$, the components G_R and G_I take their maximum values, and $G_I > 0$ displaying an

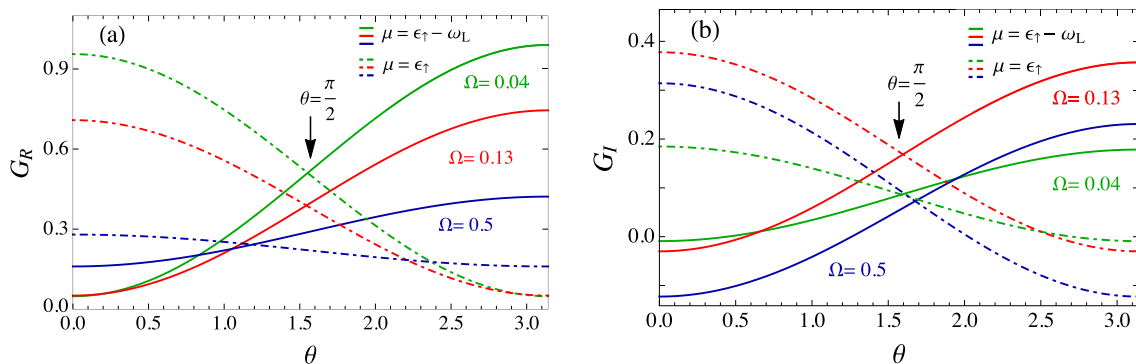


FIG. 5. (a) Real part G_R and (b) imaginary part G_I of the dynamic conductance as functions of the tilt angle θ of the molecular spin \vec{S} from the magnetic field $\vec{B} = B\vec{e}_z$. The plots are obtained for different values of Ω and μ , with $\mu = \mu_L = \mu_R$, at zero temperature. All energies are given in the units of ϵ_0 . The other parameters are set to $S = 100$, $J = 0.01$, $\omega_L = 0.5$, $\Gamma = 0.2$, and $\Gamma_L = \Gamma_R = \Gamma/2$. In the limit of low frequency Ω , for $\theta \rightarrow \pi/2$, the conductance component G_R , as well as G_I , approaches equal value at each resonance. The conductance components G_R and G_I are given in the units of conductance quantum e^2/h .

inductive-like behavior. For $\mu = \epsilon_{\uparrow} - \omega_L$ and $\theta = 0$, both G_R and G_I take their minimum values. There is no transmission channel at this energy for $\theta = 0$, but Γ is relatively large, and $G_I < 0$ displays a capacitive-like response. With the increase of θ , the additional two channels at energies $\epsilon_{\uparrow} - \omega_L$ and $\epsilon_{\downarrow} + \omega_L$ appear and become available for electron transport. This leads to the increase of conductance components G_R and G_I at $\mu = \epsilon_{\uparrow} - \omega_L$, and their decrease at $\mu_L = \epsilon_{\uparrow}$, as functions of θ (see Fig. 5). For $\theta \rightarrow \pi/2$, in the case of small Ω the complex components of the effective transmission function $T(\epsilon, \Omega)$ approach the same height at resonant energies ϵ_i , so the probability of transmission reaches equal value at each level. Thus, both G_R and G_I show peaks of the same height at the resonances. The points of intersection of solid and dot-dashed lines of the same color in Fig. 5 correspond to this particular case. For larger frequencies Ω , these points are shifted away from $\theta \rightarrow \pi/2$, since the peaks broaden and overlap and the suppression or increase of G_R and G_I is much faster. Finally, for $\theta = \pi$ the situation is reversed compared to the one with $\theta = 0$, as again the static spin \vec{S} is in the direction opposite that of the external field \vec{B} . The Zeeman splitting in this case is equal to $\omega_L - JS$, so the only two levels available for electron transport are ϵ_2 and ϵ_3 . Therefore, for $\theta = \pi$, when the system is at the resonance $\mu = \epsilon_3$, the conductance components G_R and G_I reach their maximum values, with $G_I > 0$. For $\mu = \epsilon_4$, which is off resonance for $\theta = \pi$, both G_R and G_I take minimum values, with $G_I < 0$.

V. SPIN TRANSPORT AND SPIN-TRANSFER TORQUE

A. Spin transport under dc-bias voltage

In the absence of ac harmonic potentials in the leads, tunneling under dc-bias voltage takes place. The spin-angular momenta between the itinerant electronic spins and the precessing molecular spin are exchanged via exchange interaction, governed by the coupling constant J . The molecular spin precession pumps spin currents into the system but remains undamped using external sources, which compensate effects of the interaction with electron spins. Further simplification of Eq. (11) gives time-independent z components of the spin current, $I_{Lz}^{\omega_L}$, and the in-plane $j = x, y$ time-dependent spin-current components from the left lead,

$$I_{Lj}^{\omega_L}(t) = [I_{Lj}(\omega_L)e^{-i\omega_L t} + I_{Lj}^*(\omega_L)e^{i\omega_L t}]. \quad (27)$$

The expressions for complex time-independent functions $I_{Lx}(\omega_L)$ and $I_{Ly}(\omega_L)$, and the spin current $I_{Lz}^{\omega_L}$ are given by Eqs. (A1)–(A3) in the Appendix.

The spin-transport properties are characterized by elastic, i.e., energy-conserving, tunnel processes [terms involving factors $[f_L(\epsilon) - f_R(\epsilon)]$ in Eqs. (A1) and (A3)] and inelastic, i.e., energy-nonconserving, tunnel processes [terms involving factors $[f_{\xi}(\epsilon - \omega_L) - f_{\zeta}(\epsilon)]$ in Eqs. (A1) and (A3)]. In the latter ones an electron changes its energy by ω_L and flips its spin due to the exchange interaction with the rotational component of the molecular spin. The spin-flip processes occur between levels with quasienergies ϵ_{\uparrow} and $\epsilon_{\uparrow} - \omega_L$ and between levels with quasienergies ϵ_{\downarrow} and $\epsilon_{\downarrow} + \omega_L$.

The STT exerted by the inelastic spin-currents onto the spin of the molecule is given by [49–52]

$$\vec{T}^{\omega_L}(t) = -[\vec{I}_L^{\omega_L}(t) + \vec{I}_R^{\omega_L}(t)] \quad (28)$$

and can be expressed in terms of the matrix elements of the Green's functions $\hat{G}^{0r}(\epsilon)$ and $\hat{G}^{0a}(\epsilon)$ as

$$T_j^{\omega_L}(t) = - \int \frac{d\epsilon}{2\pi} \sum_{\xi\zeta} \frac{\Gamma_{\xi}\Gamma_{\zeta}}{\Gamma} [f_{\xi}(\epsilon - \omega_L) - f_{\zeta}(\epsilon)] \times \text{Im} \left\{ (\hat{\sigma}_j)_{21} \frac{\gamma G_{11}^{0r}(\epsilon) G_{22}^{0a}(\epsilon - \omega_L)}{|1 - \gamma^2 G_{11}^{0r}(\epsilon) G_{22}^{0r}(\epsilon - \omega_L)|^2} \times [1 - \gamma^2 G_{11}^{0a}(\epsilon) G_{22}^{0r}(\epsilon - \omega_L)] e^{-i\omega_L t} \right\}, \quad (29)$$

$$T_z^{\omega_L} = - \int \frac{d\epsilon}{2\pi} \sum_{\xi\zeta} \Gamma_{\xi}\Gamma_{\zeta} [f_{\xi}(\epsilon - \omega_L) - f_{\zeta}(\epsilon)] \times \frac{\gamma^2 |G_{11}^{0r}(\epsilon) G_{22}^{0r}(\epsilon - \omega_L)|^2}{|1 - \gamma^2 G_{11}^{0r}(\epsilon) G_{22}^{0r}(\epsilon - \omega_L)|^2}. \quad (30)$$

Regarding the molecular spin \vec{S} , the STT can be presented as

$$\vec{T}^{\omega_L}(t) = \frac{\alpha}{S} \dot{\vec{S}}(t) \times \vec{S}(t) + \beta \dot{\vec{S}}(t) + \eta \vec{S}(t), \quad (31)$$

with the Gilbert damping coefficient α in the first term. The coefficient β that characterizes the modulation of the precession frequency of the molecular spin $\vec{S}(t)$ is given by the second term. The third coefficient η can be written in terms of α and $T_z^{\omega_L}$ as $\eta = [T_z^{\omega_L} + \omega_L S \alpha \sin^2(\theta)]/S_z$. Using Eqs. (29) and (30), and comparing them with Eq. (31), one obtains exact expressions for the torque coefficients α and β as

$$\alpha = - \frac{1}{\omega_L S} \int \frac{d\epsilon}{2\pi} \sum_{\xi\zeta} \Gamma_{\xi}\Gamma_{\zeta} [f_{\xi}(\epsilon - \omega_L) - f_{\zeta}(\epsilon)] \frac{(JS_z/2\Gamma) \text{Im}\{G_{11}^{0r}(\epsilon) G_{22}^{0a}(\epsilon - \omega_L)\} - \gamma^2 |G_{11}^{0r}(\epsilon) G_{22}^{0r}(\epsilon - \omega_L)|^2}{|1 - \gamma^2 G_{11}^{0r}(\epsilon) G_{22}^{0r}(\epsilon - \omega_L)|^2}, \quad (32)$$

$$\beta = - \frac{J}{\omega_L} \int \frac{d\epsilon}{4\pi} \sum_{\xi\zeta} \frac{\Gamma_{\xi}\Gamma_{\zeta}}{\Gamma} [f_{\xi}(\epsilon - \omega_L) - f_{\zeta}(\epsilon)] \frac{\text{Re}\{G_{11}^{0r}(\epsilon) G_{22}^{0a}(\epsilon - \omega_L)\} - \gamma^2 |G_{11}^{0r}(\epsilon) G_{22}^{0r}(\epsilon - \omega_L)|^2}{|1 - \gamma^2 G_{11}^{0r}(\epsilon) G_{22}^{0r}(\epsilon - \omega_L)|^2}. \quad (33)$$

In the limit $\gamma^2 \rightarrow 0$, the expressions (29)–(33) are in agreement with Ref. [64]. In the strong exchange coupling limit $J \gg \Gamma$ both Gilbert damping coefficient α and the torque coefficient β drop to zero.

B. Photon-assisted spin transport under ac-bias voltage

We consider spin transport in the double-driving experiment, where we first establish molecular spin precession at Larmor frequency ω_L and then apply the oscillating potentials

with frequency Ω in the leads. The spin current components indicating photon-assisted inelastic spin transport can be obtained by further simplification of Eq. (12). The in-plane x and y spin-current components consist of oscillating terms involving both ac frequency Ω and Larmor frequency ω_L . Experimentally, by adjusting $\Omega = \pm\omega_L$, these currents may be measurable. In this case they have one dc component and one component oscillating with frequency 2Ω . The photon-assisted spin currents are given by Eqs. (A4)–(A7) in the Appendix.

The time average of a periodic function $F(t)$, with a period T is defined as

$$\langle F \rangle_t = \frac{1}{T} \int_0^T F(t) dt. \quad (34)$$

According to Eq. (A4), the time-averaged $j = x, y$ components of the total spin current $\vec{I}_L(t)$ are nonzero only for $\Omega = \pm\omega_L$ and read

$$\langle I_{Lj} \rangle_t = \langle I_{Lj}^{\Omega=\pm\omega_L} \rangle_t = \sum_{\xi} \text{Re} \{ I_{L\xi}^j(-\omega_L) e^{\pm i\phi_{\xi}} \}, \quad (35)$$

while the time-averaged z component of the spin-current equals

$$\langle I_{Lz} \rangle_t = I_{Lz}^{\omega_L}. \quad (36)$$

Hence, the in-plane time-averaged x and y spin-current components contain only contributions from photon-assisted spin tunneling processes, while the z component contains only contributions from spin tunneling under dc-bias voltage. The time-averaged STT is then given by

$$\langle \vec{T} \rangle_t = - \sum_{\xi} \langle \vec{I}_{\xi} \rangle_t. \quad (37)$$

All the torques are compensated by external means, which keep the molecular spin precession undamped during the experiment.

C. Analysis of the time-averaged spin transport

The in-plane components of the time-averaged spin current and STT are presented in Figs. 6(a) and 6(b) as functions of the bias-voltage $eV = \mu_L - \mu_R$. According to Eqs. (A6) and (35),

$\langle I_{Lx} \rangle_t$ and $\langle I_{Ly} \rangle_t$ differ in phase by $\pi/2$. The plots are obtained at zero temperature for two different phases of the ac field in the left lead. We set $\Omega = \omega_L$, the right lead's Fermi energy $\mu_R = 0$, and apply an ac harmonic chemical potential only to the left lead. According to the segment $[f_L(\epsilon - \Omega) - f_L(\epsilon)]$ in Eq. (A5), electrons with energies within the window $[\mu_L - \Omega, \mu_L]$ participate in the photon-assisted spin transport. Each of these processes is followed by a spin-flip and emission (absorption) of an amount of energy ω_L . This is caused by the interaction of the electron spin with the precessing component of the molecular spin. In turn, during the exchange interaction, a photon-assisted STT is generated onto $\vec{S}(t)$. In regard to photon-assisted transmission of 1/2-spin particles, the in-plane spin-current components show significant changes in either magnitude or direction, controlled by the change of the phase of the ac field in the left lead ϕ_L . Similarly to the case of charge transport, the necessary condition for photon-assisted spin tunneling is given by the inequality (23). The cases with equality sign in (23) are represented by the black arrows in Fig. 6, pointing to the eV scale. Each level satisfying this condition corresponds to two black arrows. In the region between each two black arrows the inequality (23) is satisfied for at least one molecular quasienergy level. Here the components of spin current and STT approach constant values. If $\epsilon_1 \leq \mu_L \leq \epsilon_2$ or $\epsilon_3 \leq \mu_L \leq \epsilon_4$, then the inequality (23) is satisfied for both ϵ_1 and ϵ_2 or ϵ_3 and ϵ_4 . As a result, the magnitude of spin currents and STT is enhanced under these conditions, due to the involvement of both levels ϵ_1 and ϵ_2 , or ϵ_3 and ϵ_4 , in photon-assisted spin transport and photon-assisted spin-flip processes. We should point out that both spin-current components and STTs are antisymmetric functions of eV with respect to the position of ϵ_0 . This is a consequence of the antisymmetric position of levels ϵ_i attributed to the spin-up or spin-down state of the electron with respect to ϵ_0 . Using Eq. (35) with $v_{ac}^R = 0$, $\phi_R = 0$, we obtain the largest magnitudes of the $j = x, y$ time-averaged spin-current components for

$$\phi_L = \arctan \left(\frac{\text{Im} \{ I_{LL}^j(-\omega_L) \}}{\text{Re} \{ I_{LL}^j(-\omega_L) \}} \right). \quad (38)$$

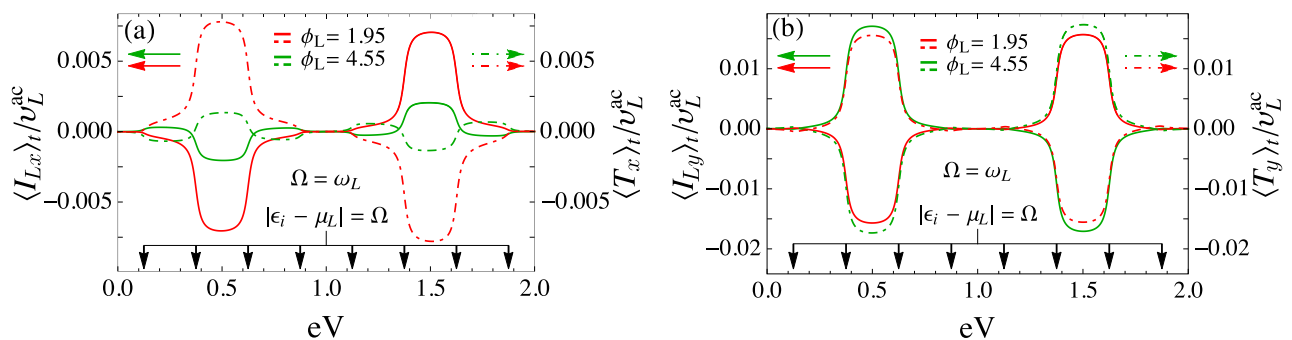


FIG. 6. Bias-voltage dependence of the time-averaged components of the spin-current and spin-transfer torque (a) $\langle I_{Lx} \rangle_t / v_L^{ac}$ and $\langle T_x \rangle_t / v_L^{ac}$ and (b) $\langle I_{Ly} \rangle_t / v_L^{ac}$ and $\langle T_y \rangle_t / v_L^{ac}$. The plots are obtained at zero temperature for two different phases ϕ_L , with $B = B\hat{z}$. All energies are given in the units of ϵ_0 . The other parameters are set to $\Gamma = 0.04$, $\Gamma_L = \Gamma_R = \Gamma/2$, $\mu_R = 0$, $\phi_R = 0$, $v_{ac}^R = 0$, $\theta = 1.25$, $S = 100$, $J = 0.01$, and $\Omega = \omega_L = 0.25$. Photon-assisted spin transport is enhanced for $\epsilon_1 < \mu_L < \epsilon_2$ and $\epsilon_3 < \mu_L < \epsilon_4$, where the in-plane components of the spin-current and spin-transfer torque approach the constant largest magnitudes.

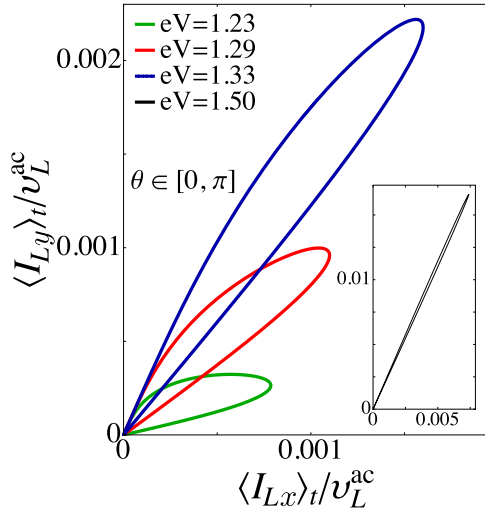


FIG. 7. Time-averaged spin currents $\langle I_{Lx} \rangle_t / v_L^{\text{ac}}$ and $\langle I_{Ly} \rangle_t / v_L^{\text{ac}}$ for $\theta \in [0, \pi]$ and $\phi_L = 1.95$, with maximal magnitudes around $\theta = \pi/2$. The plots are obtained at zero temperature for four different bias-voltages varied as $eV = \mu_L$. All energies are given in the units of ϵ_0 . The other parameters are the same as in Fig. 6. Inset: In-plane spin-current components for $eV = 1.5$, where $\epsilon_3 < \mu_L < \epsilon_4$.

Simultaneously, the other in-plane time-averaged spin-current equals zero.

The magnitude of the time-averaged spin currents (and STTs) can also be controlled by tuning the tilt angle θ , as presented in Fig. 7. For $\theta = 0$, the in-plane spin currents are equal to 0. Since the spin-flip is most probable with the largest magnitude of the rotating field, the maximal magnitudes of $\langle I_{Lx} \rangle_t$ and $\langle I_{Ly} \rangle_t$ are obtained around $\theta = \pi/2$ and increase significantly if μ_L lies between any two levels connected with spin-flip mechanism (see the inset in Fig. 7).

Some of the photon-assisted tunneling processes contributing to the spin transport are presented in Fig. 8. We show examples of two opposite photon-assisted spin-flip processes. Figure 8(a) corresponds to the case in which $\epsilon_1 - \mu_L < \Omega$ (or $\epsilon_3 - \mu_L < \Omega$). Here an electron from the left lead excited by a photon of energy $\Omega = \omega_L$ tunnels into the level ϵ_1

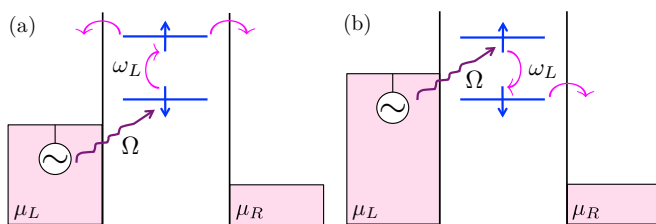


FIG. 8. Sketch of two opposite photon-assisted spin-flip processes between molecular quasienergy levels in the presence of ac harmonic potential with frequency Ω in the left lead. (a) Excited electron with energy Ω tunnels into spin-down level ϵ_1 (or $\epsilon_\uparrow - \omega_L$). It absorbs an amount of energy ω_L , flips its spin due to the exchange interaction with the precessing component of the molecular spin, and exits into either lead. (b) Excited electron tunnels into spin-up level $\epsilon_4 + \omega_L$ (or ϵ_\uparrow), flips its spin, and emits an energy quantum ω_L . Then it tunnels out to the right lead.

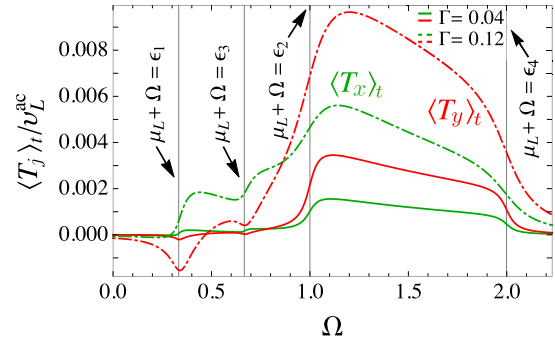


FIG. 9. Time-averaged spin-transfer torque components $\langle T_j \rangle_t$ for $j = x, y$ as functions of ac frequency Ω . The plots are obtained at zero temperature for two different Γ , with $\Gamma_L = \Gamma_R = \Gamma/2$, $\vec{B} = B\vec{e}_z$, and $\Omega = \omega_L$. All energies are given in the units of ϵ_0 . The other parameters are set to: $\mu_L = 0.25$, $\mu_R = 0$, $\phi_L = 1.95$, $v_R^{\text{ac}} = 0$, $\phi_R = 0$, $\theta = 1.25$, $J = 0.005$, and $S = 100$. Each step or peak coincides with a change in the number of available channels for photon-assisted spin tunneling.

(or ϵ_3). During the exchange interaction with the precessing component of $\vec{S}(t)$, it absorbs an energy ω_L and flips its spin, ending up in the level ϵ_2 (or ϵ_4), and then tunnels into either of the leads. One photon-assisted spin-flip process through level ϵ_2 (or ϵ_4) for $\epsilon_1 \leq \mu_L \leq \epsilon_2$ (or $\epsilon_3 \leq \mu_L \leq \epsilon_4$) is presented in Fig. 8(b). In this case, an electron absorbs an energy $\Omega = \omega_L$ interacting with ac field in the left lead and enter the spin-up level ϵ_2 (or ϵ_4). Then, it emits energy quantum ω_L , flips its spin due to the interaction with the precessing component of the molecular spin, and tunnels into the right lead.

In Fig. 9 the time-averaged x and y components of STT are plotted as functions of ac frequency $\Omega = \omega_L$, for two different tunnel coupling constants $\Gamma = 0.04$ (solid lines) and $\Gamma = 0.12$ (dot-dashed lines), at zero temperature. The grid lines correspond to $\epsilon_i - \mu_L = \Omega$. For Ω such that $\epsilon_1 - \mu_L = \Omega$ the molecular quasienergy level ϵ_1 participates in photon-assisted spin transport, followed by an electron spin-flip and hence a finite STT. In this case $\langle T_x \rangle_t$ is initially enhanced while $\langle T_y \rangle_t$ has a minimum value and increases after $\Omega = \epsilon_1 - \mu_L$ [first grid line in Fig. 9]. As Ω increases the inequality (23) is satisfied for level ϵ_1 leading to a nonzero STT. With further increase of ac frequency Ω the photon-assisted spin transport begins to take place in the level ϵ_3 . Both $\langle T_x \rangle_t$ and $\langle T_y \rangle_t$ increase around $\Omega = \epsilon_3 - \mu_L$, after going to a local minimum, due to the fact that level ϵ_3 is now available for spin-flip tunneling processes.

For larger Ω the inequality (23) is satisfied for both ϵ_1 and ϵ_3 . Consequently, both $\langle T_x \rangle_t$, and $\langle T_y \rangle_t$ increase. Finally, as Ω increases further, level ϵ_2 also becomes available for photon-assisted spin tunneling, leading to the largest enhancement of both in-plane STT components. As Ω increases further, inequality (23) is satisfied for levels ϵ_1 , ϵ_2 , and ϵ_3 , and photon-assisted STT components are large and decreasing. After the level ϵ_4 becomes available for photon-assisted spin transport, both components $\langle T_x \rangle_t$ and $\langle T_y \rangle_t$ drop to zero. This is due to the previously mentioned antisymmetry. Namely, in this case, the contributions of the photon-assisted STTs for $\epsilon_1 < \mu_L < \epsilon_2$ and $\epsilon_3 < \mu_L < \epsilon_4$ are equal in magnitude but have

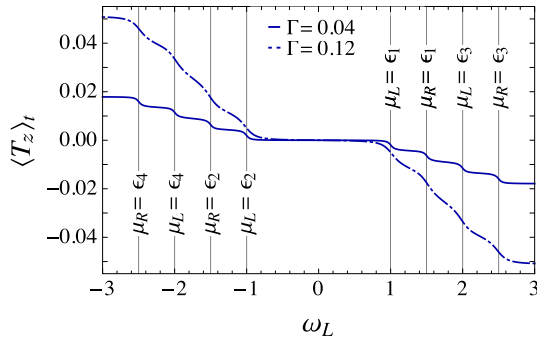


FIG. 10. Time-averaged z component of the spin-transfer torque $\langle T_z \rangle_t$ as a function of the Larmor precession frequency ω_L . The plots are obtained for two different tunneling rates Γ at zero temperature, with $\vec{B} = B\vec{e}_z$ and $\Gamma_L = \Gamma_R = \Gamma/2$. All energies are given in the units of ϵ_0 . The other parameters are set to: $\mu_L = 0.25, \mu_R = 0, \theta = 1.25, J = 0.005$, and $S = 100$. Each step corresponds to a spin-tunneling process involving a spin-flip.

opposite directions. Therefore, they cancel each other as μ_L satisfies both these inequalities simultaneously. Conditions of inequality (23) are relaxed for larger Γ due to the broadening of the levels ϵ_i .

The z component of the time-averaged STT, $\langle T_z \rangle_t$ is plotted as a function of the Larmor frequency ω_L in Fig. 10. This component does not contain contributions from photon-assisted spin tunneling but only from tunneling under dc-bias voltage, followed by an electron spin flip due to the interaction with the precessing component of the molecular spin $\vec{S}(t)$. In turn, an STT is exerted on the molecular spin. The STT component $\langle T_z \rangle_t$ is an odd function of ω_L since the change of the direction of \vec{B} gives negative ω_L . Each step in Fig. 10 denotes a new available spin-transport channel, and an additional spin-flip process, contributing to the STT, which takes place for $\mu_\xi = \epsilon_i$.

VI. CONCLUSIONS

In this paper we have theoretically studied photon-assisted spin and charge transport through a molecular magnet junction. The junction consists of single molecular orbital in the presence of a molecular spin precessing with Larmor frequency ω_L in a constant magnetic field. The orbital is connected to

two metal leads subject to harmonically varying chemical potentials with frequency Ω , treated as a perturbation. We used the Keldysh nonequilibrium Green's functions method to derive charge and spin currents and the spin-transfer torque. We employed the displacement current partitioning scheme of Wang *et al.* [48] to obtain gauge-invariant expressions for the dynamic conductance of the charge current. The dynamic response of the system is controlled by photon-assisted transport. In the low-ac-frequency limit this junction displays an inductive-like or capacitive-like behavior depending on the system parameters. When the chemical potentials are in resonance with a molecular quasienergy level ϵ_i , the real and imaginary components of the ac conductance both increase around the ac frequency which coincides with the Larmor frequency, after going to a local minimum, thus allowing to reveal the Larmor frequency by a conductance measurement. The photon-assisted x and y spin-current components consist of a dc part and a part that oscillates with frequency $2\omega_L$ for $\Omega = \omega_L$. This opens the possibility of experimentally investigating photon-assisted spin-transfer torque exerted on the molecular magnet, which can be detected through the presence of nonzero time-averaged contributions. By manipulating the phases of the harmonic potentials in the leads with respect to the precession, and the tilt angle between the magnetic field and the molecular spin, the control of the direction and the magnitude of the time-averaged photon-assisted spin current components and spin-transfer torque is achievable. Finally, in this work we present the nonperturbative Gilbert damping and other STT coefficients with respect to the coupling γ , in the zero ac frequency limit. Remarkably, the Gilbert damping vanishes in the strong-coupling limit.

In the future it might be interesting to investigate further transport properties like the current noise or the spin-torque noise, as well as to find ways to manipulate the magnetic moment using, e.g., ferromagnetic leads.

ACKNOWLEDGMENTS

We thank Gianluca Rastelli, Federica Haupt, and Cecilia Holmqvist for useful discussions. We gratefully acknowledge the financial support from the Deutsche Forschungsgemeinschaft through the SFB 767 "Controlled Nanosystems" and the SPP 1285 "Semiconductor Spintronics" and an ERC Advanced Grant "UltraPhase" of Alfred Leitenstorfer.

APPENDIX: EXPRESSIONS FOR SPIN-CURRENT COMPONENTS

Here we present the expressions for spin-current complex components $I_{Lx}(\omega_L)$ and $I_{Ly}(\omega_L)$, spin current $I_{Lz}^{\omega_L}$ in the presence of dc-bias voltage, and spin currents in the presence of ac voltage in terms of the matrix elements of the Green's functions $\hat{G}^{0r}(\epsilon)$ and $\hat{G}^{0a}(\epsilon)$.

The expressions for spin-current complex components introduced by Eq. (27) are given by

$$I_{Lx}(\omega_L) = -i \int \frac{d\epsilon}{4\pi} \left\{ \frac{\Gamma_L \Gamma_R}{\Gamma} [f_L(\epsilon) - f_R(\epsilon)] \left[\frac{\gamma G_{11}^{0r}(\epsilon + \omega_L) G_{22}^{0r}(\epsilon)}{|1 - \gamma^2 G_{11}^{0r}(\epsilon + \omega_L) G_{22}^{0r}(\epsilon)|^2} + \frac{2i\gamma \text{Im}\{G_{11}^{0r}(\epsilon)\} G_{22}^{0a}(\epsilon - \omega_L) + \gamma^3 |G_{11}^{0r}(\epsilon) G_{22}^{0r}(\epsilon - \omega_L)|^2}{|1 - \gamma^2 G_{11}^{0r}(\epsilon) G_{22}^{0r}(\epsilon - \omega_L)|^2} \right] \right. \\ \left. + \sum_{\xi, \zeta=L,R} \frac{\Gamma_\xi \Gamma_\zeta}{\Gamma} [f_\xi(\epsilon - \omega_L) - f_\zeta(\epsilon)] [\delta_{\zeta L} - \delta_{\xi L} \gamma^2 G_{11}^{0a}(\epsilon) G_{22}^{0r}(\epsilon - \omega_L)] \frac{\gamma G_{11}^{0r}(\epsilon) G_{22}^{0a}(\epsilon - \omega_L)}{|1 - \gamma^2 G_{11}^{0r}(\epsilon) G_{22}^{0r}(\epsilon - \omega_L)|^2} \right\}, \quad (\text{A1})$$

$$I_{Ly}(\omega_L) = i I_{Lx}(\omega_L), \quad (\text{A2})$$

$$\text{while } I_{Lz}^{\omega_L} = \int \frac{d\epsilon}{4\pi} \left\{ \frac{\Gamma_L \Gamma_R}{\Gamma} [f_L(\epsilon) - f_R(\epsilon)] \left[\frac{2\text{Im}\{G_{11}^{0r}(\epsilon)\}}{|1 - \gamma^2 G_{11}^{0r}(\epsilon) G_{22}^{0r}(\epsilon - \omega_L)|^2} - \frac{2\text{Im}\{G_{22}^{0r}(\epsilon)\}}{|1 - \gamma^2 G_{11}^{0r}(\epsilon + \omega_L) G_{22}^{0r}(\epsilon)|^2} \right] \right. \\ \left. + \sum_{\xi, \zeta=L,R} \Gamma_\xi \Gamma_\zeta [f_\xi(\epsilon - \omega_L) - f_\zeta(\epsilon)] (\delta_{\xi L} + \delta_{\zeta L}) \frac{\gamma^2 |G_{11}^{0r}(\epsilon) G_{22}^{0r}(\epsilon - \omega_L)|^2}{|1 - \gamma^2 G_{11}^{0r}(\epsilon) G_{22}^{0r}(\epsilon - \omega_L)|^2} \right\}. \quad (\text{A3})$$

The spin-current components in the presence of oscillating chemical potentials in the leads, introduced as the second term in Eq. (10), for $\xi = L$ can be expressed in the following way:

$$I_{Lj}^\Omega(t) = \sum_{\xi=L,R} \text{Re} \left\{ I_{L\xi}^j(\Omega) e^{-i(\Omega t + \phi_\xi)} + I_{L\xi}^j(-\Omega) e^{i(\Omega t + \phi_\xi)} \right\} e^{-i\omega_L t}, \quad j = x, y, \quad (\text{A4})$$

$$\text{where } I_{L\xi}^x(\Omega) = \gamma \Gamma_L \Gamma_\xi \frac{v_{ac}^\xi}{\Omega} \int \frac{d\epsilon}{4\pi} [f_\xi(\epsilon - \Omega) - f_\xi(\epsilon)] \\ \times \left\{ \frac{G_{11}^{0a}(\epsilon - \Omega) G_{22}^{0a}(\epsilon - \Omega - \omega_L) \{G_{11}^{0r}(\epsilon) + i \frac{\delta_{L\xi}}{\Gamma_\xi} [1 - \gamma^2 G_{11}^{0r}(\epsilon) G_{22}^{0r}(\epsilon - \omega_L)]\}}{[1 - \gamma^2 G_{11}^{0r}(\epsilon) G_{22}^{0r}(\epsilon - \omega_L)] [1 - \gamma^2 G_{11}^{0a}(\epsilon - \Omega) G_{22}^{0a}(\epsilon - \Omega - \omega_L)]} \right. \\ \left. + \frac{G_{11}^{0r}(\epsilon + \omega_L) G_{22}^{0r}(\epsilon) \{G_{22}^{0a}(\epsilon - \Omega) - i \frac{\delta_{L\xi}}{\Gamma_\xi} [1 - \gamma^2 G_{11}^{0a}(\epsilon - \Omega + \omega_L) G_{22}^{0a}(\epsilon - \Omega)]\}}{[1 - \gamma^2 G_{11}^{0a}(\epsilon - \Omega + \omega_L) G_{22}^{0a}(\epsilon - \Omega)] [1 - \gamma^2 G_{11}^{0r}(\epsilon + \omega_L) G_{22}^{0r}(\epsilon)]} \right\}, \quad (\text{A5})$$

$$\text{while } I_{L\xi}^y(\Omega) = i I_{L\xi}^x(\Omega), \quad (\text{A6})$$

$$\text{and } I_{Lz}^\Omega(t) = \sum_{\xi=L,R} \sum_{\sigma=\pm 1} \text{Re} \left\{ \Gamma_L \Gamma_\xi \frac{v_{ac}^\xi}{\Omega} \int \frac{d\epsilon}{4\pi} [f_\xi(\epsilon - \Omega) - f_\xi(\epsilon)] e^{-i(\Omega t + \phi_\xi)} \right. \\ \left. \times \frac{[\hat{\sigma}_z \hat{G}^{0r}(\epsilon) \hat{G}^{0a}(\epsilon - \Omega)]_{\sigma\sigma} \{2 - [1 - i \frac{\delta_{L\xi}}{\Gamma_\xi} (\Omega + i\Gamma)] [1 + \gamma^2 G_{-\sigma-\sigma}^{0r}(\epsilon_\sigma) G_{-\sigma-\sigma}^{0a}(\epsilon_\sigma - \Omega)]\}}{[1 - \gamma^2 G_{\sigma\sigma}^{0r}(\epsilon) G_{-\sigma-\sigma}^{0r}(\epsilon_\sigma)] [1 - \gamma^2 G_{\sigma\sigma}^{0a}(\epsilon - \Omega) G_{-\sigma-\sigma}^{0a}(\epsilon_\sigma - \Omega)]} \right\}. \quad (\text{A7})$$

-
- [1] A. Aviram and M. Ratner, *Chem. Phys. Lett.* **29**, 277 (1974).
[2] A. Nitzan and M. Ratner, *Science* **300**, 1384 (2003).
[3] J. C. Cuevas and E. Scheer, *Molecular Electronics: An Introduction to Theory and Experiment* (World Scientific, Singapore, 2010).
[4] J. Lehmann, S. Kohler, P. Hänggi, and A. Nitzan, *J. Chem. Phys.* **118**, 3283 (2003); S. Kohler, J. Lehmann, and P. Hänggi, *Phys. Rep.* **406**, 379 (2005).
[5] D. Dulić, S. J. van der Molen, T. Kudernac, H. T. Jonkman, J. J. D. de Jong, T. N. Bowden, J. van Esch, B. L. Feringa, and B. J. van Wees, *Phys. Rev. Lett.* **91**, 207402 (2003).
[6] S. van der Molen, J. Liao, T. Kudernac, J. Agustsson, L. Bernard, M. Calame, B. van Wees, B. Feringa, and C. Schönenberger, *Nano Lett.* **9**, 76 (2009).
[7] H. Song, Y. Kim, Y. H. Jang, H. Jeong, M. A. Reed, and T. Lee, *Nature (London)* **462**, 1039 (2009).
[8] Y. Kim, T. J. Hellmuth, D. Sysoiev, F. Pauly, T. Pietsch, J. Wolf, A. Erbe, T. Huhn, U. Groth, U. E. Steiner, and E. Scheer, *Nano Lett.* **12**, 3736 (2012).
[9] R. Sessoli, D. Gatteschi, A. Caneschi, and M. A. Novak, *Nature (London)* **365**, 141 (1993).
[10] W. Wernsdorfer and R. Sessoli, *Science* **284**, 133 (1999).
[11] J. R. Friedman, M. P. Sarachik, J. Tejada, and R. Ziolo, *Phys. Rev. Lett.* **76**, 3830 (1996); L. Thomas, F. Lioni, R. Ballou, D. Gatteschi, R. Sessoli, and B. Barbara, *Nature (London)* **383**, 145 (1996); C. Sangregorio, T. Ohm, C. Paulsen, R. Sessoli, and D. Gatteschi, *Phys. Rev. Lett.* **78**, 4645 (1997); W. Wernsdorfer, M. Murugesu, and G. Christou, *ibid.* **96**, 057208 (2006).
[12] A. Ardavan, O. Rival, J. J. L. Morton, S. J. Blundell, A. M. Tyryshkin, G. A. Timco, and R. E. P. Winpenny, *Phys. Rev. Lett.* **98**, 057201 (2007); S. Carretta, P. Santini, G. Amoretti, T. Guidi, J. R. D. Copley, Y. Qiu, R. Caciuffo, G. A. Timco, and R. E. P. Winpenny, *ibid.* **98**, 167401 (2007); S. Bertaina, S. Gambarelli, T. Mitra, B. Tsukerblat, A. Muller, and B. Barbara, *Nature (London)* **453**, 203 (2008).
[13] A. Garg, *EuroPhys. Lett.* **22**, 205 (1993); W. Wernsdorfer, N. E. Chakov, and G. Christou, *Phys. Rev. Lett.* **95**, 037203 (2005).
[14] D. D. Awschalom, M. E. Flatte, and N. Samarth, *Spintronics* (Scientific American, New York, 2002), pp. 67–73.
[15] S. Voss, M. Fonin, U. Rüdiger, M. Burgert, and U. Groth, *Appl. Phys. Lett.* **90**, 133104 (2007).
[16] E. Burzuri, A. S. Zyazin, A. Cornia, and H. S. J. van der Zant, *Phys. Rev. Lett.* **109**, 147203 (2012).
[17] S. Kahle, Z. Deng, N. Malinowski, C. Tonnoir, A. Forment-Aliaga, N. Thontasen, G. Rinke, D. Le, V. Turkowski, T. Rahman, S. Rauschenbach, M. Ternes, and K. Kern, *Nano Lett.* **12**, 518 (2012).
[18] N. S. Wingreen, A.-P. Jauho, and Y. Meir, *Phys. Rev. B* **48**, 8487 (1993).
[19] A.-P. Jauho, N. S. Wingreen, and Y. Meir, *Phys. Rev. B* **50**, 5528 (1994).
[20] A.-P. Jauho and H. Haug, *Quantum Kinetics in Transport and Optics of Semiconductors* (Springer, Berlin, 1998).
[21] B. Dong, H. L. Cui, and X. L. Lei, *Phys. Rev. B* **69**, 205315 (2004).

- [22] Y. Zhu, J. Maciejko, T. Ji, H. Guo, and J. Wang, *Phys. Rev. B* **71**, 075317 (2005).
- [23] E. Runge and E. K. U. Gross, *Phys. Rev. Lett.* **52**, 997 (1984).
- [24] G. Stefanucci and C. O. Almbladh, *Europhys. Lett.* **67**, 14 (2004).
- [25] K. Burke and R. Car, and R. Gebauer, *Phys. Rev. Lett.* **94**, 146803 (2005).
- [26] S. Kurth, G. Stefanucci, C. O. Almbladh, A. Rubio, and E. K. U. Gross, *Phys. Rev. B* **72**, 035308 (2005).
- [27] E. Khosravi, S. Kurth, G. Stefanucci, and E. K. U. Gross, *Appl. Phys. A* **93**, 355 (2008).
- [28] G. Q. Li, S. Welack, M. Schreiber, and U. Kleinekathöfer, *Phys. Rev. B* **77**, 075321 (2008).
- [29] A. H. L. Dayem and R. J. Martin, *Phys. Rev. Lett.* **8**, 246 (1962).
- [30] P. K. Tien and J. P. Gordon, *Phys. Rev.* **129**, 647 (1963).
- [31] G. Platero and R. Aguado, *Phys. Rep.* **395**, 1 (2004).
- [32] W. Zheng, Y. Wei, J. Wang, and H. Guo, *Phys. Rev. B* **61**, 13121 (2000); J. Wu, B. Wang, J. Wang, and H. Guo, *ibid.* **72**, 195324 (2005).
- [33] A. Tikhonov, R. D. Coalson, and Y. Dahnovsky, *J. Chem. Phys.* **116**, 10909 (2002).
- [34] U. Kleinekathöfer, G.-Q. Li, S. Welack, and M. Schreiber, *Europhys. Lett.* **75**, 139 (2006); G.-Q. Li and M. Schreiber, and U. Kleinekathöfer, *ibid.* **79**, 27006 (2007).
- [35] J. K. Viljas and J. C. Cuevas, *Phys. Rev. B* **75**, 075406 (2007); J. K. Viljas, F. Pauly, and J. C. Cuevas, *ibid.* **76**, 033403 (2007); **77**, 155119 (2008).
- [36] L.-Y. Hsu and H. Rabitz, *Phys. Rev. Lett.* **109**, 186801 (2012).
- [37] B. D. Fainberg, *Phys. Rev. B* **88**, 245435 (2013).
- [38] M. Chauvin, P. vom Stein, H. Pothier, P. Joyez, M. E. Huber, D. Esteve, and C. Urbina, *Phys. Rev. Lett.* **97**, 067006 (2006).
- [39] D. C. Guhr, D. Rettinger, J. Boneberg, A. Erbe, P. Leiderer, and E. Scheer, *Phys. Rev. Lett.* **99**, 086801 (2007).
- [40] N. Ittah, G. Noy, I. Yutsis, and Y. Selzer, *Nano Lett.* **9**, 1615 (2009).
- [41] G. Noy, A. Ophir, and Y. Selzer, *Angew. Chem. Int. Ed.* **49**, 5734 (2010).
- [42] M. A. Mangold, M. Calame, M. Mayor, and A. W. Holleitner, *J. Am. Chem. Soc.* **133**, 12185 (2011).
- [43] S. Loth, K. von Bergmann, M. Ternes, A. F. Otte, C. P. Lutz, and A. J. Heinrich, *Nat. Phys.* **6**, 340 (2010).
- [44] M. Büttiker, H. Thomas, and A. Prêtre, *Phys. Lett. A* **180**, 364 (1993).
- [45] M. Büttiker, A. Prêtre, and H. Thomas, *Phys. Rev. Lett.* **70**, 4114 (1993).
- [46] M. Büttiker, *J. Phys. Cond. Mat.* **5**, 9361 (1993).
- [47] Y. Wei and J. Wang, *Phys. Rev. B* **79**, 195315 (2009).
- [48] B. G. Wang, J. Wang, and H. Guo, *Phys. Rev. Lett.* **82**, 398 (1999).
- [49] J. C. Slonczewski, *J. Magn. Magn. Mater.* **159**, L1 (1996).
- [50] L. Berger, *Phys. Rev. B* **54**, 9353 (1996).
- [51] Y. Tserkovnyak, A. Brataas, G. E. W. Bauer, and B. I. Halperin, *Rev. Mod. Phys.* **77**, 1375 (2005).
- [52] D. C. Ralph and M. D. Stiles, *J. Magn. Magn. Mater.* **320**, 1190 (2008).
- [53] J. C. Slonczewski, *Phys. Rev. B* **71**, 024411 (2005).
- [54] C. Timm and F. Elste, *Phys. Rev. B* **73**, 235304 (2006); F. Elste and C. Timm, *ibid.* **73**, 235305 (2006).
- [55] M. Misiorny and J. Barnaś, *Phys. Rev. B* **75**, 134425 (2007).
- [56] J. C. Sankey, Y-T. Cui, J. Z. Sun, J. C. Slonczewski, R. A. Buhrman, and D. C. Ralph, *Nat. Phys.* **4**, 67 (2008).
- [57] J. Xiao, G. E. W. Bauer, and A. Brataas, *Phys. Rev. B* **77**, 224419 (2008).
- [58] F. Delgado, J. J. Palacios, and J. Fernández-Rossier, *Phys. Rev. Lett.* **104**, 026601 (2010).
- [59] N. Bode, L. Arrachea, G. S. Lozano, T. S. Nunner, and F. von Oppen, *Phys. Rev. B* **85**, 115440 (2012).
- [60] G. Floquet, *Ann. Sci. École Normale Supérieure* **12**, 47 (1883).
- [61] Jon H. Shirley, Ph.D. thesis, California Institute of Technology, 1963.
- [62] M. Grifoni and P. Hänggi, *Phys. Rep.* **304**, 229 (1998).
- [63] B. H. Wu and C. Timm, *Phys. Rev. B* **81**, 075309 (2010).
- [64] M. Filipović, C. Holmqvist, F. Haupt, and W. Belzig, *Phys. Rev. B* **87**, 045426 (2013); **88**, 119901 (2013).
- [65] T. L. Gilbert, *IEEE Trans. Magn.* **40**, 3443 (2004).
- [66] C. Kittel, *Phys. Rev.* **73**, 155 (1948).
- [67] B. Wang, J. Wang, and H. Guo, *Phys. Rev. B* **67**, 092408 (2003).
- [68] H. Bruus and K. Flensberg, *Many-Body Quantum Theory in Condensed Matter Physics* (Oxford University Press, Oxford, 2004).
- [69] P. Stadler, W. Belzig, and G. Rastelli, *Phys. Rev. Lett.* **113**, 047201 (2014).
- [70] A. Prêtre and H. Thomas, and M. Büttiker, *Phys. Rev. B* **54**, 8130 (1996).
- [71] M. Büttiker and T. Christen, in *Quantum Transport in Semiconductor Submicron Structures*, edited by B. Kramer (Kluwer Academic, Dordrecht, 1996).
- [72] M. Büttiker, A. Prêtre, and H. Thomas, *Z. Phys. B: Conens. Matter* **94**, 133 (1994).
- [73] V. Gasparian, T. Christen, and M. Büttiker, *Phys. Rev. A* **54**, 4022 (1996).

Shot noise of charge and spin transport in a junction with a precessing molecular spin

Milena Filipović and Wolfgang Belzig

Fachbereich Physik, Universität Konstanz, D-78457 Konstanz, Germany
 (Received 17 November 2017; revised manuscript received 19 February 2018; published 26 March 2018; corrected 13 April 2018)

Magnetic molecules and nanomagnets can be used to influence the electronic transport in mesoscopic junction. In a magnetic field, the precessional motion leads to resonances in the dc- and ac-transport properties of a nanocontact, in which the electrons are coupled to the precession. Quantities such as the dc conductance or the ac response provide valuable information, such as the level structure and the coupling parameters. Here, we address the current-noise properties of such contacts. This encompasses the charge current and spin-torque shot noise, which both show a steplike behavior as functions of bias voltage and magnetic field. The charge-current noise shows pronounced dips around the steps, which we trace back to interference effects of electrons in quasienergy levels coupled by the molecular spin precession. We show that some components of the noise of the spin-torque currents are directly related to the Gilbert damping, and hence are experimentally accessible. Our results show that the noise characteristics allow us to investigate in more detail the coherence of spin transport in contacts containing magnetic molecules.

DOI: [10.1103/PhysRevB.97.115441](https://doi.org/10.1103/PhysRevB.97.115441)**I. INTRODUCTION**

Shot noise of charge current has become an active research topic in recent decades, since it enables the investigation of microscopic transport properties, which cannot be obtained from the charge current or conductance [1]. It has been demonstrated that spin-flip induced fluctuations in diffusive conductors connected to ferromagnetic leads enhance the noise power, approaching the Poissonian value [2,3]. Accordingly, the Fano factor defined as $F = S(0)/e|I|$, which describes the deviation of the shot noise from the average charge current, equals 1 in this case. On the other hand, it has been shown that shot noise in a ferromagnet–quantum-dot–ferromagnet system with antiparallel magnetization alignments can be suppressed due to spin flip, with $F < 1/2$ [4].

The quantum-interference phenomenon, which is a manifestation of the wave nature of electrons, has attracted a lot of attention. The quantum-interference effects occur between coherent electron waves in nanoscale junctions [5]. Quantum interference in molecular junctions influences their electronic properties [6–10]. The Fano effect [11] due to the interference between a discrete state and the continuum has an important role in investigation of the interference effects in nanojunctions, which behave in an analogous way, and are manifested in the conductance or noise spectra [5,12,13]. Particularly interesting examples involve spin-flip processes, such as in the presence of Rashba spin-orbit interaction [14,15], a rotating magnetic field [16], or in the case of magnetotransport [17–19].

In the domain of spin transport it is interesting to investigate the noise properties, as the discrete nature of electron spin leads to the correlations between spin-carrying particles. The spin current is usually a nonconserved quantity that is difficult to measure, and its shot noise depends on spin-flip processes leading to spin-current correlations with opposite spins [20–22]. The investigation of spin-dependent scattering, spin accumulation [23], and attractive or repulsive interactions

in mesoscopic systems can be obtained using the shot noise of a spin current [24], as well as measuring the spin relaxation time [20,24]. Even in the absence of charge current, a nonzero spin current and its noise can still emerge [22,25,26]. Several works have studied the shot noise of a spin current using, e.g., the nonequilibrium Green's function method and scattering matrix theory [22,27–29].

It was demonstrated that magnetization noise originates from transferred spin current noise via a fluctuating spin-transfer torque in ferromagnetic-normal-ferromagnetic systems [30] and magnetic tunnel junctions [31]. Experimentally, spin Hall noise measurements have been demonstrated [32], and in a similar fashion the spin-current shot noise due to magnon currents can be related to the nonquantized spin of interacting magnons in ferri-, ferro-, and antiferromagnets [33,34]. Quantum noise generated from the scatterings between the magnetization of a nanomagnet and spin-polarized electrons has been studied theoretically as well [35,36]. The shot noise of spin-transfer torque was studied recently using a magnetic quantum dot connected to two noncollinear magnetic contacts [29]. According to the definition of spin-transfer torque [37,38], both autocorrelations and cross-correlations of the spin-current components contribute to the spin-torque noise.

In this article, we study theoretically the noise of charge and spin currents and spin-transfer torque in a junction connected to two normal metallic leads. The transport occurs via a single electronic energy level interacting with a molecular magnet in a constant magnetic field. The spin of the molecular magnet precesses around the magnetic field with the Larmor frequency, which is kept undamped, e.g., due to external driving. The electronic level may belong to a neighboring quantum dot or it may be an orbital of the molecular magnet itself. The electronic level and the molecular spin are coupled via exchange interaction. We derive expressions for the noise components using the Keldysh nonequilibrium Green's functions formalism [39–41].

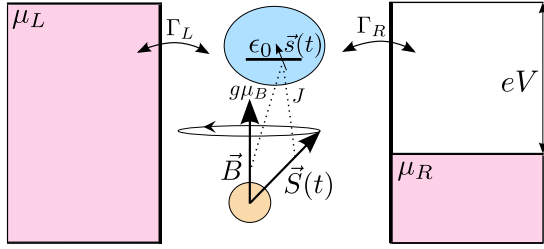


FIG. 1. Tunneling through a single molecular level with energy ϵ_0 in the presence of a precessing molecular spin $\vec{S}(t)$ in a constant magnetic field \vec{B} , connected to two metallic leads with chemical potentials μ_{ξ} , $\xi = L, R$. The molecular level is coupled to the spin of the molecule via exchange interaction with the coupling constant J . The applied dc-bias voltage $eV = \mu_L - \mu_R$, and the tunnel rates are Γ_{ξ} .

The noise of charge current is contributed by both elastic processes driven by the bias voltage, and inelastic tunneling processes driven by the molecular spin precession. We observe diplike features in the shot noise due to inelastic tunneling processes and destructive quantum interference between electron transport channels involved in the spin-flip processes. The driving mechanism of the correlations of the spin-torque components in the same spatial direction involves both the precession of the molecular spin and the bias voltage. Hence, they are contributed by elastic and inelastic processes, with the change of energy equal to one or two Larmor frequencies. The nonzero correlations of the perpendicular spin-torque components are driven by the molecular spin precession, with contributions of spin-flip tunneling processes only. These components are related to the previously obtained Gilbert damping coefficient [42,43], which characterize the Gilbert damping term of the spin-transfer torque [44–46] at arbitrary temperature.

The article is organized as follows. The model and theoretical framework based on the Keldysh nonequilibrium Green's functions formalism [39–41] are given in Sec. II. Here we derive expressions for the noise of spin and charge currents. In Sec. III we investigate and analyze the properties of the charge-current shot noise. In Sec. IV, we derive and analyze the noise of spin-transfer torque. The conclusions are given in Sec. V.

II. MODEL AND THEORETICAL FRAMEWORK

The junction under consideration consists of a noninteracting single-level quantum dot in the presence of a precessing molecular spin in a magnetic field along the z axis, $\vec{B} = B\vec{e}_z$, coupled to two noninteracting leads (Fig. 1).

The junction is described by the Hamiltonian

$$\hat{H}(t) = \sum_{\xi \in \{L, R\}} \hat{H}_{\xi} + \hat{H}_T + \hat{H}_D(t) + \hat{H}_S, \quad (1)$$

where

$$\hat{H}_{\xi} = \sum_{k, \sigma} \epsilon_{k\xi} \hat{c}_{k\sigma\xi}^{\dagger} \hat{c}_{k\sigma\xi} \quad (2)$$

is the Hamiltonian of contact $\xi = L, R$. The spin- (up or down) state of the electrons is denoted by the subscript $\sigma = \uparrow, \downarrow = 1, 2 = \pm 1$. The tunnel coupling between the quantum dot and the leads reads

$$\hat{H}_T = \sum_{k, \sigma, \xi} [V_{k\xi} \hat{c}_{k\sigma\xi}^{\dagger} \hat{d}_{\sigma} + V_{k\xi}^* \hat{d}_{\sigma}^{\dagger} \hat{c}_{k\sigma\xi}], \quad (3)$$

with spin-independent matrix element $V_{k\xi}$. The creation (annihilation) operators of the electrons in the leads and the quantum dot are given by $\hat{c}_{k\sigma\xi}^{\dagger}$ ($\hat{c}_{k\sigma\xi}$) and $\hat{d}_{\sigma}^{\dagger}$ (\hat{d}_{σ}). The Hamiltonian of the electronic level equals

$$\hat{H}_D(t) = \sum_{\sigma} \epsilon_0 \hat{d}_{\sigma}^{\dagger} \hat{d}_{\sigma} + g\mu_B \hat{s} \vec{B} + J \hat{s} \vec{S}(t). \quad (4)$$

The first term in Eq. (4) is the Hamiltonian of the non-interacting single-level quantum dot with energy ϵ_0 . The second term describes the electronic spin in the dot, $\hat{s} = (\hbar/2) \sum_{\sigma\sigma'} (\vec{\sigma})_{\sigma\sigma'} \hat{d}_{\sigma}^{\dagger} \hat{d}_{\sigma'}$, in the presence of a constant magnetic field \vec{B} , and the third term represents the exchange interaction between the electronic spin and the molecular spin $\vec{S}(t)$. The vector of the Pauli matrices is given by $\hat{\sigma} = (\hat{\sigma}_x, \hat{\sigma}_y, \hat{\sigma}_z)^T$. The g -factor of the electron and the Bohr magneton are g and μ_B , whereas J is the exchange coupling constant between the electronic and molecular spins.

The last term of Eq. (4) can be written as

$$\hat{H}_S = g\mu_B \vec{S} \vec{B}, \quad (5)$$

and it represents the energy of the molecular spin \vec{S} in the magnetic field \vec{B} . We assume that $|\vec{S}| \gg \hbar$, and neglecting quantum fluctuations we treat \vec{S} as a classical variable. The magnetic field \vec{B} generates a torque on the spin \vec{S} that causes the spin to precess around the field axis with Larmor frequency $\omega_L = g\mu_B B/\hbar$. The dynamics of the molecular spin is kept constant, which can be realized, e.g., by external rf fields [47] to cancel the loss of magnetic energy due to the interaction with the itinerant electrons. Thus, the precessing spin $\vec{S}(t)$ pumps spin currents into the leads, but its dynamics remains unaffected by the spin currents, i.e., the spin-transfer torque exerted on the molecular spin is compensated by the above-mentioned external means. The undamped precessional motion of the molecular spin, supported by the external sources, is then given by $\vec{S}(t) = S_{\perp} \cos(\omega_L t) \vec{e}_x + S_{\perp} \sin(\omega_L t) \vec{e}_y + S_z \vec{e}_z$, with θ the tilt angle between \vec{B} and \vec{S} , and $S_{\perp} = S \sin(\theta)$ the magnitude of the instantaneous projection of $\vec{S}(t)$ onto the xy plane. The component of the molecular spin along the field axis equals $S_z = S \cos(\theta)$.

The charge- and spin-current operators of the lead ξ are given by the Heisenberg equation [39,40]

$$\hat{I}_{\xi v}(t) = q_v \frac{d\hat{N}_{\xi v}}{dt} = q_v \frac{i}{\hbar} [\hat{H}, \hat{N}_{\xi v}], \quad (6)$$

where $[\cdot, \cdot]$ denotes the commutator, while $\hat{N}_{L\nu} = \sum_{k, \sigma, \sigma'} \hat{c}_{k\sigma L}^{\dagger} (\sigma_{\nu})_{\sigma\sigma'} \hat{c}_{k\sigma' L}$ is the charge ($\nu = 0$ and $q_0 = -e$) and spin ($\nu = x, y, z$ and $q_{\nu \neq 0} = \hbar/2$) occupation number operator of the contact ξ . Here $\hat{\sigma}_0 = \hat{1}$ is the identity matrix. Taking into account that only the tunneling Hamiltonian \hat{H}_T generates a nonzero commutator in Eq. (6), the current operator $\hat{I}_{\xi v}(t)$ can be expressed as

$$\hat{I}_{\xi v}(t) = -q_v \frac{i}{\hbar} \sum_{\sigma, \sigma'} (\sigma_{\nu})_{\sigma\sigma'} \hat{I}_{\xi, \sigma\sigma'}(t), \quad (7)$$

where the operator component $\hat{I}_{\xi, \sigma\sigma'}(t)$ equals

$$\hat{I}_{\xi, \sigma\sigma'}(t) = \sum_k [V_{k\xi} \hat{c}_{k\sigma\xi}^{\dagger}(t) \hat{d}_{\sigma'}(t) - V_{k\xi}^* \hat{d}_{\sigma}^{\dagger}(t) \hat{c}_{k\sigma'\xi}(t)]. \quad (8)$$

The nonsymmetrized noise of charge and spin current is defined as the correlation between fluctuations of currents $I_{\xi\nu}$ and $I_{\zeta\mu}$ [1,40],

$$S_{\xi\zeta}^{\nu\mu}(t, t') = \langle \delta \hat{I}_{\xi\nu}(t) \delta \hat{I}_{\zeta\mu}(t') \rangle, \quad (9)$$

with $\nu = \mu = 0$ for the charge-current noise. The fluctuation operator of the charge and spin current in lead ξ is given by

$$\delta \hat{I}_{\xi\nu}(t) = \hat{I}_{\xi\nu}(t) - \langle \hat{I}_{\xi\nu}(t) \rangle. \quad (10)$$

Using Eqs. (7) and (10), the noise becomes

$$S_{\xi\zeta}^{\nu\mu}(t, t') = -\frac{q_\nu q_\mu}{\hbar^2} \sum_{\sigma\sigma'} \sum_{\lambda\eta} (\sigma_\nu)_{\sigma\sigma'} (\sigma_\mu)_{\lambda\eta} S_{\xi\zeta}^{\sigma\sigma', \lambda\eta}(t, t'), \quad (11)$$

where $S_{\xi\zeta}^{\sigma\sigma', \lambda\eta}(t, t') = \langle \delta \hat{I}_{\xi, \sigma\sigma'}(t) \delta \hat{I}_{\zeta, \lambda\eta}(t') \rangle$. The formal expression for $S_{\xi\zeta}^{\nu\mu}(t, t')$ is given by Eq. (A10) in the Appendix, where it is obtained using Eq. (11) and Eqs. (A1)–(A9).

Using Fourier transformations of the central-region Green's functions given by Eqs. (A6)–(A8) and self-energies in the wide-band limit, the correlations given by Eq. (A9) can be further simplified. Some correlation functions are not just functions of the time difference $t - t'$. Thus, as in Ref. [48], we used a Wigner representation assuming that in experiments fluctuations are measured on time scales much larger than the driving period $\mathcal{T} = 2\pi/\omega_L$, which is the period of one molecular spin precession. The Wigner coordinates are given by $T' = (t + t')/2$ and $\tau = t - t'$, while the correlation functions are defined as

$$S_{\xi\zeta}^{\sigma\sigma', \lambda\eta}(\tau) = \frac{1}{\mathcal{T}} \int_0^{\mathcal{T}} dt \langle \delta \hat{I}_{\xi, \sigma\sigma'}(t + \tau) \delta \hat{I}_{\zeta, \lambda\eta}(t) \rangle. \quad (12)$$

The Fourier transform of $S_{\xi\zeta}^{\sigma\sigma', \lambda\eta}(\tau)$ is given by

$$S_{\xi\zeta}^{\sigma\sigma', \lambda\eta}(\Omega, \Omega') = 2\pi \delta(\Omega - \Omega') S_{\xi\zeta}^{\sigma\sigma', \lambda\eta}(\Omega), \quad (13)$$

where

$$S_{\xi\zeta}^{\sigma\sigma', \lambda\eta}(\Omega) = \int d\tau e^{i\Omega\tau} S_{\xi\zeta}^{\sigma\sigma', \lambda\eta}(\tau). \quad (14)$$

For the correlations that depend only on $t - t'$, the Wigner representation is identical to the standard representation.

The symmetrized noise of charge and spin currents reads [1,40]

$$S_{\xi\zeta S}^{\nu\mu}(t, t') = \frac{1}{2} \langle \{ \delta \hat{I}_{\xi\nu}(t), \delta \hat{I}_{\zeta\mu}(t') \} \rangle, \quad (15)$$

where $\{, \}$ denotes the anticommutator. According to Eqs. (11), (12), (14), and (15), in the Wigner representation the nonsymmetrized noise spectrum reads

$$\begin{aligned} S_{\xi\zeta}^{\nu\mu}(\Omega) &= \int d\tau e^{i\Omega\tau} S_{\xi\zeta}^{\nu\mu}(\tau) \\ &= \int d\tau e^{i\Omega\tau} \frac{1}{\mathcal{T}} \int_0^{\mathcal{T}} dt \langle \delta \hat{I}_{\xi\nu}(t + \tau) \delta \hat{I}_{\zeta\mu}(t) \rangle \\ &= -\frac{q_\nu q_\mu}{\hbar^2} \sum_{\sigma\sigma'} \sum_{\lambda\eta} (\sigma_\nu)_{\sigma\sigma'} (\sigma_\mu)_{\lambda\eta} S_{\xi\zeta}^{\sigma\sigma', \lambda\eta}(\Omega), \end{aligned} \quad (16)$$

while the symmetrized noise spectrum equals

$$\begin{aligned} S_{\xi\zeta S}^{\nu\mu}(\Omega) &= \frac{1}{2} [S_{\xi\zeta}^{\nu\mu}(\Omega) + S_{\xi\zeta}^{\mu\nu}(-\Omega)] \\ &= -\frac{q_\nu q_\mu}{2\hbar^2} \sum_{\sigma\sigma'} \sum_{\lambda\eta} (\sigma_\nu)_{\sigma\sigma'} (\sigma_\mu)_{\lambda\eta} S_{\xi\zeta S}^{\sigma\sigma', \lambda\eta}(\Omega), \end{aligned} \quad (17)$$

where $S_{\xi\zeta S}^{\sigma\sigma', \lambda\eta}(\Omega) = [S_{\xi\zeta}^{\sigma\sigma', \lambda\eta}(\Omega) + S_{\xi\zeta}^{\lambda\eta, \sigma\sigma'}(-\Omega)]/2$. The experimentally most easily accessible quantity is the zero-frequency noise power.

III. SHOT NOISE OF CHARGE CURRENT

For the charge-current noise, it is convenient to drop the superscripts $\nu = \mu = 0$. The charge-current noise spectrum can be obtained as [24]

$$S_{\xi\zeta}(\Omega) = -\frac{e^2}{\hbar^2} [S_{\xi\zeta}^{11,11} + S_{\xi\zeta}^{11,22} + S_{\xi\zeta}^{22,11} + S_{\xi\zeta}^{22,22}](\Omega). \quad (18)$$

In this section, we analyze the zero-frequency noise power of the charge current $S_{\xi\zeta} = S_{\xi\zeta}(0)$ at zero temperature. Taking into account that thermal noise disappears at zero temperature, the only contribution to the charge-current noise comes from the shot noise. The tunnel couplings between the molecular orbital and the leads, $\Gamma_\xi(\epsilon) = 2\pi \sum_k |V_{k\xi}|^2 \delta(\epsilon - \epsilon_{k\xi})$, are considered symmetric and in the wide-band limit $\Gamma_L = \Gamma_R = \Gamma/2$.

The average charge current from lead ξ can be expressed as

$$\begin{aligned} I_\xi &= \frac{e\Gamma_\xi\Gamma_\zeta}{\hbar} \int \frac{d\epsilon}{2\pi} [f_\xi(\epsilon) - f_\zeta(\epsilon)] \\ &\times \sum_{\substack{\sigma\sigma' \\ \sigma \neq \sigma'}} \frac{|G_{\sigma\sigma}^{0r}(\epsilon)|^2 [1 + \gamma^2 |G_{\sigma\sigma'}^{0r}(\epsilon + \sigma'\omega_L)|^2]}{|1 - \gamma^2 G_{\sigma\sigma}^{0r}(\epsilon) G_{\sigma\sigma'}^{0r}(\epsilon + \sigma'\omega_L)|^2}, \end{aligned} \quad (19)$$

where $\xi \neq \zeta$, while $G_{\sigma\sigma}^{0r}(\epsilon)$ are matrix elements of $\hat{G}^{0r}(\epsilon) = [\epsilon - \epsilon_0 + i \sum_\xi \Gamma_\xi/2 - \hat{\sigma}_z(g\mu_B B + JS_z)/2]^{-1}$ [49,50]. In the above expression, $f_\xi(\epsilon) = [e^{(\epsilon - \mu_\xi)/k_B T} + 1]^{-1}$ is the Fermi-Dirac distribution of the electrons in lead ξ , with k_B the Boltzmann constant and T the temperature. The conservation of the charge current implies that $S_{LL}(0) + S_{LR}(0) = 0$. Thus, it is sufficient to study only one correlation function.

Tuning the parameters in the system such as the bias voltage $eV = \mu_L - \mu_R$ (where μ_L and μ_R are the chemical potentials of the leads), B , and the tilt angle θ , the shot noise can be controlled and minimized. The shot noise in the small precession frequency limit $\omega_L \ll k_B T$ is in agreement with Ref. [22] for $eV = 0$.

In Fig. 2(a) we present the average charge current as a staircase function of bias voltage, where the bias is varied in four different ways. In the presence of the external magnetic field and the precessing molecular spin, the initially degenerate electronic level with energy ϵ_0 results in four nondegenerate transport channels, which has an important influence on the noise. Each step corresponds to a new available transport channel. The transport channels are located at the Floquet quasienergies [43] $\epsilon_1 = \epsilon_0 - (\omega_L/2) - (JS/2)$, $\epsilon_2 = \epsilon_0 + (\omega_L/2) - (JS/2)$, $\epsilon_3 = \epsilon_0 - (\omega_L/2) + (JS/2)$, and $\epsilon_4 = \epsilon_0 + (\omega_L/2) + (JS/2)$, which are calculated using the Floquet theorem [16,51–54].

The correlated current fluctuations give nonzero noise power, which is presented in Fig. 2(b). The noise power shows the molecular quasienergy spectrum, and each step or diplike feature in the noise denotes the energy of a new available transport channel. The noise has two steps and two diplike features that correspond to these resonances. Charge current and noise power are saturated for large bias voltages. If the Fermi levels of the leads lie below the resonances, the shot

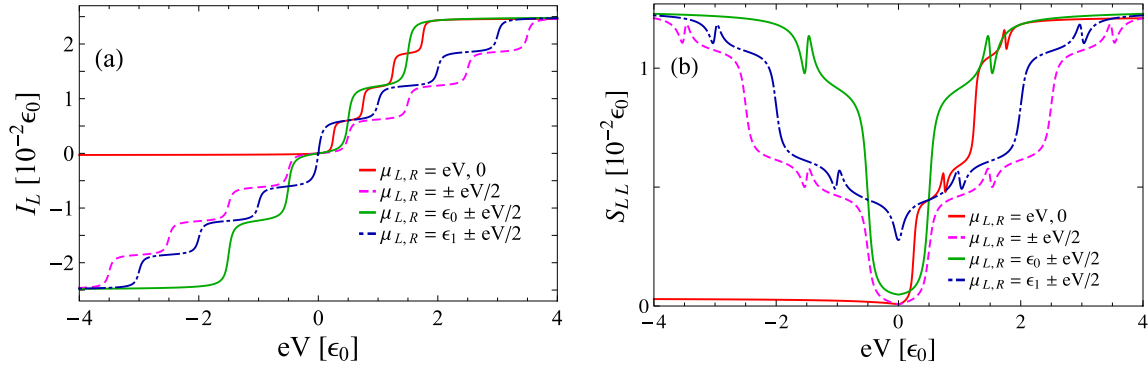


FIG. 2. (a) Charge current I_L and (b) autocorrelation shot noise S_{LL} as functions of bias-voltage eV . All plots are obtained at zero temperature, with $\vec{B} = B\vec{e}_z$. The other parameters are $\Gamma_L = \Gamma_R = \Gamma/2$, $\Gamma = 0.05 \epsilon_0$, $\omega_L = 0.5 \epsilon_0$, $J = 0.01 \epsilon_0$, $S = 100$, and $\theta = \pi/2$. The molecular quasienergy levels are located at $\epsilon_1 = 0.25 \epsilon_0$, $\epsilon_2 = 0.75 \epsilon_0$, $\epsilon_3 = 1.25 \epsilon_0$, and $\epsilon_4 = 1.75 \epsilon_0$.

noise approaches zero for $eV \rightarrow 0$ [red and dashed pink lines in Fig. 2(b)]. This is due to the fact that a small number of electron states can participate in transport inside this small bias window and both current and noise are close to 0. If the bias voltage is varied with respect to the resonant energy ϵ_1 such that $\mu_{L,R} = \epsilon_1 \pm eV/2$ [dot-dashed blue line in Fig. 2(b)], or with respect to ϵ_0 such that $\mu_{L,R} = \epsilon_0 \pm eV/2$ [green line in Fig. 2(b)], we observe a valley at zero bias $eV = 0$, which corresponds to $\mu_L = \mu_R = \epsilon_1$ in the first case and nonzero noise in the second case. For $eV = 0$, the charge current is zero, but the precession-assisted inelastic processes involving the absorption of an energy quantum ω_L give rise to the noise here.

At small bias voltage, the Fano factor $F = S_{LL}/e|I_L|$ is inversely proportional to eV and hence diverges as $eV \rightarrow 0$, indicating that the noise is super-Poissonian, as depicted in Fig. 3. Due to absorption (emission) processes [16] and quantum-interference effects, the Fano factor is a deformed steplike function, where each step corresponds to a resonance. As the bias voltage is increased, the noise is enhanced since the number of correlated electron pairs increases with the increase of the Fermi level. For larger bias, due to the absorption and emission of an energy quantum ω_L , electrons can jump to a level with higher energy or lower level during the transport,

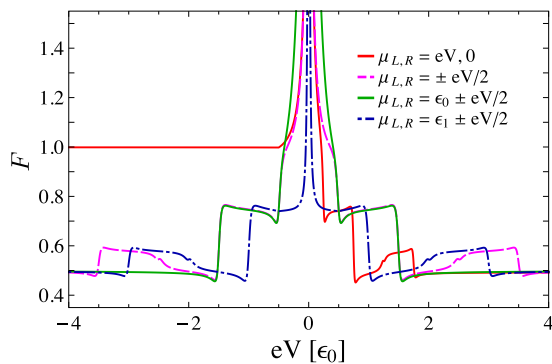


FIG. 3. Fano factor F as a function of bias voltage eV . All plots are obtained at zero temperature, with $\vec{B} = B\vec{e}_z$. The other parameters are set to $\Gamma = 0.05 \epsilon_0$, $\Gamma_L = \Gamma_R = \Gamma/2$, $\omega_L = 0.5 \epsilon_0$, $J = 0.01 \epsilon_0$, $S = 100$, and $\theta = \pi/2$. The positions of the molecular quasienergy levels are $\epsilon_1 = 0.25 \epsilon_0$, $\epsilon_2 = 0.75 \epsilon_0$, $\epsilon_3 = 1.25 \epsilon_0$, and $\epsilon_4 = 1.75 \epsilon_0$.

and the Fano factor $F < 1$ indicates the sub-Poissonian noise. Around the resonances $\mu_{L,R} = \epsilon_i$, $i = 1, 2, 3, 4$, the probability of transmission is very high, resulting in a small Fano factor. Elastic tunneling contributes to the sub-Poissonian Fano factor around the resonances and competes with the spin-flip events caused by the molecular spin precession. However, if the resonant quasienergy levels are much higher than the Fermi energy of the leads, the probability of transmission is very low and the Fano factor is close to 1, as shown in Fig. 3 (red line). This means that the stochastic processes are uncorrelated. If the two levels connected with the inelastic photon emission (absorption) tunnel processes, or all four levels, lie between the Fermi levels of the leads, the Fano factor approaches $1/2$, which is in agreement with Ref. [55]. For $eV = \epsilon_3$ [see Fig. 3 (red line)], a spin-down electron can tunnel elastically or inelastically in a spin-flip process, leading to the increase of the Fano factor. Spin-flip processes increase the electron traveling time, leading to sub-Poissonian noise. Similarly, the Pauli exclusion principle is known to lead to sub-Poissonian noise, since it prevents the double occupancy of a level.

The precessing molecular spin induces quantum interference between the transport channels connected with spin-flip events and the change of energy by one energy quantum ω_L , i.e., between levels with energies ϵ_1 and $\epsilon_2 = \epsilon_1 + \omega_L$, or ϵ_3 and $\epsilon_4 = \epsilon_3 + \omega_L$. The destructive quantum-interference effects manifest themselves in the form of diplike features in Fig. 2(b). When one or both pairs of the levels connected with spin-flip events enter the bias-voltage window, then an electron from the left lead can tunnel through both levels via elastic or inelastic spin-flip processes. Different tunneling pathways ending in the final state with the same energy destructively interfere, as in the Fano effect [11]. Namely, the state with lower energy ϵ_1 (or ϵ_3) mimics the discrete state in the Fano effect. An electron tunnels into the state ϵ_1 (or ϵ_3), undergoes a spin flip, and absorbs an energy quantum ω_L . The other state with energy ϵ_2 (or ϵ_4) is an analog of the continuum in the Fano effect, and the electron tunnels elastically through this level. These two tunneling processes (one elastic and the other inelastic) interfere, leading to a diplike feature in the noise power. If we vary, for instance, the bias voltage as $eV = \mu_L$, where $\mu_R = 0$ [Fig. 2(b), red line], we observe diplike features for $eV = \epsilon_2$ and $eV = \epsilon_4$.

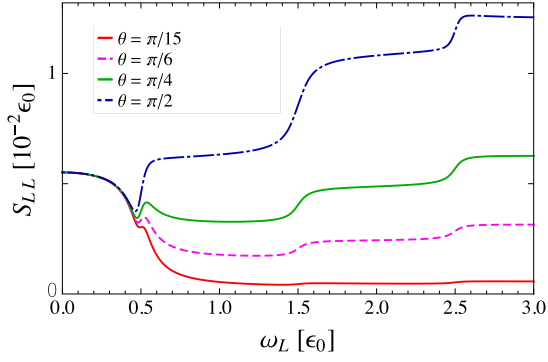


FIG. 4. Shot noise of charge current S_{LL} as a function of the Larmor frequency ω_L for different tilt angles θ , with $\vec{B} = B\vec{e}_z$, at zero temperature. The other parameters are $\Gamma = 0.05 \epsilon_0$, $\Gamma_L = \Gamma_R = \Gamma/2$, $\mu_L = 0.75 \epsilon_0$, $\mu_R = 0.25 \epsilon_0$, $J = 0.01 \epsilon_0$, and $S = 100$. For $\omega_L = \mu_L - \mu_R$, we observe a dip due to destructive quantum interference.

The destructive interference effect is also presented in Fig. 4, where noise power S_{LL} is depicted as a function of ω_L . Here, we observe a dip due to the quantum-interference effect around $\omega_L = 0.5 \epsilon_0$, which corresponds to $\mu_L = \epsilon_2$ and $\mu_R = \epsilon_1$. The other two steps in Fig. 4 occur when the Fermi energy of the right or left lead is in resonance with one of the quasienergy levels. The magnitude of the precessing component of the molecular spin, which induces spin-flip processes between molecular quasienergy levels, equals $JS \sin(\theta)/2$. Therefore, the dip increases with the increase of the tilt angle θ , and it is maximal and distinct for $\theta = \pi/2$.

Finally, in Fig. 5 we plotted the noise power of charge current S_{LL} as a function of $\mu = \mu_L = \mu_R$ at zero temperature. It shows a nonmonotonic dependence on the tunneling rates Γ . For small Γ (Fig. 5, red line) the noise is increased if μ is positioned between levels connected with spin-flip events, and it is contributed only by absorption processes of an energy quantum ω_L as we vary the chemical potentials. For larger Γ (Fig. 5, green line), the charge-current noise is increased since levels broaden and overlap, and more electrons can tunnel. With a further increase of Γ (Fig. 5, dotted blue line) the noise starts to de-

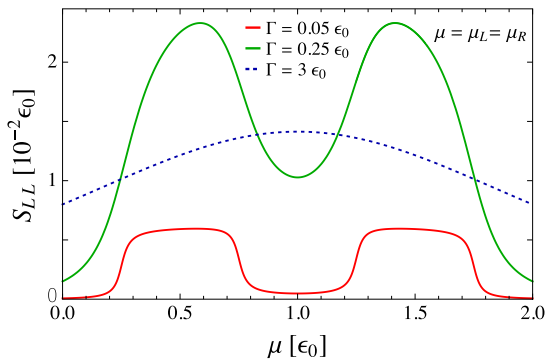


FIG. 5. Shot noise of charge current S_{LL} as a function of the chemical potential of the leads $\mu = \mu_L = \mu_R$, with $\vec{B} = B\vec{e}_z$, for three different couplings Γ , where $\Gamma_L = \Gamma_R = \Gamma/2$, at zero temperature. The other parameters are $\omega_L = 0.5 \epsilon_0$, $J = 0.01 \epsilon_0$, $S = 100$, and $\theta = \pi/2$. The molecular quasienergy levels are positioned at $\epsilon_1 = 0.25 \epsilon_0$, $\epsilon_2 = 0.75 \epsilon_0$, $\epsilon_3 = 1.25 \epsilon_0$, and $\epsilon_4 = 1.75 \epsilon_0$.

crease, and it is finally suppressed for $\Gamma \gg \omega_L$ since a current-carrying electron sees the molecular spin as nearly static in this case, leading to a reduction of the inelastic spin-flip processes.

IV. SHOT NOISE OF SPIN CURRENT AND SPIN-TRANSFER TORQUE

In this section, we present the spin-current noise spectrum components and relations between them. Later we introduce the noise of spin-transfer torque, and we investigate the zero-frequency spin-torque shot noise at zero temperature. The components of the nonsymmetrized spin-current noise spectrum read

$$S_{\xi\xi}^{xx}(\Omega) = -\frac{1}{4}[S_{\xi\xi}^{12,21} + S_{\xi\xi}^{21,12}](\Omega), \quad (20)$$

$$S_{\xi\xi}^{xy}(\Omega) = -\frac{i}{4}[S_{\xi\xi}^{12,21} - S_{\xi\xi}^{21,12}](\Omega), \quad (21)$$

$$S_{\xi\xi}^{zz}(\Omega) = -\frac{1}{4}[S_{\xi\xi}^{11,11} - S_{\xi\xi}^{11,22} - S_{\xi\xi}^{22,11} + S_{\xi\xi}^{22,22}](\Omega), \quad (22)$$

where Eq. (22) denotes the noise of the z component of the spin current [22,24]. Since the polarization of the spin current precesses in the xy plane, the remaining components of the spin-current noise spectrum satisfy the following relations:

$$S_{\xi\xi}^{yy}(\Omega) = S_{\xi\xi}^{xx}(\Omega), \quad (23)$$

$$S_{\xi\xi}^{yx}(\Omega) = -S_{\xi\xi}^{xy}(\Omega), \quad (24)$$

$$S_{\xi\xi}^{xz}(\Omega) = S_{\xi\xi}^{zx}(\Omega) = S_{\xi\xi}^{yz}(\Omega) = S_{\xi\xi}^{zy}(\Omega) = 0. \quad (25)$$

Taking into account that the spin current is not a conserved quantity, it is important to notice that the complete information from the noise spectrum can be obtained by studying both the autocorrelation noise spectrum $S_{\xi\xi}^{jk}(\Omega)$ and the cross-correlation noise spectrum $S_{\xi\xi}^{jk}(\Omega)$, $\zeta \neq \xi$. Therefore, it is more convenient to investigate the spin-torque noise spectrum, where both autocorrelation and cross-correlation noise components of spin currents are included. The spin-transfer torque operator can be defined as

$$\hat{T}_j = -(\hat{I}_{Lj} + \hat{I}_{Rj}), \quad j = x, y, z, \quad (26)$$

while its fluctuation reads

$$\delta\hat{T}_j(t) = -[\delta\hat{I}_{Lj}(t) + \delta\hat{I}_{Rj}(t)]. \quad (27)$$

Accordingly, the nonsymmetrized and symmetrized spin-torque noise can be obtained using the spin-current noise components as

$$\begin{aligned} S_T^{jk}(t, t') &= \langle \delta\hat{T}_j(t) \delta\hat{T}_k(t') \rangle \\ &= \sum_{\xi\zeta} S_{\xi\xi}^{jk}(t, t'), \quad j, k = x, y, z; \end{aligned} \quad (28)$$

$$S_{TS}^{jk}(t, t') = \frac{1}{2}[S_T^{jk}(t, t') + S_T^{kj}(t', t)], \quad (29)$$

with the corresponding noise spectrums given by

$$S_T^{jk}(\Omega) = \sum_{\xi\zeta} S_{\xi\xi}^{jk}(\Omega), \quad (30)$$

$$S_{TS}^{jk}(\Omega) = \sum_{\xi\zeta} S_{\xi\xi}^{jk}(\Omega). \quad (31)$$

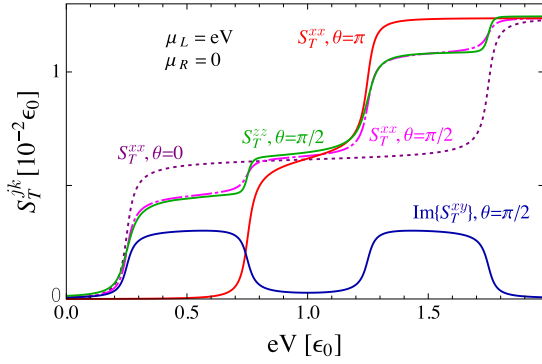


FIG. 6. Spin-torque shot-noise components S_T^{jk} as functions of the bias voltage eV for $\mu_R = 0$, $\mu_L = eV$. All plots are obtained at zero temperature, with $\vec{B} = B\vec{e}_z$, and $\Gamma_L = \Gamma_R = \Gamma/2$, for $\Gamma = 0.05 \epsilon_0$. The other parameters are set to $\omega_L = 0.5 \epsilon_0$, $J = 0.01 \epsilon_0$, and $S = 100$. The molecular quasienergy levels lie at $\epsilon_1 = 0.25 \epsilon_0$, $\epsilon_2 = 0.75 \epsilon_0$, $\epsilon_3 = 1.25 \epsilon_0$, and $\epsilon_4 = 1.75 \epsilon_0$.

According to Eqs. (23), (24), and (30), $S_T^{xx}(\Omega) = S_T^{yy}(\Omega)$ and $S_T^{yx}(\Omega) = -S_T^{xy}(\Omega)$.

In the remainder of the section, we investigate the zero-frequency spin-torque shot noise $S_T^{jk} = S_T^{jk}(0)$ at zero temperature, where $S_T^{xx}(0) = S_T^{xx}(0)$, $S_T^{yy}(0) = S_T^{yy}(0)$, $S_T^{zz}(0) = S_T^{zz}(0)$, while $S_T^{xy}(0)$ is a complex imaginary function, and $S_T^{yx}(0) = 0$ according to Eqs. (24) and (31). Since $S_T^{yx}(0) = S_T^{xy}(0)$, all results and discussions related to $S_T^{xx}(0)$ also refer to $S_T^{yy}(0)$.

Spin currents $I_{\xi x}$ and $I_{\xi y}$ are periodic functions of time, with period $\mathcal{T} = 2\pi/\omega_L$, while $I_{\xi z}$ is time-independent. It has already been demonstrated that spin-flip processes contribute to the noise of spin current [22]. The presence of the precessing molecular spin affects the spin-current noise. Since the number of particles with different spins changes due to spin-flip processes, additional spin-current fluctuations are generated. Currents with the same and with different spin orientations are correlated during transport. Due to the precessional motion of the molecular spin, inelastic spin currents with spin-flip events induce noise of spin currents and spin-torque noise, which can be nonzero even for $eV = 0$. The noise component S_T^{xy} is induced by the molecular spin precession and vanishes for a static molecular spin. The noises of spin currents and spin-transfer torque are driven by the bias voltage and by the molecular spin precession. Hence, in the case when both the molecular spin is static (absence of inelastic spin-flip processes) and $eV = 0$ (no contribution of elastic tunneling processes), they are all equal to zero. The noise of spin-transfer torque can be modified by adjusting system parameters such as the bias voltage eV , the magnetic field \vec{B} , or the tilt angle θ .

In Fig. 6 we present the zero-frequency spin-torque noise components $S_T^{xx} = S_T^{yy}$, $\text{Im}\{S_T^{xy}\}$, and S_T^{zz} as functions of the bias voltage $eV = \mu_L - \mu_R$ for $\mu_R = 0$ and different tilt angles θ between \vec{B} and \vec{S} at zero temperature. They give information on available transport channels and inelastic spin-flip processes. The magnitude of the torque noise at resonance energies ϵ_i , $i = 1, 2, 3, 4$, is determined by θ . In cases $\theta = 0$ and $\theta = \pi$, there are only two transport channels of opposite spins determined by the resulting Zeeman field $B \pm JS/g\mu_B$. The component S_T^{xx} shows two steps with equal heights

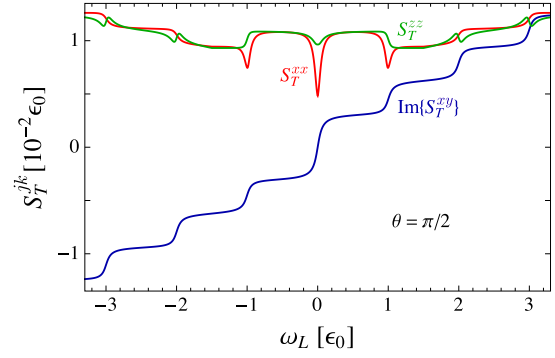


FIG. 7. Spin-torque shot-noise components S_T^{jk} as functions of the Larmor frequency ω_L for $\theta = \pi/2$, $\mu_R = 0$, and $\mu_L = 1.5 \epsilon_0$. All plots are obtained for $\vec{B} = B\vec{e}_z$ at zero temperature. The other parameters are $\Gamma_L = \Gamma_R = \Gamma/2$, $\Gamma = 0.05 \epsilon_0$, $J = 0.01 \epsilon_0$, and $S = 100$.

located at these resonances, where the only contribution to the spin-torque noise comes from elastic tunneling events (dotted purple and red lines in Fig. 6). For $\theta = \pi/2$, the elastic tunneling contributes with four steps with equal heights located at resonances ϵ_i , but due to the contributions of the inelastic precession-assisted processes between quasienergy levels $\epsilon_1(\epsilon_3)$ and $\epsilon_2(\epsilon_4)$, the heights of the steps in S_T^{xx} are not equal anymore (dot-dashed pink line in Fig. 6). Here, we observed that the contribution of the inelastic tunneling processes to S_T^{xx} , involving absorption of an energy quantum ω_L and a spin flip, shows steps at spin-down quasienergy levels ϵ_1 and ϵ_3 , while it is constant between and after the bias has passed these levels. The component S_T^{zz} shows similar behavior (green line in Fig. 6). As in the case of the inelastic tunneling involving the absorption of one energy quantum ω_L , in $S_T^{xx} = S_T^{yy}$ we observed inelastic spin-flip processes involving the absorption of two energy quanta $2\omega_L$ in the form of steps at spin-down levels ϵ_1 , ϵ_3 , $\epsilon_2 - 2\omega_L$, and $\epsilon_4 - 2\omega_L$, which have a negligible contribution compared to the other terms. These processes are a result of correlations of two oscillating spin-currents. For large bias voltage, the spin-torque noise components S_T^{xx} and S_T^{zz} saturate.

The behavior of the component $\text{Im}\{S_T^{xy}\}$ is completely different in nature. It is contributed only by one energy quantum ω_L absorption (emission) spin-flip process. Interestingly, we obtained the following relation between the Gilbert damping parameter α [42,43] and $\text{Im}\{S_T^{xy}\}$ at arbitrary temperature:

$$\text{Im}\{S_T^{xy}\} = \frac{\omega_L S \sin^2(\theta)}{2} \alpha. \quad (32)$$

Hence, the component $\text{Im}\{S_T^{xy}\}$ is increased for Fermi levels of the leads positioned in the regions where inelastic tunneling processes occur (blue line in Fig. 6).

The spin-torque noise is influenced by the magnetic field \vec{B} since it determines the spin-up and spin-down molecular quasienergy levels. The dependence of S_T^{xx} , $\text{Im}\{S_T^{xy}\}$, and S_T^{zz} on the Larmor frequency ω_L is depicted in Fig. 7. The steps, dips, or peaks in the plots are located at resonant tunneling frequencies $\omega_L = \pm|2\mu_{L,R} - 2\epsilon_0 \pm JS|$. For $\omega_L = 0$ there are only two transport channels, one at energy $\epsilon_0 + JS/2$, which is equal to the Fermi energy of the left lead, and the other

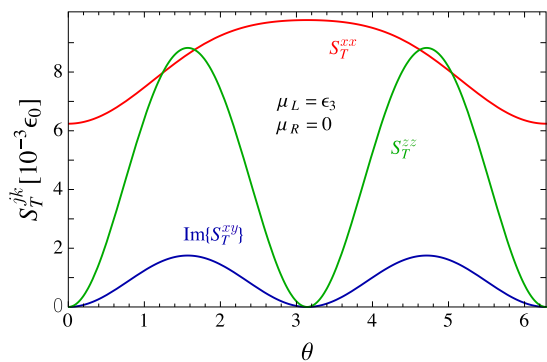


FIG. 8. Spin-torque shot-noise components as functions of the tilt angle θ for $\mu_L = \epsilon_3$, $\mu_R = 0$. All plots are obtained at zero temperature, with $B = B\bar{e}_z$, $\Gamma = 0.05\epsilon_0$, and $\Gamma_L = \Gamma_R = \Gamma/2$. The other parameters are $\omega_L = 0.5\epsilon_0$, $J = 0.01\epsilon_0$, and $S = 100$.

at $\epsilon_0 - JS/2$ located between μ_L and μ_R . The contributions of the elastic spin transport processes through these levels result in dips in the components S_T^{xx} and S_T^{zz} , while $\text{Im}\{S_T^{xy}\} = 0$. For $\omega = \epsilon_0$ corresponding to $\mu_R = \epsilon_1$ and $\mu_R = \epsilon_4 - 2\omega_L$, both the elastic and spin-flip tunneling events involving the absorption of energy of one quantum ω_L contribute with a dip, while the spin-flip processes involving the absorption of an energy equal to $2\omega_L$ contribute with a peak to the component S_T^{xx} . For $\omega_L = 2\epsilon_0$ and $\omega_L = 3\epsilon_0$ corresponding to $\mu_L = \epsilon_2$ and $\mu_R = \epsilon_3$, both elastic and spin-flip processes with the absorption of an energy equal to ω_L contribute with a step, while the inelastic processes involving the absorption of an energy $2\omega_L$ give negligible contribution to S_T^{xx} . The component S_T^{zz} shows dips at these two points, since here the dominant contribution comes from inelastic tunneling spin-flip events. The component S_T^{zz} is an even function of ω_L , while $\text{Im}\{S_T^{xy}\}$ is an odd function of ω_L . The spin-torque noise S_T^{xx} is an even function of ω_L for $\theta = \pi/2$.

The spin-torque noise components as functions of θ for $\mu_L = \epsilon_3$ and $\mu_R = 0$ at zero temperature are shown in Fig. 8. The magnitudes and the appearance of the spin-torque noise components at resonance energies ϵ_i can be controlled by θ , since it influences the polarization of the spin current. Here we see that both S_T^{zz} and $\text{Im}\{S_T^{xy}\}$ are zero for $\theta = 0$ and $\theta = \pi$, as the molecular spin is static and its magnitude is constant along the z direction in both cases. These torque-noise components take their maximum values for $\theta = \pi/2$, where both elastic and inelastic tunneling contributions are maximal. The component S_T^{xx} takes its minimum value for $\theta = 0$ and its maximum

value for $\theta = \pi$, with only elastic tunneling contributions in both cases. For $\theta = \pi/2$, the inelastic tunneling events make a maximal contribution while energy-conserving processes make a minimal contribution to S_T^{xx} .

V. CONCLUSIONS

In this article, we studied theoretically the noise of charge and spin transport through a small junction, consisting of a single molecular orbital in the presence of a molecular spin precessing with Larmor frequency ω_L in a constant magnetic field. The orbital is connected to two Fermi leads. We used the Keldysh nonequilibrium Green's function method to derive the noise components of charge and spin currents and spin-transfer torque.

Then, we analyzed the shot noise of charge current and observed characteristics that differ from the ones in the current. In the noise power, we observed diplike features that we attribute to inelastic processes, due to the molecular spin precession, leading to the quantum-interference effect between correlated transport channels.

Since the inelastic tunneling processes lead to a spin-transfer torque acting on the molecular spin, we have also investigated the spin-torque noise components contributed by these processes, involving the change of energy by an energy quantum ω_L . The spin-torque noise components are driven by both the bias voltage and the molecular spin precession. The in-plane noise components S_T^{xx} and S_T^{yy} are also contributed by the processes involving the absorption of an energy equal to $2\omega_L$. We obtained the relation between $\text{Im}\{S_T^{xy}\}$ and the Gilbert damping coefficient α at arbitrary temperature.

Taking into account that the noise of charge and spin transport can be controlled by parameters such as the bias voltage and external magnetic field, our results might be useful in molecular electronics and spintronics. The experimental observation of the predicted noise properties might be a challenging task due to complicated tunneling processes through molecular magnets. Finding a way to control the spin states of single-molecule magnets in tunnel junctions might be a future task.

ACKNOWLEDGMENTS

We would like to thank Fei Xu for useful discussions. We gratefully acknowledge the financial support from the Deutsche Forschungsgemeinschaft through the SFB 767 *Controlled Nanosystems*, the Center of Applied Photonics, the DAAD through a STIBET scholarship, and an ERC Advanced Grant *UltraPhase* of Alfred Leitenstorfer.

APPENDIX: FORMAL EXPRESSION FOR THE NONSYMMETRIZED NOISE

Here, we present the derivation of the formal expression for the nonsymmetrized noise $S_{\xi\xi}^{\nu\mu}(t, t')$. The correlation functions $S_{\xi\xi}^{\sigma\sigma', \lambda\eta}(t, t')$, introduced in Eq. (11), can be expressed by means of Wick's theorem [56] as

$$\begin{aligned}
 S_{\xi\xi}^{\sigma\sigma', \lambda\eta}(t, t') = & \sum_{kk'} [V_{k\xi} V_{k'\zeta} G_{\sigma', k'\lambda\xi}^>(t, t') G_{\eta, k\sigma\xi}^<(t', t) - V_{k\xi} V_{k'\zeta}^* G_{\sigma', \lambda}^>(t, t') G_{k'\eta\xi, k\sigma\xi}^<(t', t) \\
 & - V_{k\xi}^* V_{k'\zeta} G_{k\sigma'\xi, k'\lambda\xi}^>(t, t') G_{\eta\sigma}^<(t', t) + V_{k\xi}^* V_{k'\zeta} G_{k\sigma'\xi, \lambda}^>(t, t') G_{\xi k'\eta\xi, \sigma}^<(t', t)], \quad (\text{A1})
 \end{aligned}$$

with the mixed Green's functions defined, using units in which $\hbar = e = 1$, as

$$G_{\eta,k\sigma\xi}^<(t,t') = i\langle\hat{c}_{k\sigma\xi}^\dagger(t')\hat{d}_\eta(t)\rangle, \quad (\text{A2})$$

$$G_{\sigma',k'\lambda\xi}^>(t,t') = -i\langle\hat{d}_{\sigma'}(t)\hat{c}_{k'\lambda\xi}^\dagger(t')\rangle, \quad (\text{A3})$$

while Green's functions $G_{k\sigma\xi,\eta}^<(t,t') = -[G_{\eta,k\sigma\xi}^<(t',t)]^*$ and $G_{k'\lambda\xi,\sigma'}^>(t,t') = -[G_{\sigma',k'\lambda\xi}^>(t',t)]^*$. The Green's functions of the leads and the central region are defined as

$$G_{k\sigma\xi,k'\sigma'\zeta}^<(t,t') = i\langle\hat{c}_{k'\sigma'\zeta}^\dagger(t')\hat{c}_{k\sigma\xi}(t)\rangle, \quad (\text{A4})$$

$$G_{k\sigma\xi,k'\sigma'\zeta}^>(t,t') = -i\langle\hat{c}_{k\sigma\xi}(t)\hat{c}_{k'\sigma'\zeta}^\dagger(t')\rangle, \quad (\text{A5})$$

$$G_{\sigma\sigma'}^<(t,t') = i\langle\hat{d}_{\sigma'}^\dagger(t')\hat{d}_\sigma(t)\rangle, \quad (\text{A6})$$

$$G_{\sigma\sigma'}^>(t,t') = -i\langle\hat{d}_\sigma(t)\hat{d}_{\sigma'}^\dagger(t')\rangle, \quad (\text{A7})$$

$$G_{\sigma\sigma'}^{r,a}(t,t') = \mp i\theta(\pm t \mp t')\langle\{\hat{d}_\sigma(t),\hat{d}_{\sigma'}^\dagger(t')\}\rangle. \quad (\text{A8})$$

Since the self-energies originating from the coupling between the electronic level and the lead ξ are diagonal in the electron spin space, their entries can be written as $\Sigma_\xi^{<,>,r,a}(t,t') = \sum_k V_{k\xi} g_{k\xi}^{<,>,r,a}(t,t') V_{k\xi}^*$, where $g^{<,>,r,a}(t,t')$ are the Green's functions of the free electrons in lead ξ . Applying Langreth analytical continuation rules [57], Eq. (A1) transforms into

$$\begin{aligned} S_{\xi\xi}^{\sigma\sigma',\lambda\eta}(t,t') = & \int dt_1 \int dt_2 \{ [G_{\sigma'\lambda}^r(t,t_1)\Sigma_\zeta^>(t_1,t') + G_{\sigma'\lambda}^>(t,t_1)\Sigma_\zeta^a(t_1,t')] [G_{\eta\sigma}^r(t',t_2)\Sigma_\xi^<(t_2,t) + G_{\eta\sigma}^<(t',t_2)\Sigma_\xi^a(t_2,t)] \\ & + [\Sigma_\xi^>(t,t_1)G_{\sigma'\lambda}^a(t_1,t') + \Sigma_\xi^r(t,t_1)G_{\sigma'\lambda}^>(t_1,t')] [\Sigma_\zeta^<(t',t_2)G_{\eta\sigma}^a(t_2,t) + \Sigma_\zeta^r(t',t_2)G_{\eta\sigma}^<(t_2,t)] \\ & - G_{\sigma'\lambda}^>(t,t') [\Sigma_\zeta^r(t',t_1)G_{\eta\sigma}^r(t_1,t_2)\Sigma_\xi^<(t_2,t) + \Sigma_\zeta^<(t',t_1)G_{\eta\sigma}^a(t_1,t_2)\Sigma_\xi^a(t_2,t) \\ & + \Sigma_\zeta^r(t',t_1)G_{\eta\sigma}^<(t_1,t_2)\Sigma_\xi^a(t_2,t)] - [\Sigma_\xi^r(t,t_1)G_{\sigma'\lambda}^r(t_1,t_2)\Sigma_\zeta^>(t_2,t') \\ & + \Sigma_\xi^>(t,t_1)G_{\sigma'\lambda}^a(t_1,t_2)\Sigma_\zeta^a(t_2,t') + \Sigma_\xi^r(t,t_1)G_{\sigma'\lambda}^>(t_1,t_2)\Sigma_\zeta^a(t_2,t')] G_{\eta\sigma}^<(t',t) \} \\ & - \delta_{\xi\zeta} [\delta_{\eta\sigma} G_{\sigma'\lambda}^>(t,t')\Sigma_\xi^<(t',t) + \delta_{\sigma'\lambda} \Sigma_\xi^>(t,t')G_{\eta\sigma}^<(t',t)]. \end{aligned} \quad (\text{A9})$$

Finally, using Eqs. (11) and (A9), the obtained formal expression for the nonsymmetrized noise of charge current [40,58] and spin currents in standard coordinates t and t' can be written as

$$\begin{aligned} S_{\xi\xi}^{v\mu}(t,t') = & -\frac{q_v q_\mu}{\hbar^2} \text{Tr} \left\{ \int dt_1 \int dt_2 \{ \hat{\sigma}_v [\hat{G}^r(t,t_1)\hat{\Sigma}_\zeta^>(t_1,t') + \hat{G}^>(t,t_1)\hat{\Sigma}_\zeta^a(t_1,t')] \hat{\sigma}_\mu [\hat{G}^r(t',t_2)\hat{\Sigma}_\xi^<(t_2,t) + \hat{G}^<(t',t_2)\hat{\Sigma}_\xi^a(t_2,t)] \right. \\ & + \hat{\sigma}_v [\hat{\Sigma}_\xi^>(t,t_1)\hat{G}^a(t_1,t') + \hat{\Sigma}_\xi^r(t,t_1)\hat{G}^>(t_1,t')] \hat{\sigma}_\mu [\hat{\Sigma}_\zeta^<(t',t_2)\hat{G}^a(t_2,t) + \hat{\Sigma}_\zeta^r(t',t_2)\hat{G}^<(t_2,t)] \\ & - \hat{\sigma}_v \hat{G}^>(t,t') \hat{\sigma}_\mu [\hat{\Sigma}_\zeta^r(t',t_1)\hat{G}^r(t_1,t_2)\hat{\Sigma}_\xi^<(t_2,t) + \hat{\Sigma}_\zeta^<(t',t_1)\hat{G}^a(t_1,t_2)\hat{\Sigma}_\xi^a(t_2,t) + \hat{\Sigma}_\zeta^r(t',t_1)\hat{G}^<(t_1,t_2)\hat{\Sigma}_\xi^a(t_2,t)] \\ & - \hat{\sigma}_v [\hat{\Sigma}_\xi^r(t,t_1)\hat{G}^r(t_1,t_2)\hat{\Sigma}_\zeta^>(t_2,t') + \hat{\Sigma}_\xi^>(t,t_1)\hat{G}^a(t_1,t_2)\hat{\Sigma}_\zeta^a(t_2,t') + \hat{\Sigma}_\xi^r(t,t_1)\hat{G}^>(t_1,t_2)\hat{\Sigma}_\zeta^a(t_2,t')] \hat{\sigma}_\mu \hat{G}^<(t',t) \} \\ & \left. - \delta_{\xi\zeta} \hat{\sigma}_v [\hat{G}^>(t,t') \hat{\sigma}_\mu \hat{\Sigma}_\xi^<(t',t) + \hat{\Sigma}_\xi^>(t,t') \hat{\sigma}_\mu \hat{G}^<(t',t)] \right\}, \end{aligned} \quad (\text{A10})$$

where Tr denotes the trace in the electronic spin space.

-
- | | |
|---|--|
| [1] Y. M. Blanter and M. Büttiker, <i>Phys. Rep.</i> 336 , 1 (2000). | [7] H. Vázquez, R. Skouta, S. Schneebeli, M. Kamenetska, R. Beslov, L. Venkataraman, and M. S. Hybertsen, <i>Nat. Nanotech.</i> 7 , 663 (2012). |
| [2] E. G. Mishchenko, <i>Phys. Rev. B</i> 68 , 100409(R) (2003). | [8] R. Stadler, <i>Phys. Rev. B</i> 80 , 125401 (2009). |
| [3] W. Belzig and M. Zareyan, <i>Phys. Rev. B</i> 69 , 140407 (2004). | [9] M. A. Ratner, <i>J. Phys. Chem.</i> 94 , 4877 (1990). |
| [4] F. M. Souza, A. P. Jauho, and J. C. Egues, <i>Phys. Rev. B</i> 78 , 155303 (2008). | [10] T. Hansen, G. C. Solomon, D. Q. Andrews, and M. A. Ratner, <i>J. Chem. Phys.</i> 131 , 194704 (2009). |
| [5] A. E. Miroshnichenko, S. Flach, and Y. S. Kivshar, <i>Rev. Mod. Phys.</i> 82 , 2257 (2010). | [11] U. Fano, <i>Phys. Rev.</i> 124 , 1866 (1961). |
| [6] C. M. Guédon, H. Valkenier, T. Markussen, K. S. Thygesen, J. C. Hummelen, and S. J. van der Molen, <i>Nat. Nanotech.</i> 7 , 305 (2012). | [12] J. Faist, F. Capasso, C. Sirtori, K. W. West, and L. N. Pfeiffer, <i>Nature (London)</i> 390 , 589 (1997). |

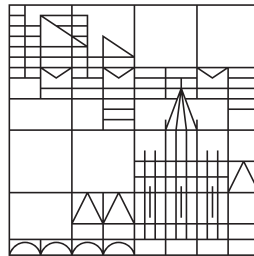
- [13] O. Entin-Wohlman, Y. Imry, S. A. Gurvitz, and A. Aharony, *Phys. Rev. B* **75**, 193308 (2007).
- [14] D. Sánchez and L. Serra, *Phys. Rev. B* **74**, 153313 (2006).
- [15] P. Stefański, *J. Phys.: Condens. Matter* **22**, 505303 (2010).
- [16] B. H. Wu and C. Timm, *Phys. Rev. B* **81**, 075309 (2010).
- [17] S. A. Gurvitz, D. Mozysky, and G. P. Berman, *Phys. Rev. B* **72**, 205341 (2005).
- [18] S. A. Gurvitz, *IEEE Trans. Nanotech.* **4**, 45 (2005).
- [19] D. Mozysky, L. Fedichkin, S. A. Gurvitz, and G. P. Berman, *Phys. Rev. B* **66**, 161313 (2002).
- [20] A. Lamacraft, *Phys. Rev. B* **69**, 081301(R) (2004).
- [21] M. Zareyan and W. Belzig, *Europhys. Lett.* **70**, 817 (2005).
- [22] B. Wang, J. Wang, and H. Guo, *Phys. Rev. B* **69**, 153301 (2004).
- [23] S. H. Ouyang, C. H. Lam, and J. Q. You, *Euro. Phys. J. B* **64**, 67 (2008).
- [24] O. Sauret and D. Feinberg, *Phys. Rev. Lett.* **92**, 106601 (2004).
- [25] M. J. Stevens, A. L. Smirl, R. D. R. Bhat, A. Najmaie, J. E. Sipe, and H. M. van Driel, *Phys. Rev. Lett.* **90**, 136603 (2003).
- [26] A. Brataas, Y. Tserkovnyak, G. E. W. Bauer, and B. I. Halperin, *Phys. Rev. B* **66**, 060404(R) (2002).
- [27] R. L. Dragomirova and B. K. Nikolić, *Phys. Rev. B* **75**, 085328 (2007).
- [28] Y. He, D. Hou, and R. Han, *J. Appl. Phys.* **101**, 023710 (2007).
- [29] Y. Yu, H. Zhan, L. Wan, B. Wang, Y. Wei, Q. Sun, and J. Wang, *Nanotechnology* **24**, 155202 (2013).
- [30] J. Foros, A. Brataas, Y. Tserkovnyak, and G. E. W. Bauer, *Phys. Rev. Lett.* **95**, 016601 (2005).
- [31] A. L. Chudnovskiy, J. Swiebodzinski, and A. Kamenev, *Phys. Rev. Lett.* **101**, 066601 (2008).
- [32] A. Kamra, F. P. Witek, S. Meyer, H. Huebl, S. Geprägs, R. Gross, G. E. W. Bauer, and S. T. B. Goennenwein, *Phys. Rev. B* **90**, 214419 (2014).
- [33] A. Kamra and W. Belzig, *Phys. Rev. Lett.* **116**, 146601 (2016); *Phys. Rev. B* **94**, 014419 (2016).
- [34] A. Kamra and W. Belzig, *Phys. Rev. Lett.* **119**, 197201 (2017).
- [35] Y. Wang and L. J. Sham, *Phys. Rev. B* **85**, 092403 (2012).
- [36] Y. Wang and L. J. Sham, *Phys. Rev. B* **87**, 174433 (2013).
- [37] J. C. Slonczewski, *J. Magn. Magn. Mater.* **159**, L1 (1996).
- [38] L. Berger, *Phys. Rev. B* **54**, 9353 (1996).
- [39] A.-P. Jauho, N. S. Wingreen, and Y. Meir, *Phys. Rev. B* **50**, 5528 (1994).
- [40] A.-P. Jauho and H. Haug, *Quantum Kinetics in Transport and Optics of Semiconductors* (Springer, Berlin, 2008).
- [41] N. S. Wingreen, A.-P. Jauho, and Y. Meir, *Phys. Rev. B* **48**, 8487 (1993).
- [42] M. Filipović, C. Holmqvist, F. Haupt, and W. Belzig, *Phys. Rev. B* **87**, 045426 (2013); **88**, 119901(E) (2013).
- [43] M. Filipović and W. Belzig, *Phys. Rev. B* **93**, 075402 (2016).
- [44] T. L. Gilbert, *Phys. Rev.* **100**, 1243 (1955); *IEEE Trans. Magn.* **40**, 3443 (2004).
- [45] Y. Tserkovnyak, A. Brataas, G. E. W. Bauer, and B. I. Halperin, *Rev. Mod. Phys.* **77**, 1375 (2005).
- [46] D. C. Ralph and M. D. Stiles, *J. Magn. Magn. Mater.* **320**, 1190 (2008).
- [47] C. Kittel, *Phys. Rev.* **73**, 155 (1948).
- [48] M. H. Pedersen and M. Büttiker, *Phys. Rev. B* **58**, 12993 (1998).
- [49] B. Wang, J. Wang, and H. Guo, *Phys. Rev. B* **67**, 092408 (2003).
- [50] N. Bode, L. Arrachea, G. S. Lozano, T. S. Nunner, and F. von Oppen, *Phys. Rev. B* **85**, 115440 (2012).
- [51] G. Floquet, *Ann. Sci. Ecole Norm. Supér.* **12**, 47 (1883).
- [52] Jon H. Shirley, Ph.D. thesis, California Institute of Technology, 1963.
- [53] M. Grifoni and P. Hänggi, *Phys. Rep.* **304**, 229 (1998).
- [54] S.-I. Chu and D. A. Telnov, *Phys. Rep.* **390**, 1 (2004).
- [55] A. Thielmann, M. H. Hettler, J. König, and G. Schön, *Phys. Rev. B* **68**, 115105 (2003).
- [56] A. Fetter and J. D. Walecka, *Quantum Theory of Many-Particle Systems* (Dover, Mineola, NY, 2003).
- [57] D. C. Langreth, in *Linear and Nonlinear Electron Transport in Solids*, edited by J. T. Devreese and E. Van Doren (Plenum, New York, 1976).
- [58] Z. Feng, J. Maciejko, J. Wang, and H. Guo, *Phys. Rev. B* **77**, 075302 (2008).

Correction: Two sentences were improperly edited and subsequently fixed (on page 2, left, fifth sentence and on page 7, left, second sentence of the second paragraph).

Quantum Transport Through Molecular Magnets

DISSERTATION
zur Erlangung des
akademischen Grades eines
Doktors der Naturwissenschaften
Dr. rer. nat.

vorgelegt von
Milena Filipović
aus Serbien



UNIVERSITÄT KONSTANZ
Mathematisch-Naturwissenschaftliche Sektion
Fachbereich Physik

Tag der mündlichen Prüfung: 23.07.2015

1. Referent: Prof. Dr. Wolfgang Belzig
2. Referent: Prof. Dr. Guido Burkard

“It is strange that we need just a little to be happy, and it is even more strange how often we miss just that little.”

Ivo Andrić

Abstract

In this thesis we theoretically study time-dependent electronic and spin transport through a molecular orbital connected to two Fermi leads, and coupled to a molecular magnet via exchange interaction. The molecular spin is considered as a classical variable and is assumed to precess around an external magnetic field with Larmor frequency. We derive expressions for charge and spin currents using the Keldysh nonequilibrium Green's functions formalism. The coupling between the electronic spins and the magnetization dynamics of the molecule leads to inelastic tunneling processes, which contribute to the spin currents. The inelastic spin currents exert a spin-transfer torque on the molecular spin, which is compensated by external means. This back-action includes a contribution to the Gilbert damping and a change of the precession frequency. The Gilbert damping coefficient can be controlled by the bias and gate voltages, or via the external magnetic field, and has a nonmonotonic dependence on the broadening of the molecular level.

Next, we study the ac-charge and -spin transport through the molecular orbital, where we assume that the source and drain contacts have time-dependent electrochemical potentials. By means of the Keldysh nonequilibrium Green's functions method we calculate the spin and charge currents in linear order with respect to the time-dependent potentials. Oscillating electrochemical potentials allow to detect the Larmor frequency by a measurement of the conductance if the ac-frequency matches the Larmor frequency. In the low ac-frequency regime the junction behaves as an equivalent classical circuit, which can be tuned from capacitive-like to inductive-like response. Furthermore, we show that the setup can be used to generate dc-spin currents, which are controlled by the molecular magnetization direction and the relative phases between the Larmor precession and the ac-voltage.

Finally, we study the nonequilibrium noise of charge and spin transport through the junction, in the presence of dc-bias voltage. Using the Keldysh Green's functions method we obtain the noise components of charge and spin currents and spin-transfer torque. Then we analyze the shot noise of charge current and observe dip-like features due to inelastic tunneling processes involving the change of energy by one Larmor frequency. These processes are driven by the molecular spin precession and lead to a quantum interference effect between correlated currents, with electron waves passing through the levels connected with inelastic processes. The spin-torque noise components are driven by both the dc-bias voltage and the molecular spin precession. The torque noise components correlating spin-transfer torques in the same spatial direction in the precession plane are contributed by elastic tunneling processes, and by inelastic processes, where current-carrying spin particles change their energy by one or two Larmor frequencies. In the end, we show that the correlations of the perpendicular components of the spin-transfer torque in the precession plane are related to the Gilbert damping coefficient at zero temperature.

Zusammenfassung

Diese Arbeit beschäftigt sich mit der theoretischen Untersuchung des zeitabhängigen Ladungs- und Spin-Transport durch ein molekulares Energieniveau, das an zwei Kontakte gekoppelt ist, sowie mit einem molekularen Magneten wechselwirkt. Der molekulare Spin, der als klassische Größe behandelt wird, präzediert mit der Larmorfrequenz um ein externes Magnetfeld. Unter Anwendung des Keldysh-Formalismus für Nichtgleichgewichts Green'sche Funktionen werden die Ausdrücke für Ladungs- und Spin-Ströme hergeleitet. Die Wechselwirkung des Spins der Elektronen mit der dynamischen Magnetisierung des Moleküls führt zu inelastischen Tunnelprozessen, welche zum Spinstrom beitragen. Dieser inelastische Beitrag im Spinstrom führt zu einem Drehmoment auf das magnetische Moment, was extern kompensiert wird. Diese Rückkopplung beinhaltet einen Beitrag zur Gilbert-Dämpfung sowie eine Änderung der Drehfrequenz. Der Dämpfungskoeffizient wird entweder durch die Transport- und Gatter-Spannungen kontrolliert oder über das externe Magnetfeld und hängt nichtmonoton mit der Verbreiterung des molekularen Energieniveaus zusammen.

Als nächstes untersuchen wir den zeitabhängigen Ladungs- und Spin-Transport durch das molekulare Energieniveau, wobei wir annehmen dass die beiden Kontakte zeitabhängige elektrochemische Potenziale haben. Mithilfe des Keldysh-Formalismus berechnen wir Spin und Ladungsströme in linearer Ordnung bezüglich der zeitabhängigen Potenziale. Oszillierende elektrochemische Potenziale erlauben eine Bestimmung der Larmorfrequenz durch Messen des Gleichstrom-Leitwerts, wenn die Wechselspannungsfrequenz mit der Larmorfrequenz übereinstimmt. Bei kleinen Wechselspannungsfrequenzen verhält sich der Kontakt äquivalent zu einem klassischen Schwingkreis, der von einem induktiven zu einem kapazitiven Verhalten gesteuert werden kann. Des Weiteren zeigen wir, dass dieser Aufbau dazu verwendet werden kann Gleichgewichts-Spinströme zu erzeugen, die durch die Magnetisierungsrichtung und die relative Phase zwischen Larmorpräzession und Wechselspannung kontrolliert werden.

Als letztes untersuchen wir das quantenmechanische Rauschen der Ladungs- und Spinströme durch den Kontakt bei Gleichspannung. Der Keldysh-Formalismus liefert uns hierbei die Rauschkomponenten des Ladungs- und Spinstromrauschens, sowie des mit dem Spin-Transport verbundenen Drehmoments. Hierbei analysieren wir das Schrotrauschen des Ladungstransports und beobachten peakartige Strukturen, die auf inelastische Tunnelprozesse zurückzuführen sind, bei denen sich die Energie um das Äquivalent einer Larmorfrequenz ändert. Solche Prozesse werden durch die molekulare Spin-Präzession ausgelöst und führen zu quantenmechanischen Interferenzeffekten zwischen korrelierten Strömen, bei denen Elektronenwellen durch Energieniveaus propagieren, die durch inelastische Prozesse verknüpft sind. Das Spin-Drehmoment-Rauschen wird sowohl durch die Gleichspannung als auch durch die Präzession des molekularen Spins ausgelöst. Die Komponenten des Drehmoment-Rauschens, die Spin-Transport Drehmomente in derselben

räumlichen Richtung in der Präzessions-Ebene korrelieren, werden durch elastische Tunnelprozesse, sowie durch inelastische Prozesse mit einer Energieänderung von ein oder zwei Larmorfrequenzen verursacht. Zuletzt zeigen wir, dass die Korrelationen der senkrechten Komponenten der Spin-Transport-Drehmomente in der Präzessionsebene, am Temperaturnullpunkt mit dem Gilbert-Dämpfungs-Koeffizienten zusammenhängen.

Acknowledgements

I would like to express my deep gratitude to Prof. Wolfgang Belzig for accepting me as a PhD student in theoretical condensed matter physics and for introducing me to the exciting field of quantum transport. I thank Prof. Belzig for his patience, excellent pedagogic approach, guidance and supervision during my PhD studies. His frequent availability for discussions and the inspiration I gained from him are gratefully acknowledged.

I am grateful to Prof. Guido Burkard for agreeing to be the second referee of my thesis, and to Prof. Georg Maret who accepted to be the thesis committee chair.

I wish to thank Dr. Federica Haupt who introduced the Keldysh nonequilibrium Green's functions formalism to me, and Dr. Cecilia Holmqvist who introduced me to the concept of spin-transfer torque, for fruitful collaboration.

I am very grateful to the following physicists who contributed to the creation of this work through useful discussions, and/or computer help: Dr. Christian Wickles, Dr. Jan Hammer, Dr. Mihajlo Vanević, Dr. Gianluca Rastelli, Dr. Angelo Di Marco, Dr. Stefan Gerlach, Johannes Reutlinger, Pascal Stadler, Fei Xu, the other present and former members of our research group, and all colleagues who broadened my knowledge and understanding of physics at seminars, office discussions and conferences.

Many thanks to our secretaries Sabine Lucas, Marianne Griesser and Letizia Brusaglioni for their kindness, help and assistance.

I sincerely thank the Welcome Center Team at the University of Konstanz, especially Dr. Johannes Dingler, and Elisabeth Grübel from the Tax and Social Security Services, for their help, kindness, support, and always warm and welcoming atmosphere every time I visited them.

I gratefully acknowledge financial support from the DFG through SFB 767, an ERC Advanced Grant *UltraPhase* of Prof. Alfred Leitenstorfer, and a DAAD stipend granted by the International Office at the University of Konstanz.

Finally, I owe many special thanks to God and my loved ones, especially to my mother Bogdanka, my sister Desanka and her family, my grandmother Desanka who was my great supporter and unfortunately passed away in the meantime, my cousins Anita and Tanja, my aunt Zorica, and to all my dear friends from the Chestnut street in Belgrade, where I grew up, for their love, care, support, and encouragement throughout this journey.

...

*To the memory
of my father Milorad
who was my first mentor
and remains
my closest soulmate
until today*

...

Contents

Abstract	vii
Zusammenfassung	ix
Acknowledgements	xi
1 Introduction	1
1.1 Molecular electronics and spintronics	1
1.2 Thesis outline	4
2 Theory of quantum transport	7
2.1 Nonequilibrium Green's functions formalism	7
2.1.1 Introduction	7
2.1.2 Average of an observable in nonequilibrium	8
2.1.3 Nonequilibrium perturbation expansion	11
2.1.4 Analytic continuation and Langreth theorem	13
2.1.5 Keldysh equation	16
2.1.6 Physical meaning of real-time Green's functions	17
2.1.7 Nonequilibrium formalism in mesoscopic transport	18
2.1.7.1 Stationary mesoscopic transport	21
2.1.8 Nonequilibrium current fluctuations	22
2.2 Single-molecule magnets	26
2.2.1 Giant spin approximation	27
2.2.2 Quantum tunneling of magnetization	29
2.2.3 Large spin and classical limit	30
2.3 Spin-transfer torque	31
3 Spin transport and tunable Gilbert damping in a molecular magnet junction	35
3.1 Introduction	35
3.2 Current response to a time-dependent magnetic field	37
3.2.1 Model and formalism	37
3.2.2 Analysis of the spin and current responses	42
3.3 Spin-transfer torque and molecular spin dynamics	43

3.3.1	Model with a precessing molecular spin	43
3.3.2	Analysis of the spin-transfer torque	49
3.4	Conclusions	56
4	Photon-assisted electronic and spin transport through a precessing spin of a molecular magnet	59
4.1	Introduction	59
4.2	Model setup	61
4.3	Theoretical formalism	63
4.4	Charge transport	66
4.4.1	Dynamic charge conductance	66
4.4.2	Density of states in the quantum dot	68
4.4.3	Analysis of the dynamic conductance	69
4.4.4	Frequency dependence of the ac conductance and equivalent circuit	72
4.4.5	Effects of other parameters on the ac conductance	76
4.5	Spin transport and spin-transfer torque	81
4.5.1	Spin transport under dc-bias voltage	81
4.5.2	Photon-assisted spin transport under ac-bias voltage	83
4.5.3	Analysis of the time-averaged spin transport	84
4.6	Conclusions	91
5	Shot noise of charge and spin transport in a molecular magnet junction	93
5.1	Introduction	93
5.2	Model and theoretical framework	95
5.3	Shot noise of charge current	100
5.4	Shot noise of spin current and spin-transfer torque	105
5.5	Conclusions	112
6	Conclusions and outlook	113
A	Floquet theorem	115
B	Noise power of charge and spin transport	119
	Bibliography	129

Quantum Transport Through Molecular Magnets

Chapter 1

Introduction

1.1 Molecular electronics and spintronics

One of the challenges in modern electronics is to create high-speed processing devices of miniature size. New advancements in technology enable investigation of transport on nanoscale, using quantum dots, quantum wires, molecules, etc. The pioneers of molecular electronics A. Aviram and M. Ratner first proposed the potential use of molecules as components of electronic circuitry [1]. Transport through single molecules or molecular clusters has attracted much attention in the last decades [2, 3]. This is in accordance with the Moore's law which tells that the number of transistors in computer processors exponentially increases in time [4]. The research in molecular electronics involve the study of molecular level structure, transport properties such as charge current, conductance, and noise, as well as the possible applications as memory devices, wires, switches, rectifiers [4–6], etc. Besides various technological motives, from the physical point of view the research in this field is useful, to comprehend the transport properties on the molecular scale. Many kinds of molecules are considered as good candidates for fabrication of devices, from small organic polymers [4, 7, 8] and large biomolecules [9–11], to carbon nanotubes [12–14].

Using chemical engineering various types of molecules with desired characteristics can be synthesized for quantum transport investigations. If the Coulomb interactions are weak one finds that the current as a function of bias voltage increases with the increase of the number of the available transport channels. However, in the presence of strong Coulomb interactions and due to the Pauli exclusion principle, important effects such as e.g., Coulomb blockade [15], Kondo effect [16–19], and negative differential resistance [20, 21] can arise. The dynamics

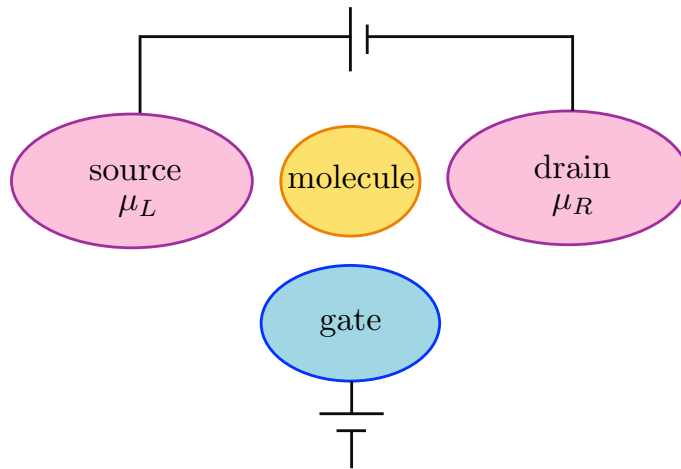


FIGURE 1.1: Setup of a molecular transport junction. The molecule is coupled to two metallic leads with chemical potentials μ_L and μ_R . The charge current is driven by the bias voltage $eV = \mu_L - \mu_R$. An additional gate electrode can be used to modify the molecular electrostatic potential.

of current-carrying electrons in molecular transport junctions is complicated since they move in the field of other electrons and nuclei in molecules. The geometry and organization of the molecule can be changed, under the influence of charge current. Unique transport characteristics were observed in molecular junctions due to the interaction between electrons and vibrational degrees of freedom [15, 22–27] and spins [28–30], which are absent in quantum dots and carbon nanotubes.

The molecular conduction behavior range from the absence of the electron conduction (insulators) [31] to superconducting behavior [32]. The conduction properties of molecules can be controlled by the application of lasers, since external electromagnetic fields excite the electrons in molecules to orbitals with higher energy, thus changing the current-voltage characteristics of charge transport [33–39]. Photon-assisted tunneling is a phenomenon based on the influence of the external time-dependent periodic fields in molecular junctions, where excited electrons participate in inelastic tunneling processes [33]. The control of electron transport through molecules can also be obtained by employing magnetic fields [29, 40, 41], e.g., in the presence of Kondo effect [18], or in junctions with single-molecule magnets [42].

Molecular transport junction is an open system, consisting of two leads (source and drain), coupled to a molecule or group of molecules [7]. The leads are considered large reservoirs, treated as grand canonical ensembles of free electrons, with different chemical potentials, where the current through the interacting (central) region is generated by the bias-voltage $eV = \mu_L - \mu_R$. A gate electrode can be used to control the position of molecular orbitals with respect to the chemical potentials of the leads [43, 44]. A typical molecular junction is shown in Fig. 1.1. The setup

of the molecule coupled to contacts is described by the following Hamiltonian

$$\hat{H} = \hat{H}_{\text{leads}} + \hat{H}_T + \hat{H}_{\text{molecule}}, \quad (1.1)$$

where \hat{H}_{leads} is the Hamiltonian of the leads, while \hat{H}_T represents the tunnel coupling between the leads and the molecule, and $\hat{H}_{\text{molecule}}$ is the Hamiltonian of the molecule. In calculations, the wide-band limit is a frequently used approximation, where one assumes that the self-energy originating from the coupling of the molecule with the leads is energy-independent, including only the broadening of the molecular level, while the energy shift of the level is neglected [45].

The nonequilibrium Green's functions method has been widely used in study of both dc and ac transport through molecules [46–49]. Many works using this method include perturbation theory [22, 50, 51], equation of motion technique [52], etc. Employing nonequilibrium Green's functions technique one can take into account electron-phonon interactions, external magnetic field and decoherence in the calculation of transport properties through molecular devices. Theoretically, quantum transport through molecules has also been investigated using various other methods, such as scattering theory [53–56], density functional theory [57, 58], time-dependent density functional theory [59–61], density-matrix theory [62–66], real-time path integration [67, 68], and numerical renormalization group method [69–71].

Various experimental techniques have been used to manufacture molecular junctions. Molecules can be contacted to leads using scanning tunneling microscopy, where a molecule is placed between tip and substrate [27, 72–75]. The other possibility is to use break junction method [7, 44, 76, 77] or electromigration [15, 78, 79], with a molecule placed in the gap of a wire between two ends where bias-voltage is applied. Usually, a gate electrode is also present to control and shift energy spectrum of the molecular orbitals [80]. Atomic force microscopy has also been widely used [81, 82]. Using these techniques, the current and its derivative with respect to the applied voltage (conductance) are measured. Inelastic electron tunneling spectroscopy measures the second derivative of current with respect to voltage, and gives information about the vibrations of atoms in the molecular junction [83–85].

Besides charge, electrons possess intrinsic spin degree of freedom. Spin dependent electron transport i.e., spintronics is a new field of research where electron spins are the carriers of transport [40, 86]. Many spintronic devices use giant magnetoresistance effect where the resistance of the system, consisting of alternating ferromagnetic and nonmagnetic layers, depends on the spin of the conduction electrons and is controlled by changing the orientation of the magnetization in the ferromagnetic layers [87, 88]. Here, the antiparallel alignment of the electron

spins and the magnetization of a ferromagnetic layer lead to the high resistance, while for their parallel alignment the resistance is low. The research in spintronics started with the discovery of the giant magnetoresistance effect. Spintronic devices can also be manufactured e.g., by using ferromagnetic leads as sources of spin-polarized currents [40, 89, 90]. Spintronic devices are smaller, cheaper, spend less energy, with faster information processing, than devices using electron charge, which makes them more convenient for applications in technology.

Single-molecule magnets are an important group of molecules [91]. They are nanomagnets with both quantum [92–101] and classical [92] characteristics, and due to their properties are good candidates for quantum computing [102, 103] and information storage [104, 105], molecular electronics and spintronics [2, 5, 86, 106, 107]. Molecular spintronics investigates the influence of spin-polarized currents on the state of the magnetization of the molecular magnets. The spin state of the molecular magnet can be controlled and manipulated using spin-polarized currents. During the transfer of spin-angular momentum between the molecular spin and spin-polarized current a spin-transfer torque is exerted onto the molecular spin [108–111]. Current-induced magnetization switching of single-molecule magnets has been experimentally observed [90, 112–114]. Solving the dynamics of the molecular spin in the presence of the spin-polarized currents could lead to its efficient manipulation and control. Experimental realization of spintronic devices aiming to control and manipulate the spin states of the molecules are e.g., molecular spin transistor, spin-valve, and multi-dot devices [40].

1.2 Thesis outline

In this thesis we theoretically study the time-dependent spin and charge transport through a molecular level in the presence of the precessing molecular spin in a magnetic field. The molecular spin is treated as a classical variable, while for the electron spin and charge transport we use a quantum-mechanical description.

In Chapter 2 we introduce the Keldysh nonequilibrium Green's functions technique which is used to derive and analyze spin and charge currents and noise. Later, in the same chapter, we briefly introduce single-molecule magnets and the concept of spin-transfer torque.

In Chapter 3 we derive expressions for charge and spin currents in the presence of an arbitrary time-dependent magnetic field in linear approximation with respect to the field. Then we analyze the inelastic tunneling processes created by the coupling between the electronic and precessing molecular spins in a constant magnetic field. The inelastic spin currents in turn exert a spin-transfer torque

on the spin of the molecule, including the Gilbert damping term and a term that modifies the precession frequency. The molecular spin precession is kept steady by external means and pumps electron spins into the leads. The Gilbert damping coefficient and the coefficient related to the change of the precession frequency can be controlled by the bias and gate voltages, or via the external magnetic field.

In Chapter 4 we go beyond and turn on time-dependent periodic fields in the leads. Here, we calculate the spin and charge currents, linear in time-dependent chemical potentials. Then we analyze the dynamic charge conductance and show that in the low ac-frequency limit the junction behaves as a classical electric circuit. The real and imaginary components of the ac conductance are both enhanced after going to a local minimum, for resonant positions of the chemical potentials with molecular quasienergy levels, around the ac frequency that matches the Larmor frequency of the molecular spin precession. Later, we calculate and analyze the photon-assisted spin currents and spin-transfer torque. We show that the system can be employed to obtain dc-spin currents with arbitrary magnetization direction for the ac frequency matching the Larmor frequency.

In Chapter 5 we investigate shot noise of charge and spin currents and spin-transfer torque in the presence of only dc-bias voltage. The competition between the contributions of elastic and inelastic precession-assisted tunneling, including the possibility of quantum interference between correlated currents, result in the dip-like features in the shot noise of charge current. The driving mechanism of the spin-torque noise components involves both precession of the molecular spin and the bias-voltage. The correlations of spin-torques in the same spatial direction in the plane of precession are contributed by elastic processes, and by inelastic processes where current-carrying spin particles change the energy by one or two Larmor frequencies. The elastic tunneling contributions are not present in the correlations of the perpendicular spin-torque components in the precession plane. We obtained relations which connect these components of the spin-torque noise and the Gilbert damping coefficient at zero temperature.

Finally, in Chapter 6 we conclude and give an outlook of the possible directions in future research.

Chapter 2

Theory of quantum transport

2.1 Nonequilibrium Green's functions formalism

2.1.1 Introduction

In condensed matter physics quantum mechanical systems are modeled by the Hamiltonian operator, which is usually not solvable exactly. In order to attack this problem, various perturbative techniques are used. In the presence of time-dependent magnetic or electric fields, or if the system is connected to electric contacts with different chemical potentials, for example, the system is in a nonequilibrium state. In these cases, the Keldysh nonequilibrium Green's functions technique is used as an efficient method to obtain ensemble and quantum averages of various observables that characterize the system under consideration [46, 115, 116]. This technique is particularly useful to analyze quantum transport in mesoscopic systems [46]. Section 2.1 is based on [46, 117–120].

In equilibrium, in the presence of interactions, the Hamiltonian of a system consists of a solvable, noninteracting, diagonalizable Hamiltonian \hat{H}_0 , and an interacting part \hat{H}^i ,¹

$$\hat{H} = \hat{H}_0 + \hat{H}^i. \quad (2.1)$$

Considering the grand canonical ensemble, with the particle number operator \hat{N} , and the chemical potential μ maintained by a particle reservoir, one needs to incorporate the term $-\mu\hat{N}$ in \hat{H}_0 . The system is in contact with the thermostat at temperature T .

¹We use a hat "^^" over a symbol to denote an operator and/or a matrix.

At zero temperature, the system is in the ground state $|\Psi_0\rangle$, and the single-particle Green's function is given by [117, 121, 122]

$$G(\vec{r}, t; \vec{r}', t') = -i \frac{\langle \Psi_0 | T_t \{ \hat{\psi}_H(\vec{r}, t) \hat{\psi}_H^\dagger(\vec{r}', t') \} | \Psi_0 \rangle}{\langle \Psi_0 | \Psi_0 \rangle}, \quad (2.2)$$

where we use units in which $\hbar = 1$, and T_t is the time-ordering operator. In Eq. (2.2), $\hat{\psi}_H(\vec{r}, t)$ are the field operators in the Heisenberg picture, with respect to the Hamiltonian \hat{H} .

Since the ground state $|\Psi_0\rangle$ is unknown, the Green's functions are obtained using the scattering \hat{S} -matrix, which connects the initial and final states of a system in the interaction picture, $|\Psi(t)\rangle = \hat{S}(t, t')|\Psi(t')\rangle$. The \hat{S} -matrix is given by [118, 122]

$$\hat{S}(t, t') = T_t \{ e^{-i \int_{t'}^t dt'' \hat{H}_{H_0}^i(t'')} \}, \quad (2.3)$$

where $\hat{H}_{H_0}^i(t)$ is the interaction operator \hat{H}^i in the interaction picture. The Gell-Mann-Low theorem relates the exact ground state of the system $|\Psi_0\rangle$ and the noninteracting ground state $|\Phi_0\rangle$ as $|\Psi_0\rangle = \hat{S}(0, -\infty)|\Phi_0\rangle$ [123]. Using this theorem the single-particle Green's function at zero temperature becomes [46, 117]

$$G(\vec{r}, t; \vec{r}', t') = -i \frac{\langle \Phi_0 | T_t \{ \hat{S}(\infty, -\infty) \hat{\psi}_{H_0}(\vec{r}, t) \hat{\psi}_{H_0}^\dagger(\vec{r}', t') \} | \Phi_0 \rangle}{\langle \Phi_0 | \hat{S}(\infty, -\infty) | \Phi_0 \rangle}, \quad (2.4)$$

where $\hat{\psi}_{H_0}(\vec{r}, t)$ is the field operator in the interaction picture. In Eq. (2.4) one can apply the Wick's theorem, and obtain the perturbation expansion of the Green's function [117].

When the system is in a nonequilibrium state, or in an equilibrium state at nonzero temperature, the Gell-Mann-Low theorem fails, since the system usually does not return to its initial state after infinitely long time. In these cases, the perturbation expansion can be constructed by employing closed time path formalism, in which contour-ordering operator is used instead of time-ordering operator [46, 115, 116, 119, 124, 125]. With the contour-ordered Green's functions, the nonequilibrium approach is formally equivalent to the equilibrium theory [125].

2.1.2 Average of an observable in nonequilibrium

In a nonequilibrium situation, the total Hamiltonian of the system can be formulated as follows:

$$\hat{\mathcal{H}}(t) = \hat{H} + \hat{H}'(t), \quad (2.5)$$

where \hat{H} is the time-independent part given by Eq. (2.1), while $\hat{H}'(t)$ represents the nonequilibrium term, which is turned on at time $t = t_0$. Assuming that the system is in thermal equilibrium before turning on the time-dependent perturbation, it can be described by density matrix

$$\hat{\rho}(\hat{H}) = \frac{e^{-\beta\hat{H}}}{\text{Tr}[e^{-\beta\hat{H}}]}, \quad (2.6)$$

where $\beta = 1/(k_B T)$. In the Heisenberg picture the operators evolve in accordance with the Hamiltonian $\hat{\mathcal{H}}(t)$, i.e.,

$$\hat{O}_{\mathcal{H}}(t) = \hat{u}_{\mathcal{H}}^\dagger(t, t_0) \hat{O} \hat{u}_{\mathcal{H}}(t, t_0), \quad (2.7)$$

where $\hat{O} = \hat{O}_{\mathcal{H}}(t_0)$ is the corresponding operator in the Schrödinger picture. In Eq. (2.7) the evolution operator is given by

$$\hat{u}_{\mathcal{H}}(t, t_0) = T_t \{ e^{-i \int_{t_0}^t dt' \hat{\mathcal{H}}(t')} \}. \quad (2.8)$$

The quantum statistical expectation value of the observable $\hat{O}_{\mathcal{H}}(t)$ with respect to $\hat{\rho}(\hat{H})$ for $t > t_0$ is given by

$$\langle \hat{O}_{\mathcal{H}}(t) \rangle = \text{Tr}[\hat{\rho}(\hat{H}) \hat{O}_{\mathcal{H}}(t)]. \quad (2.9)$$

If the system evolves according to the time-independent Hamiltonian \hat{H} , where the evolution operator can be written as

$$\hat{u}_H(t, t_0) = e^{-i\hat{H}(t-t_0)}, \quad (2.10)$$

then the time evolution of the operator $\hat{O}_H(t)$ in the Heisenberg picture is given by

$$\hat{O}_H(t) = \hat{u}_H^\dagger(t, t_0) \hat{O} \hat{u}_H(t, t_0). \quad (2.11)$$

According to Eqs. (2.7) and (2.11) the time evolution of the observable $\hat{O}_{\mathcal{H}}(t)$ can be further expressed as

$$\hat{O}_{\mathcal{H}}(t) = \hat{v}_H^\dagger(t, t_0) \hat{O}_H(t) \hat{v}_H(t, t_0), \quad (2.12)$$

where

$$\hat{v}_H(t, t_0) = T_t \{ e^{-i \int_{t_0}^t dt' \hat{H}'_H(t')} \}. \quad (2.13)$$

The contour-ordering operator T_{C_t} on the contour C_t which is depicted in Fig. 2.1(a), applied to a product of n fermion operators, orders them in a way

that the latest time on the contour C_t comes first

$$T_{C_t}\{\hat{O}_1(t_1)\hat{O}_2(t_2)\dots\hat{O}_n(t_n)\} = (-1)^P \hat{O}_{p1}(t_{p1})\hat{O}_{p2}(t_{p2})\dots\hat{O}_{pn}(t_{pn}), \quad (2.14)$$

$t_{p1} >_{C_t} t_{p2} >_{C_t} \dots >_{C_t} t_{pn}$. In the factor $(-1)^P$, the number of permutations of operators from the original order is given by P .

Using the contour-ordering operator T_{C_t} , an equivalent form of Eq. (2.12) can be written as [46, 119, 125]

$$\hat{O}_{\mathcal{H}}(t) = T_{C_t}\{e^{-i\int_{C_t} d\tau \hat{H}'_{\mathcal{H}}(\tau)} \hat{O}_H(t)\}. \quad (2.15)$$

The goal is to express the time-dependent part of the average value $\langle \hat{O}_{\mathcal{H}}(t) \rangle$ using the interaction picture, in which the evolution of the operator is governed by the noninteracting Hamiltonian \hat{H}_0 ,

$$\hat{O}_{H_0}(t) = \hat{u}_{H_0}^\dagger(t, t_0) \hat{O} \hat{u}_{H_0}(t, t_0). \quad (2.16)$$

Here, the evolution operator reads

$$\hat{u}_{H_0}(t, t_0) = e^{-i\hat{H}_0(t-t_0)}. \quad (2.17)$$

Employing Eqs. (2.7) and (2.16), one obtains the relation

$$\hat{O}_{\mathcal{H}}(t) = \hat{v}_{H_0}^\dagger(t, t_0) \hat{O}_{H_0}(t) \hat{v}_{H_0}(t, t_0), \quad (2.18)$$

with $\hat{v}_{H_0}(t, t_0) = \hat{u}_{H_0}^\dagger(t, t_0) \hat{u}_{\mathcal{H}}(t, t_0)$. Finding $\partial_t \hat{v}_{H_0}(t, t_0)$, and integrating the obtained expression over time interval from t_0 to t , with the boundary condition $\hat{v}_{H_0}(t, t_0) = \hat{1}$, where $\hat{1}$ is the identity operator, one transforms Eq. (2.18) with the help of the contour-ordering operator T_{C_t} into [119, 125]

$$\hat{O}_{\mathcal{H}}(t) = T_{C_t}\{e^{-i\int_{C_t} d\tau [\hat{H}_{H_0}^i(\tau) + \hat{H}'_{H_0}(\tau)]} \hat{O}_{H_0}(t)\}. \quad (2.19)$$

In order to enable the application of the Wick's theorem, the expectation value in Eq. (2.9) needs to be transformed to the one in the interaction picture with respect to the quadratic density matrix $\hat{\rho}(\hat{H}_0)$. This can be easily obtained by using the following relation [119, 125]

$$e^{-\beta \hat{H}} = e^{-\beta \hat{H}_0} T_{C_\beta} \{e^{-i\int_{t_0}^{t_0-i\beta} d\tau \hat{H}_{H_0}^i(\tau)}\}, \quad (2.20)$$

and the closed contour C running from t_0 to t and back to t_0 , where the contour-time variable τ lies on either the upper or lower part of the contour, depicted in

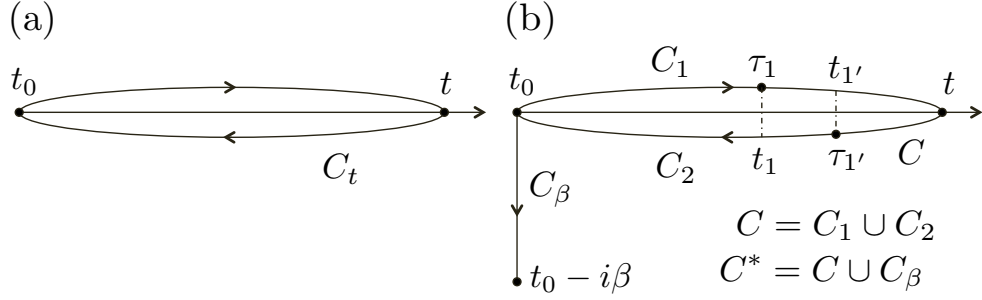


FIGURE 2.1: (a) Contour C_t running from t_0 to t and back to t_0 on the real-time axis. (b) Keldysh contour in the complex-time plane, $C^* = C \cup C_\beta$, where C runs from t_0 to t and back to t_0 , passing through contour-times τ_1 and τ_1' only once. The contour time $\tau_1' >_C \tau_1$, where $>_C$ denotes greater in the contour sense. The contour part C_β runs from t_0 to $t_0 - i\beta$.

Fig. 2.1(b). The contour C_β runs from t_0 to $t_0 - i\beta$, with the corresponding contour-ordering operator denoted as T_{C_β} . The contour-ordering operator T_C which orders operators along the contour C , places the operators with the latest contour times first, regardless of their projections on the real-time axis. The contours C and C_β form the Keldysh contour $C^* = C \cup C_\beta$ shown in Fig. 2.1(b) [116]. According to Eqs. (2.19) and (2.20), the expectation value given by Eq. (2.9) can be written using the Keldysh contour C^* as [119, 120, 125]

$$\begin{aligned} \langle \hat{O}_{\mathcal{H}}(t) \rangle &= \frac{\text{Tr} [e^{-\beta \hat{H}_0} T_{C_\beta} \{ e^{-i \int_{t_0}^{t_0 - i\beta} d\tau \hat{H}_{H_0}^i(\tau)} \} T_C \{ \hat{S}_C^i \hat{S}'_C \hat{O}_{H_0}(t) \}]}{\text{Tr} [e^{-\beta \hat{H}_0} T_{C_\beta} \{ e^{-i \int_{t_0}^{t_0 - i\beta} d\tau \hat{H}_{H_0}^i(\tau)} \}]} \\ &= \frac{\text{Tr} [\hat{\rho}(\hat{H}_0) T_{C^*} \{ \hat{S}_{C^*}^i \hat{S}'_C \hat{O}_{H_0}(t) \}]}{\text{Tr} [\hat{\rho}(\hat{H}_0) T_{C^*} \{ \hat{S}_{C^*}^i \hat{S}'_C \}]} \end{aligned} \quad (2.21)$$

where

$$\hat{S}_C^i = e^{-i \int_C d\tau \hat{H}_{H_0}^i(\tau)}, \quad (2.22)$$

$$\hat{S}'_C = e^{-i \int_C d\tau \hat{H}'_{H_0}(\tau)}, \quad (2.23)$$

$$\hat{S}_{C^*}^i = e^{-i \int_{C^*} d\tau \hat{H}_{H_0}^i(\tau)}. \quad (2.24)$$

In this factorization, the time-dependent part is reduced only to the evolution of the operator with respect to the noninteracting Hamiltonian \hat{H}_0 . The main result for the further consideration is contained in Eq. (2.21), since it can be decomposed using Wick's theorem.

2.1.3 Nonequilibrium perturbation expansion

Using the contour-ordering operator T_C and the fermion field operator in the Heisenberg picture $\hat{\psi}_{\mathcal{H}}$ and its adjoint, one can define the contour-ordered Green's

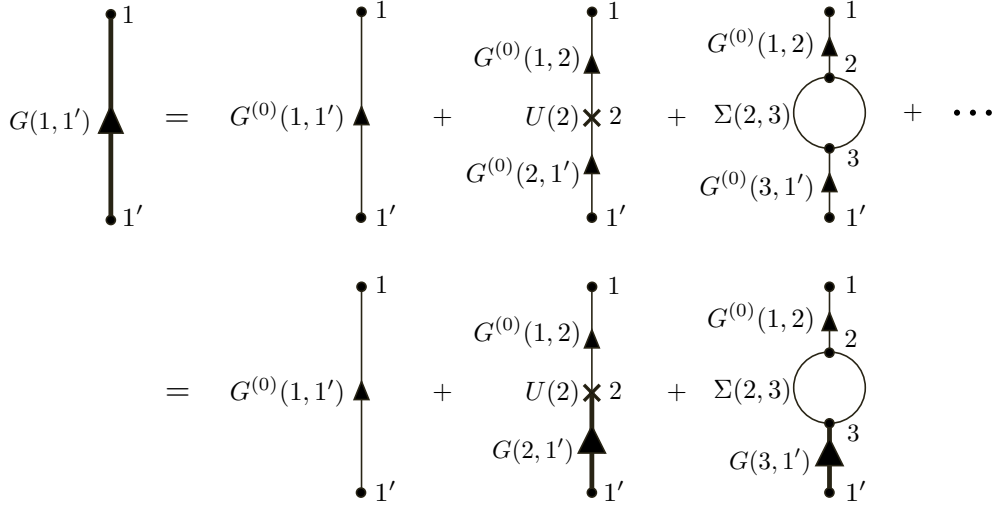


FIGURE 2.2: Representation of the Dyson equation in terms of Feynman diagrams.

function of a single particle as

$$G(1, 1') = -i \langle T_C \{ \hat{\psi}_{\mathcal{H}}(1) \hat{\psi}_{\mathcal{H}}^\dagger(1') \} \rangle. \quad (2.25)$$

In the abbreviation $(1) \equiv (\vec{x}_1, \tau_1)$, the variable \vec{x}_1 symbolizes the particle position in space, and may include other degrees of freedom, like spin, while τ_1 is the contour time. The contour C runs from t_0 to $\max\{t_1, t'_1\}$ or infinity and back to t_0 .

According to Eq. (2.21), the Green's function given by Eq. (2.25) can be obtained in the interaction picture as [119, 125]

$$G(1, 1') = -i \frac{\text{Tr}[\hat{\rho}(\hat{H}_0) T_{C^*} \{ \hat{S}_{C^*}^i \hat{S}'_C \hat{\psi}_{H_0}(1) \hat{\psi}_{H_0}^\dagger(1') \}]}{\text{Tr}[\hat{\rho}(\hat{H}_0) T_{C^*} \{ \hat{S}_{C^*}^i \hat{S}'_C \}]} \quad (2.26)$$

Presuming that the system was in equilibrium before turning on the external perturbation, so that the initial correlations can be neglected, one can use the initial time limit $t_0 \rightarrow -\infty$. This means that the integration over C_β can be discarded in Eq. (2.26), since the perturbation caused by the external field vanishes on this segment of the contour, i.e., $C^* \equiv C$ [119, 125]. With this boundary condition, the denominator in Eq. (2.26), $\text{Tr}[\hat{\rho}(\hat{H}_0) T_C \{ \hat{S}_C^i \hat{S}'_C \}] = 1$, as the contour C is closed, leading to $T_C \{ \hat{S}_C^i \hat{S}'_C \} = \hat{1}$, and the Green's function can be obtained in the interaction picture as [119, 125]

$$G(1, 1') = -i \text{Tr}[\hat{\rho}(\hat{H}_0) T_C \{ \hat{S}_C^i \hat{S}'_C \hat{\psi}_{H_0}(1) \hat{\psi}_{H_0}^\dagger(1') \}]. \quad (2.27)$$

The right-hand side of Eq. (2.27) can be expanded in terms of products of field operators averaged with respect to $\hat{\rho}(\hat{H}_0)$. Assuming for simplicity that the

time-dependent perturbation term in the Hamiltonian is presented by coupling of particles to an external potential $U(\vec{x}, t)$, the first two terms in this expansion read² [46, 119, 125]

$$G^{(0)}(1, 1') = -i\text{Tr}[\hat{\rho}(\hat{H}_0)T_C\{\hat{\psi}_{H_0}(1)\hat{\psi}_{H_0}^\dagger(1')\}], \quad (2.28)$$

$$\begin{aligned} G^{(1)}(1, 1') &= (-i)^2 \int d\vec{x}_2 \int_C d\tau_2 U(2)\text{Tr}[\hat{\rho}(\hat{H}_0)T_C\{\hat{\psi}_{H_0}^\dagger(2)\hat{\psi}_{H_0}(2)\hat{\psi}_{H_0}(1)\hat{\psi}_{H_0}^\dagger(1')\}] \\ &= \int d\vec{x}_2 \int_C d\tau_2 G^{(0)}(1, 2)U(2)G^{(0)}(2, 1'). \end{aligned} \quad (2.29)$$

Each term $G^{(n)}(1, 1')$, where n denotes the order of expansion can be further decomposed into products, using Wick's theorem which works also for contour-ordered products of field operators. Every product contains the free particle Green's function $G^{(0)}(1, 1')$. The terms of the expansion can be summed up by the Dyson's equation [46, 119, 125]

$$\begin{aligned} G(1, 1') &= G^{(0)}(1, 1') + G^{(1)}(1, 1') + G^{(2)}(1, 1') + \dots \\ &= G^{(0)}(1, 1') + \int d\vec{x}_2 \int_C d\tau_2 G^{(0)}(1, 2)U(2)G(2, 1') \\ &\quad + \int d\vec{x}_2 \int_C d\tau_2 \int d\vec{x}_3 \int_C d\tau_3 G^{(0)}(1, 2)\Sigma(2, 3)G(3, 1'), \end{aligned} \quad (2.30)$$

where the interactions are included in a functional of G , called the self-energy $\Sigma[G]$.

All perturbation expansion terms and the Dyson's equation can be represented diagrammatically, using Feynman diagrams [46, 117–119], as shown in Fig. 2.2. Thin lines from one argument to the other, with an arrow in the middle depict the free contour-ordered Green's function $G^{(0)}$. The full Green's function G is illustrated by a thick line. The interaction of the particles with the potential U is represented by a cross, while the self-energy Σ joins the rest of the diagram by two external fermion lines. Nonequilibrium perturbation theory with contour-ordered Green's functions is rather formal. In order to solve practical problems, one needs to replace contour integrals by integrals over real time.

2.1.4 Analytic continuation and Langreth theorem

Analytic continuation is a method to generate real-time Green's functions from a contour-ordered Green's function [115, 126]. Since $t_0 \rightarrow -\infty$, the part of the contour C that starts at $-\infty$ and ends at ∞ , can be denoted as C_1 , while C_2 symbolizes the branch from ∞ to $-\infty$. Depending on the position of the time

²An integral in space denotes an integration over the entire real space.

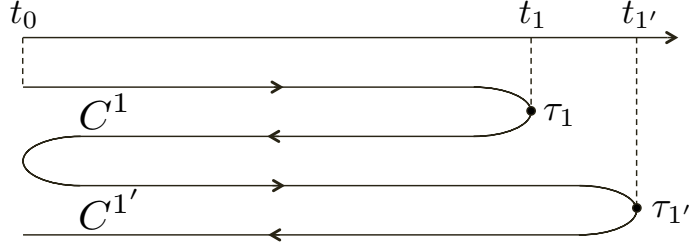


FIGURE 2.3: Deformation of the contour C into two loops C^1 and $C^{1'}$ for τ_1 on the upper half and $\tau_{1'}$ on the lower half of the contour.

arguments on the contour C , the contour-ordered Green's function includes the following functions:

$$G(1, 1') = \begin{cases} G_{C_1}(1, 1') & \tau_1, \tau_{1'} \in C_1 \\ G^<(1, 1') & \tau_1 \in C_1, \tau_{1'} \in C_2 \\ G^>(1, 1') & \tau_1 \in C_2, \tau_{1'} \in C_1 \\ G_{C_2}(1, 1') & \tau_1, \tau_{1'} \in C_2 \end{cases}, \quad (2.31)$$

where, $G_{C_1}(1, 1')$, $G^<(1, 1')$, $G^>(1, 1')$, and $G_{C_2}(1, 1')$ are the time-ordered, lesser, greater and antitime-ordered Green's functions defined as

$$\begin{aligned} G_{C_1}(1, 1') &= -i\langle T_t[\hat{\psi}_{\mathcal{H}}(1)\hat{\psi}_{\mathcal{H}}^\dagger(1')] \rangle \\ &= -i\theta(t_1 - t_{1'})\langle \hat{\psi}_{\mathcal{H}}(1)\hat{\psi}_{\mathcal{H}}^\dagger(1') \rangle + i\theta(t_{1'} - t_1)\langle \hat{\psi}_{\mathcal{H}}^\dagger(1')\hat{\psi}_{\mathcal{H}}(1) \rangle, \end{aligned} \quad (2.32)$$

$$G^<(1, 1') = +i\langle \hat{\psi}_{\mathcal{H}}^\dagger(1')\hat{\psi}_{\mathcal{H}}(1) \rangle, \quad (2.33)$$

$$G^>(1, 1') = -i\langle \hat{\psi}_{\mathcal{H}}(1)\hat{\psi}_{\mathcal{H}}^\dagger(1') \rangle, \quad (2.34)$$

$$\begin{aligned} G_{C_2}(1, 1') &= -i\langle \tilde{T}_t[\hat{\psi}_{\mathcal{H}}(1)\hat{\psi}_{\mathcal{H}}^\dagger(1')] \rangle \\ &= -i\theta(t_{1'} - t_1)\langle \hat{\psi}_{\mathcal{H}}(1)\hat{\psi}_{\mathcal{H}}^\dagger(1') \rangle + i\theta(t_1 - t_{1'})\langle \hat{\psi}_{\mathcal{H}}^\dagger(1')\hat{\psi}_{\mathcal{H}}(1) \rangle. \end{aligned} \quad (2.35)$$

It is useful to introduce the retarded and advanced Green's functions $G^r(1, 1')$ and $G^a(1, 1')$, which appear in analytic continuation,

$$G^r(1, 1') = -i\theta(t_1 - t_{1'})\langle \{\hat{\psi}_{\mathcal{H}}(1), \hat{\psi}_{\mathcal{H}}^\dagger(1')\} \rangle, \quad (2.36)$$

$$G^a(1, 1') = i\theta(t_{1'} - t_1)\langle \{\hat{\psi}_{\mathcal{H}}(1), \hat{\psi}_{\mathcal{H}}^\dagger(1')\} \rangle, \quad (2.37)$$

where the brackets $\{\cdot, \cdot\}$ indicate an anticommutator.

According to the above definitions, the Green's functions are connected by the important relations given by

$$G_{C_1, C_2}(1, 1') = \theta(t_{1,1'} - t_{1',1})G^>(1, 1') + (t_{1',1} - t_{1,1'})G^<(1, 1'), \quad (2.38)$$

$$G_{C_1}(1, 1') + G_{C_2}(1, 1') = G^>(1, 1') + G^<(1, 1'), \quad (2.39)$$

$$G^{r,a}(1, 1') = \theta(t_{1,1'} - t_{1',1})[G^{>,<}(1, 1') - G^{<,>}(1, 1')], \quad (2.40)$$

$$G^r(1, 1') - G^a(1, 1') = G^>(1, 1') - G^<(1, 1'). \quad (2.41)$$

Using general functions of two contour times $A(\tau, \tau')$, $B(\tau, \tau')$, $C(\tau, \tau')$, and $D(\tau, \tau')$ instead of the contour-ordered Green's functions, one notices that the contour integrations in Dyson equation take the forms

$$C(\tau_1, \tau_{1'}) = \int_C d\tau_2 A(\tau_1, \tau_2)B(\tau_2, \tau_{1'}), \quad (2.42)$$

$$D(\tau_1, \tau_{1'}) = \int_C d\tau_2 \int_C d\tau_3 A(\tau_1, \tau_2)B(\tau_2, \tau_3)C(\tau_3, \tau_{1'}). \quad (2.43)$$

The transition from contour-ordered Green's function to real time Green's functions is obtained using Langreth theorem [126], which tells that components of the function given by Eq. (2.42) on the real-time axis can be expressed as

$$C^{<,>}(t_1, t_{1'}) = \int_{-\infty}^{\infty} dt [A^r(t_1, t)B^{<,>}(t, t_{1'}) + A^{<,>}(t_1, t)B^a(t, t_{1'})], \quad (2.44)$$

$$C^{r,a}(t_1, t_{1'}) = \int_{-\infty}^{\infty} dt A^{r,a}(t_1, t)B^{r,a}(t, t_{1'}). \quad (2.45)$$

The proof is obtained by proper deformations of the contour C , depending on the choice of contour-time variables. For the choice of variables $\tau_1 \in C_1$ and $\tau_{1'} \in C_2$, one finds $C^<(t_1, t_{1'})$ using the deformation contour depicted in Fig. 2.3 in the following way

$$\begin{aligned} C^<(t_1, t_{1'}) &= \int_{C^1} d\tau_2 A(\tau_1, \tau_2)B(\tau_2, \tau_{1'}) + \int_{C^{1'}} d\tau_2 A(\tau_1, \tau_2)B(\tau_2, \tau_{1'}) \\ &= \int_{-\infty}^{t_1} dt_2 A^>(t_1, t_2)B^<(t_2, t_{1'}) + \int_{t_1}^{-\infty} dt_2 A^<(t_1, t_2)B^<(t_2, t_{1'}) \\ &\quad + \int_{-\infty}^{t_{1'}} dt_2 A^<(t_1, t_2)B^<(t_2, t_{1'}) + \int_{t_{1'}}^{-\infty} dt_2 A^<(t_1, t_2)B^>(t_2, t_{1'}) \\ &= \int_{-\infty}^{\infty} dt_2 \theta(t_1 - t_2)[A^>(t_1, t_2) - A^<(t_1, t_2)]B^<(t_2, t_{1'}) \\ &\quad + \int_{-\infty}^{\infty} dt_2 \theta(t_{1'} - t_2)A^<(t_1, t_2)[B^<(t_2, t_{1'}) - B^>(t_2, t_{1'})], \end{aligned} \quad (2.46)$$

with $\tau_2 <_{C^1} \tau_{1'}$ and $\tau_2 >_{C^{1'}} \tau_1$, where $<_{C^1}$ and $>_{C^{1'}}$ denote lesser or greater in the contour sense. Using Eq. (2.40), one gets Eq. (2.44) for $C^<(t_1, t_{1'})$, while the proof for $C^>(t_1, t_{1'})$ can be carried out in a similar way, by choosing $\tau_1 \in C_2$ and $\tau_{1'} \in C_1$. The proof of Eq. (2.45) can be obtained by using Eqs. (2.40) and (2.44). The rules for product of three functions of two contour times given by Eq. (2.43), can be generated from the rules found for product of two functions. They are

given by

$$D^{<, >} = A^r B^r C^{<, >} + A^r B^{<, >} C^a + A^{<, >} B^a C^a, \quad (2.47)$$

$$D^{r, a} = A^{r, a} B^{r, a} C^{r, a}, \quad (2.48)$$

where products denote internal integrations over space (and spin), and internal real-time integrations. For the products of two functions of two parallel or antiparallel contour times

$$C(\tau, \tau') = A(\tau, \tau') B(\tau, \tau'), \quad (2.49)$$

$$D(\tau, \tau') = A(\tau, \tau') B(\tau', \tau), \quad (2.50)$$

one obtains on the real-time axis the lesser, greater and retarded components as

$$C^{<, >}(t, t') = A^{<, >}(t, t') B^{<, >}(t, t'), \quad (2.51)$$

$$D^{<, >}(t, t') = A^{<, >}(t, t') B^{>, <}(t', t), \quad (2.52)$$

$$C^r(t, t') = A^{<}(t, t') B^r(t, t') + A^r(t, t') B^{<}(t, t') + A^r(t, t') B^r(t, t'), \quad (2.53)$$

$$D^r(t, t') = A^{<}(t, t') B^a(t', t) + A^r(t, t') B^{<}(t', t). \quad (2.54)$$

Employing analytic continuation rules obtained by the application of the Langreth theorem [126], one can express any contour-ordered Green's function or any term in its perturbation expansion through real-time Green's functions.

2.1.5 Keldysh equation

By means of analytic continuation rules given by Eqs. (2.44) and (2.47), applied to the Dyson's equation, the expression for the lesser Green's function $G^{<}$ can be written as

$$G^{<} = G_0^{<} + G_0^r U G^{<} + G_0^{<} U G^a + G_0^r \Sigma^r G^{<} + G_0^r \Sigma^{<} G^a + G_0^{<} \Sigma^a G^a. \quad (2.55)$$

Since the potential U can be incorporated into G_0 , one can neglect it and obtain $G^{<}$ as

$$\begin{aligned} G^{<} &= G_0^{<} + G_0^r \Sigma^r (G_0^{<} + G_0^r \Sigma^r G^{<} + G_0^r \Sigma^{<} G^a + G_0^{<} \Sigma^a G^a) + G_0^r \Sigma^{<} G^a + G_0^{<} \Sigma^a G^a \\ &= (1 + G^r \Sigma^r) G_0^{<} (1 + \Sigma^a G^a) + G^r \Sigma^{<} G^a, \end{aligned} \quad (2.56)$$

known as the Keldysh integral equation [46, 116]. If the system was in an equilibrium state in infinite past, the first term in Eq. (2.56) drops to zero. The Keldysh

equation for the steady state systems then reads [46]

$$G^< = G^r \Sigma^< G^a. \quad (2.57)$$

The Keldysh equation (2.57) is widely used in calculations related to mesoscopic transport properties, such as charge current, shot noise etc.

2.1.6 Physical meaning of real-time Green's functions

According to the definition of the greater Green's function, in the real time domain $iG^>(\vec{x}, t, \vec{x}', t') = \langle \hat{\psi}_{\mathcal{H}}(\vec{x}, t) \hat{\psi}_{\mathcal{H}}^\dagger(\vec{x}', t') \rangle$ can be interpreted as the probability amplitude of finding a particle at the point (\vec{x}, t) , given that it is added to the system at the point (\vec{x}', t') . In a similar way, $-iG^<(\vec{x}, t, \vec{x}', t') = \langle \hat{\psi}_{\mathcal{H}}^\dagger(\vec{x}', t') \hat{\psi}_{\mathcal{H}}(\vec{x}, t) \rangle$ represents the propagation of a 'hole' from the point (\vec{x}, t) to the point (\vec{x}', t') .

The expectation values of experimentally measurable observables can be computed using Green's functions [46, 117]. Let $\hat{O} = \sum_i \hat{o}(\vec{x}_i)$ be the single-particle operator in the first quantization, where $\hat{o}(\vec{x}_i)$ acts on the i -th particle. Its second-quantized form in the Heisenberg picture is given by

$$\hat{O}_{\mathcal{H}}(t) = \int d\vec{x} \hat{\psi}_{\mathcal{H}}^\dagger(\vec{x}, t) \hat{o}(\vec{x}) \hat{\psi}_{\mathcal{H}}(\vec{x}, t). \quad (2.58)$$

The expectation value of $\hat{O}_{\mathcal{H}}(t)$ can be written as [117]

$$\begin{aligned} \langle \hat{O}_{\mathcal{H}}(t) \rangle &= \int d\vec{x} \langle \hat{\psi}_{\mathcal{H}}^\dagger(\vec{x}, t) \hat{o}(\vec{x}) \hat{\psi}_{\mathcal{H}}(\vec{x}, t) \rangle \\ &= \int d\vec{x} \lim_{\vec{x}' \rightarrow \vec{x}} \lim_{t' \rightarrow t} \hat{o}(\vec{x}) \langle \hat{\psi}_{\mathcal{H}}^\dagger(\vec{x}', t') \hat{\psi}_{\mathcal{H}}(\vec{x}, t) \rangle \\ &= -i \int d\vec{x} \lim_{\vec{x}' \rightarrow \vec{x}} \hat{o}(\vec{x}) G^<(\vec{x}, t, \vec{x}', t). \end{aligned} \quad (2.59)$$

For instance, the particle density operator in the first quantization can be written as $\hat{n}(\vec{x}) = \sum_i \delta(\vec{x} - \vec{x}_i)$ [117]. The average of the corresponding second-quantized operator in the Heisenberg picture $\hat{n}(\vec{x}, t) = \hat{\psi}_{\mathcal{H}}^\dagger(\vec{x}, t) \hat{\psi}_{\mathcal{H}}(\vec{x}, t)$ can be directly obtained using the real-time lesser Green's function as

$$\langle \hat{n}(\vec{x}, t) \rangle = -iG^<(\vec{x}, t, \vec{x}, t), \quad (2.60)$$

which is in agreement with Eq. (2.59). Other quantities such as charge current and current noise in nanoscale conductors can be evaluated using lesser Green's functions.

The real-time retarded Green's function $G^r(t, t')$ contains $\theta(t - t')$ and is interpreted as response of a given system at time t to a perturbation occurred at time $t' < t$.

The spectral function is defined as [46]

$$A(t, t') = i[G^r(t, t') - G^a(t, t')], \quad (2.61)$$

and represents the time-dependent local density of states.

2.1.7 Nonequilibrium formalism in mesoscopic transport

Let us investigate the time-dependent tunneling current in a system which is in nonequilibrium. The system consists of two metallic leads, left (L) and right (R), with free, noninteracting electrons, and chemical potentials μ_ξ , $\xi = L, R$, and the interacting central region. In the distant past, each region was in thermal equilibrium and they were uncoupled. Upon turning on the time-dependent tunnel coupling the charge current starts to flow. Time-dependent external driving is applied to the leads and the central region, and the system is now far from equilibrium.

The Hamiltonian of the system is given by [45, 46]

$$\hat{H}(t) = \sum_{\xi \in \{L, R\}} \hat{H}_\xi(t) + \hat{H}_T(t) + \hat{H}_C(t), \quad (2.62)$$

where $\hat{H}_\xi(t)$ is the Hamiltonian of the electrons in the lead $\xi = L, R$ given by

$$\hat{H}_\xi(t) = \sum_k \epsilon_{k\xi}(t) \hat{c}_{k\xi}^\dagger \hat{c}_{k\xi}, \quad (2.63)$$

with the single-particle energy in the lead ξ modulated by an external time-dependent driving $\Delta_\xi(t)$ as $\epsilon_{k\xi}(t) = \epsilon_{k\xi} + \Delta_\xi(t)$. The tunnel coupling between the leads and the central region is described by

$$\hat{H}_T(t) = \sum_{k, \xi, n} [V_{k\xi, n}(t) \hat{c}_{k\xi}^\dagger \hat{d}_n + V_{k\xi, n}^*(t) \hat{d}_n^\dagger \hat{c}_{k\xi}], \quad (2.64)$$

with matrix element $V_{k\xi, n}(t)$, and can be modulated with time-dependent gate voltages. The operators $\hat{c}_{k\xi}^\dagger (\hat{c}_{k\xi})$ are the creation (annihilation) operators of the electrons in the leads, while $\{\hat{d}_n^\dagger\}$ and $\{\hat{d}_n\}$ are the complete, orthonormal set of the creation and annihilation operators of electrons in the central region. The Hamiltonian of the central region \hat{H}_C reads

$$\hat{H}_C(t) = [\{\hat{d}_n^\dagger\}; \{\hat{d}_n\}, t], \quad (2.65)$$

and its exact description depends on the system under investigation.

The average charge current from lead ξ to the central region is given by [45, 46]

$$\begin{aligned} I_\xi(t) &= -e \left\langle \frac{d}{dt} \hat{N}_\xi \right\rangle \\ &= -e \frac{i}{\hbar} \langle [\hat{H}(t), \hat{N}_\xi] \rangle \\ &= -e \frac{i}{\hbar} \langle [\hat{H}_T(t), \hat{N}_\xi] \rangle \\ &= \frac{ie}{\hbar} \sum_{k,n} [V_{k\xi,n}(t) \langle \hat{c}_{k\xi}^\dagger \hat{d}_n \rangle - V_{k\xi,n}^*(t) \langle \hat{d}_n^\dagger \hat{c}_{k\xi} \rangle], \end{aligned} \quad (2.66)$$

where $\hat{N}_\xi = \sum_k \hat{c}_{k\xi}^\dagger \hat{c}_{k\xi}$ is the charge occupation number operator of the contact ξ . Defining two new Green's functions

$$G_{n,k\xi}^<(t, t') = i \langle \hat{c}_{k\xi}^\dagger(t') \hat{d}_n(t) \rangle, \quad (2.67)$$

$$G_{k\xi,n}^<(t, t') = i \langle \hat{d}_n^\dagger(t') \hat{c}_{k\xi}(t) \rangle, \quad (2.68)$$

and taking into account that $G_{k\xi,n}^<(t, t') = -[G_{n,k\xi}^<(t', t)]^*$, the expression for the current can be further simplified as [45, 46]

$$I_\xi(t) = \frac{2e}{\hbar} \text{Re} \left\{ \sum_{k,n} V_{k\xi,n}(t) G_{n,k\xi}^<(t, t) \right\}. \quad (2.69)$$

Employing the equation of motion technique [118] by applying partial derivative $-i\partial_{t'}$ to the time-ordered Green's function $G_{n,k\xi}^t(t, t') = -i \langle T_t \{ \hat{d}_n(t) \hat{c}_{k\xi}^\dagger(t') \} \rangle$, and replacing the intermediate time integration with the integration on the complex contour, one obtains the Dyson equation for the contour-ordered Green's function $G_{n,k\xi}(\tau, \tau') = -i \langle T_C \{ \hat{d}_n(\tau) \hat{c}_{k\xi}^\dagger(\tau') \} \rangle$,

$$G_{n,k\xi}(\tau, \tau') = \sum_m \int_C d\tau_1 G_{nm}(\tau, \tau_1) V_{k\xi,m}^*(\tau_1) g_{k\xi}(\tau_1, \tau'). \quad (2.70)$$

Here, $G_{nm}(\tau, \tau') = -i \langle T_C \{ \hat{d}_n(\tau) \hat{d}_m^\dagger(\tau') \} \rangle$ and $g_{k\xi}(\tau, \tau') = -i \langle T_C \{ \hat{c}_{k\xi}(\tau) \hat{c}_{k\xi}^\dagger(\tau') \} \rangle$ are the contour-ordered Green's functions of the central region and the leads. Applying analytic continuation rules and Langreth theorem [126] to Eq. (2.70), one obtains³

$$G_{n,k\xi}^<(t, t') = \sum_m \int dt_1 V_{k\xi,m}^*(t_1) [G_{nm}^r(t, t_1) g_{k\xi}^<(t_1, t') + G_{nm}^<(t, t_1) g_{k\xi}^a(t_1, t')], \quad (2.71)$$

³An integral without limits over one variable denotes an integral from $-\infty$ to ∞ .

with the real-time Green's functions of the contact ξ given by

$$g_{k\xi}^<(t, t') = i\langle \hat{c}_{k\xi}^\dagger(t') \hat{c}_{k\xi}(t) \rangle = if(\epsilon_{k\xi})e^{-i\int_{t'}^t dt_1 \epsilon_{k\xi}(t_1)}, \quad (2.72)$$

$$g_{k\xi}^r(t, t') = -i\theta(t-t')\langle \{ \hat{c}_{k\xi}(t), \hat{c}_{k\xi}^\dagger(t') \} \rangle = -i\theta(t-t')e^{-i\int_{t'}^t dt_1 \epsilon_{k\xi}(t_1)}, \quad (2.73)$$

and $g_{k\xi}^a(t, t') = [g_{k\xi}^r(t', t)]^*$. Inserting the expression for the real-time Green's function $G_{n,k\xi}^<(t, t')$ given by Eq. (2.71) into Eq. (2.69), and defining the matrix components of the tunneling self-energy in the indices of the central region m, n as

$$\Sigma_{\xi, mn}^{r,a,<,>}(t, t') = \sum_k V_{k\xi, m}^*(t) g_{k\xi}^{r,a,<,>}(t, t') V_{k\xi, n}(t'), \quad (2.74)$$

one arrives at the expression for the charge current from contact ξ given by [45, 46]

$$I_\xi(t) = \frac{2e}{\hbar} \text{Re} \int dt' \text{Tr} \{ [\hat{G}^r(t, t') \hat{\Sigma}_\xi^<(t', t) + \hat{G}^<(t, t') \hat{\Sigma}_\xi^a(t', t)] \}, \quad (2.75)$$

where the Green's functions $\hat{G}^{r,<}(t, t')$ and self-energies $\hat{\Sigma}_\xi^{<,a}(t', t)$ are matrices in the central-region indices m, n . The self-energy $\hat{\Sigma}_\xi^<$ is related to the occupation in the lead ξ , while $\hat{G}^<$ is related to the occupation in the central region. Accordingly, the first term in Eq. (2.75) can be associated to the current tunneling from the lead ξ to the central region, while the second term can be related to the tunneling into the lead ξ .

The summation over k in the leads can be converted into an energy integration $\int d\epsilon \rho_\alpha(\epsilon)$, where $\rho_\alpha(\epsilon)$ is the density of states in channel α . Defining the level-width function, which describes the coupling between the lead ξ and the central region as [45, 46]

$$[\Gamma_\xi(\epsilon, t_1, t)]_{mn} = 2\pi \sum_{\alpha \in \xi} \rho_\alpha(\epsilon) V_{\alpha, n}(\epsilon, t) V_{\alpha, m}^*(\epsilon, t_1) e^{-i\int_{t_1}^t dt_2 \Delta_\alpha(\epsilon, t_2)}, \quad (2.76)$$

the equation (2.75) can be rewritten as [45, 46]

$$I_\xi(t) = -\frac{2e}{\hbar} \int_{-\infty}^t dt_1 \int \frac{d\epsilon}{2\pi} \text{Im} \text{Tr} \{ e^{-i\epsilon(t_1-t)} \hat{\Gamma}_\xi(\epsilon, t_1, t) [\hat{G}^<(t, t_1) + f_\xi(\epsilon) \hat{G}^r(t, t_1)] \}. \quad (2.77)$$

Eqs. (2.75) and (2.77) express the tunneling current through an interacting central region, tunnel-coupled to noninteracting leads. They are rather formal since the calculation of $\hat{G}^{r,<}(t, t')$ is usually a complicated task. It is particularly useful for stationary transport, time-dependent resonant-level model, transport in the presence of harmonic time modulation, linear response [45, 46], etc.

2.1.7.1 Stationary mesoscopic transport

In the absence of external time-dependent driving in the leads and the central region, upon turning on the time-independent tunnel coupling, a charge current starts to flow under dc-bias voltage $eV = \mu_L - \mu_R$. This nonequilibrium problem can be solved taking into account that in the stationary limit the Green's functions and self-energies depend on the time difference $t - t'$. Applying Fourier transformations in Eq. (2.75) one obtains stationary current flowing from lead ξ as [46, 127]

$$I_\xi = \frac{2e}{\hbar} \text{Re} \int \frac{d\epsilon}{2\pi} \text{Tr} \{ [\hat{G}^r(\epsilon) \hat{\Sigma}_\xi^<(\epsilon) + \hat{G}^<(\epsilon) \hat{\Sigma}_\xi^a(\epsilon)] \}. \quad (2.78)$$

Employing Eq. (2.41) in Fourier space, $\hat{G}^r(\epsilon) - \hat{G}^a(\epsilon) = \hat{G}^>(\epsilon) - \hat{G}^<(\epsilon)$, which also holds for matrices of self-energies, $\hat{\Sigma}^r(\epsilon) - \hat{\Sigma}^a(\epsilon) = \hat{\Sigma}^>(\epsilon) - \hat{\Sigma}^<(\epsilon)$, one finds [46, 120]

$$I_\xi = \frac{e}{\hbar} \int \frac{d\epsilon}{2\pi} \text{Tr} \{ [\hat{G}^>(\epsilon) \hat{\Sigma}_\xi^<(\epsilon) - \hat{G}^<(\epsilon) \hat{\Sigma}_\xi^>(\epsilon)] \}. \quad (2.79)$$

The Green's function $\hat{G}^<(\epsilon)$ ($\hat{G}^>(\epsilon)$) is related to the number of occupied (available) states in the central region, while $\hat{\Sigma}_\xi^>(\epsilon)$ ($\hat{\Sigma}_\xi^<(\epsilon)$) gives the tunneling rate into (out of) lead ξ . Thus, the first term in Eq. (2.79) represents the charge current flowing from the lead ξ to the central region, while the second term is the tunneling current into the lead ξ .

In the stationary limit, the Fourier transforms of the tunneling self-energies given by Eq. (2.74) result in [46, 120]

$$\Sigma_{\xi,mn}^{r,a}(\epsilon) = \Lambda_{\xi,mn}(\epsilon) \mp \frac{i}{2} \Gamma_{\xi,mn}(\epsilon), \quad (2.80)$$

$$\Sigma_{\xi,mn}^<(\epsilon) = i \Gamma_{\xi,mn}(\epsilon) f_\xi(\epsilon), \quad (2.81)$$

$$\Sigma_{\xi,mn}^>(\epsilon) = -i \Gamma_{\xi,mn}(\epsilon) [1 - f_\xi(\epsilon)]. \quad (2.82)$$

In the presence of the interactions in the central region, with the corresponding self energy $\hat{\Sigma}_{\text{int}}^<, >(\epsilon)$, the total lesser or greater self-energy equals [46, 120]

$$\hat{\Sigma}^<, >(\epsilon) = \hat{\Sigma}_{\text{int}}^<, >(\epsilon) + \hat{\Sigma}_L^<, >(\epsilon) + \hat{\Sigma}_R^<, >(\epsilon). \quad (2.83)$$

Combining the Keldysh equation (2.57) and Eq. (2.41) in Fourier space leads to the following relation

$$\text{Tr} [\hat{\Sigma}^<(\epsilon) \hat{G}^>(\epsilon) - \hat{\Sigma}^>(\epsilon) \hat{G}^<(\epsilon)] = 0. \quad (2.84)$$

Using Eqs. (2.79), (2.83) and (2.84) the necessary condition for the charge current conservation can be obtained as [46, 120]

$$\begin{aligned} 0 &= \sum_{\xi} I_{\xi} = \frac{e}{\hbar} \int \frac{d\epsilon}{2\pi} \text{Tr}\{[\hat{G}^{>}(\epsilon)[\hat{\Sigma}^{<}(\epsilon) - \hat{\Sigma}_{\text{int}}^{<}(\epsilon)] - \hat{G}^{<}(\epsilon)[\hat{\Sigma}^{>}(\epsilon) - \hat{\Sigma}_{\text{int}}^{>}(\epsilon)]\} \\ &= \frac{e}{\hbar} \int \frac{d\epsilon}{2\pi} \text{Tr}\{[\hat{G}^{<}(\epsilon)\hat{\Sigma}_{\text{int}}^{>}(\epsilon) - \hat{G}^{>}(\epsilon)\hat{\Sigma}_{\text{int}}^{<}(\epsilon)]\}, \end{aligned} \quad (2.85)$$

which is ensured by the proper model of the interacting self-energy $\Sigma_{\text{int}}^{<,>}(\epsilon)$, and in noninteracting case.

In the case of stationary current, Eq. (2.77) becomes [46, 127]

$$I_{\xi} = \frac{ie}{\hbar} \int \frac{d\epsilon}{2\pi} \text{Tr}[\hat{\Gamma}_{\xi}(\epsilon)\{\hat{G}^{<}(\epsilon) + f_{\xi}(\epsilon)[\hat{G}^r(\epsilon) - \hat{G}^a(\epsilon)]\}]. \quad (2.86)$$

Assuming constant ratio between level-width functions of the left and right leads, $\hat{\Gamma}_L(\epsilon)\hat{\Gamma}_R^{-1}(\epsilon)=\text{const.}$, the conserved steady-state current $I_L = -I_R = (I_L - I_R)/2$ can be expressed as [46, 127]

$$I_L = \frac{e}{\hbar} \int \frac{d\epsilon}{2\pi} [f_L(\epsilon) - f_R(\epsilon)]\mathcal{T}(\epsilon), \quad (2.87)$$

where $\mathcal{T}(\epsilon) = \text{Tr}\{\hat{T}(\epsilon)\}$, $\hat{T}(\epsilon) = [\hat{\Gamma}_L(\epsilon)\hat{\Gamma}_R(\epsilon)\hat{\Gamma}^{-1}(\epsilon)\hat{A}(\epsilon)]$. The level-width function $\hat{\Gamma}(\epsilon) = \hat{\Gamma}_L(\epsilon) + \hat{\Gamma}_R(\epsilon)$, while $\hat{A}(\epsilon) = i[\hat{G}^r(\epsilon) - \hat{G}^a(\epsilon)]$ is the spectral function of the interacting region. If the central region is noninteracting, the function $\mathcal{T}(\epsilon)$ is the elastic transmission probability. In that case the zero-temperature conductance at small bias-voltages $G = I_L/V$ is given by the Landauer formula $G = (e^2/h)\mathcal{T}(E_f)$ (should be multiplied by a factor of 2 for spin degeneracy), where E_f is the Fermi energy of the leads [54, 128, 129]. Note that in the interacting case, the function $\mathcal{T}(\epsilon)$ cannot be considered as the elastic transmission probability, since one needs to include the interactions into the Green's functions of the central region [46]. Namely, if a current-carrying electron undergoes a spin-flip, or interacts with a phonon, for example, it emits or absorbs energy, which leads to an inelastic contribution to the tunneling current.

2.1.8 Nonequilibrium current fluctuations

Besides charge current and conductance, additional information concerning transport in mesoscopic conductors can be obtained by the investigation of the current correlations, referred to as noise [130]. Noise measurements can give information on the transmission eigenvalues, effective transferred charge, quantum entanglement, etc. We will discuss the properties of shot noise, which arises due

to discreteness of electron charge [131], in more detail in Chapter 5. In this subsection we first present the calculation of noise using the nonequilibrium Green's functions formalism in the case of time-dependent transport [46, 49], where the Hamiltonian of the system is given by Eq. (2.62) [45, 46]. Later, we discuss noise in stationary-transport regime, where time-dependent external fields are absent [46, 132–136, 138].

The current operator in lead ξ is given by [45, 46]

$$\begin{aligned}\hat{I}_\xi(t) &= -e \frac{d}{dt} \hat{N}_\xi \\ &= \frac{ie}{\hbar} \sum_{k,n} [V_{k\xi,n}(t) \hat{c}_{k\xi}^\dagger(t) \hat{d}_n(t) - V_{k\xi,n}^*(t) \hat{d}_n^\dagger(t) \hat{c}_{k\xi}(t)].\end{aligned}\quad (2.88)$$

Symmetrized charge-current noise is defined via temporal correlations between charge currents in contacts ξ and η as [130]

$$S_{\xi\eta}(t, t') = \frac{1}{2} \langle \{ \delta \hat{I}_\xi(t), \delta \hat{I}_\eta(t') \} \rangle, \quad (2.89)$$

where $\delta \hat{I}_\xi(t) = \hat{I}_\xi(t) - \langle \hat{I}_\xi(t) \rangle$ is the current-fluctuation operator in contact ξ . According to the definition of the current-fluctuation operator, Eq. (2.89) can be further expressed as

$$S_{\xi\eta}(t, t') = \frac{1}{2} [\langle \hat{I}_\xi(t) \hat{I}_\eta(t') \rangle + \text{h.c.} - 2I_\xi(t) I_\eta(t')]. \quad (2.90)$$

Using Eq. (2.88), the noise of charge current can be computed as [46, 49]

$$\begin{aligned}S_{\xi\eta}(t, t') &= -\frac{e^2}{2\hbar^2} \sum_{kk'\eta m} \{ V_{k\xi,n}(t) V_{k'\eta,m}(t') \langle \hat{c}_{k\xi}^\dagger(t) \hat{d}_n(t) \hat{c}_{k'\eta}^\dagger(t') \hat{d}_m(t') \rangle \\ &\quad - V_{k\xi,n}(t) V_{k'\eta,m}^*(t') \langle \hat{c}_{k\xi}^\dagger(t) \hat{d}_n(t) \hat{d}_m^\dagger(t') \hat{c}_{k'\eta}(t') \rangle \\ &\quad - V_{k\xi,n}^*(t) V_{k'\eta,m}(t') \langle \hat{d}_n^\dagger(t) \hat{c}_{k\xi}(t) \hat{c}_{k'\eta}^\dagger(t') \hat{d}_m(t') \rangle \\ &\quad + V_{k\xi,n}^*(t) V_{k'\eta,m}^*(t') \langle \hat{d}_n^\dagger(t) \hat{c}_{k\xi}(t) \hat{d}_m^\dagger(t') \hat{c}_{k'\eta}(t') \rangle \} \\ &\quad + \text{h.c.} - I_\xi(t) I_\eta(t').\end{aligned}\quad (2.91)$$

According to the Wick's theorem the quantum and ensemble averages of four operator products in Eq. (2.91) can be decomposed into sums of products of correlations [117]. The mixed Green's functions can be expressed in terms of correlations involving one creation (annihilation) operator of electrons in lead ξ , and the other creation (annihilation) operator of electrons in the central region,

$$G_{n,k\xi}^>(t, t') = -i \langle \hat{d}_n(t) \hat{c}_{k\xi}^\dagger(t') \rangle, \quad (2.92)$$

$$G_{k\xi,n}^>(t, t') = -i \langle \hat{c}_{k\xi}(t) \hat{d}_n^\dagger(t') \rangle. \quad (2.93)$$

The definitions of the corresponding lesser Green's functions were already introduced in Eqs. (2.67) and (2.68). The Green's functions of the leads and the central region are defined as

$$G_{k\xi,k'\eta}^<(t, t') = i\langle \hat{c}_{k'\eta}^\dagger(t') \hat{c}_{k\xi}(t) \rangle, \quad (2.94)$$

$$G_{k\xi,k'\eta}^>(t, t') = -i\langle \hat{c}_{k\xi}(t) \hat{c}_{k'\eta}^\dagger(t') \rangle, \quad (2.95)$$

$$G_{nm}^<(t, t') = i\langle \hat{d}_m^\dagger(t') \hat{d}_n(t) \rangle, \quad (2.96)$$

$$G_{nm}^>(t, t') = -i\langle \hat{d}_n(t) \hat{d}_m^\dagger(t') \rangle. \quad (2.97)$$

Since the four-operator products in Eq. (2.91) can be expressed in terms of sums of products of the above Green's functions, while the average current is given by Eq. (2.69), the charge current noise becomes [46, 49]

$$\begin{aligned} S_{\xi\eta}(t, t') = -\frac{e^2}{\hbar^2} \text{Re} \left\{ \sum_{kk'nm} [V_{k\xi,n}(t)V_{k'\eta,m}(t')G_{n,k'\eta}^>(t, t')G_{m,k\xi}^<(t', t) \right. \\ - V_{k\xi,n}(t)V_{k'\eta,m}^*(t')G_{nm}^>(t, t')G_{k'\eta,k\xi}^<(t', t) \\ - V_{k\xi,n}^*(t)V_{k'\eta,m}(t')G_{k\xi,k'\eta}^>(t, t')G_{mn}^<(t', t) \\ \left. + V_{k\xi,n}^*(t)V_{k'\eta,m}^*(t')G_{k\xi,m}^>(t, t')G_{k'\eta,n}^<(t', t)] \right\}. \quad (2.98) \end{aligned}$$

Following the same procedure as in Section 2.1.7, i.e., applying analytic continuation rules and Langreth theorem [126], one obtains the above Green's functions in terms of $g_{k\xi}^{r,a,<,>}(t, t')$ [see e.g., Eqs. (2.72) and (2.73)], and the Green's functions of the central region. Substituting them in Eq. (2.98), and using Eq. (2.74) which defines the tunneling self-energies, yields [46, 49]

$$\begin{aligned} S_{\xi\eta}(t, t') = -\frac{e^2}{\hbar^2} \text{Re} \text{Tr} \left\{ \int dt_1 \int dt_2 \{ [\hat{G}^r(t, t_1) \hat{\Sigma}_\eta^>(t_1, t') + \hat{G}^>(t, t_1) \hat{\Sigma}_\eta^a(t_1, t')] \right. \\ \times [\hat{G}^r(t', t_2) \hat{\Sigma}_\xi^<(t_2, t) + \hat{G}^<(t', t_2) \hat{\Sigma}_\xi^a(t_2, t)] \\ + [\hat{\Sigma}_\xi^>(t, t_1) \hat{G}^a(t_1, t') + \hat{\Sigma}_\xi^r(t, t_1) \hat{G}^>(t_1, t')] \\ \times [\hat{\Sigma}_\eta^<(t', t_2) \hat{G}^a(t_2, t) + \hat{\Sigma}_\eta^r(t', t_2) \hat{G}^<(t_2, t)] \\ - \hat{G}^>(t, t') [\hat{\Sigma}_\eta^r(t', t_1) \hat{G}^r(t_1, t_2) \hat{\Sigma}_\xi^<(t_2, t) + \hat{\Sigma}_\eta^<(t', t_1) \hat{G}^a(t_1, t_2) \hat{\Sigma}_\xi^a(t_2, t) \\ + \hat{\Sigma}_\eta^r(t', t_1) \hat{G}^<(t_1, t_2) \hat{\Sigma}_\xi^a(t_2, t)] \\ - [\hat{\Sigma}_\xi^r(t, t_1) \hat{G}^r(t_1, t_2) \hat{\Sigma}_\eta^>(t_2, t') + \hat{\Sigma}_\xi^>(t, t_1) \hat{G}^a(t_1, t_2) \hat{\Sigma}_\eta^a(t_2, t')] \\ + \hat{\Sigma}_\xi^r(t, t_1) \hat{G}^>(t_1, t_2) \hat{\Sigma}_\eta^a(t_2, t') \hat{G}^<(t', t) \} \\ \left. - \delta_{\xi\eta} [\hat{G}^>(t, t') \hat{\Sigma}_\xi^<(t', t) + \hat{\Sigma}_\xi^>(t, t') \hat{G}^<(t', t)] \right\}, \quad (2.99) \end{aligned}$$

where the Green's functions $\hat{G}^{r,a,<,>}$ are matrices in the central-region indices m, n .

Together, Eqs. (2.75) and (2.99) represent important tools in solving charge-transport problems through various interacting systems connected to two noninteracting terminals. These formal expressions enable the calculation of the charge current and noise in terms of known Green's functions of the central, interacting region, and the self-energies associated with the tunnel coupling to the leads.

In the rest of this section we focus on the stationary limit, with the interacting central region, where noise depends only on time difference $t - t'$. The Fourier transform of noise is known as spectral density or power spectrum of noise [130]

$$2\pi\delta(\Omega - \Omega')S_{\xi\eta}(\Omega) = \int_{-\infty}^{\infty} \int_{-\infty}^{\infty} dt dt' e^{i\Omega t} e^{-i\Omega' t'} S_{\xi\eta}(t - t'). \quad (2.100)$$

A number of works derived noise power spectrum employing nonequilibrium Green's functions formalism [133, 134, 136, 139]. Considering zero-frequency noise power which is usual case in experimental setups, and taking into account that the condition for the charge-current conservation requires that [130]

$$S \equiv S_{LL}(\Omega = 0) = S_{RR}(\Omega = 0) = -S_{LR}(\Omega = 0) = -S_{RL}(\Omega = 0), \quad (2.101)$$

one obtains [46, 134, 135, 138]

$$\begin{aligned} S = & \frac{e^2}{\hbar^2} \int \frac{d\epsilon}{2\pi} \{ -f_L(\epsilon)[1 - f_L(\epsilon)](\text{Tr}\{[\hat{\Gamma}_L(\epsilon)\hat{G}^r(\epsilon)]^2 + [\hat{\Gamma}_L(\epsilon)\hat{G}^a(\epsilon)]^2\} \\ & + if_L \text{Tr}\{\hat{\Gamma}_L(\epsilon)\hat{G}^>(\epsilon)\} - i[1 - f_L(\epsilon)]\text{Tr}\{\hat{\Gamma}_L(\epsilon)\hat{G}^<(\epsilon)\} \\ & + f_L(\epsilon)\text{Tr}\{\hat{\Gamma}_L(\epsilon)\hat{G}^>(\epsilon)\hat{\Gamma}_L(\epsilon)[\hat{G}^r(\epsilon) - \hat{G}^a(\epsilon)]\} + \text{Tr}\{\hat{\Gamma}_L(\epsilon)\hat{G}^>(\epsilon)\hat{\Gamma}_L(\epsilon)\hat{G}^<(\epsilon)\} \\ & - [1 - f_L(\epsilon)]\text{Tr}\{\hat{\Gamma}_L(\epsilon)[\hat{G}^r(\epsilon) - \hat{G}^a(\epsilon)]\hat{\Gamma}_L(\epsilon)\hat{G}^<(\epsilon)\} \}. \end{aligned} \quad (2.102)$$

This is a general expression for zero-frequency noise power in the presence of interactions, expressed in terms of Fermi-Dirac distributions of the leads and local Green's functions of the central region.

In noninteracting case, Eq. (2.102) reduces to the Landauer-Büttiker expression for noise power obtained by using scattering matrix formalism [130, 140, 141]

$$\begin{aligned} S = & \frac{e^2}{\hbar^2} \int \frac{d\epsilon}{2\pi} (\{f_L(\epsilon)[1 - f_L(\epsilon)] + f_R(\epsilon)[1 - f_R(\epsilon)]\} \text{Tr}\{\hat{T}(\epsilon)\} \\ & + [f_L(\epsilon) - f_R(\epsilon)]^2 \text{Tr}\{[1 - \hat{T}(\epsilon)]\hat{T}(\epsilon)\}), \end{aligned} \quad (2.103)$$

where matrix $\hat{T}(\epsilon) = [\hat{\Gamma}_L(\epsilon)\hat{\Gamma}_R(\epsilon)\hat{\Gamma}^{-1}(\epsilon)\hat{A}(\epsilon)]$ is the transmission coefficient matrix introduced in Eq. (2.87). The first two terms in Eq. (2.103) represent the contribution due to the thermal excitations in the leads, called the thermal or Johnson-Nyquist noise [130, 142, 143]. In equilibrium, where $eV = 0$, the Fermi distribution

functions of the leads are equal $f(\epsilon) = f_L(\epsilon) = f_R(\epsilon)$, and S in Eq. (2.103) reduces to the thermal noise which is connected with the linear conductance G via the fluctuation-dissipation theorem as [142–145]

$$S = 2k_B T G, \quad (2.104)$$

where the Fermi-Dirac distributions satisfy $f(\epsilon)[1 - f(\epsilon)] = -k_B T \partial f(\epsilon) / \partial \epsilon$, while the conductance reads

$$G = \frac{e^2}{\hbar} \int \frac{d\epsilon}{2\pi} \left[-\frac{\partial f(\epsilon)}{\partial \epsilon} \right] \text{Tr}\{\hat{T}(\epsilon)\}. \quad (2.105)$$

In nonequilibrium, where $eV \neq 0$, the third term in Eq. (2.103) represents the shot noise contribution [130, 131]. Since it contains nondiagonal matrix elements of the transmission matrix $\hat{T}(\epsilon)$, it gives additional information about the charge transport, which is not contained in the conductance. In the low bias-voltage limit $eV \ll k_B T$ the noise is predominantly thermal, while in the low temperature limit $k_B T \ll eV$ the dominant contribution comes from the shot noise. At zero temperature, thermal noise vanishes and S reduces to the shot noise, making this special case particularly interesting.

In the presence of interactions in the central region, like e.g., electron-phonon interactions, the zero-frequency noise power cannot be divided into thermal and shot noise contributions like in Eq. (2.103) [136].

2.2 Single-molecule magnets

One challenge of modern electronics is to incorporate single-molecule magnets into quantum computers [97, 102]. Due to the bistability of the single-molecule magnets [146], they can be used in quantum computing with superpositions of spin states performing the roles of qubits, which can be entangled with each other [102]. Single-molecule magnets can be used for magnetic memory storage due to their slow magnetization relaxation at low temperatures [97, 146, 147].

In this section we describe physical properties of isolated single-molecule magnets, or subject to external magnetic fields at low temperatures. Single-molecule magnets are quantum magnets, i.e., mesoscopic quantum objects with a permanent magnetization [146, 148, 149]. They are typically formed by paramagnetic ions stabilized by surrounding organic ligands [148]. Single-molecule magnets show both classical properties such as magnetization hysteresis [92], and quantum properties such as magnetization tunneling [93–96], coherence [97–99], quantum phase

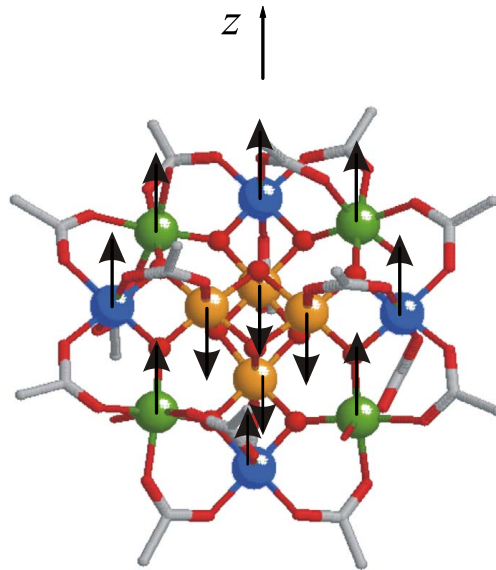


FIGURE 2.4: Crystal structure of Mn_{12} -acetate $[\text{Mn}_{12}\text{O}_{12}(\text{CH}_3\text{COO})_{16}(\text{H}_2\text{O})_4]$. The ground state spin $S = 10$. Four positive ions Mn^{4+} with spins $S = 3/2$ (orange spheres) are surrounded with eight positive ions Mn^{3+} with spins $S = 2$ (blue and green spheres). Adapted from [137].

interference [92, 100, 101], and Kondo effect [150–152]. The two crucial characteristics of single-molecule magnets are a large spin ground state and strong easy axis anisotropy [153].

One frequently studied single-molecule magnet with strong uniaxial anisotropy is Mn_{12} -acetate [154], which is presented in Fig. 2.4. Its ground state spin $S = 10$ and geometric structure obeys S_4 symmetry [91]. Due to the strong exchange interactions between the metal ions in Mn_{12} -acetate, which are dominant in the spin Hamiltonian, the giant spin approximation is used to describe this nanomagnet [155, 156]. The tunnel splitting between the ground states of this single-molecule magnet at low temperatures is negligible, since the transverse anisotropy is weak. For Mn_{12} -acetate the anisotropy constants are given by $D = 0.057 \text{ meV}$ and $E = 0.27 \times 10^{-5} \text{ meV}$ [156].

2.2.1 Giant spin approximation

In the giant spin approximation the effective molecular spin is considered large and rigid [28, 42, 149, 157, 158]. This approximation is limited in the sense that the contributions of the individual ions to the magnetic behavior of the single-molecule magnet remain unknown. The form of the Hamiltonian depends on the symmetry of the system. One simple model of the Hamiltonian of a single-molecule magnet, like Mn_{12} -acetate or Fe_8 , in the presence of an external magnetic field \vec{B} , in the

giant spin approximation can be written as

$$\hat{H} = -D\hat{S}_z^2 + E(\hat{S}_x^2 - \hat{S}_y^2) + g\mu_B\vec{B}\hat{S}. \quad (2.106)$$

where z -axis is the easy magnetization axis. The molecular spin operators along the $i = x, y, z$ axes are given by \hat{S}_i , while D is the axial anisotropy constant [149]. This constant is positive, to ensure that the lowest-energy state is the ground state of the spin. The second term is a transverse anisotropy term with transverse anisotropy constant E [149]. Some of the causes of anisotropy can be molecular symmetry [149], spin orbit coupling [159], exchange coupling [160] and magnetic fields [96, 153]. The Zeeman interaction is presented in the third term of the Hamiltonian, where g is the Landé factor, while μ_B is the Bohr magneton. All the eigenstates of the Hamiltonian in Eq. (2.106) are linear combinations of the eigenstates of \hat{S}_z , denoted as $|m\rangle$, where the spin projections along the easy axis $m \in \{-S, S\}$.

For the beginning, let us assume that the transverse anisotropy is weak $|E/D| \ll 1$, like in the case of Mn_{12} -acetate [156], and the external magnetic field is directed along the easy z -axis. In other words we neglect the transverse anisotropy and transverse magnetic fields. In this limit, the operator \hat{S}_z can be considered a conserved quantity, and $\{|m\rangle\}$ is a common eigenbasis of the Hamiltonian and \hat{S}_z . In the absence of the longitudinal external magnetic field, the corresponding eigenvalues of the Hamiltonian $E_m^0 = -Dm^2$ are degenerate, with the ground-state energy $-DS^2$. Axial anisotropy leads to an energy barrier to spin reversal of single-molecule magnets. The barrier height which separates states with $m > 0$ (spin-up) and $m < 0$ (spin-down) equals $U^0 = DS^2$ and the system is bistable. This type of anisotropy removes the energy degeneracy of the spin states in the absence of external fields and is called zero-field splitting [161].

Applying the magnetic field along the easy axis, the degeneracy of the Hamiltonian is removed due to the Zeeman splitting. In this case the eigenenergies are modified as [149]

$$E_m = -Dm^2 + g\mu_B B_z m. \quad (2.107)$$

Thus, for the spin in the state with $m = -S$ the energy $E_{m=-S}$ decreases if $B_z > 0$, whereas the energy barrier increases as [149]

$$U = D \left(S + \frac{g\mu_B B_z}{2D} \right)^2. \quad (2.108)$$

The energy spectrum of a single-molecule magnet can be presented as a double well potential, with states corresponding to $m < 0$ in one well, and states corresponding to $m > 0$ in the other well. In the absence of the longitudinal magnetic

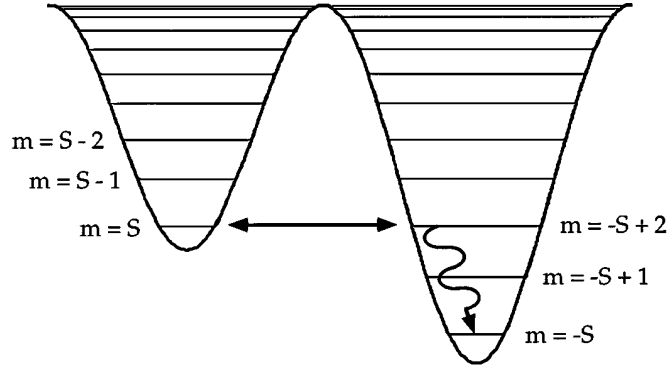


FIGURE 2.5: Double-well potential and energy levels of Mn_{12} -acetate in the presence of a magnetic field with the longitudinal component $B_z^r = 2D/g\mu_B$. Energy levels corresponding to the states $|m = S\rangle$ and $|m = -S + 2\rangle$ match. A small transverse component of the magnetic field induces tunneling of the magnetization, followed by a spontaneous decay into the ground state. Taken from [93].

field the eigenenergies $E_m^0 = E_{-m}^0$, while for $B_z \neq 0$ the eigenenergies of the states with $m < 0$ and $m > 0$ shift in the opposite directions, as shown in Fig. 2.5. For some values of the longitudinal field B_z the two energy levels corresponding to the eigenstates $|m\rangle$ in one well and $|m'\rangle$ in the other well match, where $|m| \neq |m'|$. These resonant fields are given by [93, 94]

$$B_z^r = \frac{(m + m')D}{g\mu_B}. \quad (2.109)$$

Due to the conservation of \hat{S}_z the transitions between its eigenstates are forbidden. The energy barrier prevents the reversal of magnetization along the easy axis. Hence, transverse magnetic fields or transverse anisotropy induce quantum tunneling of the magnetization [153].

2.2.2 Quantum tunneling of magnetization

Since the spin operators \hat{S}_x and \hat{S}_y do not commute with the Hamiltonian of the system, upon turning on the transverse magnetic field, the resonant-field degeneracy of energy levels corresponding to $|m\rangle$ and $|m'\rangle$ is removed. Namely, there is an energy gap $\Delta_{m,m'}$, called tunnel splitting [92, 149, 162, 163], between the new eigenstates, which are symmetric and antisymmetric superpositions of the initial degenerate states $|m\rangle$ and $|m'\rangle$. These superpositions allow quantum tunneling of the magnetic moment [93–96], as the spin can flip from the state $|m\rangle$ to the state $|m'\rangle$, with the rate of transitions given by the tunneling frequency $\omega_{m,m'} = \Delta_{m,m'}/\hbar$ [92, 149, 162, 163]. The barrier height and tunnel splittings can

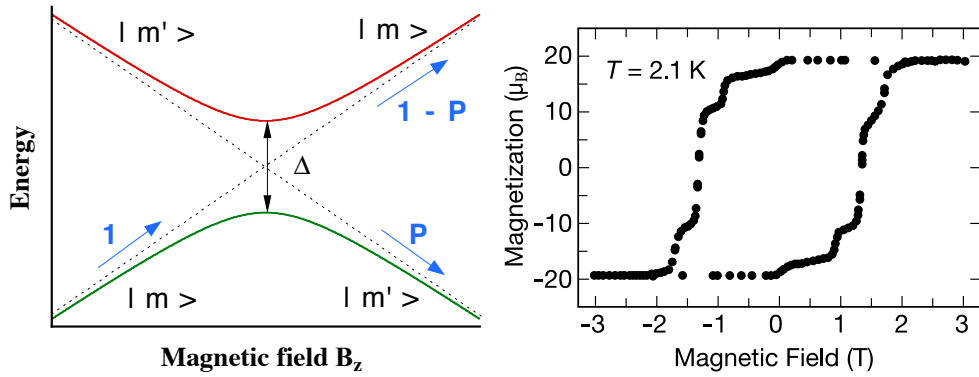


FIGURE 2.6: (left) Quantum tunneling of magnetization of a single-molecule magnet, where P denotes the Landau-Zener probability of spin tunneling from state $|m\rangle$ to state $|m'\rangle$, whereas Δ is the tunnel splitting. Adapted from [167]. (right) Magnetization hysteresis loop for an Mn_{12} -acetate at low temperature. Taken from [148].

be varied using magnetic fields. The Landau-Zener model with the probability of tunneling for a two-level system [164, 165] can be applied to spin tunneling in single-molecule magnets [92, 166]. The quantum magnetization tunneling of a single-molecule magnet is shown in Fig. 2.6 (left). The energy gaps appear at the resonant magnetic fields, where in the absence of the transverse field, only the crossings of levels are present. It has been shown that tunnel splitting oscillates as a function of the transverse magnetic field if the angle between the field and the hard axis is small. This is due to the Berry-phase interference of two tunneling paths [100, 101].

Classically, in the low temperature regime, where $k_B T \ll U$, the spin of a single-molecule magnet cannot overcome the potential energy barrier, leading to the hysteresis in the magnetization [92]. Fig. 2.6 (right) plots the magnetization of Mn_{12} -acetate as a function of longitudinal magnetic field at a low temperature. The steps in the hysteresis loop occur at resonant fields, where the relaxation of the magnetization is much faster due to the quantum tunneling of magnetization [93–96].

2.2.3 Large spin and classical limit

A single-molecule magnet with a large spin $S \gg 1$ has a large number of spin states, $2S + 1$. Its spin can be considered as a classical variable under some conditions. Tunnel splitting $\Delta_{m,m'}$ vanishes for large S [149]. For single-molecule magnets typically $|E/D| < 1$, and transverse Zeeman energy is lower than axial anisotropy energy. In the classical limit, it is required that the magnetic field along the easy axis B_z is strong, so that the corresponding Zeeman energy is much

larger than the anisotropy barrier, i.e., $g\mu_B B_z S \gg DS^2$ [168]. In many cases, the required field B_z can be on the order of tesla. For strong longitudinal magnetic fields the energy barrier and bistability disappear, allowing complete reversal of the magnetization.

2.3 Spin-transfer torque

Besides quantum tunneling due to transverse anisotropy, or transverse external magnetic fields, another interesting way to manipulate the magnetization of a single-molecule magnet is by employing spin-polarized currents. In the absence of charge current, spin currents can be injected into the magnetic nanostructures and manipulate their magnetization via spin-transfer torques [169]. The study of spin-transfer torque in view of control and manipulation of nanomagnets has attracted both technological and academic interest. Current-induced spin-transfer torque was first predicted independently by Slonczewski and Berger in magnetic multilayer systems [108, 109], and later experimentally confirmed [111, 170–172].

In the macrospin model, the individual spins in a magnetic nanostructure are aligned, coupled with strong exchange interactions and form a giant spin [111, 173]. If the orbital angular momentum can be neglected, then the magnetization and spin of the magnetic nanostructure are related as $\vec{M}(t) = -\gamma_s \vec{S}(t)$. The macrospin dynamics in this approximation, with neglected internal spin degrees of freedom, can be described by the Landau-Lifshitz-Gilbert-Slonczewski equation [108, 174–176], where Slonczewski remodeled the Landau-Lifshitz-Gilbert equation by adding one additional term that accounts for current-induced spin-transfer torque as

$$\dot{\vec{S}}(t) = \gamma_s \vec{B}_{\text{eff}} \times \vec{S}(t) + \frac{\alpha_0}{S} \dot{\vec{S}}(t) \times \vec{S}(t) + \vec{T}(t). \quad (2.110)$$

In Eq. (2.110) the magnitude of the macrospin is constant, $|\vec{S}(t)| = S$.

In the ideal case the energy of the system is conserved and the field-like torque, given by the first term in Eq. (2.110), acts on the macrospin. The spin precesses around the effective magnetic field axis with Larmor frequency $\omega_L = \gamma_s B_{\text{eff}}$, where $\gamma_s = g_s \mu_B$ is the gyromagnetic ratio, with the Landé factor g_s . The effective field includes the applied external magnetic field, anisotropy, demagnetization, exchange, and magnetoelastic fields [175].

However, the system interacts with the environment, and due to energy dissipation the macrospin $\vec{S}(t)$ is moving along spiral trajectory towards the equilibrium antiparallel alignment with the effective magnetic field \vec{B}_{eff} . The damping term is phenomenologically introduced as the second term in Eq. (2.110), where α_0 is the intrinsic Gilbert damping parameter.

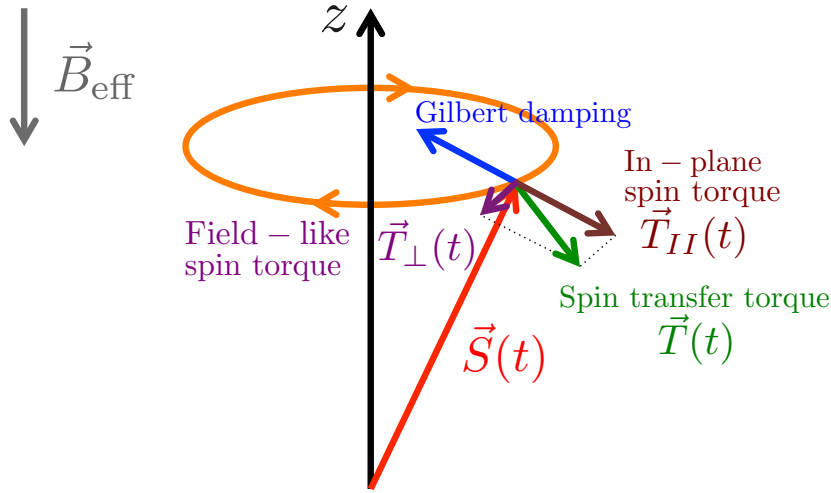


FIGURE 2.7: Sketch of a spin-transfer torque $\vec{T}(t)$, induced by spin currents, acting on a magnetic nanostructure with spin $\vec{S}(t)$ in an effective magnetic field \vec{B}_{eff} . The in-plane component $T_{II}(t)$ is (anti)parallel to the intrinsic Gilbert damping torque, whereas the perpendicular component $T_{\perp}(t)$ modifies the precession frequency of the spin.

In the presence of spin current, the incoming flow of spin carriers interacts with the macrospin via exchange interactions, and transfers spin-angular momentum to the macrospin [108–111]. The torque generated on the macrospin during these interactions is called spin-transfer torque, given by the third term in Eq. (2.110). The outgoing flow of spin current differs from the incoming flow by the amount of spin-transfer torque exerted on the macrospin [108, 110, 177, 178]

$$\vec{T}(t) = \vec{I}_{\text{out}}(t) - \vec{I}_{\text{in}}(t), \quad (2.111)$$

where we assume that the incoming electron spins are not subject to any additional spin interactions. Taking into account that the magnitude of the spin, S , is preserved, the spin-transfer torque can be written as [108, 110, 177, 178]

$$\vec{T}(t) = \vec{e}_S \times \left([\vec{I}_{\text{out}}(t) - \vec{I}_{\text{in}}(t)] \times \vec{e}_S \right), \quad (2.112)$$

where the unit vector $\vec{e}_S = \vec{S}/S$ indicates the direction of the spin. On the other hand, since the total spin angular momentum is conserved, the macrospin exerts a torque $-\vec{T}(t)$ on the spin current. This process of generating spin currents by the macrospin dynamics is called spin pumping [110, 179]. Thus, spin-transfer torque (reaction) and spin pumping (action) are two opposite effects caused by the interaction of the spin current with the macrospin dynamics.

Devices with stable macrospin precession, which occurs if the intrinsic Gilbert damping term is balanced by the spin-transfer torque acting in the opposite direction, are called spin-transfer nano-oscillators [171, 180]. Due to the stable precession of magnetization, these devices can convert dc current into microwave signals. If the spin current is strong enough, it can induce macrospin (magnetization) switching [108, 170, 181].

Since the spin-transfer torque is perpendicular to the macrospin \vec{S} , it can be written as [182]

$$\vec{T}(t) = \vec{T}_{II}(t) + \vec{T}_{\perp}(t). \quad (2.113)$$

The in-plane component $\vec{T}_{II}(t)$ is collinear with the intrinsic Gilbert damping torque [182], as presented in Fig. 2.7, and can either enhance the damping of the macrospin (dissipate energy), or act in the opposite direction (add energy), leading to the stable precession, or magnetization reversal, for sufficiently large currents. Effectively, the in-plane component $T_{II}(t)$ modifies the Gilbert damping coefficient into $\alpha_0 + \alpha$, where α is the contribution attributed to the spin-transfer torque [110, 179]. The out-of plane (perpendicular) component $\vec{T}_{\perp}(t)$ acts as an additional field-like torque induced by the spin currents, thus modifying the precession frequency [182].

Chapter 3

Spin transport and tunable Gilbert damping in a molecular magnet junction

3.1 Introduction

Currently, a goal in the field of nanophysics is to control and manipulate individual quantum systems, in particular, individual spins [40, 183]. Some theoretical works have investigated electronic transport through a molecular magnet contacted to leads [42, 150, 151, 184–193]. In this case, the transport properties are modified due to the exchange interaction between the itinerant electrons and the single-molecule magnet [194], making it possible to read out the spin state of the molecule using transport currents. Conversely, the spin dynamics and hence the state of a single-molecule magnet can also be controlled by transport currents. Efficient control of the molecule's spin state can be achieved by coupling to ferromagnetic contacts as well [195].

Experiments have addressed the electronic transport properties through magnetic molecules such as Mn_{12} and Fe_8 [28, 29], which have been intensively studied as they are promising candidates for memory devices [102]. Various phenomena such as large conductance gaps [196], switching behavior [197–199], negative differential conductance, dependence of the transport on magnetic fields and Coulomb

This chapter is adapted from M. Filipović, C. Holmqvist, F. Haupt, and W. Belzig, *Phys. Rev. B* **87**, 045426 (2013); **88**, 119901(E) (2013). See also: arXiv:1211.3611.

blockades have been experimentally observed [28, 29, 200, 201]. Experimental techniques, including, e.g., scanning tunneling microscopy [28, 29, 202–204], break junctions [7, 44, 205], and three-terminal devices [28, 29, 200], have been employed to measure electronic transport through a single-molecule magnet. Scanning tunneling spectroscopy and scanning tunneling microscopy experiments show that quantum properties of single-molecule magnets are preserved when deposited on substrates [204]. The Kondo effect in single-molecule magnets with magnetic anisotropy has been investigated both theoretically [150, 151] and experimentally [206, 207]. It has been suggested [208] and experimentally verified [209] that a spin-polarized tip can be used to control the magnetic state of a single Mn atom.

In some limits, the large spin S of a molecular magnet can be treated as a classical magnetic moment. In that case, the spin dynamics is described by the Landau-Lifshitz-Gilbert equation that incorporates effects of external magnetic fields as well as torques originating from damping phenomena [174, 175]. In tunnel junctions with magnetic particles, Landau-Lifshitz-Gilbert equations have been derived using perturbative couplings [210, 211] and the nonequilibrium Born-Oppenheimer approximation [189]. Current-induced magnetization switching is driven by a generated spin-transfer torque [108–111] as a back-action effect of the electronic spin transport on the magnetic particle [189, 212–215]. A spin-polarized scanning tunneling microscopy [209] has been used to experimentally study spin-transfer torques in relation to a molecular magnetization [216, 217]. This experimental achievement opens new possibilities for data storage technology and applications using current-induced spin-transfer torques.

Our goal is to study the interplay between electronic spin currents and the spin dynamics of a molecular magnet. We focus on the spin-transport properties of a tunnel junction through which transport occurs via a single electronic energy level in the presence of a molecular magnet. The electronic level may belong to a neighboring quantum dot or it may be an orbital related to the molecular magnet itself. The electronic level and the molecular spin are coupled via exchange interaction, allowing for interaction between the spins of the itinerant electrons tunneling through the electronic level and the spin dynamics of the molecular magnet. We use a semiclassical approach in which the magnetization of the molecular magnet is treated as a classical spin, whose dynamics is controlled by an external magnetic field and kept nondissipative by external means [218], while for the electronic spin and charge transport we use instead a quantum description. The magnetic field is assumed to be constant, leading to a precessional motion of the molecular spin around the magnetic field axis. The electronic level is subjected to both the effects of the molecular spin and the external magnetic field, generating a Zeeman split of the level. The spin precession makes additional channels available for transport,

which leads to the possibility of precession-assisted inelastic tunneling. During a tunnel event, spin-angular momentum may be transferred between the inelastic spin currents and the molecular spin, leading to a spin-transfer torque that may be used to manipulate the spin of the molecular magnet. This torque includes the so-called *Gilbert damping*, which is a phenomenologically introduced damping term of the Landau-Lifshitz-Gilbert-Slonczewski equation [108, 174–176], and a term corresponding to a modification of the precession frequency. We show that the spin-transfer torque and hence the spin dynamics of the molecular magnet can be controlled by the external magnetic field, the bias voltage across the junction, and the gate voltage acting on the electronic level [219].

The chapter is organized as follows: We introduce our model and formalism based on the Keldysh nonequilibrium Green’s functions technique [45, 46, 220] in Sec. 3.2, where we derive expressions for the charge and spin currents in linear order with respect to a time-dependent magnetic field and analyze the spin-transport properties at zero temperature. In Sec. 3.3 we replace the general magnetic field of Sec. 3.2 by a molecular magnet whose spin precesses in an external constant magnetic field, calculate the components of the spin-transfer torque related to the Gilbert damping, and the modification of the precession frequency, and analyze the effects of the external magnetic field as well as the bias and gate voltages on the spin dynamics. Conclusions are given in Sec. 3.4.

3.2 Current response to a time-dependent magnetic field

3.2.1 Model and formalism

For the sake of clarity, we start by considering a junction consisting of a noninteracting single-level quantum dot coupled with two normal, metallic leads in the presence of an external, time-dependent magnetic field (see Fig. 3.1). The leads are assumed to be noninteracting and unaffected by the external field. The total Hamiltonian describing the junction is given by

$$\hat{H}(t) = \sum_{\xi \in \{L,R\}} \hat{H}_{\xi} + \hat{H}_T + \hat{H}_D(t), \quad (3.1)$$

where the Hamiltonian of the free electrons in the lead $\xi = L, R$ reads

$$\hat{H}_{\xi} = \sum_{k,\sigma} \epsilon_{k\xi} \hat{c}_{k\sigma\xi}^{\dagger} \hat{c}_{k\sigma\xi}, \quad (3.2)$$

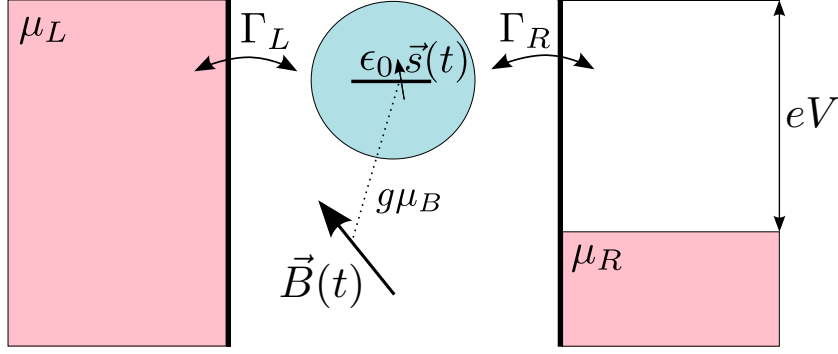


FIGURE 3.1: A quantum dot with a single electronic energy level ϵ_0 coupled to two metallic leads with chemical potentials μ_L and μ_R in the presence of an external time-dependent magnetic field $\vec{B}(t)$. The spin-transport properties of the junction are determined by the dc-bias voltage $eV = \mu_L - \mu_R$, the position of the electronic energy level ϵ_0 , the tunnel rates Γ_L and Γ_R , and the external magnetic field.

whereas the tunnel coupling between the quantum dot and the leads can be written as

$$\hat{H}_T = \sum_{k,\sigma,\xi \in \{L,R\}} [V_{k\xi} \hat{c}_{k\sigma\xi}^\dagger \hat{d}_\sigma + V_{k\xi}^* \hat{d}_\sigma^\dagger \hat{c}_{k\sigma\xi}]. \quad (3.3)$$

Here, the spin-independent tunnel matrix element is given by $V_{k\xi}$. The operators $\hat{c}_{k\sigma\xi}^\dagger$ ($\hat{c}_{k\sigma\xi}$) and \hat{d}_σ^\dagger (\hat{d}_σ) are the creation (annihilation) operators of the electrons in the leads and the quantum dot, respectively. The subscript $\sigma = \uparrow, \downarrow$ denotes the spin-up or spin-down state of the electrons. The electronic level ϵ_0 of the quantum dot is influenced by an external magnetic field $\vec{B}(t)$ consisting of a constant part \vec{B}^c and a time-dependent part $\vec{B}'(t)$. The Hamiltonian of the quantum dot with the magnetic field $\vec{B}(t)$ acting on the electronic spin \hat{s} is then given by

$$\hat{H}_D(t) = \hat{H}_D^c + \hat{H}'(t), \quad (3.4)$$

where the constant part reads

$$\hat{H}_D^c = \sum_{\sigma} \epsilon_0 \hat{d}_\sigma^\dagger \hat{d}_\sigma + g\mu_B \hat{s} \vec{B}^c, \quad (3.5)$$

while the time-dependent part $\hat{H}'(t)$ can be written as

$$\hat{H}'(t) = g\mu_B \hat{s} \vec{B}'(t). \quad (3.6)$$

The proportionality factor g is the gyromagnetic ratio of the electron and μ_B is the Bohr magneton.

The average charge and spin currents from the left lead to the electronic level are given by

$$I_{L\nu}(t) = q_\nu \left\langle \frac{d}{dt} \hat{N}_{L\nu} \right\rangle = q_\nu \frac{i}{\hbar} \langle [\hat{H}, \hat{N}_{L\nu}] \rangle, \quad (3.7)$$

where $\hat{N}_{L\nu} = \sum_{k,\sigma,\sigma'} \hat{c}_{k\sigma L}^\dagger (\sigma_\nu)_{\sigma\sigma'} \hat{c}_{k\sigma' L}$ is the charge and spin occupation number operator of the left contact. The index $\nu = 0$ corresponds to the charge current, while $\nu = x, y, z$ indicates the different components of the spin-polarized current. The current coefficients q_ν are then $q_0 = -e$ and $q_{\nu \neq 0} = \hbar/2$. In addition, it is useful to define the vector $\hat{\sigma}_\nu = (\hat{1}, \hat{\vec{\sigma}})$, where $\hat{1}$ is the identity matrix and $\hat{\vec{\sigma}}$ consists of the Pauli matrices with matrix elements $(\vec{\sigma})_{\sigma\sigma'}$. Using the Keldysh nonequilibrium Green's functions technique, the currents can then be obtained as [45, 46]

$$I_{L\nu}(t) = -\frac{2q_\nu}{\hbar} \text{Re} \int dt' \text{Tr} \{ \hat{\sigma}_\nu [\hat{G}^r(t, t') \hat{\Sigma}_L^<(t', t) + \hat{G}^<(t, t') \hat{\Sigma}_L^a(t', t)] \}, \quad (3.8)$$

where $\hat{G}^{r,a,<}$ are the retarded, advanced, and lesser Green's functions of the electrons in the quantum dot. The matrix elements of these Green's functions are given by $G_{\sigma\sigma'}^{r,a}(t, t') = \mp i \theta(\pm t \mp t') \langle \{ \hat{d}_\sigma(t), \hat{d}_{\sigma'}^\dagger(t') \} \rangle$ and $G_{\sigma\sigma'}^<(t, t') = i \langle \hat{d}_{\sigma'}^\dagger(t') \hat{d}_\sigma(t) \rangle$, while $\hat{\Sigma}_L^{r,a,<}(t, t')$ are self-energies from the coupling between the quantum dot and the left lead. Their nonzero matrix elements are diagonal in the electronic spin space with respect to the basis of eigenstates of \hat{s}_z , and can be written as $\Sigma_L^{r,a,<}(t, t') = \sum_k V_{kL} g_{kL}^{r,a,<}(t, t') V_{kL}^*$. The Green's functions $g_{kL}^{r,a,<}(t, t')$ are the retarded, advanced and lesser Green's functions of the free electrons in the left lead. The retarded Green's functions \hat{G}_0^r of the electrons in the quantum dot, in the presence of the constant magnetic field \vec{B}^c , are found using the equation of motion technique [118], while the lesser Green's functions $\hat{G}_0^<$ are obtained from the Keldysh equation $\hat{G}_0^< = \hat{G}_0^r \hat{\Sigma}^< \hat{G}_0^a$, where multiplication implies internal time integrations [46].

The time-dependent part of the magnetic field can be expressed as

$$\vec{B}'(t) = \sum_\omega (\vec{B}_\omega e^{-i\omega t} + \vec{B}_\omega^* e^{i\omega t}), \quad (3.9)$$

where \vec{B}_ω is a complex amplitude. This magnetic field acts as a time-dependent perturbation that can be expressed as

$$\hat{H}'(t) = \sum_\omega (\hat{H}_\omega e^{-i\omega t} + \hat{H}_\omega^\dagger e^{i\omega t}), \quad (3.10)$$

where \hat{H}_ω is an operator in the electronic spin space and its matrix representaton

in the basis of eigenstates of \hat{s}_z is given by

$$\hat{H}_\omega = \frac{g\mu_B}{2} \begin{pmatrix} B_{\omega z} & B_{\omega x} - iB_{\omega y} \\ B_{\omega x} + iB_{\omega y} & -B_{\omega z} \end{pmatrix}. \quad (3.11)$$

Applying Dyson's expansion, analytic continuation rules and the Keldysh equation [46], one obtains a first-order approximation of the Green's functions describing the electrons in the quantum dot that can be written as

$$\hat{G}^r \approx \hat{G}_0^r + \hat{G}_0^r \hat{H}' \hat{G}_0^r, \quad (3.12)$$

$$\hat{G}^< \approx \hat{G}_0^r \hat{\Sigma}^< \hat{G}_0^a + \hat{G}_0^r \hat{H}' \hat{G}_0^r \hat{\Sigma}^< \hat{G}_0^a + \hat{G}_0^r \hat{\Sigma}^< \hat{G}_0^a \hat{H}' \hat{G}_0^a. \quad (3.13)$$

The expression for the currents in this linear approximation is given by

$$I_{L\nu}(t) = -\frac{2q_\nu}{\hbar} \text{Re Tr} \{ \hat{\sigma}_\nu [\hat{G}_0^r \hat{\Sigma}_L^< + \hat{G}_0^< \hat{\Sigma}_L^a + \hat{G}_0^r \hat{H}' \hat{G}_0^r \hat{\Sigma}_L^< + \hat{G}_0^r \hat{H}' \hat{G}_0^r \hat{\Sigma}_L^a + \hat{G}_0^< \hat{H}' \hat{G}_0^a \hat{\Sigma}_L^a] \}. \quad (3.14)$$

Eq. (3.14) is then Fourier transformed in the wide-band limit, in which the level width function, $\Gamma(\epsilon) = -2 \text{Im}\{\Sigma^r(\epsilon)\}$, is constant, $\text{Re}\{\Sigma^r(\epsilon)\} = 0$, and one can hence write the retarded self-energy originating from the dot-lead coupling as $\Sigma^{r,a}(\epsilon) = \mp i\Gamma/2$. From this transformation, one obtains

$$I_{L\nu}(t) = I_{L\nu}^{\text{dc}} + \sum_{\omega} [I_{L\nu}(\omega) e^{-i\omega t} + I_{L\nu}^*(\omega) e^{i\omega t}]. \quad (3.15)$$

Using units in which $\hbar = 1$, the dc part of the currents [46] $I_{L\nu}^{\text{dc}}$ and the time-independent complex components $I_{L\nu}(\omega)$ are given by

$$I_{L\nu}^{\text{dc}} = q_\nu \int \frac{d\epsilon}{\pi} \frac{\Gamma_L \Gamma_R}{\Gamma} [f_L(\epsilon) - f_R(\epsilon)] \text{Tr Im} \{ \hat{\sigma}_\nu \hat{G}_0^r(\epsilon) \} \quad (3.16)$$

and

$$I_{L\nu}(\omega) = -iq_\nu \int \frac{d\epsilon}{2\pi} \frac{\Gamma_L \Gamma_R}{\Gamma} \left\{ [f_L(\epsilon) - f_R(\epsilon)] \times \text{Tr} \{ \hat{\sigma}_\nu [\hat{G}_0^r(\epsilon + \omega) \hat{H}_\omega \hat{G}_0^r(\epsilon) + 2i \text{Im} \{ \hat{G}_0^r(\epsilon) \} \hat{H}_\omega \hat{G}_0^a(\epsilon - \omega)] \} + \sum_{\xi=L,R} \frac{\Gamma_\xi}{\Gamma_R} [f_\xi(\epsilon - \omega) - f_L(\epsilon)] \text{Tr} [\hat{\sigma}_\nu \hat{G}_0^r(\epsilon) \hat{H}_\omega \hat{G}_0^a(\epsilon - \omega)] \right\}. \quad (3.17)$$

In the above expressions, $f_\xi(\epsilon) = [e^{(\epsilon - \mu_\xi)/k_B T} + 1]^{-1}$ is the Fermi distribution of the electrons in lead ξ , where k_B is the Boltzmann constant. The retarded Green's function $\hat{G}_0^r(\epsilon)$ is given by $\hat{G}_0^r(\epsilon) = [\epsilon - \epsilon_0 - \Sigma^r(\epsilon) - (1/2)g\mu_B \hat{\sigma} \vec{B}^e]^{-1}$ [189, 221].

The linear response of the spin current with respect to the applied time-dependent magnetic field can be expressed in terms of complex spin-current susceptibilities defined as

$$\chi_{\nu j}^L(\omega) = \frac{\partial I_{L\nu}(\omega)}{\partial B_{\omega j}}, \quad j = x, y, z. \quad (3.18)$$

The complex components $I_{L\nu}(\omega)$ are conversely given by $I_{L\nu}(\omega) = \sum_j \chi_{\nu j}^L(\omega) B_{\omega j}$. Taking into account that $\partial \hat{H}_\omega / \partial B_{\omega j} = (1/2)g\mu_B \hat{\sigma}_j$ and using Eq. (3.17), the current susceptibilities can be written as

$$\begin{aligned} \chi_{\nu j}^L(\omega) = & -iq_\nu g\mu_B \int \frac{d\epsilon}{4\pi} \frac{\Gamma_L \Gamma_R}{\Gamma} \left\{ [f_L(\epsilon) - f_R(\epsilon)] \right. \\ & \times \text{Tr} \{ \hat{\sigma}_\nu [\hat{G}_0^r(\epsilon + \omega) \hat{\sigma}_j \hat{G}_0^r(\epsilon) + 2i \text{Im} \{ \hat{G}_0^r(\epsilon) \} \hat{\sigma}_j \hat{G}_0^a(\epsilon - \omega)] \} \\ & \left. + \sum_\xi \frac{\Gamma_\xi}{\Gamma_R} [f_\xi(\epsilon - \omega) - f_L(\epsilon)] \text{Tr} [\hat{\sigma}_\nu \hat{G}_0^r(\epsilon) \hat{\sigma}_j \hat{G}_0^a(\epsilon - \omega)] \right\}. \end{aligned} \quad (3.19)$$

The components obey $\chi_{\nu j}^L(-\omega) = \chi_{\nu j}^{L*}(\omega)$. In other words, they satisfy the Kramers-Kronig relations [145] that can be written in a compact form as

$$\chi_{\nu j}^L(\omega) = \frac{1}{i\pi} P \int_{-\infty}^{\infty} \frac{\chi_{\nu j}^L(\xi)}{\xi - \omega} d\xi, \quad (3.20)$$

with P denoting the principal value.

For any $i, j, k = x, y, z$ such that $j \neq k$ and $j, k \neq i$, where i indicates the direction of the constant part of the magnetic field $\vec{B}^c = B^c \vec{e}_i$, the complex current susceptibilities satisfy the relations

$$\chi_{jj}^L(\omega) = \chi_{kk}^L(\omega) \quad (3.21)$$

$$\text{and} \quad \chi_{jk}^L(\omega) = -\chi_{kj}^L(\omega), \quad (3.22)$$

in addition to Eq. (3.20). The other nonzero components are $\chi_{0i}^L(\omega)$ and $\chi_{ii}^L(\omega)$. In the absence of a constant magnetic field, the only nonvanishing components obey $\chi_{xx}^L(\omega) = \chi_{yy}^L(\omega) = \chi_{zz}^L(\omega)$.

Finally, the average value of the electronic spin in the quantum dot reads $\vec{s}(t) = \langle \hat{s}(t) \rangle = (1/2) \sum_{\sigma\sigma'} \vec{\sigma}_{\sigma\sigma'} \langle \hat{d}_\sigma^\dagger(t) \hat{d}_{\sigma'}(t) \rangle = -(i/2) \sum_{\sigma\sigma'} \vec{\sigma}_{\sigma\sigma'} G_{\sigma'\sigma}^<(t, t)$ and the complex spin susceptibilities are defined as

$$\chi_{ij}^s(\omega) = \frac{\partial s_i(\omega)}{\partial B_{\omega j}}. \quad (3.23)$$

They represent the linear responses of the electronic spin components to the applied time-dependent magnetic field and satisfy the relations similar to Eqs. (3.20), (3.21), and (3.22) given above.

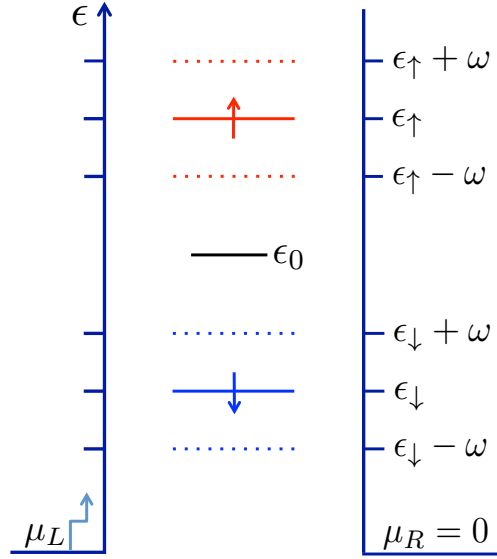


FIGURE 3.2: Sketch of the electronic levels of the quantum dot in the presence of a time-dependent magnetic field. In a static magnetic field, the electronic level ϵ_0 (solid black line) splits into the Zeeman levels $\epsilon_{\uparrow,\downarrow}$ (solid red and blue lines). If the magnetic field in addition to the static component also includes a time-dependent part with a characteristic frequency ω , additional levels appear at energies $\epsilon_{\uparrow} \pm \omega$ (dotted red lines) and $\epsilon_{\downarrow} \pm \omega$ (dotted blue lines). Hence, there are six channels available for transport.

3.2.2 Analysis of the spin and current responses

We start by analyzing the transport properties of the junction at zero temperature in response to the external time-dependent magnetic field $\vec{B}(t)$. The constant component of the magnetic field \vec{B}^c generates a Zeeman split of the quantum dot level ϵ_0 , resulting in the levels $\epsilon_{\uparrow,\downarrow}$, where $\epsilon_{\uparrow,\downarrow} = \epsilon_0 \pm g\mu_B B^c/2$ in this subsection. The time-dependent periodic component of the magnetic field $\vec{B}'(t)$ then creates additional states, i.e., sidebands, at energies $\epsilon_{\uparrow} \pm \omega$ and $\epsilon_{\downarrow} \pm \omega$ (see Fig. 3.2). These Zeeman levels and sidebands contribute to the elastic transport properties of the junction when their energies lie inside the bias-voltage window of $eV = \mu_L - \mu_R$.

However, electronic levels of the quantum dot which lie outside the bias-voltage window may also contribute to the electronic transport due to inelastic tunnel processes generated by the time-dependent magnetic field. In these inelastic processes, an electron transmitted from the left lead to the quantum dot can change its energy by ω and either tunnel back to the left lead or out into the right lead. If this perturbation is small, as is assumed in this chapter where we consider first-order corrections, the transport properties are still dominated by the elastic, energy-conserving tunnel processes that are associated with the Zeeman levels.

The levels of the quantum dot determine transport properties such as the spin-current susceptibilities and the spin susceptibilities, which are shown in Figs. 3.3 and 3.4. The imaginary and real parts of the susceptibilities are plotted as functions of the frequency ω in Figs. 3.3(a) and 3.3(b). In this case, the position of the unperturbed level ϵ_0 is symmetric with respect to the Fermi energies of the leads and a peak or step in the spin-current susceptibilities and spin susceptibilities appears at a value of ω , for which a quantum dot level is aligned with one of the Fermi energies of the leads.

In Figs. 3.4(a) and 3.4(b), the susceptibilities are instead plotted as functions of the bias voltage, eV . Here, each peak or step in the susceptibilities corresponds to a change in the number of available transport channels. The bias voltage is applied in such a way that the Fermi energy of the right lead is fixed at $\mu_R = 0$, while the Fermi energy of the left lead is varied according to $\mu_L = eV$.

3.3 Spin-transfer torque and molecular spin dynamics

3.3.1 Model with a precessing molecular spin

Now we apply the formalism of the previous section to the case of resonant tunneling through a quantum dot in the presence of a constant external magnetic field and a molecular magnet [see Fig. 3.5(a)]. A molecular magnet with a spin S lives in a $(2S + 1)$ -dimensional Hilbert space. We assume that the spin S of the molecular magnet is large and neglecting the quantum fluctuations, one can treat it as a classical vector whose end point moves on a sphere of radius S . In the presence of a constant magnetic field $\vec{B}^c = B^c \vec{e}_z$, the molecular spin precesses around the field axis according to $\vec{S}(t) = S_\perp \cos(\omega_L t) \vec{e}_x + S_\perp \sin(\omega_L t) \vec{e}_y + S_z \vec{e}_z$, where S_\perp is the projection of \vec{S} onto the xy plane, $\omega_L = g\mu_B B^c$ is the Larmor precession frequency and S_z is the projection of the spin on the z -axis [see Fig. 3.5(b)]. The spins of the electrons in the electronic level are coupled to the spin of the molecular magnet via the exchange interaction J . The contribution of the external magnetic field and the precessional motion of the molecular spin create an effective time-dependent magnetic field acting on the electronic level.

The Hamiltonian of the system is now given by

$$\hat{H}(t) = \sum_{\xi \in \{L,R\}} \hat{H}_\xi + \hat{H}_T + \hat{H}_D(t) + \hat{H}_S, \quad (3.24)$$

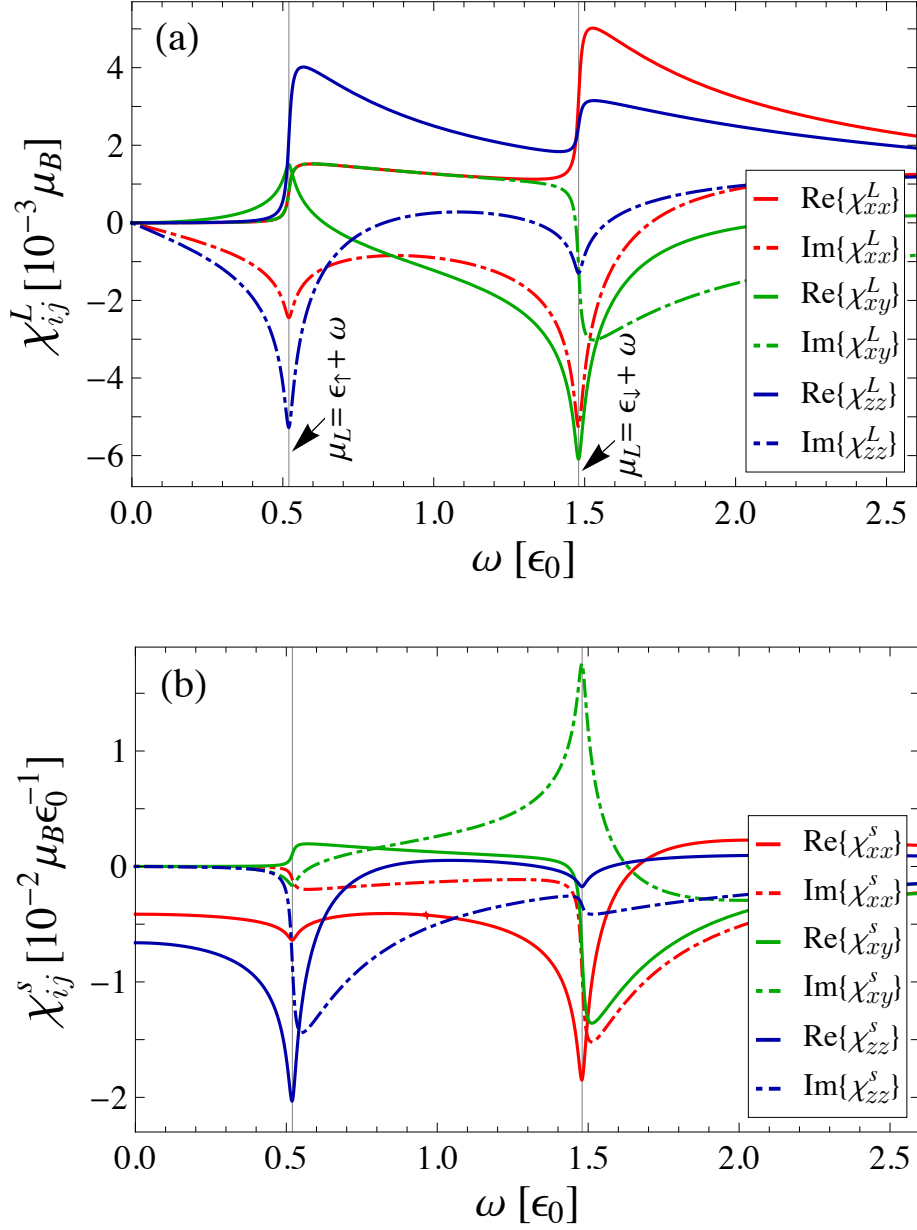


FIGURE 3.3: Frequency dependence of (a) the spin-current susceptibilities and (b) the spin susceptibilities. The chemical potential of the left lead is equal to $\mu_L = 2\epsilon_0$. All plots are obtained at zero temperature, with $\vec{B}^c = B^c \vec{e}_z$, and the other parameters set to: $\mu_R = 0$, $\epsilon_\uparrow = 1.48\epsilon_0$, $\epsilon_\downarrow = 0.52\epsilon_0$, $\Gamma = 0.02\epsilon_0$, and $\Gamma_L = \Gamma_R = 0.01\epsilon_0$.

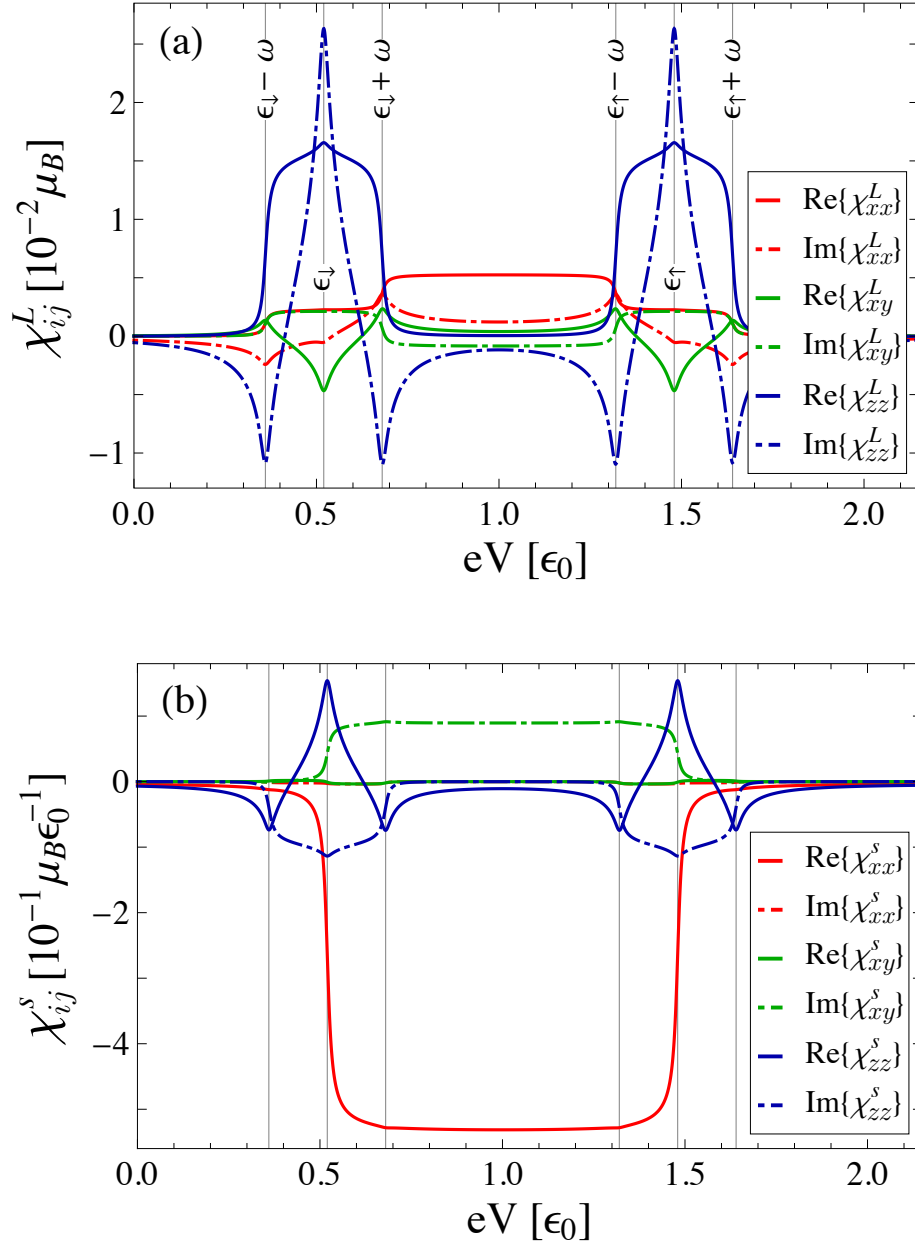


FIGURE 3.4: Bias-voltage dependence of (a) the spin-current susceptibilities and (b) the spin susceptibilities. The frequency is set to $\omega = 0.16 \epsilon_0$. All plots are obtained at zero temperature with $\vec{B}^c = B^c \vec{e}_z$, μ_L is varied as $\mu_L = eV$, and the other parameters are the same as in Fig. 3.3. Resonant transport channels manifest themselves as peaks or steps in the susceptibilities.

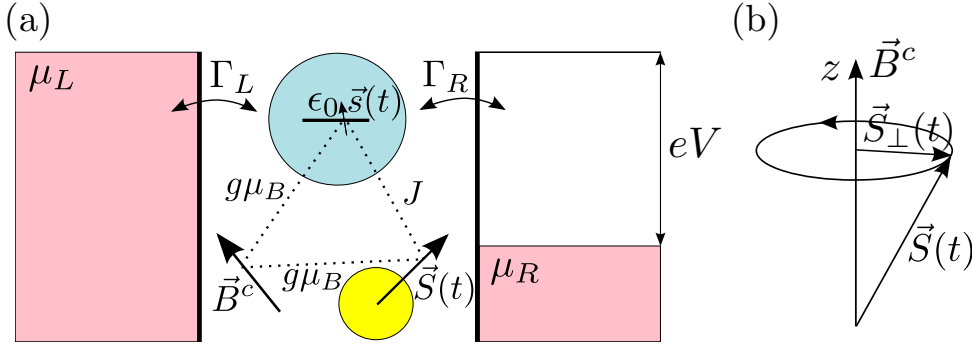


FIGURE 3.5: (a) Tunneling in the presence of a molecular magnet and an external, constant magnetic field. The electronic level of Fig. 3.1 is now coupled with the spin of the molecular magnet via exchange interaction with the coupling constant J . The dynamics of the molecular spin $\vec{S}(t)$ is controlled by the external magnetic field \vec{B}^c that also affects the electronic level. (b) Precessional motion of the spin of the molecular magnet in a constant magnetic field \vec{B}^c applied along the z -axis.

where the Hamiltonians \hat{H}_ξ and \hat{H}_T are the same as in Sec. 3.2. The Hamiltonian

$$\hat{H}_S = g\mu_B \vec{S} \vec{B}^c \quad (3.25)$$

represents the molecular spin \vec{S} in the magnetic field \vec{B}^c and contributes to the spin dynamics of the molecular magnet. The Hamiltonian of the quantum dot in this case is given by

$$\hat{H}_D(t) = \hat{H}_D^c + \hat{H}'(t), \quad (3.26)$$

where

$$\hat{H}_D^c = \sum_{\sigma} \epsilon_0 \hat{d}_{\sigma}^{\dagger} \hat{d}_{\sigma} + g\mu_B \hat{s} \vec{B}_{\text{eff}}^c \quad (3.27)$$

is the Hamiltonian of the electrons in the quantum dot in the presence of the constant part of the effective magnetic field, given by

$$\vec{B}_{\text{eff}}^c = \left[B^c + \frac{J}{g\mu_B} S_z \right] \vec{e}_z. \quad (3.28)$$

The second term of the quantum dot Hamiltonian,

$$\hat{H}'(t) = g\mu_B \hat{s} \vec{B}'_{\text{eff}}(t), \quad (3.29)$$

represents the interaction between the electronic spins of the quantum dot, \hat{s} , and the time-dependent part of the effective magnetic field, given by

$$\vec{B}'_{\text{eff}}(t) = \frac{JS_{\perp}}{g\mu_B} \left[\cos(\omega_L t) \vec{e}_x + \sin(\omega_L t) \vec{e}_y \right]. \quad (3.30)$$

The time-dependent effective magnetic field can be rewritten as

$$\vec{B}'_{\text{eff}}(t) = \vec{B}_{\omega_L} e^{-i\omega_L t} + \vec{B}_{\omega_L}^* e^{i\omega_L t}, \quad (3.31)$$

where \vec{B}_{ω_L} is the complex amplitude which consists of the components given by $B_{\omega_L x} = JS_{\perp}/2g\mu_B$, $B_{\omega_L y} = iJS_{\perp}/2g\mu_B$, and $B_{\omega_L z} = 0$. The time-dependent perturbation can then be expressed as

$$\hat{H}'(t) = \hat{H}_{\omega_L} e^{-i\omega_L t} + \hat{H}_{\omega_L}^{\dagger} e^{i\omega_L t}, \quad (3.32)$$

where \hat{H}_{ω_L} is an operator that can be written, using Eq. (3.11) and the above expressions for $B_{\omega_L j}$, $j = x, y, z$, as

$$\hat{H}_{\omega_L} = \frac{JS_{\perp}}{2} \begin{pmatrix} 0 & 1 \\ 0 & 0 \end{pmatrix}. \quad (3.33)$$

The time-dependent part of the effective magnetic field creates inelastic tunnel processes that contribute to the currents. The in-plane components of the spin current fulfill

$$\begin{aligned} I_{Lx}(\omega_L) &= -iI_{Ly}(\omega_L) \\ &= \frac{JS_{\perp}}{2g\mu_B} [\chi_{xx}^L(\omega_L) + i\chi_{xy}^L(\omega_L)], \end{aligned} \quad (3.34)$$

where \vec{B}^c is replaced by \vec{B}'_{eff} . The z component vanishes to lowest order in $H'(t)$ [222]. Therefore, the inelastic spin current has a polarization that precesses in the xy plane. The inelastic spin-current components, in turn, exert a spin-transfer torque on the molecular spin given by [108–111]

$$\vec{T}(t) = -[\vec{I}_L(t) + \vec{I}_R(t)]. \quad (3.35)$$

Using expressions (3.15), (3.17), and (3.33), the torque of Eq. (3.35) can be calculated in terms of the Green's functions $\hat{G}_0^r(\epsilon)$ and $\hat{G}_0^a(\epsilon)$ as

$$\begin{aligned} T_i(t) &= -\frac{JS_{\perp}}{2} \int \frac{d\epsilon}{2\pi} \sum_{\xi\lambda} \frac{\Gamma_{\xi}\Gamma_{\lambda}}{\Gamma} [f_{\xi}(\epsilon - \omega_L) - f_{\lambda}(\epsilon)] \\ &\quad \times \text{Im}\{(\sigma_i)_{\downarrow\uparrow} G_{0,\uparrow\uparrow}^r(\epsilon) G_{0,\downarrow\downarrow}^a(\epsilon - \omega_L) e^{-i\omega_L t}\}, \end{aligned} \quad (3.36)$$

with $\lambda = L, R$. Here $(\sigma_i)_{\downarrow\uparrow}$, $G_{0,\uparrow\uparrow}^r(\epsilon)$, and $G_{0,\downarrow\downarrow}^a(\epsilon)$ are matrix elements of $\hat{\sigma}_i$, $\hat{G}_0^r(\epsilon)$

and $\hat{G}_0^a(\epsilon)$ with respect to the basis of eigenstates of \hat{s}_z . This spin-transfer torque can be rewritten in terms of the spin vector of the molecular magnet as

$$\vec{T}(t) = \frac{\alpha}{S} \dot{\vec{S}}(t) \times \vec{S}(t) + \beta \dot{\vec{S}}(t) + \eta \vec{S}(t). \quad (3.37)$$

The first term in this back-action gives a contribution to the Gilbert damping, characterized by the Gilbert damping coefficient α . The second term acts as an effective constant magnetic field and changes the precession frequency of the spin \vec{S} with the corresponding coefficient β . The third term cancels the z component of the Gilbert damping term, thus restricting the spin-transfer torque to the xy plane. The coefficient of the third term η is related to α by $\eta/\alpha = \omega_L S_\perp^2 / S S_z$. Expressing the coefficients α and β in terms of the current susceptibilities $\chi_{xx}^\xi(\omega_L)$ and $\chi_{xy}^\xi(\omega_L)$ results in

$$\alpha = -\frac{J S_z}{g \mu_B \omega_L S} \sum_{\xi} [\text{Re}\{\chi_{xx}^\xi(\omega_L)\} - \text{Im}\{\chi_{xy}^\xi(\omega_L)\}], \quad (3.38)$$

$$\beta = \frac{J}{g \mu_B \omega_L} \sum_{\xi} [\text{Im}\{\chi_{xx}^\xi(\omega_L)\} + \text{Re}\{\chi_{xy}^\xi(\omega_L)\}]. \quad (3.39)$$

By inserting the explicit expressions for $G_{0,\uparrow\uparrow}^r(\epsilon)$ and $G_{0,\downarrow\downarrow}^a(\epsilon - \omega_L)$, one obtains the following expressions for the torque coefficients [219]

$$\alpha = \frac{J^2 S_z^2}{\omega_L S} \int \frac{d\epsilon}{8\pi} \sum_{\xi\lambda} \Gamma_\xi \Gamma_\lambda [f_\xi(\epsilon - \omega_L) - f_\lambda(\epsilon)] \times \frac{1}{[(\frac{\Gamma}{2})^2 + (\epsilon - \epsilon_\uparrow)^2][(\frac{\Gamma}{2})^2 + (\epsilon - \epsilon_\downarrow - \omega_L)^2]}, \quad (3.40)$$

$$\beta = -\frac{J}{\omega_L \Gamma} \int \frac{d\epsilon}{4\pi} \sum_{\xi\lambda} \Gamma_\xi \Gamma_\lambda [f_\xi(\epsilon - \omega_L) - f_\lambda(\epsilon)] \times \frac{(\frac{\Gamma}{2})^2 + (\epsilon - \epsilon_\uparrow)(\epsilon - \epsilon_\downarrow - \omega_L)}{[(\frac{\Gamma}{2})^2 + (\epsilon - \epsilon_\uparrow)^2][(\frac{\Gamma}{2})^2 + (\epsilon - \epsilon_\downarrow - \omega_L)^2]}, \quad (3.41)$$

where $\epsilon_{\uparrow,\downarrow} = \epsilon_0 \pm g \mu_B B_{\text{eff}}^c / 2 = \epsilon_0 \pm (\omega_L + J S_z) / 2$ are the energies of the Zeeman levels in this subsection. In the small precession frequency regime, $\omega_L \ll k_B T$, $\eta \rightarrow 0$ and in the limit of $S_z / S \rightarrow 1$ the expression for the coefficient α is in agreement with [189].

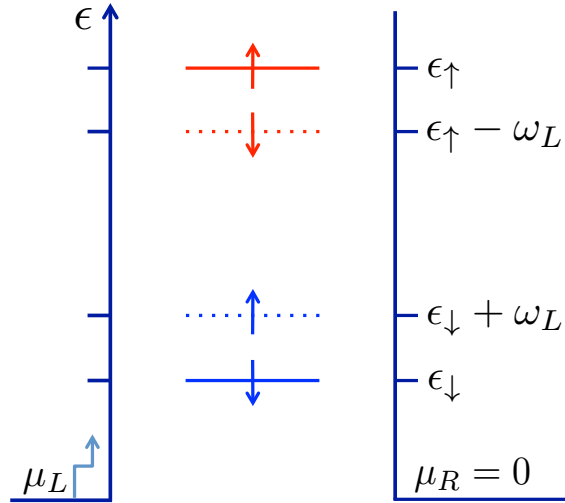


FIGURE 3.6: Sketch of the electronic quasienergy levels of the quantum dot in the presence of a molecular spin precessing with the frequency ω_L around an external, constant magnetic field. The corresponding Zeeman levels are $\epsilon_{\uparrow,\downarrow}$. The precessional motion of the molecular spin results in emission (absorption) of energy corresponding to a spin flip from spin up (down) to spin down (up). Hence, there are only four channels available for transport.

3.3.2 Analysis of the spin-transfer torque

In the case of resonant tunneling in the presence of a molecular spin precessing in a constant external magnetic field, one also needs to take the exchange of spin-angular momentum between the molecular spin and the electronic spins into account in addition to the effects of the external magnetic field. Due to the precessional motion of the molecular spin, an electron in the quantum dot emitting (absorbing) an energy ω_L also undergoes a spin flip from spin up (down) to spin down (up), as indicated by the arrows in Fig. 3.6. As a result, the levels at energies $\epsilon_{\uparrow} + \omega_L$ and $\epsilon_{\downarrow} - \omega_L$ are forbidden and hence do not contribute to the transport processes. Consequently, there are only four transport channels, which are located at energies ϵ_{\downarrow} , $\epsilon_{\downarrow} + \omega_L$, $\epsilon_{\uparrow} - \omega_L$, and ϵ_{\uparrow} . We should point out that these quasienergies can be obtained using the Floquet theorem [224–228], taking into account that we treat the periodic time-dependent part of the Hamiltonian as a perturbation (see Appendix A). In this case there are also elastic and inelastic tunnel processes. Some of the possible inelastic tunnel processes are shown in Fig. 3.7. These restrictions on the inelastic tunnel processes are also visible in Fig. 3.4(a), which identically corresponds to the case of the presence of a precessing molecular spin with the Larmor frequency $\omega_L = 0.16 \epsilon_0$, and $JS_z = 0.8 \epsilon_0$. Namely, from

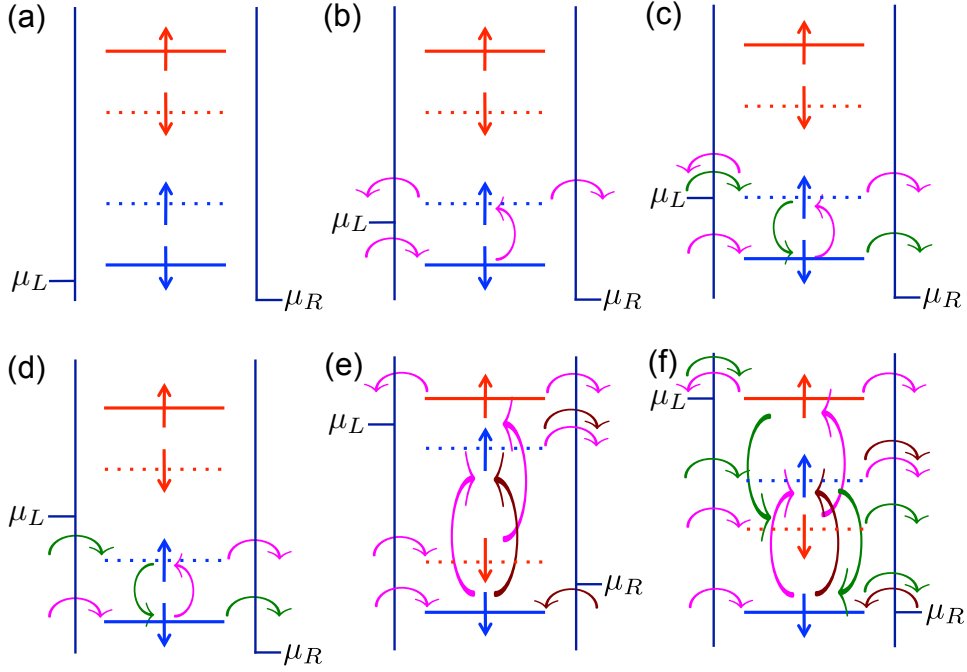


FIGURE 3.7: Sketch of the inelastic spin-tunneling processes in the quantum dot in the presence of the precessing molecular spin in the field $\vec{B}^c = B^c \vec{e}_z$, for different positions of the quasienergy levels with respect to the chemical potentials of the leads, μ_L and μ_R . Only transitions between levels with the same color (blue or red) are allowed. Different colored curved arrows (magenta, brown, or green) represent different processes.

Eq. (3.34), which is equivalent to

$$\text{Re}\{I_{Lx}(\omega_L)\} = \text{Im}\{I_{Ly}(\omega_L)\} = \frac{JS_{\perp}}{2g\mu_B} [\text{Re}\{\chi_{xx}^L(\omega_L)\} - \text{Im}\{\chi_{xy}^L(\omega_L)\}], \quad (3.42)$$

$$\text{Im}\{I_{Lx}(\omega_L)\} = -\text{Re}\{I_{Ly}(\omega_L)\} = \frac{JS_{\perp}}{2g\mu_B} [\text{Im}\{\chi_{xx}^L(\omega_L)\} + \text{Re}\{\chi_{xy}^L(\omega_L)\}], \quad (3.43)$$

and from the symmetries of the susceptibilities displayed in Fig. 3.4(a), it follows that there are no spin currents at $eV = \epsilon_{\uparrow} + \omega_L$ and $eV = \epsilon_{\downarrow} - \omega_L$.

As was mentioned, the spin currents generate a spin-transfer torque acting on the molecular spin. A necessary condition for the existence of a spin-transfer torque, and hence finite values of the coefficients α and β in Eqs. (3.40) and (3.41), is that $\vec{I}_L(t) \neq -\vec{I}_R(t)$ [see Eq. (3.35)]. This condition is met by the spin currents generated, e.g., by the inelastic tunnel processes shown in Figs. 3.7(b) and 3.7(c). These tunnel processes occur when an electron can tunnel into the quantum dot, undergo a spin flip, and then tunnel off the quantum dot into either lead. From these tunnel processes it is implied that the Gilbert damping coefficient α and the coefficient β can be controlled by the applied bias or gate voltage as well as by the external magnetic field. If a pair of quantum dot's quasienergy levels, coupled via

spin-flip processes, lie within the bias-voltage window, the spin currents instead fulfill $\vec{I}_L(t) = \vec{I}_R(t)$, leading to a vanishing spin-transfer torque [see Fig. 3.7(d)]. In Figs. 3.7(e) and 3.7(f) the position of the quasienergy levels of the quantum dot are symmetric with respect to the Fermi levels of the leads, μ_L and μ_R . When the quantum dot's level with energy ϵ_\uparrow is aligned with μ_L , this simultaneously corresponds to the level ϵ_\downarrow being aligned with μ_R [see Fig. 3.7(f)]. As a result, an electron can now tunnel from the left lead into the level ϵ_\uparrow , while a spin-down electron in the level ϵ_\downarrow can tunnel into the right lead. These additional processes enhance the spin-transfer torque compared to that of the case 3.7(e).

The two spin-torque coefficients α and β exhibit a nonmonotonic dependence on the tunneling rates Γ , as can be seen in Figs. 3.8, 3.9, and 3.10. For $\Gamma \rightarrow 0$, it is obvious that $\alpha, \beta \rightarrow 0$. In the weak coupling limit $\Gamma \ll \omega_L$, the coefficients α and β are finite if the Fermi energy of the lead ξ , μ_ξ fulfills either of the conditions

$$\epsilon_\downarrow \leq \mu_\xi \leq \epsilon_\downarrow + \omega_L, \quad (3.44)$$

$$\text{or } \epsilon_\uparrow - \omega_L \leq \mu_\xi \leq \epsilon_\uparrow, \quad (3.45)$$

in such a way that each condition is satisfied by the Fermi energy of maximum one lead. These conditions are relaxed for larger tunnel couplings as a consequence of the broadening of the quantum dot's levels, which is also responsible for the initial enhancement of α and β with increasing Γ . Notice, however, that α and β are eventually suppressed for $\Gamma \gg \omega_L$, when the quasienergy levels of the quantum dot are significantly broadened and overlap so that spin-flip processes are equally probable in each direction and there is no net effect on the molecular spin. Physically, this suppression of the spin-transfer torque can be understood by noticing that for $\Gamma \gg \omega_L$ a current-carrying electron perceives the molecular spin as almost static due to its slow precession compared to the electronic tunneling rates, and hence the exchange of angular momenta is reduced. With increasing tunneling rates, the coefficient β becomes negative before it drops to zero, causing the torque $\beta \vec{S}$ to oppose the rotational motion of the spin \vec{S} .

In Fig. 3.8, the Gilbert damping coefficient α and the coefficient β are plotted as functions of the applied bias voltage at zero temperature. We analyze the case of the smallest value of Γ (red lines), assuming that $\omega_L > 0$. For small eV , all quasienergy levels of the quantum dot lie outside the bias-voltage window and there is no spin transport [see Fig. 3.7(a)]. Hence $\alpha, \beta \rightarrow 0$. At $eV = \epsilon_\downarrow$ the tunnel processes in Fig. 3.7(b) come into play, leading to a finite spin-transfer torque and the coefficient α increases while the coefficient β has a local minimum. In the voltage region specified by inequality (3.44) for μ_L , the coefficient α approaches a constant value while the coefficient β increases. By increasing the bias voltage to

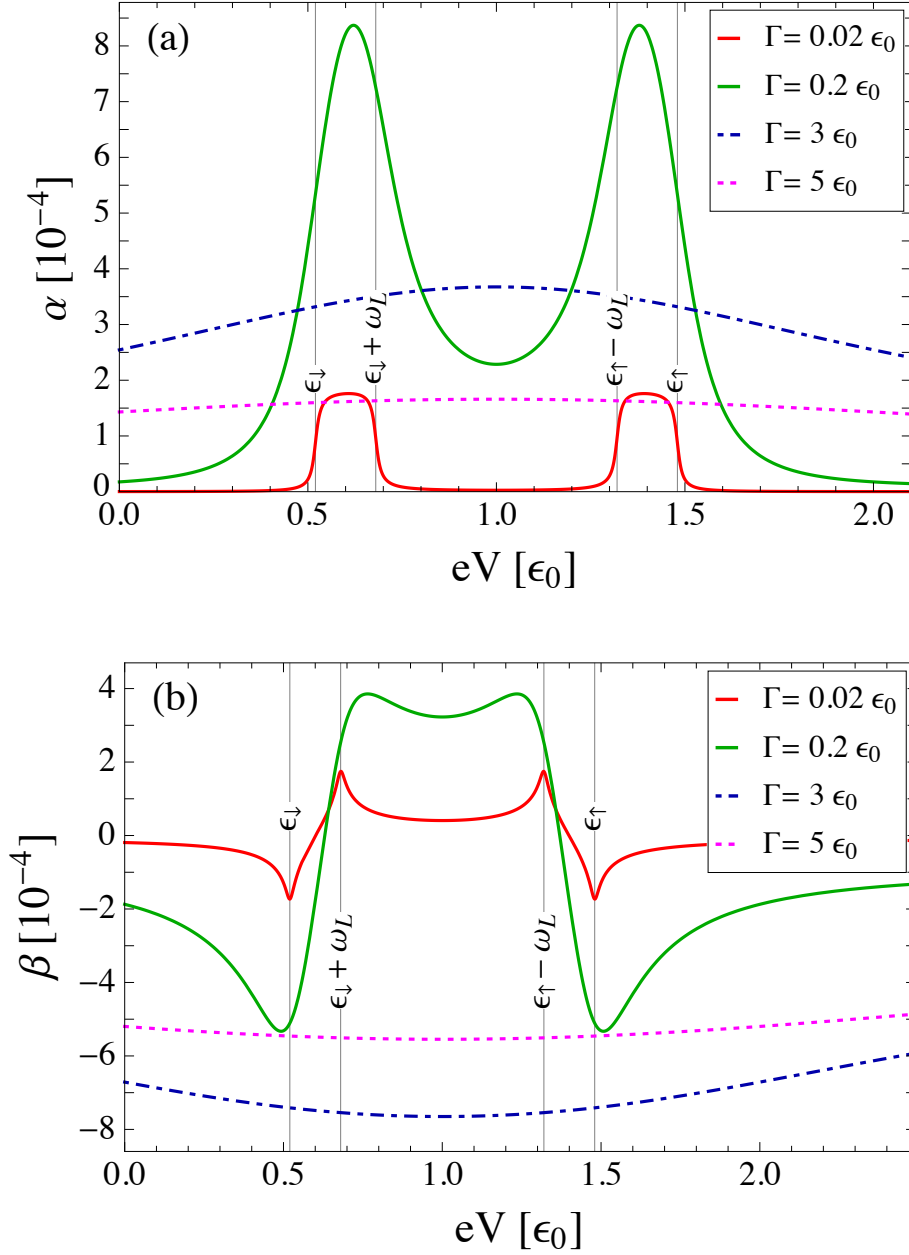


FIGURE 3.8: (a) Gilbert damping coefficient α and (b) coefficient β as functions of the applied bias voltage $eV = \mu_L - \mu_R$, with $\mu_R = 0$, and $\vec{B}^c = B^c \vec{e}_z$, for different tunneling rates Γ , at zero temperature. The other parameters are: $\Gamma_L = \Gamma_R = \Gamma/2$, $\epsilon_{\uparrow} = 1.48 \epsilon_0$, $\epsilon_{\downarrow} = 0.52 \epsilon_0$, $S = 82$, $J = 0.01 \epsilon_0$, $JS_z = 0.8 \epsilon_0$, and $\omega_L = 0.16 \epsilon_0$. In the case of the smallest value of Γ (red lines), α approaches a constant value when μ_L lies within the energy range specified by inequalities (3.44) and (3.45). The coefficient β has one local minimum and one local maximum for the same energy range.

$eV = \epsilon_{\downarrow} + \omega_L$ the tunnel processes in Fig. 3.7(c) occur, leading to a decrease of α and a local maximum of β . For $\epsilon_{\downarrow} + \omega_L < eV < \epsilon_{\uparrow} - \omega_L$, the coefficients $\alpha, \beta \rightarrow 0$ [see Fig. 3.7(d)]. In the voltage region specified by inequality (3.45) for μ_L , α approaches the same constant value mentioned above while β decreases between a local maximum at $eV = \epsilon_{\uparrow} - \omega_L$ and a local minimum at $eV = \epsilon_{\uparrow}$, which approach the same values as previously mentioned extrema. With further increase of eV , all quasienergy levels of the quantum dot lie within the bias-voltage window and the spin-transfer torque consequently vanishes.

Figure 3.9 shows the spin-torque coefficients α and β as functions of the position of the electronic level ϵ_0 . A spin-transfer torque acting on the molecular spin occurs if the electronic level ϵ_0 is positioned in such a way that the inequalities (3.44) and (3.45) may be satisfied by some values of eV , ϵ_0 and ω_L . Again, we analyze the case of the smallest value of Γ (red curve). For the particular choice of parameters in Fig. 3.9, there are four regions in which the inequalities (3.44) and (3.45) are satisfied. Within these regions, α approaches a constant value while β has a local maximum as well as a local minimum. These local extrema occur when one of the Fermi energies is aligned with one of the quasienergy levels of the quantum dot. For other values of ϵ_0 , both α and β vanish.

The coefficients α and β are plotted as functions of the precession frequency ω_L in Fig. 3.10. Here, $\epsilon_0 = eV/2$ and therefore the positions of the quasienergy levels of the quantum dot are symmetric with respect to the Fermi levels of the leads, μ_L and μ_R . Once more, we focus first on the case of the smallest value of Γ (indicated by the red curve). The energies of all four levels of the quantum dot depend on ω_L , i.e., \vec{B}^c . For $\omega_L > 0$, when the magnitude of the external magnetic field is large enough, the tunnel processes in Fig. 3.7(f) take place due to the above-mentioned symmetries. These tunnel processes lead to a finite spin-transfer torque, a maximum for the Gilbert damping coefficient α , and a negative minimum value for the β coefficient. As ω_L increases, the inequalities (3.44) and (3.45) are satisfied and the tunnel processes shown in Fig. 3.7(e) may occur. Hence, there is a contribution to the spin-transfer torque, but as is shown in Eq. (3.40), the Gilbert damping decreases with increasing precession frequency. At larger values of ω_L , resulting in $\epsilon_{\downarrow} + \omega_L = \mu_L$, the Gilbert damping coefficient has a step increase towards a local maximum, whereas, the coefficient β has a local maximum, as a consequence of the enhancement of the spin-transfer torque due to additional spin-flip processes occurring in this case. For even larger value of ω_L , the conditions (3.44) and (3.45) are no longer fulfilled and both coefficients vanish. It is energetically unfavorable to flip the spin of an electron against the antiparallel direction of the effective constant magnetic field \vec{B}_{eff}^c . Hence, as ω_L increases, more energy is needed to flip the electronic spin to the direction of the field. This causes α to decrease with

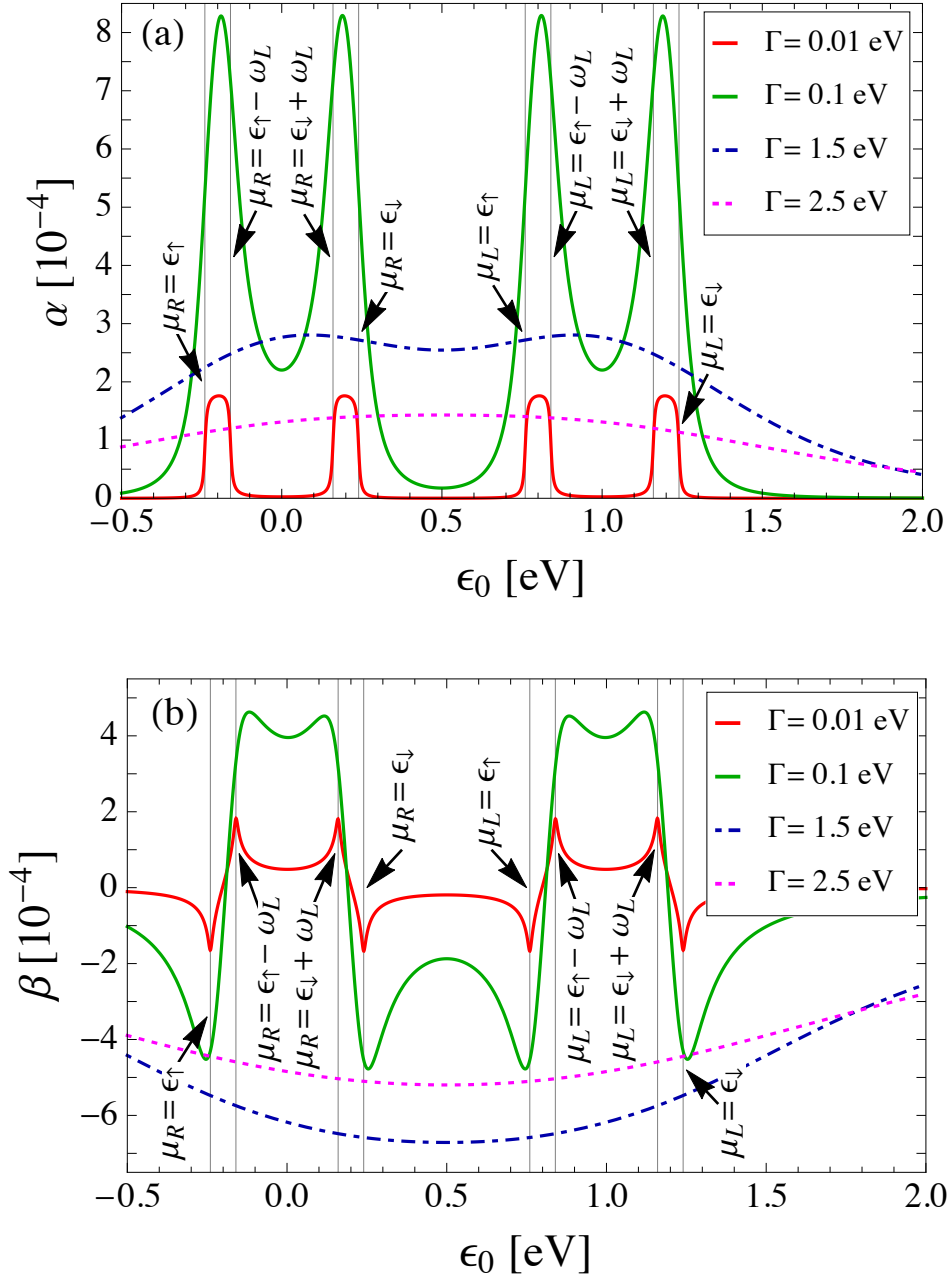


FIGURE 3.9: (a) Gilbert damping coefficient α and (b) coefficient β as functions of the position of the electronic level ϵ_0 for different tunneling rates Γ , with $\vec{B}^c = B^c \vec{e}_z$, at zero temperature. The applied bias voltage is $eV = \mu_L - \mu_R$, with $\mu_R = 0$. The other parameters are: $\Gamma_L = \Gamma_R = \Gamma/2$, $\epsilon_\uparrow - \epsilon_0 = 0.24$ eV, $S = 82$, $J = 0.005$ eV, $JS_z = 0.4$ eV, and $\omega_L = 0.08$ eV. In the case of the smallest value of Γ (red lines), there are four regions in which the Gilbert damping and the change of the precession frequency occur. In each of these regions ϵ_0 satisfies the inequalities (3.44) and (3.45), and α approaches a constant value, whereas, β has one local maximum and one local minimum.

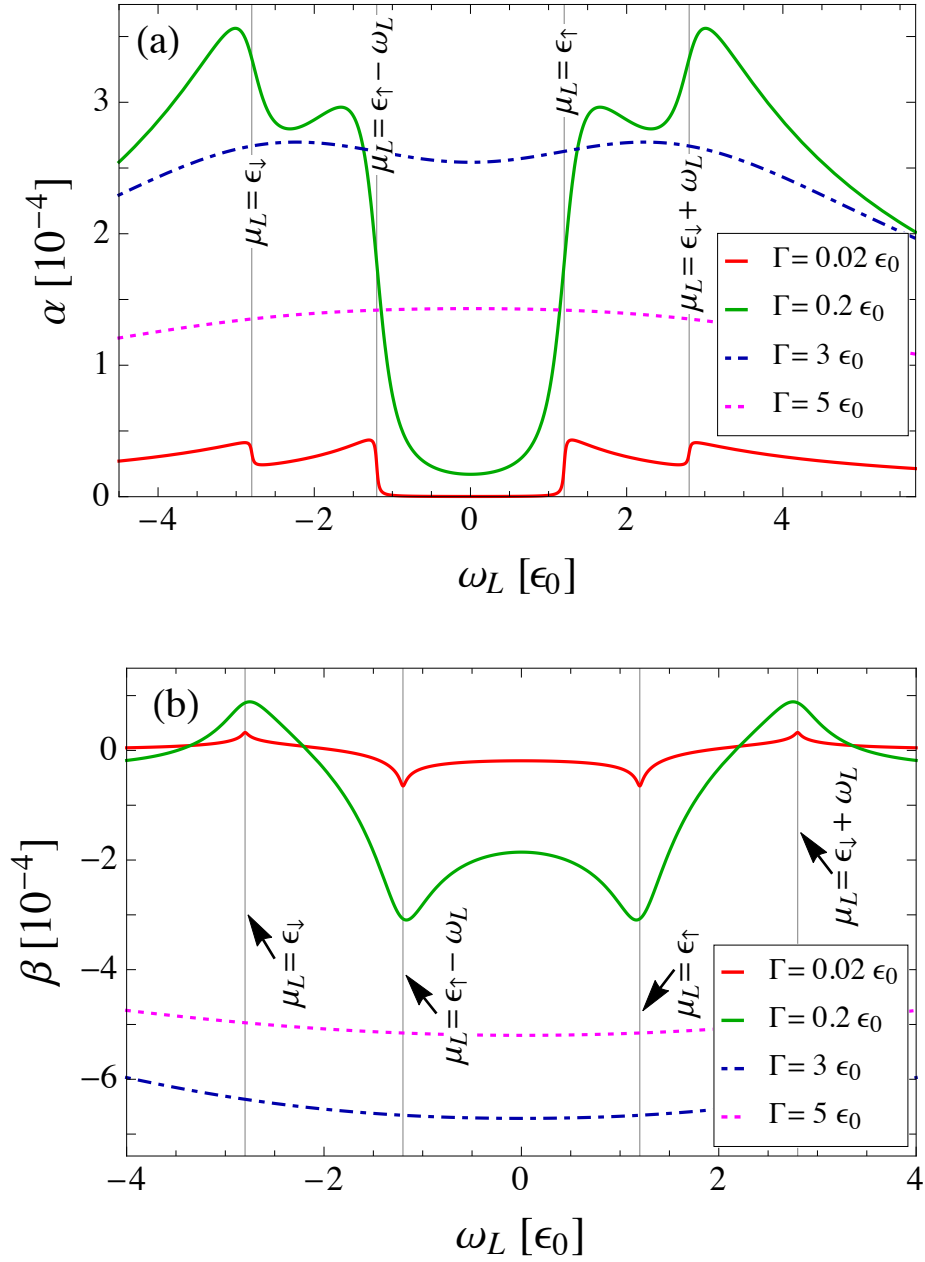


FIGURE 3.10: (a) Gilbert damping coefficient α and (b) coefficient β as functions of the precession frequency $\omega_L = g\mu_B B^c$ of the spin \vec{S} of the molecular magnet, with $\vec{B}^c = B^c \vec{e}_z$, for different tunneling rates Γ , at zero temperature. The applied bias voltage is $eV = \mu_L - \mu_R = 2\epsilon_0$, with $\mu_R = 0$. The other parameters are the same as in Fig. 3.8. In the case of the smallest Γ (red lines), the coefficient α has a step increase towards a local maximum, whereas, the coefficient β has a local maximum or minimum at a value of ω_L corresponding to a resonance of μ_L with one of the levels in the quantum dot.

increasing ω_L . Additionally, the larger the ratio ω_L/Γ , the less probable it is that spin-angular momentum will be exchanged between the molecular spin and the itinerant electrons. For $\omega_L = 0$, the molecular spin is static, i.e., $\vec{S} = 0$. In this case $\vec{T}(t) = \vec{0}$. The coefficient α then drops to zero, whereas, the coefficient β reaches a negative local maximum which is close to 0. Both α and β reach an extremum value for large values of Γ at this point. For $\omega_L < 0$ and $\Gamma \ll |\omega_L|$ (red lines), at the value of ω_L for which $\mu_L = \epsilon_\uparrow - \omega_L$, the coefficient α has a step increase towards a local maximum, whereas, the coefficient β has a negative local minimum. The coefficient α then decreases with a further decrease of ω_L as long as $\epsilon_\downarrow \leq \mu_L \leq \epsilon_\uparrow - \omega_L$. At the value of ω_L for which $\mu_L = \epsilon_\downarrow$, α has another step increase towards a local maximum, whereas, β has a maximum value. According to Eq. (3.40), the Gilbert damping also does not occur if \vec{S} is perpendicular to \vec{B}^e . In this case $\beta \lesssim 0$, and the only nonzero torque component $\beta \dot{\vec{S}}(t)$ acts in the opposite direction than the molecular spin's rotational motion.

3.4 Conclusions

In this chapter we have first theoretically studied time-dependent charge and spin transport through a small junction, consisting of a single-level quantum dot coupled to two noninteracting metallic leads in the presence of a time-dependent magnetic field. We used the Keldysh nonequilibrium Green's functions method to derive the charge and spin currents in linear order with respect to the time-dependent component of the magnetic field with a characteristic frequency ω .

We then focused on the case of a single electronic level coupled via exchange interaction to an effective magnetic field created by the precessional motion of the spin of a molecular magnet in a constant magnetic field. The inelastic tunneling processes that contribute to the spin currents produce a spin-transfer torque that acts on the molecular spin. The spin-transfer torque consists of a Gilbert damping component, characterized by the coefficient α , as well as a component, characterized by the coefficient β , that acts as an additional effective constant magnetic field, and changes the precession frequency ω_L of the molecular spin. Both α and β depend on ω_L and show a nonmonotonic dependence on the tunneling rates Γ . In the weak coupling limit $\Gamma \ll \omega_L$, α can be switched on and off as a function of bias and gate voltages. The coefficient β correspondingly has a local extremum. For $\Gamma \rightarrow 0$, both α and β vanish.

Taking into account that spin transport can be controlled by the bias and gate voltages, as well as by external magnetic fields, our results might be useful in

spintronics applications using molecular magnets. Besides a spin-polarized scanning tunneling microscopy, it may be possible to detect and manipulate the spin state of a molecular magnet in a ferromagnetic resonance experiment [229–232], and thus extract information about the effects of the current-induced spin-transfer torque on the molecular magnet. Our study could be complemented by a quantum description of a single-molecule magnet in a single-molecule magnet junction and its coherent properties, as these render the single-molecule magnet suitable for quantum information storage.

Chapter 4

Photon-assisted electronic and spin transport through a precessing spin of a molecular magnet

4.1 Introduction

Time-dependent transport through molecular junctions has been theoretically studied using different techniques, such as nonequilibrium Green's functions technique [45, 46, 48, 220, 233], time-dependent density functional theory [59, 61, 234–236], reduced density matrix approach [237], etc. Time-dependent periodic fields in electrical contacts cause photon-assisted tunneling [33, 36, 238–240], a phenomenon based on the fact that by applying an external harmonic field with frequency Ω to the contact, the conduction electrons interact with the ac field and consequently participate in the inelastic tunneling processes by absorbing or emitting an amount of energy $n\hbar\Omega$, where $n \in \mathbb{Z} \neq 0$. Theoretically, photon-assisted tunneling through atoms and molecules was investigated in numerous works [33, 36, 241–250]. Some experimental studies addressed photon-assisted tunneling through atomic-sized [251–253] and molecular [254, 255] junctions in the presence of laser fields. Time dependent electric control of the state of quantum spins of atoms has also been investigated [209]. In junctions with time-dependent

This chapter is adapted from a submitted manuscript by M. Filipović and W. Belzig, arXiv:1412.3994.

ac bias the presence of displacement currents is inevitable due to the charge accumulation in the scattering region [256, 257]. This problem can be solved either implicitly by including the Coulomb interaction in the Hamiltonian of the system [258, 259], or explicitly by adding the displacement current to the conduction current [257, 260], thus providing the conservation of the total ac current.

Spin transport through magnetic nanostructures can be used to manipulate the state of the magnetization via spin-transfer torques [108, 109]. The concept of spin-transfer torque is based on the transfer of spin angular momenta from the conduction electrons to a local magnetization in the scattering region, generating a torque as a back-action of the spin transport, and thus changing the state of the magnetic nanostructure [108–111]. Hence, current-induced magnetization reversal became an active topic in recent years [90, 189, 194, 208, 212–214]. The measurement and control of the magnetization of single-molecule magnets [146] employing spin transport may bring important applications in spintronics.

In this chapter we theoretically study the charge and spin transport through a single electronic energy level in the presence of a precessing spin of a molecular magnet in a constant magnetic field. The electronic level may be an orbital of the molecule, or it may belong to a nearby quantum dot. The molecular spin, treated as a classical magnetic moment, exhibits Larmor precession around the magnetic field axis. The Zeeman field and the interaction of the orbital with the precessing molecular spin result in four quasienergy levels in the quantum dot, obtained using the Floquet theorem [224–228]. The system is then connected to electric contacts subject to oscillating electric potentials considered as a perturbation. The oscillating chemical potentials induce photon-assisted charge and spin tunneling. A photon-assisted spin-transfer torque is exerted on the molecular spin by the photon-assisted spin-currents. This torque is not included in the dynamics of the molecular spin, since its precession is kept steady by external means, thus compensating the spin-transfer torque. The precessing molecular spin in turn pumps spin-currents into the leads, acting as an external rotating exchange field. We observe a few major effects [223]:

1. In the limit of low ac frequency the junction can be mapped onto a classical electric circuit.
2. The real and imaginary components of the dynamic conductance, associated with the resonant position of the chemical potentials with molecular quasienergy levels, are both enhanced after going to a local minimum, around the ac frequency matching the Larmor frequency, allowing the detection of the internal precession time scale.

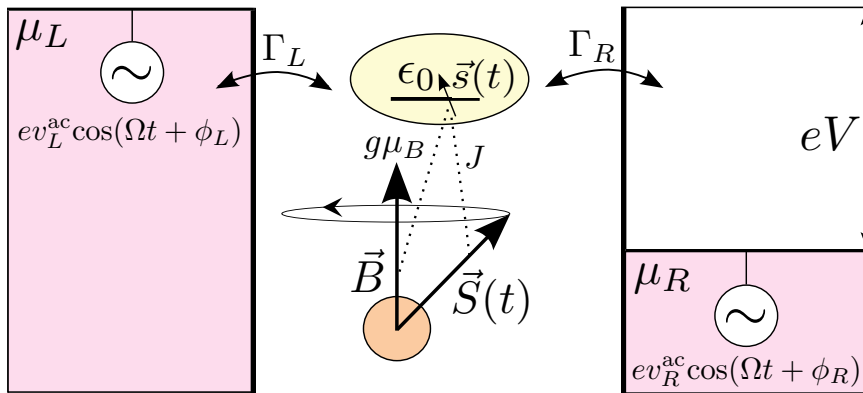


FIGURE 4.1: Photon-assisted tunneling through a single molecular level with energy ϵ_0 , coupled to the spin $\vec{S}(t)$ of a molecular magnet via exchange interaction with the coupling constant J , in the presence of a constant magnetic field \vec{B} . External ac potentials $V_\xi^{\text{ac}}(t) = v_\xi^{\text{ac}} \cos(\Omega t + \phi_\xi)$ are applied to the leads $\xi = L, R$ with chemical potentials μ_ξ and tunnel rates Γ_ξ .

3. The setup can be employed to generate and control dc-spin currents by tuning the molecular magnetization direction and the relative phases between the ac-voltage and Larmor precession, if ac frequency matches the Larmor frequency.

A part of this chapter is a complement to [219], representing the solution for the Gilbert damping coefficient [110, 175, 179], nonperturbative in the coupling to the molecular magnet in the absence of time-varying voltage. The other corresponding spin-torque coefficients, and an arising nonzero z component of the spin-transfer torque are obtained as well.

The chapter is organized in the following way: We describe the model setup of the system in Sec. 4.2. The theoretical formalism based on the Keldysh nonequilibrium Green's functions technique [45, 46, 220] is introduced in Sec. 4.3. Here we derive expressions for spin and charge currents in linear order with respect to ac harmonic potentials in the leads. In Sec. 4.4 we obtain and analyze the dynamic conductance of the charge current using the current partitioning scheme developed by Wang *et al.* in [260]. This section is followed by Sec. 4.5 in which we analyze spin transport and spin-transfer torque under dc-bias voltage and oscillating bias voltage. We finally conclude in Sec. 4.6.

4.2 Model setup

We consider a junction consisting of a single spin-degenerate molecular orbital of a molecular magnet with a precessing spin in a constant magnetic field along z -axis, $\vec{B} = B\vec{e}_z$, coupled to two normal metallic leads (see Fig. 4.1). We assume the

spin of the molecular magnet is large enough so that we can neglect the quantum fluctuations and treat it as a classical vector \vec{S} , with constant length $S = |\vec{S}|$. The magnetic field does not affect the electric contacts, which are assumed to be noninteracting. An external ac harmonic potential $V_\xi^{\text{ac}}(t) = v_\xi^{\text{ac}} \cos(\Omega t + \phi_\xi)$ is applied to each lead $\xi = L, R$, modulating the single electron energy as $\epsilon_{k\xi}(t) = \epsilon_{k\xi} + eV_\xi^{\text{ac}}(t)$, with $\epsilon_{k\xi}$ being the single-particle energy of an electron with the wave number k , in the absence of the time-varying voltage. Since we want to unravel the quantum effects induced by the tunneling electrons and the ac harmonic potentials in the leads, we consider a well coupled molecular orbital and treat it as noninteracting by disregarding the intra-orbital Coulomb interactions between the electrons.

The junction is described by the Hamiltonian

$$\hat{H}(t) = \sum_{\xi \in \{L, R\}} \hat{H}_\xi(t) + \hat{H}_T + \hat{H}_{\text{MO}}(t) + \hat{H}_S, \quad (4.1)$$

where

$$\hat{H}_\xi(t) = \sum_{k, \sigma} \epsilon_{k\xi}(t) \hat{c}_{k\sigma\xi}^\dagger \hat{c}_{k\sigma\xi} \quad (4.2)$$

is the Hamiltonian of lead $\xi = L, R$. The subscript $\sigma = \uparrow, \downarrow = 1, 2 = \pm 1$ denotes the spin-up or spin-down state of the electrons. The tunneling Hamiltonian

$$\hat{H}_T = \sum_{k, \sigma, \xi} [V_{k\xi} \hat{c}_{k\sigma\xi}^\dagger \hat{d}_\sigma + V_{k\xi}^* \hat{d}_\sigma^\dagger \hat{c}_{k\sigma\xi}] \quad (4.3)$$

introduces the spin-independent tunnel coupling between the molecular orbital and the leads, with matrix element $V_{k\xi}$. The operators $\hat{c}_{k\sigma\xi}^\dagger$ ($\hat{c}_{k\sigma\xi}$) and \hat{d}_σ^\dagger (\hat{d}_σ) represent the creation (annihilation) operators of the electrons in the leads and the molecular orbital. The next term in the Hamiltonian of the system is given by

$$\hat{H}_{\text{MO}}(t) = \sum_{\sigma} \epsilon_0 \hat{d}_\sigma^\dagger \hat{d}_\sigma + g \mu_B \hat{\vec{s}} \vec{B} + J \hat{\vec{s}} \vec{S}(t). \quad (4.4)$$

The first term in Eq. (4.4) describes the noninteracting molecular orbital with energy ϵ_0 . The second term represents the electronic spin in the molecular orbital, $\hat{\vec{s}} = (\hbar/2) \sum_{\sigma\sigma'} (\vec{\sigma})_{\sigma\sigma'} \hat{d}_\sigma^\dagger \hat{d}_{\sigma'}$, in the presence of the external constant magnetic field \vec{B} , and the third term expresses the exchange interaction between the electronic spin and the molecular spin $\vec{S}(t)$. Here, $\hat{\vec{\sigma}} = (\hat{\sigma}_x, \hat{\sigma}_y, \hat{\sigma}_z)^T$ represents the vector of the Pauli matrices. The proportionality factors g and μ_B are the gyromagnetic ratio of the electron and the Bohr magneton, respectively, while J is the exchange coupling constant between the molecular and electronic spins.

Presuming for simplicity that the molecular spin g-factor equals that of a free electron, the last term in the Hamiltonian of the junction

$$\hat{H}_S = g\mu_B \vec{S} \vec{B} \quad (4.5)$$

represents the molecular spin \vec{S} in the magnetic field \vec{B} . Accordingly, the field \vec{B} exerts a torque on the spin \vec{S} , leading to its precession around the field axis with Larmor frequency $\omega_L = g\mu_B B$. To compensate for the dissipation of the magnetic energy due to the interaction with the conduction electrons, we assume that the molecular spin is kept precessing by external means (e.g., rf fields) [218]. Hence, we keep the tilt angle θ between \vec{B} and \vec{S} fixed and determined by the initial conditions. The dynamics of the molecular spin is then given by $\vec{S}(t) = S_\perp \cos(\omega_L t) \vec{e}_x + S_\perp \sin(\omega_L t) \vec{e}_y + S_z \vec{e}_z$, where S_\perp is the magnitude of the instantaneous projection of $\vec{S}(t)$ onto the xy plane, given by $S_\perp = S \sin(\theta)$, while the projection of the molecular spin on the z -axis equals $S_z = S \cos(\theta)$. The precessing spin $\vec{S}(t)$ pumps spin-currents into the system, but the effects of spin-currents onto the molecular spin dynamics are compensated by the above mentioned external sources.

4.3 Theoretical formalism

The ensemble and quantum average charge and spin currents from the lead ξ to the molecular orbital are given by

$$I_{\xi\nu}(t) = q_\nu \left\langle \frac{d}{dt} \hat{N}_{\xi\nu} \right\rangle = q_\nu \frac{i}{\hbar} \langle [\hat{H}, \hat{N}_{\xi\nu}] \rangle, \quad (4.6)$$

with $\hat{N}_{\xi\nu} = \sum_{k,\sigma,\sigma'} \hat{c}_{k\sigma\xi}^\dagger (\sigma_\nu)_{\sigma\sigma'} \hat{c}_{k\sigma'\xi}$ representing the charge and spin occupation number operator of the contact ξ . The index ν takes values $\nu = 0$ for the charge and $\nu = 1, 2, 3$ for the components x, y, z of the spin-polarized current. The prefactors q_ν correspond to the electronic charge $q_0 = -e$ and spin $q_{\nu \neq 0} = \hbar/2$. Employing the Keldysh nonequilibrium Green's functions technique, the currents can be calculated in units in which $\hbar = e = 1$ as [45, 46]

$$I_{\xi\nu}(t) = -2q_\nu \text{Re} \int dt' \text{Tr} \{ \hat{\sigma}_\nu [\hat{G}^r(t, t') \hat{\Sigma}_\xi^<(t', t) + \hat{G}^<(t, t') \hat{\Sigma}_\xi^a(t', t)] \}, \quad (4.7)$$

where $\hat{\sigma}_0 = \hat{1}$ is the identity matrix, while $\hat{\sigma}_{\nu \neq 0}$ are the Pauli matrices. In Eq. (4.7), $\hat{\Sigma}_\xi^{r,a,<}(t, t')$ are the retarded, advanced, and lesser self-energies from the tunnel

coupling between the molecular orbital and the lead ξ , while $\hat{G}^{r,a,<}(t, t')$ are the corresponding Green's functions of the electrons in the molecular orbital. The matrices of the self-energies are diagonal in the electronic spin space with respect to the basis of eigenstates of \hat{s}_z , and their nonzero entries are given by $\Sigma_\xi^{r,a,<}(t, t') = \sum_k V_{k\xi} g_{k\xi}^{r,a,<}(t, t') V_{k\xi}^*$, where $g_{k\xi}^{r,a,<}(t, t')$ are the retarded, advanced and lesser Green's functions of the electrons in contact ξ . The matrix elements of the retarded, advanced and lesser Green's functions $\hat{G}^{r,a,<}(t, t')$ are given by $G_{\sigma\sigma'}^{r,a}(t, t') = \mp i\theta(\pm t \mp t') \langle \{ \hat{d}_\sigma(t), \hat{d}_{\sigma'}^\dagger(t') \} \rangle$ and $G_{\sigma\sigma'}^{<}(t, t') = i \langle \hat{d}_{\sigma'}^\dagger(t') \hat{d}_\sigma(t) \rangle$, where $\{ \cdot, \cdot \}$ denotes the anticommutator. The self-energies of lead ξ can be expressed as [45, 46, 220]

$$\Sigma_\xi^{<}(t, t') = i \int \frac{d\epsilon}{2\pi} e^{-i\epsilon(t-t') + i\varphi_\xi(t, t')} f_\xi(\epsilon) \Gamma_\xi(\epsilon), \quad (4.8)$$

$$\Sigma_\xi^r(t, t') = -i\theta(t - t') \int \frac{d\epsilon}{2\pi} e^{-i\epsilon(t-t') + i\varphi_\xi(t, t')} \Gamma_\xi(\epsilon). \quad (4.9)$$

Here we introduced the Faraday phases $\varphi_\xi(t, t') = e \int_t^{t'} dt'' V_\xi^{\text{ac}}(t'')$. From its definition it follows that $\Sigma_\xi^a(t, t') = [\Sigma_\xi^r(t', t)]^*$. Furthermore, $f_\xi(\epsilon) = [e^{(\epsilon - \mu_\xi)/k_B T} + 1]^{-1}$ is the Fermi-Dirac distribution of the electrons in the lead ξ , with k_B the Boltzmann constant, T the temperature, while $\Gamma_\xi(\epsilon) = 2\pi \sum_k |V_{k\xi}|^2 \delta(\epsilon - \epsilon_{k\xi})$ is the tunnel coupling to the lead ξ . Using the self-energies defined above and applying the double Fourier transformations in Eq. (4.7), in the wide-band limit in which Γ_ξ is energy independent one obtains

$$\begin{aligned} I_{\xi\nu}(t) &= 2q_\nu \Gamma_\xi \text{Im} \int \frac{d\epsilon}{2\pi} \int \frac{d\epsilon'}{2\pi} e^{-i(\epsilon - \epsilon')t} \\ &\times \sum_{m,n} J_m \left(\frac{v_\xi^{\text{ac}}}{\Omega} \right) J_n \left(\frac{v_\xi^{\text{ac}}}{\Omega} \right) e^{i(m-n)\phi_\xi} \\ &\times \text{Tr} \left\{ \hat{\sigma}_\nu [f_\xi(\epsilon'_m) \hat{G}^r(\epsilon, \epsilon'_{mn}) + \frac{1}{2} \hat{G}^{<}(\epsilon, \epsilon'_{mn})] \right\}, \end{aligned} \quad (4.10)$$

where we used the abbreviations $\epsilon_m = \epsilon - m\Omega$ and $\epsilon_{mn} = \epsilon - (m - n)\Omega$. The generating function $\exp[ia \sin(\Omega t + \phi)] = \sum_m J_m(a) \exp[im(\Omega t + \phi)]$ was used in Eq. (4.10), where J_m is the Bessel function of the first kind of order m .

The matrix components of the retarded Green's function of the electrons in the molecular orbital, in the absence of the ac harmonic potentials in the leads, can be obtained exactly by applying Dyson's expansion and analytic continuation rules [46]. Their double Fourier transforms are written as [221]

$$\mathcal{G}_{\sigma\sigma}^r(\epsilon, \epsilon') = \frac{2\pi\delta(\epsilon - \epsilon') G_{\sigma\sigma}^{0r}(\epsilon)}{1 - \gamma^2 G_{\sigma\sigma}^{0r}(\epsilon) G_{-\sigma-\sigma}^{0r}(\epsilon_\sigma)}, \quad (4.11)$$

$$\mathcal{G}_{\sigma-\sigma}^r(\epsilon, \epsilon') = \frac{2\pi\gamma\delta(\epsilon_\sigma - \epsilon') G_{\sigma\sigma}^{0r}(\epsilon) G_{-\sigma-\sigma}^{0r}(\epsilon_\sigma)}{1 - \gamma^2 G_{\sigma\sigma}^{0r}(\epsilon) G_{-\sigma-\sigma}^{0r}(\epsilon_\sigma)}, \quad (4.12)$$

with $\gamma = JS \sin(\theta)/2$ and $\epsilon_\sigma = \epsilon - \sigma\omega_L$. The matrix elements of the corresponding lesser Green's function are obtained using the Fourier-transformed Keldysh equation $\hat{\mathcal{G}}^<(\epsilon, \epsilon') = \int d\epsilon'' \hat{\mathcal{G}}^r(\epsilon, \epsilon'') \hat{\Sigma}_0^<(\epsilon'') \hat{\mathcal{G}}^a(\epsilon'', \epsilon')/2\pi$ [46]. Here $\hat{\mathcal{G}}^a(\epsilon, \epsilon') = [\hat{\mathcal{G}}^r(\epsilon', \epsilon)]^\dagger$, and $\Sigma_0^<(\epsilon) = i \sum_\xi \Gamma_\xi f_\xi(\epsilon)$ is the lesser self-energy originating from the orbital-lead coupling in the absence of harmonic potentials in the leads. The retarded Green's functions \hat{G}^{0r} of the electrons in the molecular orbital, in the presence of the static component of the molecular spin and the constant magnetic field \vec{B} , are found using the equation of motion technique [118], and Fourier transformed read $\hat{G}^{0r}(\epsilon) = [\epsilon - \epsilon_0 - \Sigma_0^r(\epsilon) - \hat{\sigma}_z(g\mu_B B + JS_z)/2]^{-1}$ [189, 221], where $\Sigma_0^r(\epsilon) = -i\Gamma/2$ and $\Gamma = \sum_\xi \Gamma_\xi$.

For a weak ac field $v_\xi^{\text{ac}} \ll \Omega$, the retarded and lesser Green's functions of the electrons in the molecular orbital can be obtained by applying Dyson's expansion, analytic continuation rules and the Keldysh equation [46]. Keeping only terms linear in v_ξ^{ac}/Ω they read

$$\hat{G}^r(\epsilon, \epsilon') \approx \hat{\mathcal{G}}^r(\epsilon, \epsilon'), \quad (4.13)$$

$$\begin{aligned} \hat{G}^<(\epsilon, \epsilon') \approx & \hat{\mathcal{G}}^<(\epsilon, \epsilon') + i \sum_{\xi, n=\pm 1} n \Gamma_\xi \frac{v_\xi^{\text{ac}}}{\Omega} e^{in\phi_\xi} \\ & \times \int \frac{d\epsilon''}{4\pi} [f_\xi(\epsilon''_n) - f_\xi(\epsilon'')] \hat{\mathcal{G}}^r(\epsilon, \epsilon''_n) \hat{\mathcal{G}}^a(\epsilon'', \epsilon'). \end{aligned} \quad (4.14)$$

In the rest of the chapter we will stay in this limit.

The particle current contains the following contributions

$$I_{\xi\nu}(t) = I_{\xi\nu}^{\omega_L}(t) + I_{\xi\nu}^\Omega(t). \quad (4.15)$$

The first component represents the transport in the absence of ac-voltages in the leads. It has a static and a time-dependent contribution, which are both created by the precession of the molecular spin. This precession-induced current reads

$$\begin{aligned} I_{\xi\nu}^{\omega_L}(t) = & 2q_\nu \Gamma_\xi \text{Im} \left\{ \int \frac{d\epsilon}{2\pi} \int \frac{d\epsilon'}{2\pi} e^{-i(\epsilon-\epsilon')t} \right. \\ & \left. \times \text{Tr} \left\{ \hat{\sigma}_\nu \left[\frac{1}{2} \hat{\mathcal{G}}^<(\epsilon, \epsilon') + f_\xi(\epsilon') \hat{\mathcal{G}}^r(\epsilon, \epsilon') \right] \right\} \right\}. \end{aligned} \quad (4.16)$$

In the limit $\gamma^2 \rightarrow 0$, Eq. (4.16) reduces to the result obtained in the previous chapter [219]. The second term of Eq. (4.15) is induced when an ac voltage is applied to lead ξ and can be expressed in linear order with respect to v_ξ^{ac}/Ω using

Eqs. (4.10), (4.13) and (4.14) as

$$\begin{aligned}
I_{\xi\nu}^{\Omega}(t) &= q_{\nu} \sum_{\zeta, n=\pm 1} n \Gamma_{\xi} \Gamma_{\zeta} \frac{v_{\zeta}^{\text{ac}}}{\Omega} \text{Re} \int \frac{d\epsilon}{2\pi} \int \frac{d\epsilon'}{2\pi} e^{-i(\epsilon-\epsilon')t + in\phi_{\zeta}} \\
&\times \left\{ \int \frac{d\epsilon''}{4\pi} \{ [f_{\zeta}(\epsilon''_n) - f_{\zeta}(\epsilon'')] \text{Tr}[\hat{\sigma}_{\nu} \hat{\mathcal{G}}^r(\epsilon, \epsilon''_n) \hat{\mathcal{G}}^a(\epsilon'', \epsilon')] \} \right. \\
&\left. - \frac{i}{\Gamma_{\zeta}} \delta_{\xi\zeta} [f_{\zeta}(\epsilon'_n) - f_{\zeta}(\epsilon')] \text{Tr}[\hat{\sigma}_{\nu} \hat{\mathcal{G}}^r(\epsilon, \epsilon'_n)] \right\}. \quad (4.17)
\end{aligned}$$

These expressions for the currents constitute the main results of the chapter. They allow us to calculate the dynamic charge and spin conductance properties of our molecular contact. Note that spin currents are more conveniently discussed in terms of the spin-transfer torque exerted by the inelastic spin-currents onto the spin of the molecule [108–111], given by

$$\vec{T}(t) = \vec{T}^{\omega_L}(t) + \vec{T}^{\Omega}(t) = -[\vec{I}_L(t) + \vec{I}_R(t)]. \quad (4.18)$$

Hence, in the remainder of the chapter we will concentrate on the ac-charge conductance and the dc spin-transfer torque.

4.4 Charge transport

4.4.1 Dynamic charge conductance

The time-dependent particle charge current from the lead ξ to the molecular orbital is induced by the ac harmonic potentials in the leads and can be written as

$$I_{\xi 0}^{\Omega}(t) = \text{Re} \left\{ \sum_{\zeta} G_{\xi\zeta}^c(\Omega) v_{\zeta}^{\text{ac}} e^{-i(\Omega t + \phi_{\zeta})} \right\}. \quad (4.19)$$

This expression defines the conductance $G_{\xi\zeta}^c(\Omega)$ between leads ξ and ζ . Combining equations (4.17) and (4.19), and taking into account that

$$G_{\sigma\sigma}^{0r}(\epsilon) - G_{\sigma\sigma}^{0a}(\epsilon - \Omega) = -(\Omega + i\Gamma) G_{\sigma\sigma}^{0r}(\epsilon) G_{\sigma\sigma}^{0a}(\epsilon - \Omega), \quad (4.20)$$

the complex components $G_{\xi\zeta}^c(\Omega)$ can be obtained as

$$G_{\xi\zeta}^c(\Omega) = -\frac{e^2}{h} [\Gamma_{\xi} \Gamma_{\zeta} - \Gamma_{\xi} \delta_{\xi\zeta} (\Gamma - i\Omega)] \int d\epsilon \frac{[f_{\zeta}(\epsilon - \Omega) - f_{\zeta}(\epsilon)]}{\Omega} T^c(\epsilon, \Omega), \quad (4.21)$$

with the energy-dependent complex function $T^c(\epsilon, \Omega)$, which can be written as

$$T^c(\epsilon, \Omega) = \sum_{\sigma=\pm 1} \frac{G_{\sigma\sigma}^{0r}(\epsilon)G_{\sigma\sigma}^{0a}(\epsilon - \Omega)[1 + \gamma^2 G_{-\sigma-\sigma}^{0r}(\epsilon_\sigma)G_{-\sigma-\sigma}^{0a}(\epsilon_\sigma - \Omega)]}{[1 - \gamma^2 G_{\sigma\sigma}^{0a}(\epsilon - \Omega)G_{-\sigma-\sigma}^{0a}(\epsilon_\sigma - \Omega)][1 - \gamma^2 G_{\sigma\sigma}^{0r}(\epsilon)G_{-\sigma-\sigma}^{0r}(\epsilon_\sigma)]}. \quad (4.22)$$

In order to determine the dynamic conductance under ac bias-voltage conditions, besides the particle current one needs to take into account the contribution from the displacement current. Coulomb interaction leads to screening of the charge accumulation in the quantum dot given by

$$\begin{aligned} I^d(t) &= \frac{dQ(t)}{dt} \\ &= -e \text{Im} \left\{ \frac{d}{dt} [\text{Tr} \hat{G}^<(t, t)] \right\}. \end{aligned} \quad (4.23)$$

According to the Kirchoff's current law,

$$I^d(t) + \sum_{\xi} I_{\xi 0}^{\Omega}(t) = 0. \quad (4.24)$$

The following expression defines the total conductance of charge current, $G_{\xi\zeta}$,

$$I_{\xi 0}^{\Omega, tot}(t) = \text{Re} \left\{ \sum_{\zeta} G_{\xi\zeta}(\Omega) v_{\zeta}^{\text{ac}} e^{-i(\Omega t + \phi_{\zeta})} \right\}, \quad (4.25)$$

while the displacement conductance G_{ζ}^d is given by

$$I^d(t) = \text{Re} \left\{ \sum_{\zeta} G_{\zeta}^d(\Omega) v_{\zeta}^{\text{ac}} e^{-i(\Omega t + \phi_{\zeta})} \right\}. \quad (4.26)$$

The conservation of the total charge current and gauge invariance with respect to the shift of the chemical potentials lead to $\sum_{\xi} G_{\xi\xi} = 0$ and $\sum_{\zeta} G_{\xi\zeta} = 0$ [257]. These conditions are satisfied by partitioning the displacement current into each lead [260]

$$I_{\xi 0}^{\Omega, tot} = I_{\xi 0}^{\Omega} + A_{\xi} I^d, \quad (4.27)$$

or equivalently

$$G_{\xi\zeta} = G_{\xi\zeta}^c + A_{\xi} G_{\zeta}^d, \quad (4.28)$$

in such a way that the sum of the partitioning factors A_{ξ} obeys $\sum_{\xi} A_{\xi} = 1$. Using the sum rules given above one obtains the expression for the dynamic conductance [257, 260]

$$G_{\xi\zeta} = G_{\xi\zeta}^c - G_{\zeta}^d \frac{\sum_{\lambda} G_{\xi\lambda}^c}{\sum_{\lambda} G_{\lambda}^d}, \quad (4.29)$$

with $\lambda = L, R$, where $A_\xi = -(\sum_\lambda G_{\xi\lambda}^c)/(\sum_\lambda G_\lambda^d)$, $G_\zeta^d = -\sum_\xi G_{\xi\zeta}^c$, and

$$G(\Omega) = G_{LL}(\Omega) = G_{RR}(\Omega) = -G_{LR}(\Omega) = -G_{RL}(\Omega). \quad (4.30)$$

The first term of Eq. (4.29) represents the dynamic response of the charge current, while the second term is the internal response to the applied external ac perturbation due to screening by the Coulomb interaction. Note that the dynamic conductance consists of a real dissipative component G_R , and an imaginary nondissipative component G_I indicating the difference in phase between the current and the voltage. Due to the total current conservation, the two terms in Eq. (4.29) should behave in a way that a minimum (maximum) of $G_{\xi\zeta}^c(\Omega)$ corresponds to a maximum (minimum) of $G_\zeta^d(\Omega)$, for both real and imaginary parts.

4.4.2 Density of states in the quantum dot

Since the dynamic conductance is an experimentally directly accessible quantity, we hope that a measurement can help to reveal the internal time scales of the coupling between the molecular and electronic spins in the transport. We begin by analyzing the density of states available for electron transport in the quantum dot

$$\rho(\epsilon) = -\frac{1}{\pi} \sum_{\sigma=\pm 1} \text{Im} \left\{ \frac{G_{\sigma\sigma}^{0r}(\epsilon)}{1 - \gamma^2 G_{\sigma\sigma}^{0r}(\epsilon) G_{-\sigma-\sigma}^{0r}(\epsilon_\sigma)} \right\}. \quad (4.31)$$

The dc-bias transmission coefficient $T_{dc}(\epsilon) = 2\pi\Gamma_L\Gamma_R\rho(\epsilon)/\Gamma$ is plotted in Fig. 4.2(a) (black line). There are four resonant transmission channels. They manifest themselves as peaks positioned at Floquet quasienergies $\epsilon_1 = \epsilon_\downarrow = \epsilon_0 - (\omega_L + JS)/2$ (spin down), $\epsilon_2 = \epsilon_\uparrow + \omega_L = \epsilon_0 + (\omega_L - JS)/2$ (spin up), $\epsilon_3 = \epsilon_\downarrow - \omega_L = \epsilon_0 - (\omega_L - JS)/2$ (spin down) and $\epsilon_4 = \epsilon_\uparrow = \epsilon_0 + (\omega_L + JS)/2$ (spin up). According to the expression for $\rho(\epsilon)$ these resonances are given by the real part of the poles of $[1 - \gamma^2 G_{\sigma\sigma}^{0r}(\epsilon) G_{-\sigma-\sigma}^{0r}(\epsilon_\sigma)]^{-1}$.

The Hamiltonian of the molecular orbital is a periodic function of time, with the period $\mathcal{T} = 2\pi/\omega_L$, $\hat{H}_{\text{MO}}(t) = \hat{H}_{\text{MO}}(t + \mathcal{T})$. Accordingly, the quasienergies ϵ_i , $i = 1, 2, 3, 4$, can be obtained using the Floquet theorem [224–228] (see Appendix A). The precessing component of the molecular spin couples state with quasienergy ϵ_1 (or ϵ_3) to the state with quasienergy ϵ_2 (or ϵ_4) which differ in energy by an energy quantum ω_L . Namely, due to the periodic motion of the molecular spin an electron can absorb or emit an energy ω_L accompanied with a spin-flip. Spin-flip processes due to rotating magnetic field were analyzed in some works [219, 221]. A similar mechanism was discussed in a recent work for a nanomechanical spin-valve in which inelastic spin-flip processes are assisted by molecular vibrations [261].

4.4.3 Analysis of the dynamic conductance

Now we analyze the charge conductance in response to the ac-voltages. The conductance of charge current under dc bias in the presence of a rotating field, or in the presence of an ac gate voltage where photon-assisted tunneling was observed was discussed in [227]. Here we consider ac conductance in a double-driving experiment, where we first induce molecular spin precession at Larmor frequency ω_L , and then turn on the oscillating fields with frequency Ω in the leads. Assuming equal chemical potentials of the leads $\mu_L = \mu_R = \mu$, we analyze the dynamic conductance $G(\Omega)$ at zero temperature. Since we work in the wide band limit, this symmetry simplifies the partitioning factors to $A_\xi = \Gamma_\xi/\Gamma$. Hence, Eq. (4.29) can be transformed into

$$G_{\xi\zeta}(\Omega) = \frac{e^2}{h} \int d\epsilon T_{\xi\zeta}(\epsilon, \Omega) \frac{f_\zeta(\epsilon - \Omega) - f_\zeta(\epsilon)}{\Omega}. \quad (4.32)$$

Here $T_{\xi\zeta}(\epsilon, \Omega)$ is the effective transmission function that can be expressed as $T(\epsilon, \Omega) = T_{LL}(\epsilon, \Omega) = T_{RR}(\epsilon, \Omega) = -T_{LR}(\epsilon, \Omega) = -T_{RL}(\epsilon, \Omega)$, which reads

$$T(\epsilon, \Omega) = \frac{\Gamma_L \Gamma_R}{\Gamma} (\Gamma - i\Omega) T^c(\epsilon, \Omega). \quad (4.33)$$

In Figs. 4.2(a) and 4.2(b) we plotted the energy dependence of the real part $T_R(\epsilon, \Omega)$ and the imaginary part $T_I(\epsilon, \Omega)$ of the effective transmission function $T(\epsilon, \Omega)$, for several ac frequencies Ω , at zero temperature. In the limit $\Omega \rightarrow 0$ (black lines in Fig. 4.2), $T_R(\epsilon, \Omega \rightarrow 0)$ coincides with the dc transmission function $T_{dc}(\epsilon)$, while $T_I(\epsilon, \Omega) \rightarrow 0$. Upon turning on the ac-bias voltage, due to the inelastic transport channels T_R decreases near each of the four resonances with increasing Ω , and splits into two different peaks distanced by Ω . Namely, the peaks positioned at ϵ_i and $\epsilon_i + \Omega$ appear as a signature of photon-assisted tunneling. They represent bands in the leads through which an electron can tunnel after it absorbs an energy Ω from the ac field. The photon-assisted bands through which the transport occurs are represented by the peaks on green (small Γ) and blue dot-dashed (larger Γ) lines in Fig. 4.2(a). Compared to Fig. 4.2(a), in Fig. 4.2(b) the peaks of T_I increase with increasing Ω .

The corresponding real part G_R and imaginary part G_I of the dynamic conductance versus chemical potential μ are plotted in Figs. 4.3(a) and 4.3(b). Both G_R and G_I achieve their maximum at $\mu_\xi = \epsilon_i$, where the resonance peaks are positioned. In accordance with Eq. (4.32) the electrons with energies $\mu_\zeta - \Omega \leq \epsilon \leq \mu_\zeta$ can participate in the transport processes by absorbing a photon of energy Ω . For ac frequency $\Omega \rightarrow 0$ the dynamic conductance reduces to dc conductance

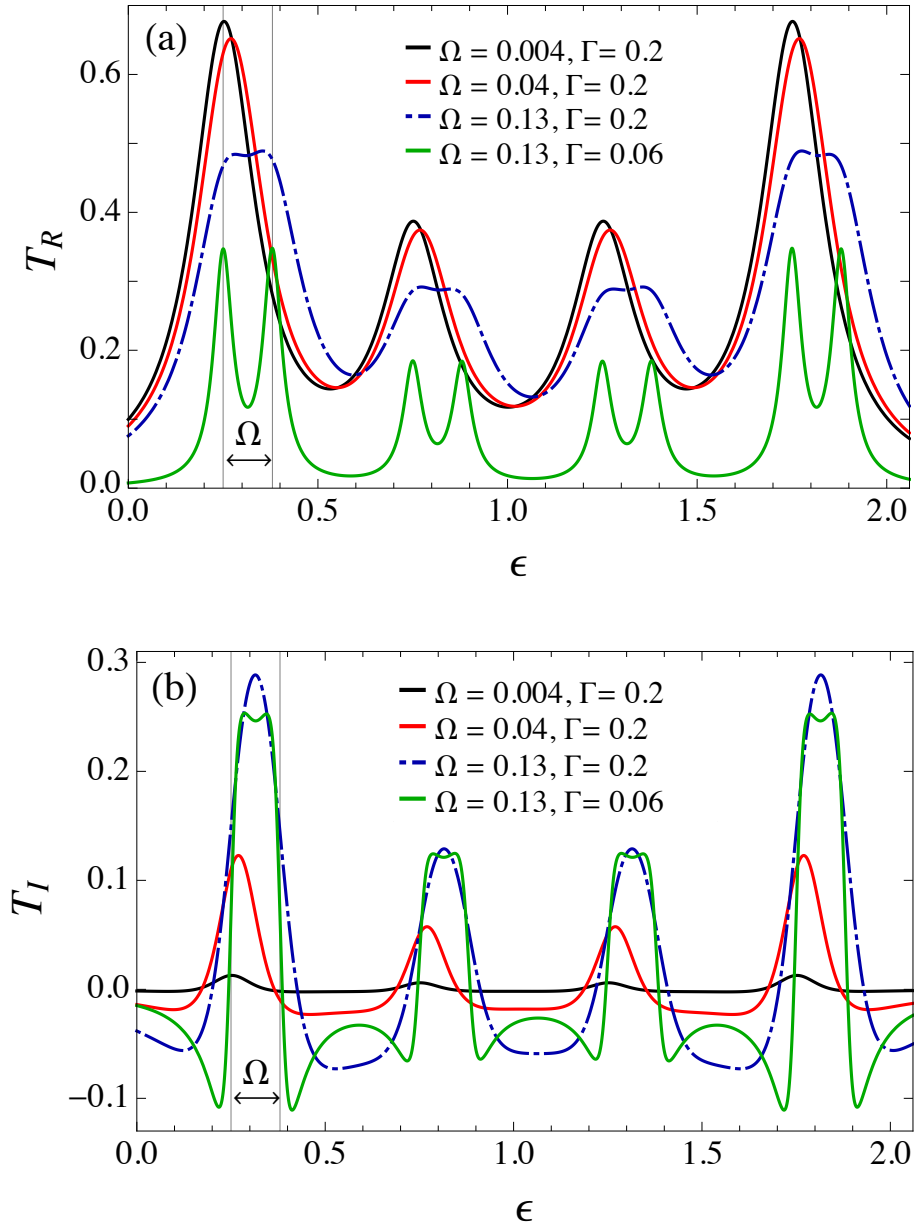


FIGURE 4.2: Energy dependence of (a) the real part T_R and (b) the imaginary part T_I of the effective transmission function. The plots are obtained for different ac frequencies Ω and tunneling rates Γ at zero temperature, with $\vec{B} = B\vec{e}_z$, and $\Gamma_L = \Gamma_R = \Gamma/2$. All energies are given in the units of ϵ_0 . The other parameters are set to: $\omega_L = 0.5$, $J = 0.01$, $S = 100$, $\theta = 1.25$, $\gamma \approx 0.474$. The positions of the molecular quasienergy levels are: $\epsilon_1 = 0.25$, $\epsilon_2 = 0.75$, $\epsilon_3 = 1.25$, and $\epsilon_4 = 1.75$.

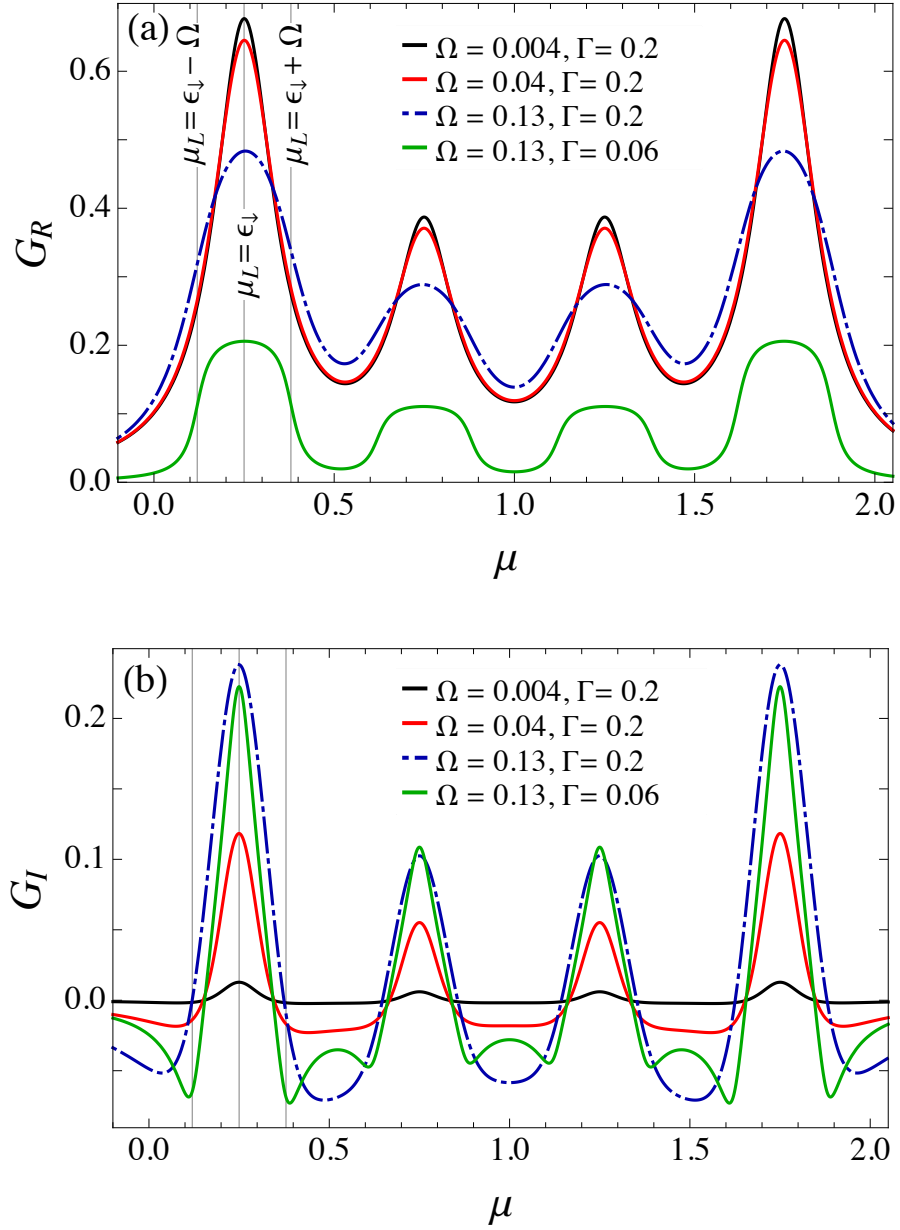


FIGURE 4.3: (a) Real part G_R and (b) imaginary part G_I of the dynamic conductance as functions of the chemical potential μ , with $\mu = \mu_L = \mu_R$. The plots are obtained for different ac frequencies Ω and tunneling rates Γ at zero temperature, with $\Gamma_L = \Gamma_R = \Gamma/2$, and $\vec{B} = B\vec{e}_z$. All energies are given in the units of ϵ_0 . The other parameters are set to: $\omega_L = 0.5$, $J = 0.01$, $S = 100$, $\theta = 1.25$, and $\gamma \approx 0.474$. The molecular quasienergy levels are positioned at: $\epsilon_1 = 0.25$, $\epsilon_2 = 0.75$, $\epsilon_3 = 1.25$, and $\epsilon_4 = 1.75$. The conductance components G_R and G_I are given in the units of conductance quantum e^2/h .

$G_{\xi\zeta}(\Omega \rightarrow 0) = e^2 T_{\xi\zeta}(\mu_\zeta, \Omega \rightarrow 0)/h$, and reaches its maximum near the resonances given by the Floquet quasienergies [227]. The dc conductance has four peaks emerging from the peaks in the resonant tunneling transmission function $T_{dc}(\epsilon)$ [black lines in Figs. 4.2(a) and 4.3(a)]. Following the behavior of T_I , the imaginary part of the dynamic conductance G_I approaches zero for $\Omega \rightarrow 0$ [black lines in Figs. 4.2(b) and 4.3(b)]. The considerable contribution of the displacement current to the total current is reflected in the decrease of G_R , and the increase of G_I near resonances with increasing Ω , as the displacement current opposes the change of the particle charge current under ac bias [red and blue dot-dashed lines in Figs. 4.3(a) and 4.3(b)]. For a small value of both Γ and Ω , complex components T_R and G_R show sharp peaks. However, with the increase of Ω , each of the peaks in G_R broadens [green line in Fig. 4.3(a)]. It approaches a constant value around the corresponding resonant level, with the width equal to 2Ω , since the inequality

$$|\epsilon_i - \mu_\xi| \leq \Omega \quad (4.34)$$

is the condition for the inelastic photon-assisted tunneling to occur.

4.4.4 Frequency dependence of the ac conductance and equivalent circuit

In this subsection we analyze the behavior of the dynamic conductance components G_R and G_I as functions of the ac frequency Ω for $\mu = \epsilon_\uparrow - \omega_L = \epsilon_3$ [Fig. 4.4, green and blue lines] and $\mu = 0.1 \epsilon_0$ [Fig. 4.4, red and purple-dotted lines], for two values of Γ at zero temperature.

The behavior of the ac-conductance components in the low ac-frequency regime can be understood using an effective circuit theory [262]. Namely, at small ac frequencies $\Omega \ll \Gamma$, the molecular magnet junction behaves as a parallel combination of two serial connections: one of a resistor and an inductor and the other of a resistor and a capacitor, i.e., as a classical electric circuit [see Fig. 4.5]. Depending on the phase difference between the voltage and the current, the circuit shows inductive-like (positive phase difference) or capacitive-like (negative phase difference) responses to the applied ac voltage. Therefore, the dynamic conductance can be expanded up to the second order in Ω in the small ac-frequency limit in

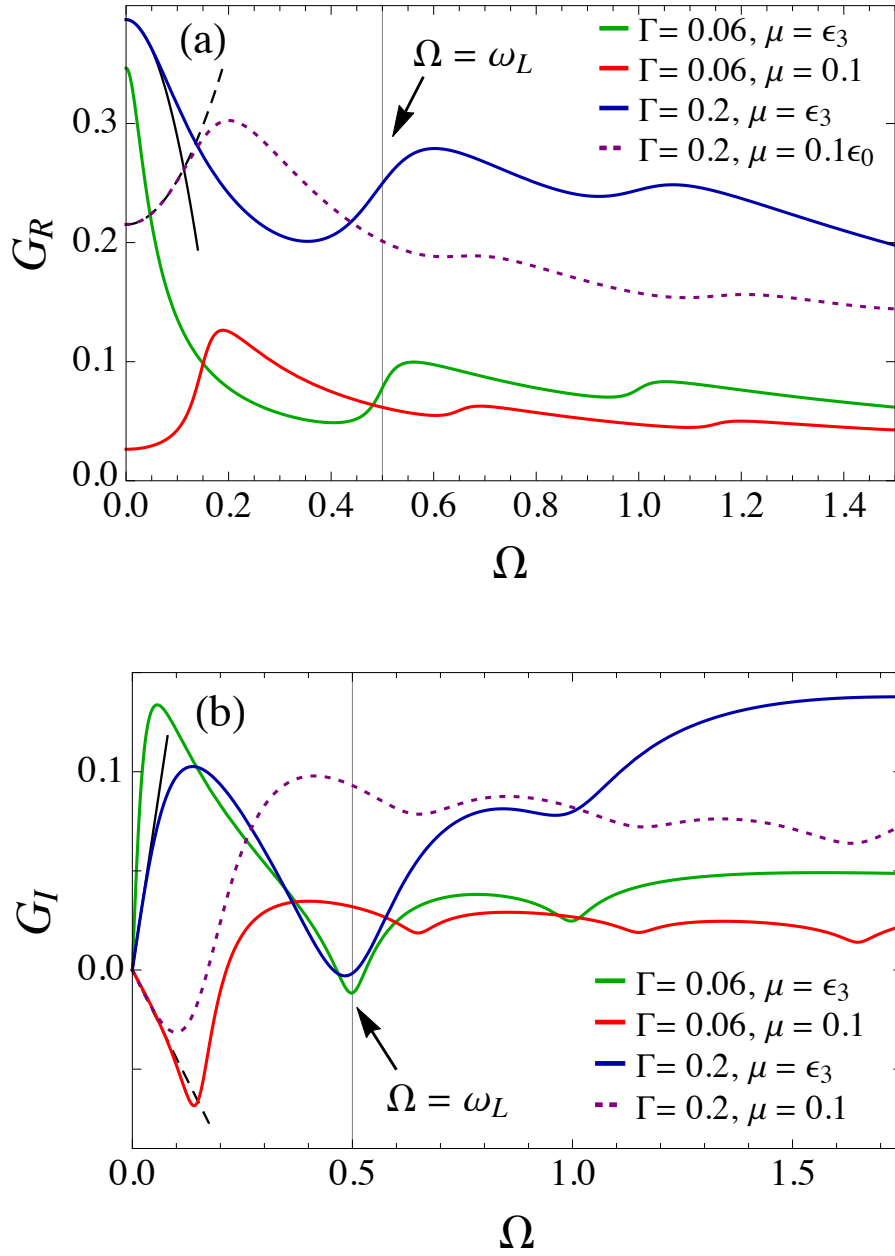


FIGURE 4.4: (a) Real part G_R and (b) imaginary part G_I of the dynamic conductance as functions of the ac frequency Ω . The plots are obtained for two different tunneling rates Γ and chemical potentials μ , with $\mu = \mu_L = \mu_R$ and $\vec{B} = B\vec{e}_z$, at zero temperature. All energies are given in the units of ϵ_0 . The other parameters are set to: $\Gamma_L = \Gamma_R = \Gamma/2$, $S = 100$, $J = 0.01$, $\omega_L = 0.5$, $\theta = 1.25$, $\gamma \approx 0.474$. The molecular quasienergy levels lie at: $\epsilon_1 = 0.25$, $\epsilon_2 = 0.75$, $\epsilon_3 = 1.25$, and $\epsilon_4 = 1.75$. In the resonant case $\mu = \epsilon_3$, the response of the system is inductive-like in the low ac frequency limit ($G_I > 0$), and G_R and G_I are both enhanced around $\Omega = \omega_L$, after going to a local minimum, as the channel with energy ϵ_4 becomes available for photon-assisted tunneling, i.e., $\mu + \Omega = \epsilon_4$. The conductance components G_R and G_I are given in the units of conductance quantum e^2/h .

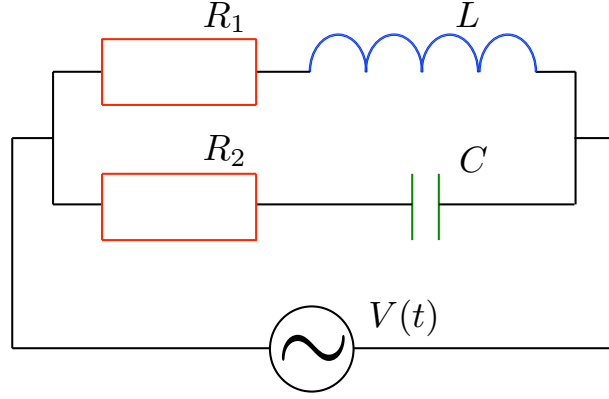


FIGURE 4.5: The equivalent classical circuit of the molecular magnet junction in the low ac frequency regime. It is composed of two serial combinations: one of a resistor and an inductor, and the other of a resistor and a capacitor, connected in parallel, and driven by a source of ac-voltage $V(t)$. The resistances are denoted by R_1 and R_2 ; L is the inductance, and C is the capacitance of the circuit elements.

the following way:

$$G(\Omega) = G(0) + G'(0)\Omega + \frac{1}{2}G''(0)\Omega^2 + O(\Omega^3) \quad (4.35)$$

$$\approx \frac{1}{R_1} + i \left(\frac{L}{R_1^2} - C \right) \Omega + \left(R_2 C^2 - \frac{L^2}{R_1^3} \right) \Omega^2, \quad (4.36)$$

where R_1 , R_2 , L and C denote the resistances, inductance and capacitance of the circuit. In our further analysis we will assume that $R_1 = R_2 = R$. The first term of Eq. (4.36) represents therefore the dc conductance $G(0) = 1/R$. The second, imaginary term, linear in Ω is iG_I in the low ac-frequency regime.

Depending on the sign of the expression $L/R^2 - C$, the linear response is inductive-like ($G_I > 0$) while G_R decreases, or capacitive-like ($G_I < 0$) while G_R increases, with the increase of Ω . For $C = L/R^2$ the system behaves like a resistor with $G = G(0)$. The nondissipative component G_I shows inductive-like behavior for

$$|\epsilon_i - \mu_\xi| < \frac{\Gamma}{2}, \quad (4.37)$$

as we have observed in Fig. 4.3(b) (red line), and capacitive-like otherwise. The equality sign corresponds to resistive behavior.

The real part G_R is an even, while the imaginary part G_I is an odd function of Ω . In the low ac-frequency regime $\Omega \ll \Gamma$, G_R is a quadratic function [black, solid and dashed lines in Fig. 4.4 (a)], while G_I is a linear function of frequency [black, solid and dashed lines in Fig. 4.4(b)]. By fitting parameters of these functions and using Eq. (4.36), one obtains R , L , and C components, confirming that in this limit the ac conductance of the system resembles the previously described

classical circuit model. The circuit parameters can be calculated in terms of the dynamic conductance according to Eqs. (4.35) and (4.36). Note that they depend on the relative position of the Fermi energy of the leads with respect to the molecular quasienergy levels.

Near the four resonances we expect the system to be highly transmissive and therefore to conduct well. This is confirmed by Figs. 4.3 and 4.4. Namely, the imaginary conductance component $G_I > 0$ around resonances and is a positive linear function of Ω in the low ac-frequency limit [see Fig. 4.4(b), black solid line]. This implies that the behavior of the system is inductive-like since the displacement current tends to reduce the charge current, as electrons reside awhile in the quantum dot, causing the delay in phase between the voltage and the current. Accordingly, the real component G_R decreases quadratically from initial value $G(0)$ upon switching on the ac frequency Ω [black solid line in Fig. 4.4(a)]. However, the off-resonance behavior is capacitive-like resulting from intra-orbital Coulomb interactions included via displacement current [260]. Hence, in the low ac-frequency limit $G_I(\Omega)$ is negative, and decreases linearly with the increase of Ω for Fermi energies of the leads which are far from the resonant energies ϵ_i [black dashed line in Fig. 4.4(b)]. In this case $G_R(\Omega)$ increases quadratically with Ω [black dashed line in Fig. 4.4(a)]. Obviously the molecular magnet junction behaves as a classical circuit only in the low ac-frequency regime.

For higher ac-frequencies Ω we use Eq. (4.32) to analyze the behavior of G_R and G_I [see Fig. 4.4], where the dynamic response of the system remains predominantly inductive-like for $\mu = \epsilon_{\uparrow} - \omega_L = \epsilon_3$. With further increase of Ω , the ac conductance $G(\Omega)$ vanishes asymptotically. Upon turning on the ac frequency while the system is on resonance $\mu = \epsilon_{\uparrow} - \omega_L = \epsilon_3$, the imaginary component G_I increases quickly from 0 to a local maximum and then decreases to its minimum value around $\Omega = \omega_L$ [green and blue lines in Fig. 4.4(b)]. The real part G_R decreases to a local minimum and then has a step-like increase towards a local maximum around $\Omega = \omega_L$ [green and blue lines in Fig. 4.4(a)]. This behavior of the dynamic conductance can be understood as follows. For $\mu = \epsilon_{\uparrow} - \omega_L = \epsilon_3$, at $\Omega = \omega_L$, besides resonant level with energy $\epsilon_{\uparrow} - \omega_L$, the upper level with energy ϵ_{\uparrow} becomes available for photon-assisted electron transport. It is then distanced by the energy Ω from the chemical potential μ . Consequently, an electron with Fermi energy equal to $\epsilon_{\uparrow} - \omega_L$ can absorb a photon of energy $\Omega = \omega_L$ and tunnel into the level with energy ϵ_{\uparrow} . This leads to an enhancement of the response functions G_R and G_I after going to a local minimum, with features corresponding to photon-assisted tunneling processes. Each step-like increase of G_R and the corresponding dip of G_I in Fig. 4.4 are determined by the difference between the quasienergy levels ϵ_i and the chemical potential μ , viz. $|\epsilon_i - \mu| = \Omega$. Thus, for $\mu = \epsilon_3$ and the set of

parameters given in Fig. 4.4, they are positioned around $\Omega/\epsilon_0 = 0.5$ and $\Omega/\epsilon_0 = 1$. For the larger tunnel couplings the step-like increases in G_R are broadened due to the level broadening Γ . We notice that the enhancement of the dynamic conductance is higher around $\Omega = \omega_L$ than around the subsequent frequency $\Omega/\epsilon_0 = 1$. This is due to the fact that the frequency has to traverse one resonant peak in G_R , or dip in G_I , to reach the second one. We need to mention that the off-diagonal conductances $G_{\xi\zeta} = -G$, where $\xi \neq \zeta$, and hence have the opposite behavior than the diagonal ones.

In the spirit of the scattering matrix formalism, the dynamic conductance of our molecular magnet junction, in the low ac-frequency regime, can be expanded as [263]

$$G_{\xi\zeta}(\Omega) = G_{\xi\zeta}(0) - i\Omega E_{\xi\zeta} + \Omega^2 K_{\xi\zeta} + O(\Omega^3), \quad (4.38)$$

where $G_{\xi\zeta}(0)$ is the dc conductance. The quantity $E_{\xi\zeta} = -\text{Im}\{\partial G_{\xi\zeta}(0)/\partial\Omega\}$ is called the emittance [263]. It contains the contribution from the displacement current and the partial density of states that characterize the scattering process [258, 264, 265]. The partial density of states can be calculated using the scattering matrix, and can be understood as density of states due to electrons injected from lead ζ and leaving through lead ξ [258, 264, 265]. The emittance $E_{\xi\zeta}$ measures the dynamic response of the system to an external oscillating ac field, and depending on its sign, the response is capacitive-like or inductive-like [263]. The matrix element of the third term, $K_{\xi\zeta} = \text{Re}\{\partial^2 G_{\xi\zeta}(0)/\partial\Omega^2\}/2$, represents the correction to the real part of the dynamic conductance, and describes the dynamic dissipation in the low ac-frequency regime [263]. Both $E_{\xi\zeta}$ and $K_{\xi\zeta}$ obey the sum rules, since the total current conservation and gauge invariance conditions have to be satisfied [257]. According to Eq. (4.38), their diagonal elements $E = E_{\xi\xi}$ and $K = K_{\xi\xi}$ can be approximated as $E \approx -G_I/\Omega$ and $K \approx [G_R - G(0)]/\Omega^2$ in the low ac-frequency limit [263]. Based on the analyzed G_R and G_I the behavior of E and K can be examined. Around all resonances $\mu = \epsilon_i$ the emittance $E < 0$ (inductive-like response), and $K < 0$ since $G_R < G(0)$, while off resonance $E > 0$ (capacitive-like response), and $K > 0$ [see Figs. 4.3 and 4.4].

4.4.5 Effects of other parameters on the ac conductance

The conductance components G_R and G_I as functions of the Larmor precession frequency ω_L are presented in Figs. 4.6(a) and 4.6(b), while Figs. 4.7(a) and 4.7(b) depict the dependence of G_R and G_I on the exchange coupling constant J . They show similar characteristics as in Fig. 4.3, with higher peaks at resonancies corresponding to $\mu_\xi = \epsilon_{1,4}$, while lower peaks correspond to $\mu_\xi = \epsilon_{2,3}$. In the

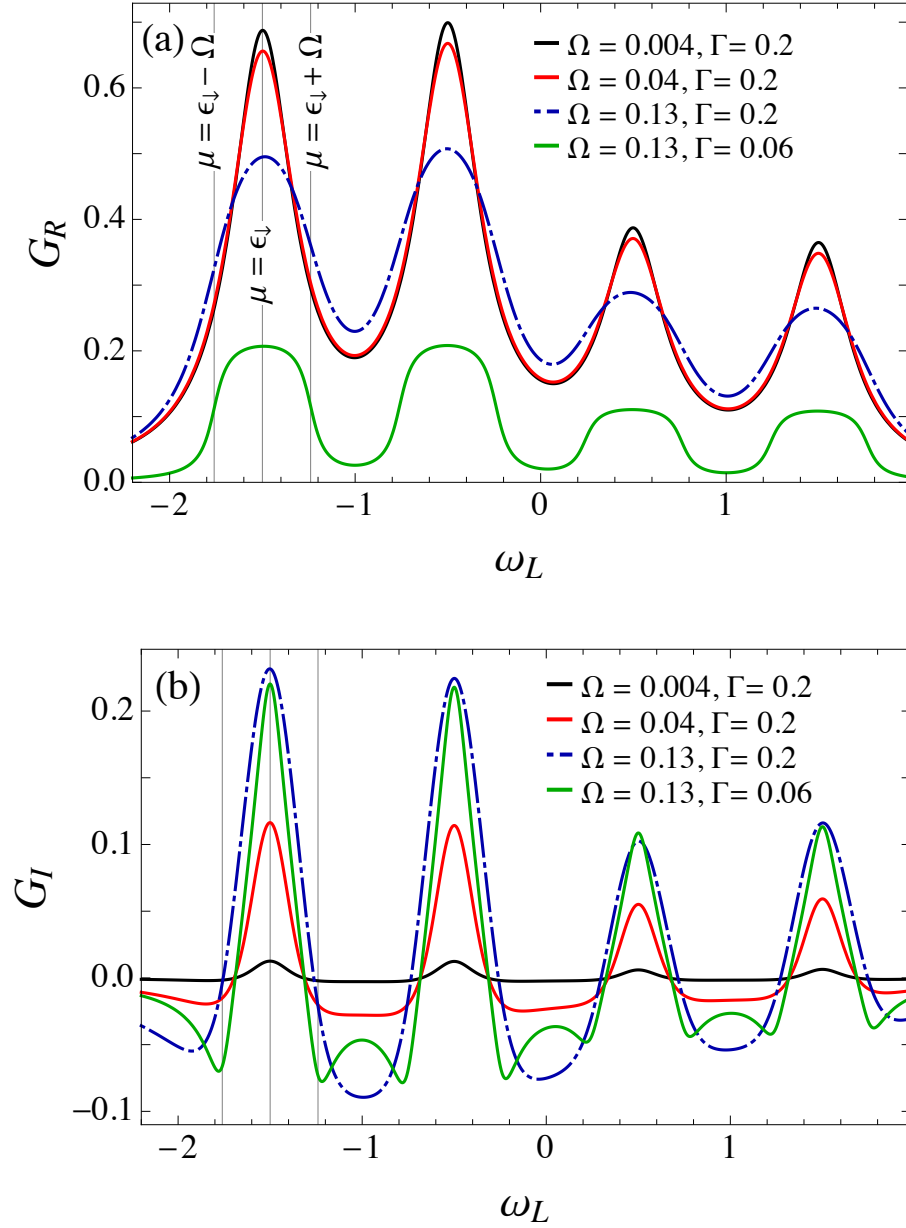


FIGURE 4.6: Larmor frequency dependence of (a) the real part G_R and (b) the imaginary part G_I of the dynamic conductance. The plots are obtained for different ac frequencies Ω and tunneling rates Γ at zero temperature, with $\Gamma_L = \Gamma_R = \Gamma/2$, and $\vec{B} = B\vec{e}_z$. All energies are given in the units of ϵ_0 . The molecular spin is set to $S = 100$, and the tilt angle to $\theta = 1.25$. The exchange coupling constant $J = 0.01$, and the chemical potentials of the leads are $\mu_L = \mu_R = 1.25$. The conductance components G_R and G_I are given in the units of conductance quantum e^2/h .

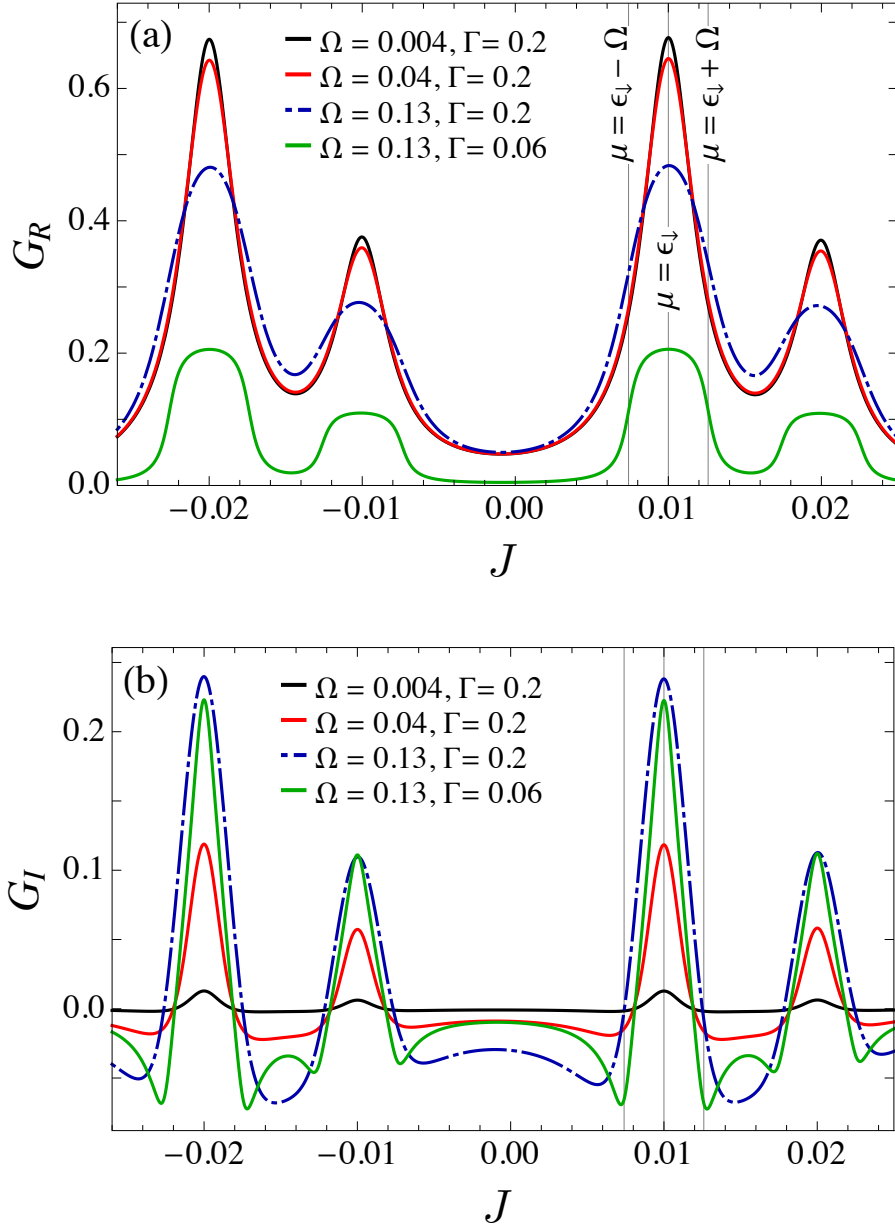


FIGURE 4.7: (a) Real part G_R and (b) imaginary part G_I of the dynamic conductance as functions of the exchange coupling J . The plots are obtained for different ac frequencies Ω and tunneling rates Γ at zero temperature, with $\Gamma_L = \Gamma_R = \Gamma/2$, and $\vec{B} = B\vec{e}_z$. All energies are given in the units of ϵ_0 . The molecular spin is set to $S = 100$, and the tilt angle to $\theta = 1.25$. The Larmor frequency is equal to $\omega_L = 0.5$, and the chemical potentials of the leads are $\mu_L = \mu_R = 0.25$. The conductance components G_R and G_I are given in the units of conductance quantum e^2/h .

low ac-frequency limit the system shows inductive-like behavior ($G_I > 0$) around resonancies for values of ω_L or J for which the inequality (4.37) is satisfied [see Figs. 4.6(b) and 4.7(b)]. The response of the system is resistive ($G_I = 0$) or capacitive-like ($G_I < 0$) otherwise. In the limit of weak tunnel coupling Γ each peak of G_R broaden for large Ω approaching a constant value. Their width is equal to 4Ω and $4\Omega/S$ in Figs. 4.6(a) and 4.7(a) (green lines), since for these values of ω_L and J the inequality (4.34) is fulfilled.

For $\theta = 1.25$ the peaks of both G_R and G_I in Figs. 4.3(a) and 4.3(b) at $\mu = \epsilon_{\uparrow,\downarrow} \mp \omega_L$ are much smaller than those at $\mu = \epsilon_{\uparrow,\downarrow}$, implying that the molecular magnet junction is less transmissive at the upper two mentioned resonances. This can be qualitatively understood by looking at Figs. 4.8(a) and 4.8(b) where we plotted G_R and G_I as functions of the tilt angle θ between the external magnetic field \vec{B} and the molecular spin $\vec{S}(t)$. The behavior of the conductance components near the resonances for $\mu = \epsilon_{\uparrow} - \omega_L$ (solid lines in Fig. 4.8) and $\mu = \epsilon_{\uparrow}$ (dot-dashed lines in Fig. 4.8) depends on the direction of \vec{S} with respect to the external magnetic field. For $\theta = 0$ the molecular spin \vec{S} is static and the only two levels available for electron transport are Zeeman levels $\epsilon_1 = \epsilon_{\downarrow}$ and $\epsilon_4 = \epsilon_{\uparrow}$. In this case, when the system is at the resonance $\mu = \epsilon_{\uparrow}$, the components G_R and G_I take their maximum values, and $G_I > 0$ displaying an inductive-like behavior. For $\mu = \epsilon_{\uparrow} - \omega_L$ and $\theta = 0$, both G_R and G_I take their minimum values. There is no transmission channel at this energy for $\theta = 0$, but Γ is relatively large, and $G_I < 0$ displaying a capacitive-like response. With the increase of θ , the additional two channels at energies $\epsilon_{\uparrow} - \omega_L$ and $\epsilon_{\downarrow} + \omega_L$ appear, and become available for electron transport. This leads to the increase of conductance components G_R and G_I at $\mu = \epsilon_{\uparrow} - \omega_L$, and their decrease at $\mu = \epsilon_{\uparrow}$, as functions of θ (see Fig. 4.8). For $\theta \rightarrow \pi/2$, in the case of small Ω the complex components of the effective transmission function $T(\epsilon, \Omega)$ approach the same height at resonant energies ϵ_i , so that the probability of transmission reaches equal value at each level. Thus, the dynamic response function G_R approaches equal characteristics at each resonance as well as G_I . The points of intersection of solid and dot-dashed lines of the same color in Fig. 4.8 correspond to this particular case. For larger frequencies Ω , these points are shifted away from $\theta \rightarrow \pi/2$, since the peaks broaden and overlap and the suppression or increase of G_R and G_I is much faster. Finally, for $\theta = \pi$ the situation is reversed compared to the one with $\theta = 0$, as the again static spin \vec{S} is in the opposite direction than that of the external field \vec{B} . The Zeeman splitting in this case is equal to $\omega_L - JS$, so that the only two levels available for electron transport are ϵ_2 and ϵ_3 . Therefore, for $\theta = \pi$, when the system is at the resonance $\mu = \epsilon_3$, the conductance components G_R and G_I reach their maximum values, with $G_I > 0$. For $\mu = \epsilon_4$, which is off resonance for $\theta = \pi$, both G_R and G_I take minimum values, with $G_I < 0$.

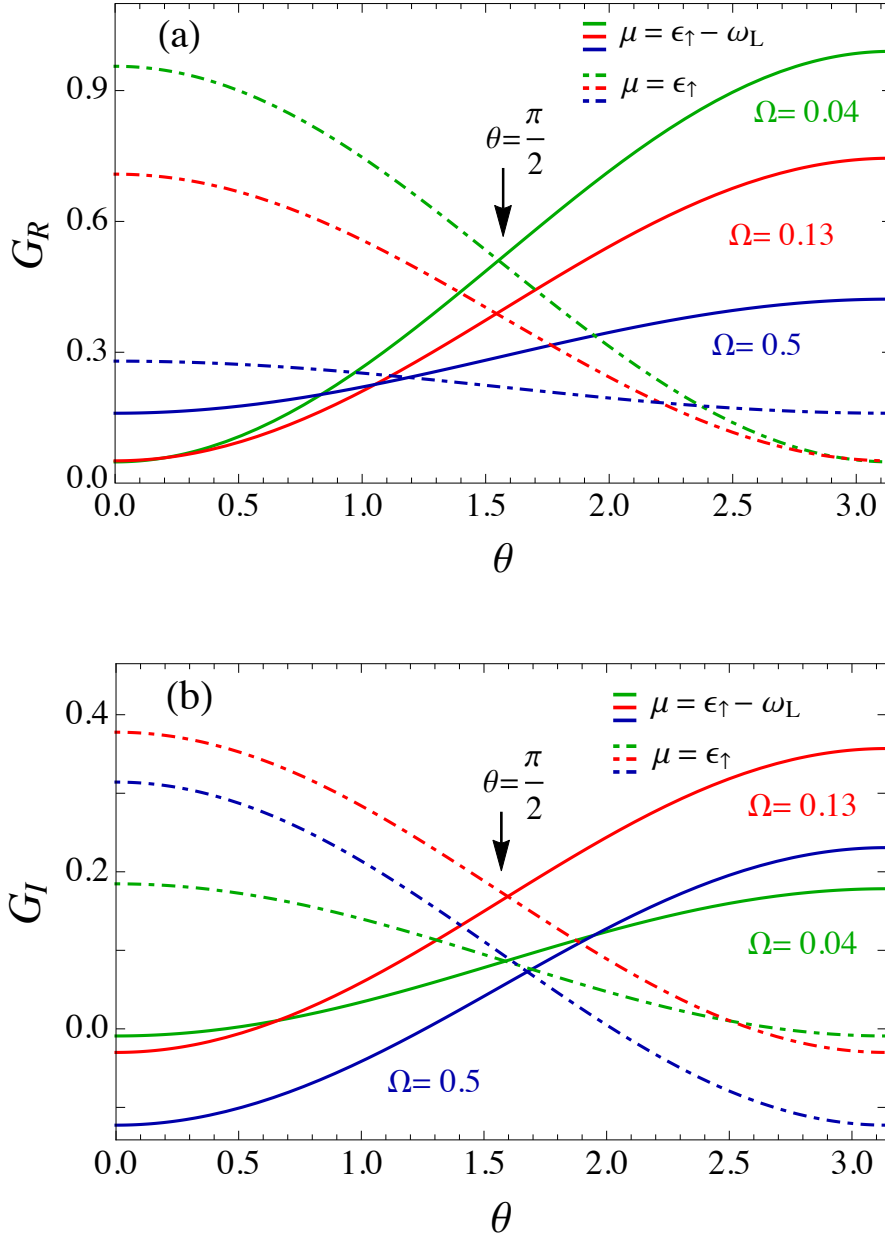


FIGURE 4.8: (a) Real part G_R and (b) imaginary part G_I of the dynamic conductance as functions of the tilt angle θ of the molecular spin \vec{S} from the magnetic field $\vec{B} = B\vec{e}_z$. The plots are obtained for different values of Ω and μ , with $\mu = \mu_L = \mu_R$, at zero temperature. All energies are given in the units of ϵ_0 . The other parameters are set to $S = 100$, $J = 0.01$, $\omega_L = 0.5$, $\Gamma = 0.2$, and $\Gamma_L = \Gamma_R = \Gamma/2$. In the limit of low frequency Ω , for $\theta \rightarrow \pi/2$, the conductance component G_R , as well as G_I , approaches equal value at each resonance. The conductance components G_R and G_I are given in the units of conductance quantum e^2/h .

4.5 Spin transport and spin-transfer torque

4.5.1 Spin transport under dc-bias voltage

In the absence of ac harmonic potentials in the leads, tunneling under dc-bias voltage takes place. The spin-angular momenta between the itinerant electronic spins and the precessing molecular spin are exchanged via exchange interaction, governed by the coupling constant J . The molecular spin precession pumps spin currents into the system, but remains undamped using external sources which compensate effects of the interaction with electron spins. Further simplification of Eq. (4.16) gives time-independent z component of the spin current, $I_{Lz}^{\omega_L}$, and the in-plane $j = x, y$ time-dependent spin-current components, from the left lead

$$I_{Lj}^{\omega_L}(t) = [I_{Lj}(\omega_L)e^{-i\omega_L t} + I_{Lj}^*(\omega_L)e^{i\omega_L t}]. \quad (4.39)$$

The complex time-independent functions $I_{Lx}(\omega_L)$ and $I_{Ly}(\omega_L)$, and the spin current $I_{Lz}^{\omega_L}$ can be expressed as

$$I_{Lx}(\omega_L) = -i \int \frac{d\epsilon}{4\pi} \left\{ \frac{\Gamma_L \Gamma_R}{\Gamma} [f_L(\epsilon) - f_R(\epsilon)] \left[\frac{\gamma G_{11}^{0r}(\epsilon + \omega_L) G_{22}^{0r}(\epsilon)}{|1 - \gamma^2 G_{11}^{0r}(\epsilon + \omega_L) G_{22}^{0r}(\epsilon)|^2} \right. \right. \quad (4.40)$$

$$+ \left. \frac{2i\gamma \text{Im}\{G_{11}^{0r}(\epsilon)\} G_{22}^{0a}(\epsilon - \omega_L) + \gamma^3 |G_{11}^{0r}(\epsilon) G_{22}^{0r}(\epsilon - \omega_L)|^2}{|1 - \gamma^2 G_{11}^{0r}(\epsilon) G_{22}^{0r}(\epsilon - \omega_L)|^2} \right]$$

$$+ \sum_{\xi, \zeta=L,R} \frac{\Gamma_\xi \Gamma_\zeta}{\Gamma} [f_\xi(\epsilon - \omega_L) - f_\zeta(\epsilon)] \left[\delta_{\zeta L} - \delta_{\xi L} \gamma^2 G_{11}^{0a}(\epsilon) G_{22}^{0r}(\epsilon - \omega_L) \right]$$

$$\times \left. \frac{\gamma G_{11}^{0r}(\epsilon) G_{22}^{0a}(\epsilon - \omega_L)}{|1 - \gamma^2 G_{11}^{0r}(\epsilon) G_{22}^{0r}(\epsilon - \omega_L)|^2} \right\},$$

$$I_{Ly}(\omega_L) = iI_{Lx}(\omega_L), \quad (4.41)$$

$$I_{Lz}^{\omega_L} = \int \frac{d\epsilon}{4\pi} \left\{ \frac{\Gamma_L \Gamma_R}{\Gamma} [f_L(\epsilon) - f_R(\epsilon)] \quad (4.42)$$

$$\times \left[\frac{2\text{Im}\{G_{11}^{0r}(\epsilon)\}}{|1 - \gamma^2 G_{11}^{0r}(\epsilon) G_{22}^{0r}(\epsilon - \omega_L)|^2} - \frac{2\text{Im}\{G_{22}^{0r}(\epsilon)\}}{|1 - \gamma^2 G_{11}^{0r}(\epsilon + \omega_L) G_{22}^{0r}(\epsilon)|^2} \right]$$

$$+ \sum_{\xi, \zeta=L,R} \Gamma_\xi \Gamma_\zeta [f_\xi(\epsilon - \omega_L) - f_\zeta(\epsilon)] (\delta_{\xi L} + \delta_{\zeta L}) \frac{\gamma^2 |G_{11}^{0r}(\epsilon) G_{22}^{0r}(\epsilon - \omega_L)|^2}{|1 - \gamma^2 G_{11}^{0r}(\epsilon) G_{22}^{0r}(\epsilon - \omega_L)|^2} \right\}.$$

The spin-transport properties are characterized by the elastic, i.e., energy-conserving tunnel processes [terms involving factors $f_L(\epsilon) - f_R(\epsilon)$ in Eqs. (4.40) and (4.42)], and the inelastic, i.e., energy-nonconserving tunnel processes [terms which involve factors $f_\xi(\epsilon - \omega_L) - f_\zeta(\epsilon)$ in Eqs. (4.40) and (4.42)]. In the later

ones an electron changes its energy by ω_L and flips its spin due to the exchange interaction with the rotational component of the molecular spin. The spin-flip processes occur between levels with energies ϵ_\uparrow and $\epsilon_\uparrow - \omega_L$, and between levels with energies ϵ_\downarrow and $\epsilon_\downarrow + \omega_L$.

The spin-transfer torque exerted by the inelastic spin-currents onto the spin of the molecule is given by [108–111]

$$\vec{T}^{\omega_L}(t) = -[\vec{I}_L^{\omega_L}(t) + \vec{I}_R^{\omega_L}(t)]. \quad (4.43)$$

Using Eqs. (4.39)–(4.43), the spatial components of the spin-transfer torque can be expressed in terms of the matrix elements of the Green's functions $\hat{G}_0^r(\epsilon)$ and $\hat{G}_0^a(\epsilon)$ as

$$\begin{aligned} T_j^{\omega_L}(t) &= - \int \frac{d\epsilon}{2\pi} \sum_{\xi\zeta} \frac{\Gamma_\xi \Gamma_\zeta}{\Gamma} [f_\xi(\epsilon - \omega_L) - f_\zeta(\epsilon)] \\ &\quad \times \text{Im} \left\{ (\hat{\sigma}_j)_{21} \frac{\gamma G_{11}^{0r}(\epsilon) G_{22}^{0a}(\epsilon - \omega_L)}{|1 - \gamma^2 G_{11}^{0r}(\epsilon) G_{22}^{0r}(\epsilon - \omega_L)|^2} \right. \\ &\quad \left. \times [1 - \gamma^2 G_{11}^{0a}(\epsilon) G_{22}^{0r}(\epsilon - \omega_L)] e^{-i\omega_L t} \right\}, \end{aligned} \quad (4.44)$$

$$\begin{aligned} T_z^{\omega_L} &= - \int \frac{d\epsilon}{2\pi} \sum_{\xi\zeta} \Gamma_\xi \Gamma_\zeta [f_\xi(\epsilon - \omega_L) - f_\zeta(\epsilon)] \\ &\quad \times \frac{\gamma^2 |G_{11}^{0r}(\epsilon) G_{22}^{0r}(\epsilon - \omega_L)|^2}{|1 - \gamma^2 G_{11}^{0r}(\epsilon) G_{22}^{0r}(\epsilon - \omega_L)|^2}. \end{aligned} \quad (4.45)$$

Regarding the molecular spin $\vec{S}(t)$, the spin-transfer torque can be presented as

$$\vec{T}^{\omega_L}(t) = \frac{\alpha}{S} \dot{\vec{S}}(t) \times \vec{S}(t) + \beta \ddot{\vec{S}}(t) + \eta \vec{S}(t), \quad (4.46)$$

with the Gilbert damping coefficient α in the first term. The coefficient β that characterizes the modulation of the precession frequency of the molecular spin $\vec{S}(t)$ is given by the second term. The third coefficient η can be written in terms of α and $T_z^{\omega_L}$ as $\eta = [T_z^{\omega_L} + \omega_L S \alpha \sin^2(\theta)]/S_z$. Using Eqs. (4.44) and (4.45), and comparing them with Eq. (4.46), one obtains exact expressions for the torque coefficients α and β as [223]

$$\begin{aligned} \alpha &= - \frac{1}{\omega_L S} \int \frac{d\epsilon}{2\pi} \sum_{\xi\zeta} \Gamma_\xi \Gamma_\zeta [f_\xi(\epsilon - \omega_L) - f_\zeta(\epsilon)] \\ &\quad \times \frac{(JS_z/2\Gamma) \text{Im}\{G_{11}^{0r}(\epsilon) G_{22}^{0a}(\epsilon - \omega_L)\} - \gamma^2 |G_{11}^{0r}(\epsilon) G_{22}^{0r}(\epsilon - \omega_L)|^2}{|1 - \gamma^2 G_{11}^{0r}(\epsilon) G_{22}^{0r}(\epsilon - \omega_L)|^2}, \end{aligned} \quad (4.47)$$

$$\beta = -\frac{J}{\omega_L} \int \frac{d\epsilon}{4\pi} \sum_{\xi\zeta} \frac{\Gamma_\xi \Gamma_\zeta}{\Gamma} [f_\xi(\epsilon - \omega_L) - f_\zeta(\epsilon)] \times \frac{\text{Re}\{G_{11}^{0r}(\epsilon)G_{22}^{0a}(\epsilon - \omega_L)\} - \gamma^2 |G_{11}^{0r}(\epsilon)G_{22}^{0r}(\epsilon - \omega_L)|^2}{|1 - \gamma^2 G_{11}^{0r}(\epsilon)G_{22}^{0r}(\epsilon - \omega_L)|^2}. \quad (4.48)$$

In the limit $\gamma^2 \rightarrow 0$, the expressions (4.40)–(4.48) are in agreement with [219] (see Section 3.3.1). In the strong exchange coupling limit $J \gg \Gamma$ both Gilbert damping coefficient α and the torque coefficient β drop to zero.

4.5.2 Photon-assisted spin transport under ac-bias voltage

We consider spin transport in the double-driving experiment, where we first establish molecular spin precession at Larmor frequency ω_L , and then apply the oscillating potentials with frequency Ω in the leads. The spin current components indicating photon-assisted inelastic spin transport can be obtained by further simplification of Eq. (4.17). The in-plane x and y spin-current components consist of oscillating terms involving both ac frequency Ω and Larmor frequency ω_L . Experimentally, by adjusting $\Omega = \pm\omega_L$, these currents may be measurable. In this case they have one dc component and one component oscillating with frequency 2Ω . The in-plane photon-assisted spin currents read

$$I_{Lj}^\Omega(t) = \sum_{\xi=L,R} \text{Re}\left\{ [I_{L\xi}^j(\Omega)e^{-i(\Omega t + \phi_\xi)} + I_{L\xi}^j(-\Omega)e^{i(\Omega t + \phi_\xi)}] e^{-i\omega_L t} \right\}, \quad (4.49)$$

where $j = x, y$. In Eq. (4.49) the time-independent complex components $I_{L\xi}^j(\Omega)$ can be written as

$$I_{L\xi}^x(\Omega) = \gamma \Gamma_L \Gamma_\xi \frac{v_\xi^{\text{ac}}}{\Omega} \int \frac{d\epsilon}{4\pi} [f_\xi(\epsilon - \Omega) - f_\xi(\epsilon)] \times \left\{ \frac{G_{11}^{0a}(\epsilon - \Omega)G_{22}^{0a}(\epsilon - \Omega - \omega_L)}{[1 - \gamma^2 G_{11}^{0a}(\epsilon - \Omega)G_{22}^{0a}(\epsilon - \Omega - \omega_L)]} \times \frac{\{G_{11}^{0r}(\epsilon) + i\frac{\delta_{L\xi}}{\Gamma_\xi} [1 - \gamma^2 G_{11}^{0r}(\epsilon)G_{22}^{0r}(\epsilon - \omega_L)]\}}{[1 - \gamma^2 G_{11}^{0r}(\epsilon)G_{22}^{0r}(\epsilon - \omega_L)]} + \frac{G_{11}^{0r}(\epsilon + \omega_L)G_{22}^{0r}(\epsilon)}{[1 - \gamma^2 G_{11}^{0r}(\epsilon + \omega_L)G_{22}^{0r}(\epsilon)]} \times \frac{\{G_{22}^{0a}(\epsilon - \Omega) - i\frac{\delta_{L\xi}}{\Gamma_\xi} [1 - \gamma^2 G_{11}^{0a}(\epsilon - \Omega + \omega_L)G_{22}^{0a}(\epsilon - \Omega)]\}}{[1 - \gamma^2 G_{11}^{0a}(\epsilon - \Omega + \omega_L)G_{22}^{0a}(\epsilon - \Omega)]} \right\}, \quad (4.51)$$

$$I_{L\xi}^y(\Omega) = iI_{L\xi}^x(\Omega).$$

The z component of the photon-assisted spin-current is given by

$$I_{Lz}^{\Omega}(t) = \sum_{\xi=L,R} \sum_{\sigma=\pm 1} \text{Re} \left\{ \Gamma_L \Gamma_{\xi} \frac{v_{\xi}^{\text{ac}}}{\Omega} \int \frac{d\epsilon}{4\pi} [f_{\xi}(\epsilon - \Omega) - f_{\xi}(\epsilon)] e^{-i(\Omega t + \phi_{\xi})} \right. \quad (4.52)$$

$$\times \frac{[\hat{\sigma}_z \hat{G}^{0r}(\epsilon) \hat{G}^{0a}(\epsilon - \Omega)]_{\sigma\sigma}}{[1 - \gamma^2 G_{\sigma\sigma}^{0r}(\epsilon) G_{-\sigma-\sigma}^{0r}(\epsilon_{\sigma})]}$$

$$\left. \times \frac{\left\{ 2 - [1 - i \frac{\delta_{L\xi}}{\Gamma_{\xi}} (\Omega + i\Gamma)] [1 + \gamma^2 G_{-\sigma-\sigma}^{0r}(\epsilon_{\sigma}) G_{-\sigma-\sigma}^{0a}(\epsilon_{\sigma} - \Omega)] \right\}}{[1 - \gamma^2 G_{\sigma\sigma}^{0a}(\epsilon - \Omega) G_{-\sigma-\sigma}^{0a}(\epsilon_{\sigma} - \Omega)]} \right\}.$$

The time average of a periodic function $F(t)$ with a period T_p is defined as

$$\langle F \rangle_t = \frac{1}{T_p} \int_0^{T_p} F(t) dt. \quad (4.53)$$

According to Eq. (4.49), the time-averaged $j = x, y$ components of the total spin current $\vec{I}_L(t)$ are nonzero only for $\Omega = \pm\omega_L$ and read

$$\langle I_{Lj} \rangle_t = \langle I_{Lj}^{\Omega=\pm\omega_L} \rangle_t = \sum_{\xi} \text{Re} \left\{ I_{L\xi}^j(-\omega_L) e^{\pm i\phi_{\xi}} \right\}, \quad (4.54)$$

while the time-averaged z component of the spin current equals

$$\langle I_{Lz} \rangle_t = I_{Lz}^{\omega_L}. \quad (4.55)$$

Hence, the in-plane time-averaged x and y spin-current components contain only contributions from photon-assisted spin tunneling processes, while the z component contains only contributions from spin tunneling under dc-bias voltage. The time-averaged spin-transfer torque is then given by

$$\langle \vec{T} \rangle_t = - \sum_{\xi} \langle \vec{I}_{\xi} \rangle_t. \quad (4.56)$$

All the torques are compensated by external means which keep the molecular spin precession undamped during the experiment.

4.5.3 Analysis of the time-averaged spin transport

We start by analyzing the in-plane x and y components of the time-averaged spin current, which differ in phase by $\pi/2$ according to Eqs. (4.51) and (4.54), and the spin-transfer torque. They are presented as functions of the bias-voltage $eV = \mu_L - \mu_R$ in Figs. 4.9(a) and 4.9(b), and as functions of the exchange coupling

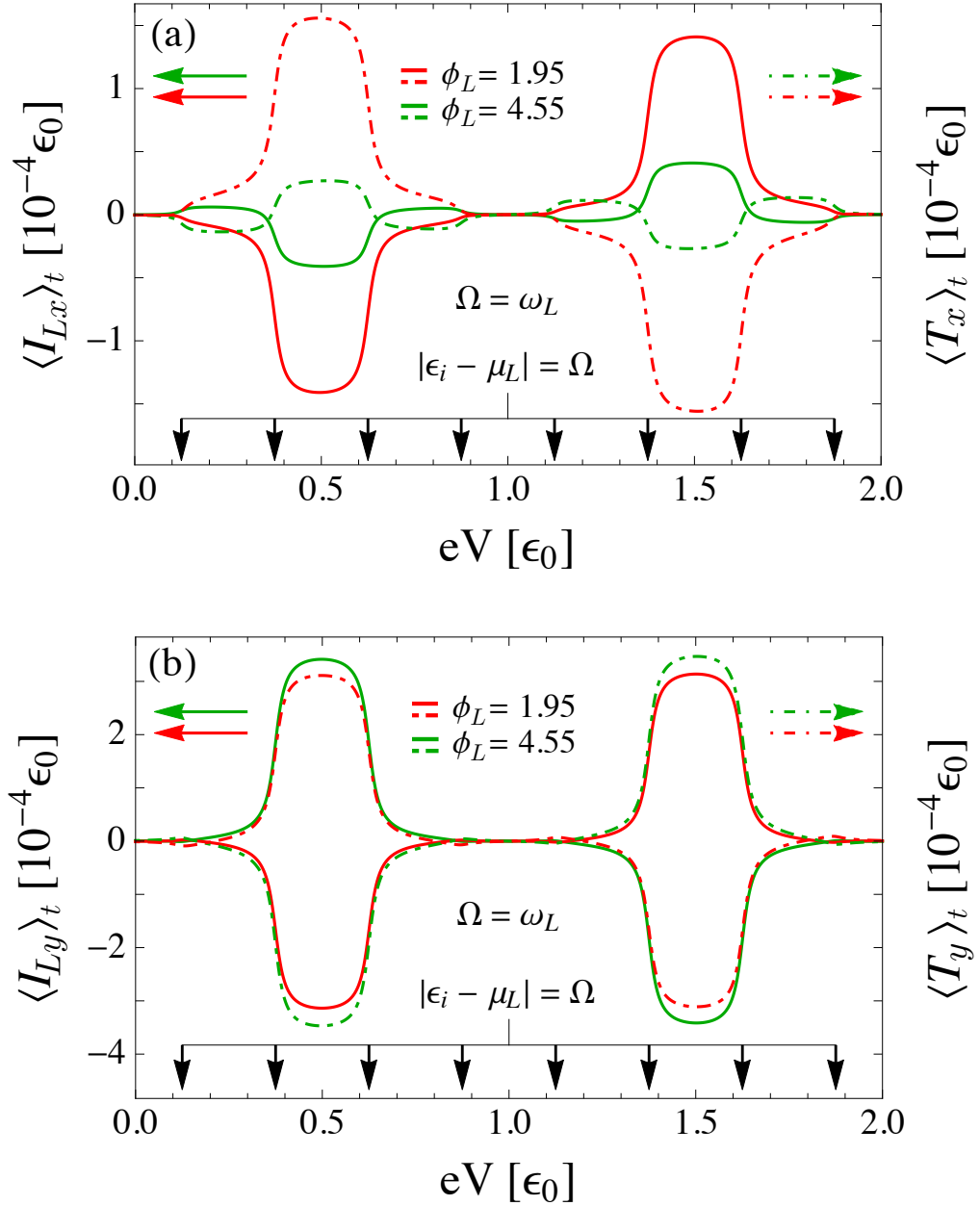


FIGURE 4.9: Bias-voltage dependence of the time-averaged components of the spin-current and spin-transfer torque (a) $\langle I_{Lx} \rangle_t$ and $\langle T_x \rangle_t$, and (b) $\langle I_{Ly} \rangle_t$ and $\langle T_y \rangle_t$. All plots are obtained at zero temperature for two different phases ϕ_L , with $\vec{B} = B\vec{e}_z$. The other parameters are set to $\Gamma_L = \Gamma_R = \Gamma/2$, $\Gamma = 0.04 \epsilon_0$, $\mu_R = 0$, $\phi_R = 0$, $v_R^{\text{ac}} = 0$, $v_L^{\text{ac}} = 0.02 \epsilon_0$, $\theta = 1.25$, $S = 100$, $J = 0.01 \epsilon_0$, and $\Omega = \omega_L = 0.25 \epsilon_0$. Photon-assisted spin transport is enhanced for $\epsilon_1 < \mu_L < \epsilon_2$ and $\epsilon_1 < \mu_L < \epsilon_2$, where the in-plane components of the spin-current and spin-transfer torque approach the constant largest magnitudes.

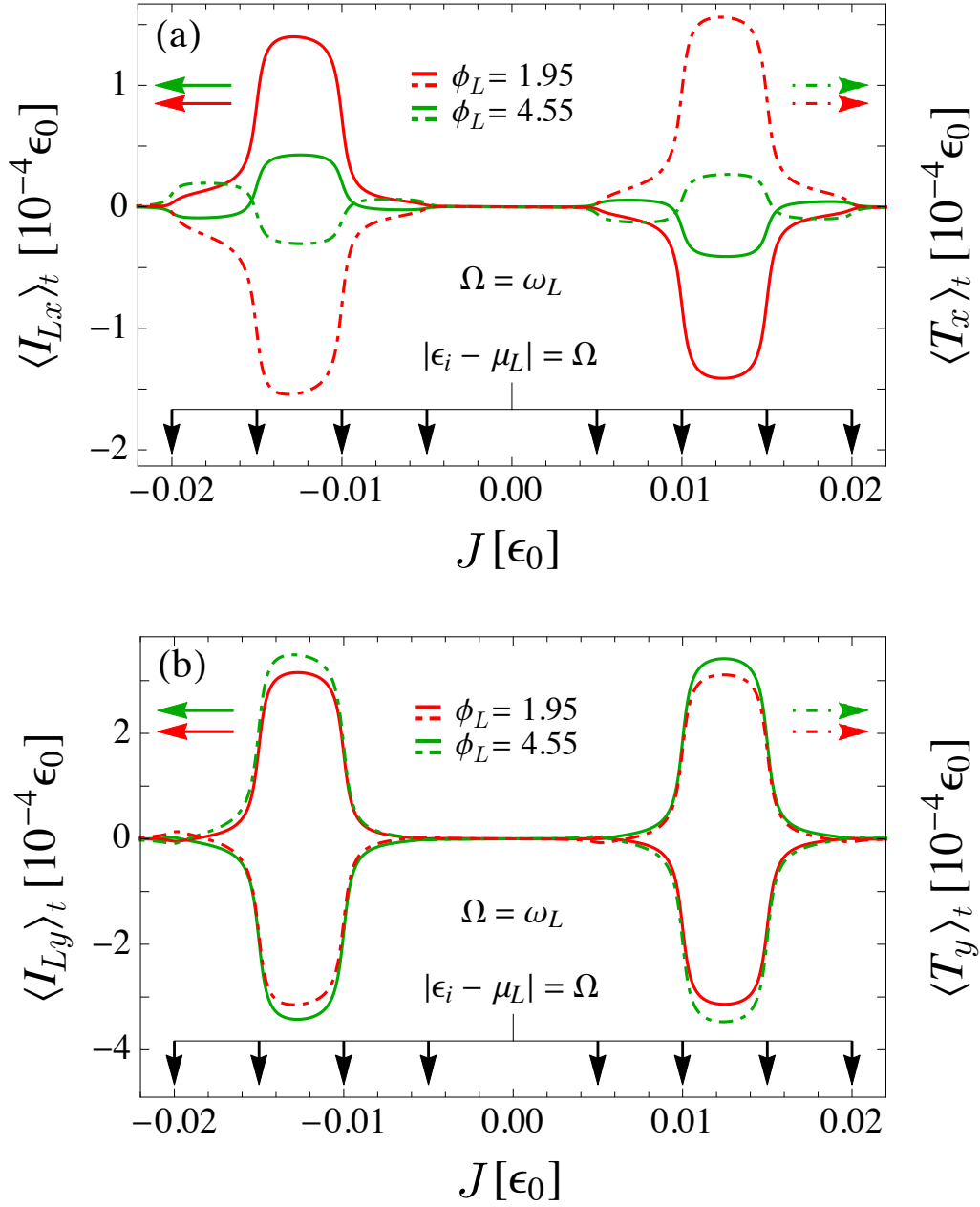


FIGURE 4.10: Time-averaged components of the spin-current and spin-transfer torque (a) $\langle I_{Lx} \rangle_t$, $\langle T_x \rangle_t$; and (b) $\langle I_{Ly} \rangle_t$, $\langle T_y \rangle_t$; as functions of the exchange coupling J . All plots are obtained at zero temperature for two different phases ϕ_L , with $\vec{B} = B\vec{e}_z$. The other parameters are set to $\Gamma_L = \Gamma_R = \Gamma/2$, $\Gamma = 0.04 \epsilon_0$, $\mu_L = 0.375 \epsilon_0$, $\mu_R = 0$, $\phi_R = 0$, $v_R^{\text{ac}} = 0$, $v_L^{\text{ac}} = 0.02 \epsilon_0$, $\theta = 1.25$, $S = 100$, and $\Omega = \omega_L = 0.25 \epsilon_0$.

constant J in Figs. 4.10(a) and 4.10(b). The plots are obtained at zero temperature, for two different phases of ac field in the left lead. We set $\Omega = \omega_L$, the right lead's Fermi energy $\mu_R = 0$, and apply an ac harmonic chemical potential only to the left lead. In Figs. 4.9(a) and 4.9(b) we vary the Fermi energy of the left lead as $\mu_L = eV$, while in Figs. 4.10(a) and 4.10(b) we set $\mu_L = 0.375\epsilon_0$. According to the segment $[f_L(\epsilon - \Omega) - f_L(\epsilon)]$ in Eq. (4.50), electrons with energies within the window $[\mu_L - \Omega, \mu_L]$ participate in the photon-assisted spin transport. Each of these processes is followed by a spin-flip and emission (absorption) of an amount of energy ω_L . This is caused by the interaction of the electron spin with the precessing component of the molecular spin. In turn, during the exchange interaction a photon-assisted spin-transfer torque is generated onto $\vec{S}(t)$. In regard to photon-assisted transmission of $1/2$ - spin particles, the in-plane spin-current components show significant changes either in magnitude, or direction, controlled by the change of the phase of the ac field in the left lead ϕ_L . Similarly to the case of charge transport, the necessary condition for photon-assisted spin tunneling is given by the inequality (4.34). The cases with equality sign in (4.34) are represented by the black arrows in Figs. 4.9 and 4.10, pointing to the eV and J scale. Each level satisfying this condition corresponds to two black arrows. In the region between each two black arrows the inequality (4.34) is satisfied for at least one molecular quasienergy level. Here, the components of spin current and spin-transfer torque approach constant values. If $\epsilon_1 \leq \mu_L \leq \epsilon_2$ or $\epsilon_3 \leq \mu_L \leq \epsilon_4$, the inequality (4.34) is satisfied for both ϵ_1 and ϵ_2 , or ϵ_3 and ϵ_4 . As a result, the magnitude of spin currents and spin-transfer torque is enhanced under these conditions, due to the involvement of both levels ϵ_1 and ϵ_2 , or ϵ_3 and ϵ_4 , in photon-assisted spin transport and photon-assisted spin-flip processes. We should point out that both spin-current components and spin-torques are antisymmetric functions of eV with respect to the position of ϵ_0 , and odd functions of exchange coupling J . This is a consequence of the antisymmetric position of levels ϵ_i attributed to spin-up or spin-down state of the electron with respect to ϵ_0 . Using Eq. (4.54) with $v_R^{\text{ac}} = 0$ and $\phi_R = 0$, we obtain the largest magnitudes of the $j = x, y$ time-averaged spin-currents for

$$\phi_L = \arctan \left(\frac{\text{Im}\{I_{LL}^j(-\omega_L)\}}{\text{Re}\{I_{LL}^j(-\omega_L)\}} \right), \quad (4.57)$$

where $\Omega = \pm\omega_L$. Simultaneously, the other in-plane time-averaged spin-current equals zero. The magnitude and direction of the time-averaged spin currents and spin-transfer torques can also be controlled by changing the tilt angle θ . For $\theta = 0$, the in-plane spin currents are equal to 0. If μ_L lies between any two levels connected with spin-flip mechanism, then the largest magnitudes of the in-plane components of the spin-current and spin-transfer torque are obtained for $\theta = \pi/2$.

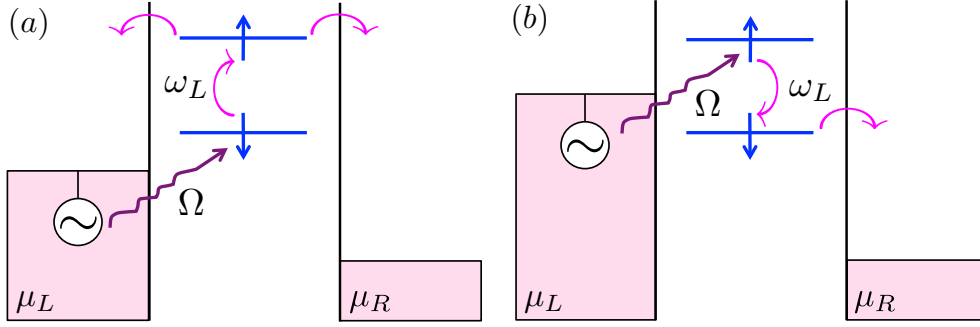


FIGURE 4.11: Sketch of two opposite photon-assisted spin-flip processes between molecular quasienergy levels in the presence of ac harmonic potential with frequency Ω in the left lead. (a) Excited electron with energy Ω tunnels into spin-down level ϵ_\downarrow (or $\epsilon_\uparrow - \omega_L$). It absorbs an amount of energy ω_L , flips its spin due to the exchange interaction with the precessing component of the molecular spin, and exits into either lead. (b) Excited electron tunnels into spin-up level $\epsilon_\downarrow + \omega_L$ (or ϵ_\uparrow), flips its spin and emits an energy quantum ω_L . Then it tunnels out to the right lead.

In this case, the spin-flip is most probable, with the largest magnitude of the rotating field.

Some of the photon-assisted tunneling processes contributing to the spin transport are presented in Fig. 4.11, where we show examples of the two opposite photon-assisted spin-flip processes. Fig. 4.11(a) corresponds to the case in which $\epsilon_1 - \mu_L < \Omega$ (or $\epsilon_3 - \mu_L < \Omega$). Here an electron from the left lead excited by energy $\Omega = \omega_L$ tunnels into the level ϵ_1 (or ϵ_3). During the exchange interaction with the precessing component of $\vec{S}(t)$ it absorbs an energy ω_L and flips its spin, ending up in the level ϵ_2 (or ϵ_4), and then tunnels into either lead. One photon-assisted spin-flip process through level ϵ_2 (or ϵ_4) for $\epsilon_1 \leq \mu_L \leq \epsilon_2$ (or $\epsilon_3 \leq \mu_L \leq \epsilon_4$) is presented in Fig. 4.11(b). In this case an electron absorbs an energy $\Omega = \omega_L$ interacting with ac field in the left lead and enter the spin-up level ϵ_2 (or ϵ_4). Then it emits energy quantum ω_L and flips its spin due to the interaction with the precessing molecular spin, and tunnels into the right lead.

We analyzed the time-averaged photon-assisted spin transport for $\Gamma \ll \omega_L$. However, for Γ comparable with ω_L , we should take into account the possibility of quantum interference between spin states with energies ϵ_1 and ϵ_2 , or ϵ_3 and ϵ_4 . This effect is presented in Fig. 4.12, where it manifests itself in the form of two peaks located at $\mu_L = (\epsilon_1 + \epsilon_2)/2$ and $\mu_L = (\epsilon_3 + \epsilon_4)/2$.

In Fig. 4.13, the time-averaged x and y components of the spin-transfer torque are plotted as functions of ac frequency $\Omega = \omega_L$, for two different tunnel coupling constants $\Gamma = 0.04 \epsilon_0$ (solid lines) and $\Gamma = 0.12 \epsilon_0$ (dot-dashed lines) at zero temperature. The grid lines correspond to $\epsilon_i - \mu_L = \Omega$. For Ω such that $\epsilon_1 - \mu_L = \Omega$, the level ϵ_1 participates in photon-assisted spin transport, followed by an electron

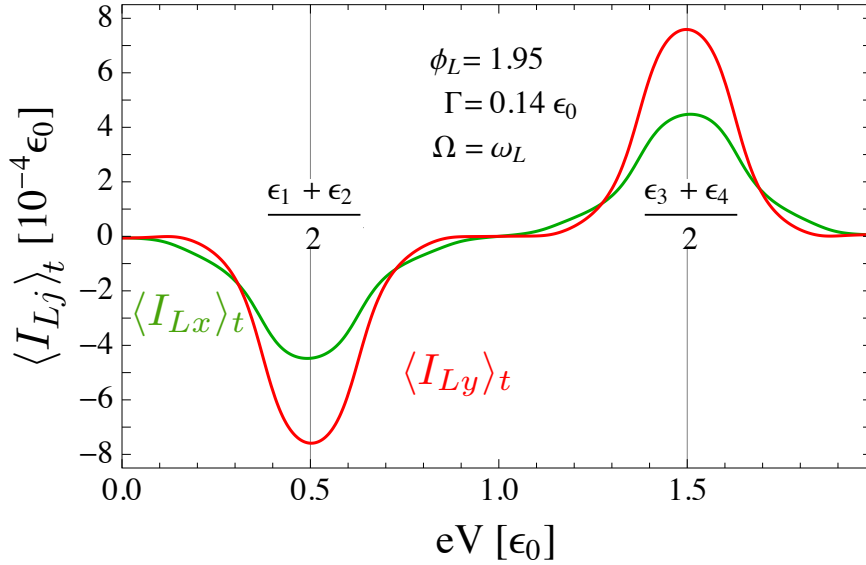


FIGURE 4.12: Time-averaged spin-current components $\langle I_{Lj} \rangle_t$ for $j = x, y$ as functions of bias-voltage eV . The plots are obtained at zero temperature, with $\vec{B} = B\vec{e}_z$, $\Gamma = 0.14 \epsilon_0$, and $\Gamma_L = \Gamma_R = \Gamma/2$. The other parameters are set to: $\Omega = \omega_L = 0.25 \epsilon_0$, $\mu_R = 0$, $v_L^{\text{ac}} = 0.02 \epsilon_0$, $\phi_L = 1.95$, $v_R^{\text{ac}} = 0$, $\phi_R = 0$, $\theta = 1.25$, $J = 0.01 \epsilon_0$, and $S = 100$. Grid lines correspond to peaks due to quantum interference effect between two opposite spin states with quasienergies ϵ_1 (or ϵ_3) and ϵ_2 (or ϵ_4), distanced by ω_L .

spin-flip, and hence a finite spin-transfer torque. In this case $\langle T_x \rangle_t$ is initially enhanced, while $\langle T_y \rangle_t$ has a minimum value and increases after $\Omega = \epsilon_1 - \mu_L$ [first grid line in Fig. 4.13]. As Ω increases the inequality (4.34) is satisfied for level ϵ_1 leading to a nonzero spin-transfer torque. With further increase of ac frequency Ω the photon-assisted spin transport begins to take place in the level ϵ_3 . Both $\langle T_x \rangle_t$ and $\langle T_y \rangle_t$ increase around $\Omega = \epsilon_3 - \mu_L$, after going to a local minimum, due to the fact that level ϵ_3 is now available for spin-flip tunneling processes. For larger Ω the inequality (4.34) is satisfied for both ϵ_1 and ϵ_3 . Consequently, both $\langle T_x \rangle_t$, and $\langle T_y \rangle_t$ increase. Finally, as Ω increases further, level ϵ_2 also becomes available for photon-assisted spin tunneling, leading to the largest enhancement of both in-plane components of the spin-transfer torque. As Ω increases inequality (4.34) is satisfied for levels ϵ_1 , ϵ_2 and ϵ_3 , and photon-assisted time-averaged components of the spin-transfer torque are large and decreasing. After the level ϵ_4 becomes available for photon-assisted spin transport, both components $\langle T_x \rangle_t$ and $\langle T_y \rangle_t$ drop to zero. This is due to the previously mentioned antisymmetry. Namely, in this case the contributions of the photon-assisted spin-transfer torques for $\epsilon_1 < \mu_L < \epsilon_2$ and $\epsilon_3 < \mu_L < \epsilon_4$ are equal in magnitude, but have opposite directions. Therefore, they cancel each other as μ_L satisfies both these inequalities simultaneously. Conditions of inequality (4.34) are relaxed for larger Γ due to the broadening of the levels ϵ_i .

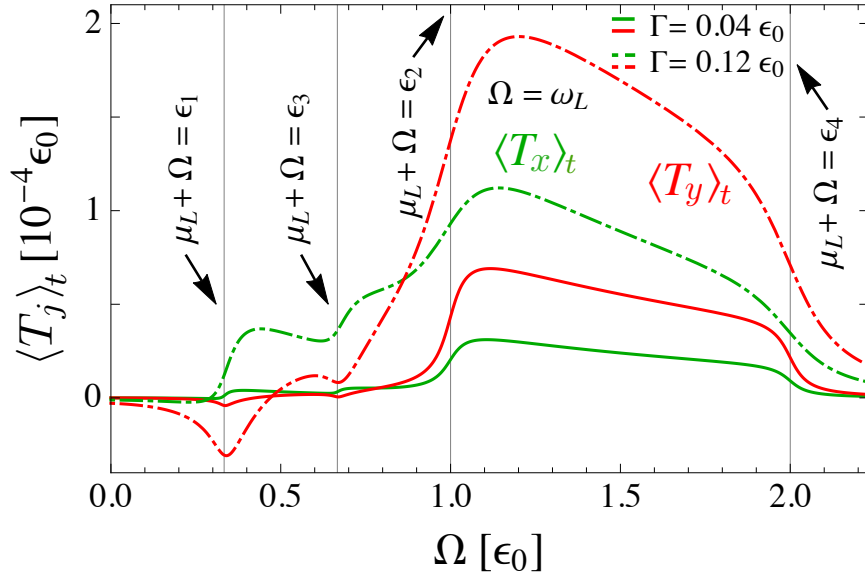


FIGURE 4.13: Time-averaged spin-transfer torque components $\langle T_j \rangle_t$ for $j = x, y$ as functions of ac frequency Ω . The plots are obtained at zero temperature for two different Γ , with $\vec{B} = B\vec{e}_z$, $\Omega = \omega_L$, and $\Gamma_L = \Gamma_R = \Gamma/2$. The other parameters are set to: $\mu_L = 0.25 \epsilon_0$, $\mu_R = 0$, $v_L^{\text{ac}} = 0.02 \epsilon_0$, $\phi_L = 1.95$, $v_R^{\text{ac}} = 0$, $\phi_R = 0$, $\theta = 1.25$, $J = 0.005 \epsilon_0$, and $S = 100$. Each step or dip coincides with a change in the number of available channels for photon-assisted spin tunneling.

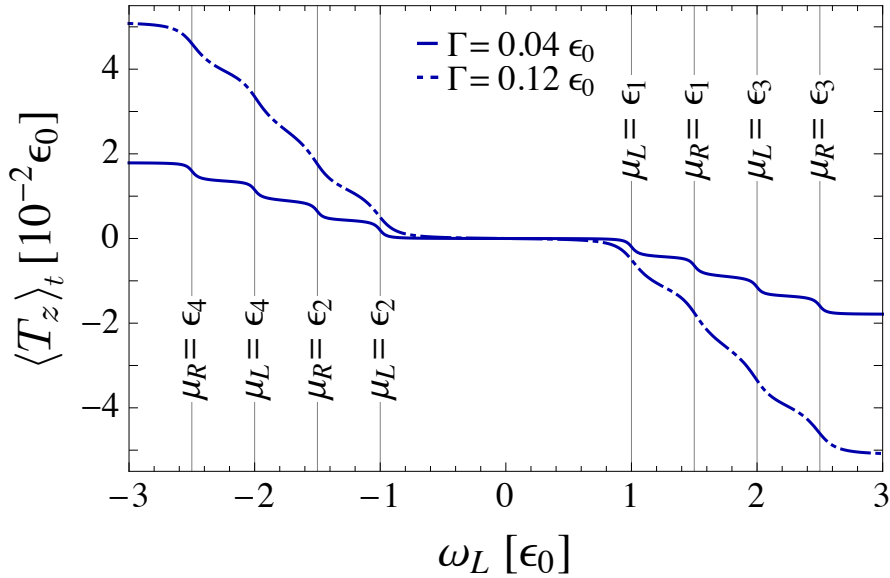


FIGURE 4.14: Time-averaged z component of the spin-transfer torque $\langle T_z \rangle_t$ as a function of the Larmor precession frequency ω_L . The plots are obtained for two different tunneling rates Γ at zero temperature, with $\Gamma_L = \Gamma_R = \Gamma/2$ and $\vec{B} = B\vec{e}_z$. The other parameters are set to: $\mu_L = 0.25 \epsilon_0$, $\mu_R = 0$, $\theta = 1.25$, $J = 0.005 \epsilon_0$, and $S = 100$. Each step corresponds to a spin-tunneling process involving a spin-flip.

The z component of the time-averaged spin-transfer torque, $\langle T_z \rangle_t = T_z^{\omega_L}$ [see Eq. (4.45)] is plotted as a function of the Larmor frequency ω_L in Fig. 4.14. This component does not contain contributions from photon-assisted spin tunneling, but only from spin tunneling under dc-bias voltage, followed by an electron spin-flip due to the interaction with the precessing component of the molecular spin $\vec{S}(t)$. Thus, it does not depend on ac frequency Ω . In turn, a spin-transfer torque is exerted on the molecular spin. The spin-torque component $\langle T_z \rangle_t$ is an odd function of ω_L , since the change of the direction of \vec{B} gives negative ω_L . Each step in Fig. 4.14 denotes a new available spin-transport channel, and an additional spin-flip process, contributing to the spin-transfer torque, which takes place for $\mu_\xi = \epsilon_i$.

4.6 Conclusions

In this chapter we have theoretically studied photon-assisted spin and charge transport through a molecular magnet junction. The junction consists of a single molecular orbital, in the presence of a molecular spin, precessing with Larmor frequency ω_L in a constant magnetic field. The orbital is connected to two metal leads subject to harmonically varying chemical potentials with frequency Ω , treated as a perturbation. We used the Keldysh nonequilibrium Green's functions method to derive charge and spin currents and the spin-transfer torque. We employed the displacement current partitioning scheme of Wang *et al.* [260] to obtain gauge invariant expressions for the dynamic conductance of the charge current.

The dynamic response of the system is controlled by photon-assisted transport. In the low ac-frequency limit, this junction displays an inductive-like or capacitive-like behavior, depending on the system parameters.

When the chemical potentials are in resonance with a molecular quasienergy level ϵ_i , the real and imaginary components of the ac conductance both increase around the ac frequency which coincides with the Larmor frequency, after going to a local minimum, thus allowing to reveal the Larmor frequency by a conductance measurement.

The photon-assisted x and y spin-current components consist of a dc part and a part that oscillates with the frequency 2Ω for $\Omega = \omega_L$. This opens a possibility to experimentally investigate photon-assisted spin-transfer torque exerted on the molecular magnet, which can be detected through the presence of nonzero time-averaged contributions. By manipulating the phases of the harmonic potentials in the leads with respect to the Larmor precession, and the tilt angle between the

magnetic field and the molecular spin, the control of the direction and the magnitude of the time-averaged photon-assisted spin currents and spin-transfer torque is achievable.

Finally, in this chapter we present the nonperturbative Gilbert damping and the other spin-torque coefficients, with respect to the coupling γ , in the zero ac-frequency limit. Remarkably, the Gilbert damping vanishes in the strong coupling limit.

In the future, it might be interesting to investigate further transport properties like the current noise or the spin-torque noise, as well as to find ways to manipulate molecular magnetic moments by using e.g., ferromagnetic leads.

Chapter 5

Shot noise of charge and spin transport in a molecular magnet junction

5.1 Introduction

Shot noise of charge current has become an active research topic in the last decades, since it enables the investigation of microscopic transport properties, which cannot be obtained from the charge current or conductance [130]. Some of these properties result from the quantization of electron charge [130]. Namely, the nonequilibrium time-dependent fluctuations of charge current arise due to discrete nature of electron charge. Classical zero-frequency shot noise given by Schottky's formula $S(0) = e\langle I \rangle$ corresponds to uncorrelated charge carriers with Poissonian distribution [131]. Accordingly, the Fano factor defined as $F = S(0)/e\langle I \rangle$, which describes the deviation of the shot noise from the charge current, equals 1 in this case. In quantum devices the Fermi-Dirac distribution and the Pauli exclusion principle suppress ($F < 1$) [140, 266, 267], while the Coulomb interaction can either suppress ($F < 1$) [268, 269] or enhance ($F > 1$) [270] the shot noise, depending on the system under consideration.

The quantum interference phenomenon, which is a manifestation of the wave nature of electrons has attracted a lot of attention. The quantum interference effects occur between coherent electron waves in nanoscale junctions [271]. Quantum

This chapter is based on a manuscript in preparation by M. Filipović and W. Belzig.

interference in molecular junctions influences their electronic properties [272–276]. The Fano effect [277] due to the interference between a discrete state and the continuum has an important role in investigation of the interference effects in nanojunctions, which behave in an analogous way, and are manifested in the conductance or noise spectra [271, 278, 279]. Particularly interesting examples involve spin-flip processes, like in the presence of Rashba spin-orbit interaction [280, 281], rotating magnetic field [227], or in the case of the magnetotransport [282–284].

It has been demonstrated that spin-flip induced fluctuations in diffusive conductors connected to ferromagnetic leads enhance the noise power, approaching the Poissonian value $F = 1$ [285]. On the other hand, it has been shown that shot noise in a ferromagnet-quantum dot-ferromagnet system with antiparallel magnetization alignments can be suppressed due to spin-flip, with $F < 1/2$ [138]. Shot noise can be used to study correlations of wave functions [286] and kinetics of electrons [287], for example. Theoretically, shot noise has been mostly investigated in mesoscopic systems under dc-bias voltage. If the charge current is conserved, only current correlation at the same contact (auto-correlation noise) or between different contacts (cross-correlation noise) is needed to describe the shot noise of the system with two probes [130]. The cross-correlations take negative definite values for fermions [140, 288]. Noise of charge current has been investigated using e.g., nonequilibrium Green’s function method [133, 134, 136, 139], scattering matrix theory [130], equation of motion method [289], and Floquet master equation approach [33].

In the domain of spin transport it is interesting to investigate the noise properties, as the discrete nature of electron spin leads to the correlations between spin-carrying particles. The spin current is usually a nonconserved quantity difficult to measure, and its shot noise depends on spin-flip processes leading to the spin-current correlations with opposite spins [290–292]. Consequently, in order to investigate the shot noise of spin current, one needs to study both auto-correlations and cross-correlations. The investigation of the spin-dependent scattering, spin accumulation [293] and attractive or repulsive interactions in mesoscopic systems can be obtained using shot noise of spin current [294], as well as measuring the spin relaxation time [290, 294]. One should mention that even in the absence of charge current, a nonzero spin current and its noise can emerge [292, 295, 296]. Several works have studied shot noise of spin current using e.g., nonequilibrium Green’s functions method and scattering matrix theory [292, 297–299].

It was demonstrated that the magnetization noise originates from transferred spin current noise via a fluctuating spin-transfer torque in ferromagnetic-normal-ferromagnetic systems [300], and magnetic tunnel junctions [215]. Quantum noise generated from the scatterings between the magnetization of a nanomagnet and

spin-polarized electrons has been shown as well [301, 302]. The shot noise of spin-transfer torque has been recently studied using a magnetic quantum dot connected to two noncollinear magnetic contacts [299]. According to the definition of the spin-transfer torque, both auto-correlations and cross-correlations of the spin-current components contribute to the spin-torque noise.

In this chapter we theoretically study noise of charge and spin currents and spin-transfer torque in a tunnel junction through which transport occurs via a single electronic energy level, in the presence of a molecular magnet in a constant magnetic field, connected to two normal metallic leads. The spin of the molecular magnet precesses around the magnetic field with Larmor frequency. Its precession is kept undamped by external sources. The electronic level may belong to a neighboring quantum dot or it may be an orbital of the molecular magnet itself. The electronic level and the molecular spin are coupled via exchange interaction. We derive expressions for the noise components using the Keldysh nonequilibrium Green's functions formalism. The noise of charge current is contributed by both elastic processes driven by the bias voltage, and inelastic tunneling processes driven by the molecular spin precession. We observe dip-like features in the shot noise due to inelastic tunneling processes and destructive quantum interference between electron transport channels involved in the spin-flip processes. The driving mechanism of the correlations of the spin-torque components in the same spatial direction involves both precession of the molecular spin and the bias-voltage. Hence, they are contributed by elastic and inelastic processes, with the change of energy equal to one or two Larmor frequencies. The nonzero correlations of the perpendicular spin-torque components are driven by the molecular spin precession, with contributions of spin-flip tunneling processes only. These components are related to the previously obtained Gilbert damping coefficient at zero temperature.

The chapter is organized as follows. The model and theoretical framework based on the Keldysh nonequilibrium Green's functions formalism[45, 46, 220] are given in Sec. 5.2. Here we derive expressions for the noise of spin and charge currents. In Sec. 5.3 we investigate and analyze the properties of the charge-current shot noise. This section is followed by Sec. 5.4 in which we derive and analyze the noise of spin-transfer torque. The conclusions are given in Sec. 5.5.

5.2 Model and theoretical framework

We use the model with a precessing molecular spin, where the system is subjected to a dc-bias voltage, which was thoroughly described in Sec. 3.3. Here we assume that the interaction between the spin of the itinerant electrons and the

precessing component of the molecular magnetization presented by the Hamiltonian $\hat{H}'(t)$ is strong enough to be treated exactly, i.e., we do not neglect nonlinear terms in γ . For the sake of clarity we repeat the Hamiltonian of the system,

$$\hat{H}(t) = \sum_{\xi \in \{L, R\}} \hat{H}_\xi + \hat{H}_T + \hat{H}_D(t) + \hat{H}_S, \quad (5.1)$$

where

$$\hat{H}_\xi = \sum_{k, \sigma} \epsilon_{k\xi} \hat{c}_{k\sigma\xi}^\dagger \hat{c}_{k\sigma\xi} \quad (5.2)$$

is the Hamiltonian of lead $\xi = L, R$. The tunneling Hamiltonian is given by

$$\hat{H}_T = \sum_{k, \sigma, \xi} [V_{k\xi} \hat{c}_{k\sigma\xi}^\dagger \hat{d}_\sigma + V_{k\xi}^* \hat{d}_\sigma^\dagger \hat{c}_{k\sigma\xi}], \quad (5.3)$$

while the Hamiltonian of the electronic level equals

$$\hat{H}_D(t) = \sum_{\sigma} \epsilon_0 \hat{d}_\sigma^\dagger \hat{d}_\sigma + g\mu_B \hat{s} \vec{B} + J \hat{s} \vec{S}(t). \quad (5.4)$$

The Hamiltonian of the molecular spin \vec{S} in the magnetic field $\vec{B} = B\vec{e}_z$ is given by

$$\hat{H}_S = g\mu_B \vec{S} \vec{B}. \quad (5.5)$$

The dynamics of the molecular spin, which we treat as a classical variable can be written as $\vec{S}(t) = S_\perp \cos(\omega_L t) \vec{e}_x + S_\perp \sin(\omega_L t) \vec{e}_y + S_z \vec{e}_z$, where $S_\perp = S \sin(\theta)$ is the magnitude of the instantaneous projection of $\vec{S}(t)$ onto the xy plane, while z component equals $S_z = S \cos(\theta)$, with θ the tilt angle between \vec{B} and \vec{S} , and $\omega_L = g\mu_B B$ the Larmor frequency.

The charge and spin current operator of the lead ξ is given by the Heisenberg equation [45, 46]

$$\hat{I}_{\xi\nu}(t) = q_\nu \frac{d\hat{N}_{\xi\nu}}{dt} = q_\nu \frac{i}{\hbar} [\hat{H}, \hat{N}_{\xi\nu}], \quad (5.6)$$

where $[,]$ denotes the commutator, while $\hat{N}_{L\nu} = \sum_{k, \sigma, \sigma'} \hat{c}_{k\sigma L}^\dagger (\sigma_\nu)_{\sigma\sigma'} \hat{c}_{k\sigma' L}$ is the charge ($\nu = 0$ and $q_0 = -e$) and spin ($\nu = x, y, z$ and $q_{\nu \neq 0} = \hbar/2$) occupation number operator of the contact ξ . Taking into account that only the tunneling Hamiltonian \hat{H}_T generates a nonzero commutator in Eq. (5.6), the current operator $\hat{I}_{\xi\nu}(t)$ can be expressed as

$$\hat{I}_{\xi\nu}(t) = -q_\nu \frac{i}{\hbar} \sum_{\sigma, \sigma'} (\sigma_\nu)_{\sigma\sigma'} \hat{I}_{\xi, \sigma\sigma'}(t), \quad (5.7)$$

where the operator component $\hat{I}_{\xi,\sigma\sigma'}(t)$ equals

$$\hat{I}_{\xi,\sigma\sigma'}(t) = \sum_k [V_{k\xi} \hat{c}_{k\sigma\xi}^\dagger(t) \hat{d}_{\sigma'}(t) - V_{k\xi}^* \hat{d}_{\sigma'}^\dagger(t) \hat{c}_{k\sigma\xi}(t)]. \quad (5.8)$$

The nonsymmetrized noise of charge and spin current is defined as the correlation between fluctuations of currents $I_{\xi\nu}$ and $I_{\zeta\mu}$ [46, 130],

$$S_{\xi\zeta}^{\nu\mu}(t, t') = \langle \delta \hat{I}_{\xi\nu}(t) \delta \hat{I}_{\zeta\mu}(t') \rangle, \quad (5.9)$$

with $\nu = \mu = 0$ for the charge current noise. The fluctuation operator of the charge and spin current in lead ξ is given by

$$\delta \hat{I}_{\xi\nu}(t) = \hat{I}_{\xi\nu}(t) - \langle \hat{I}_{\xi\nu}(t) \rangle. \quad (5.10)$$

Using Eqs. (5.7) and (5.10), the noise becomes

$$S_{\xi\zeta}^{\nu\mu}(t, t') = -\frac{q_\nu q_\mu}{\hbar^2} \sum_{\sigma\sigma'} \sum_{\lambda\eta} (\sigma_\nu)_{\sigma\sigma'} (\sigma_\mu)_{\lambda\eta} S_{\xi\zeta}^{\sigma\sigma',\lambda\eta}(t, t'), \quad (5.11)$$

where $S_{\xi\zeta}^{\sigma\sigma',\lambda\eta}(t, t') = \langle \delta \hat{I}_{\xi,\sigma\sigma'}(t) \delta \hat{I}_{\zeta,\lambda\eta}(t') \rangle$. The correlation functions $S_{\xi\zeta}^{\sigma\sigma',\lambda\eta}(t, t')$ can be expressed by means of the Wick's theorem [117] as

$$\begin{aligned} S_{\xi\zeta}^{\sigma\sigma',\lambda\eta}(t, t') &= \sum_{kk'} [V_{k\xi} V_{k'\zeta} G_{\sigma',k'\lambda\zeta}^>(t, t') G_{\eta,k\sigma\xi}^<(t', t) \\ &\quad - V_{k\xi} V_{k'\zeta}^* G_{\sigma',\lambda}^>(t, t') G_{k'\eta\zeta,k\sigma\xi}^<(t', t) \\ &\quad - V_{k\xi}^* V_{k'\zeta} G_{k\sigma\xi,k'\lambda\zeta}^>(t, t') G_{\eta\sigma}^<(t', t) \\ &\quad + V_{k\xi}^* V_{k'\zeta} G_{k\sigma\xi,\lambda}^>(t, t') G_{k'\eta\zeta,\sigma}^<(t', t)], \end{aligned} \quad (5.12)$$

with the mixed Green's functions defined as

$$G_{\eta,k\sigma\xi}^<(t, t') = i \langle \hat{c}_{k\sigma\xi}^\dagger(t') \hat{d}_\eta(t) \rangle, \quad (5.13)$$

$$G_{\sigma',k'\lambda\zeta}^>(t, t') = -i \langle \hat{d}_{\sigma'}(t) \hat{c}_{k'\lambda\zeta}^\dagger(t') \rangle, \quad (5.14)$$

while $G_{k\sigma\xi,\eta}^<(t, t') = -[G_{\eta,k\sigma\xi}^<(t', t)]^*$ and $G_{k'\lambda\zeta,\sigma'}^>(t, t') = -[G_{\sigma',k'\lambda\zeta}^>(t', t)]^*$. The Green's functions of the leads and the central region are defined as

$$G_{k\sigma\xi,k'\sigma'\zeta}^<(t, t') = i \langle \hat{c}_{k'\sigma'\zeta}^\dagger(t') \hat{c}_{k\sigma\xi}(t) \rangle, \quad (5.15)$$

$$G_{k\sigma\xi,k'\sigma'\zeta}^>(t, t') = -i \langle \hat{c}_{k\sigma\xi}(t) \hat{c}_{k'\sigma'\zeta}^\dagger(t') \rangle, \quad (5.16)$$

$$G_{\sigma\sigma'}^<(t, t') = i \langle \hat{d}_{\sigma'}^\dagger(t') \hat{d}_\sigma(t) \rangle, \quad (5.17)$$

$$G_{\sigma\sigma'}^>(t, t') = -i \langle \hat{d}_\sigma(t) \hat{d}_{\sigma'}^\dagger(t') \rangle. \quad (5.18)$$

Since the self-energies originating from the coupling between the electronic level and the lead ξ are diagonal in the electron spin space, their equal diagonal elements can be written as $\Sigma_{\xi}^{<, >, r, a}(t, t')$. Taking into account that the mixed Green's functions can be expressed in terms of Green's functions of the leads and the central region using Langreth analytical continuation rules, Eq. (5.12) transforms into

$$\begin{aligned}
S_{\xi\zeta}^{\sigma\sigma', \lambda\eta}(t, t') = & \int dt_1 \int dt_2 \{ [G_{\sigma'\lambda}^r(t, t_1)\Sigma_{\zeta}^>(t_1, t') + G_{\sigma'\lambda}^>(t, t_1)\Sigma_{\zeta}^a(t_1, t')] \\
& \times [G_{\eta\sigma}^r(t', t_2)\Sigma_{\xi}^<(t_2, t) + G_{\eta\sigma}^<(t', t_2)\Sigma_{\xi}^a(t_2, t)] \\
& + [\Sigma_{\xi}^>(t, t_1)G_{\sigma'\lambda}^a(t_1, t') + \Sigma_{\xi}^r(t, t_1)G_{\sigma'\lambda}^>(t_1, t')] \\
& \times [\Sigma_{\zeta}^<(t', t_2)G_{\eta\sigma}^a(t_2, t) + \Sigma_{\zeta}^r(t', t_2)G_{\eta\sigma}^<(t_2, t)] \\
& - G_{\sigma'\lambda}^>(t, t')[\Sigma_{\zeta}^r(t', t_1)G_{\eta\sigma}^r(t_1, t_2)\Sigma_{\xi}^<(t_2, t) + \Sigma_{\zeta}^<(t', t_1)G_{\eta\sigma}^a(t_1, t_2)\Sigma_{\xi}^a(t_2, t) \\
& + \Sigma_{\zeta}^r(t', t_1)G_{\eta\sigma}^<(t_1, t_2)\Sigma_{\xi}^a(t_2, t)] \\
& - [\Sigma_{\xi}^r(t, t_1)G_{\sigma'\lambda}^r(t_1, t_2)\Sigma_{\zeta}^>(t_2, t') + \Sigma_{\xi}^>(t, t_1)G_{\sigma'\lambda}^a(t_1, t_2)\Sigma_{\zeta}^a(t_2, t')] \\
& + \Sigma_{\xi}^r(t, t_1)G_{\sigma'\lambda}^>(t_1, t_2)\Sigma_{\zeta}^a(t_2, t')]G_{\eta\sigma}^<(t', t) \} \\
& - \delta_{\xi\zeta}[\delta_{\eta\sigma}G_{\sigma'\lambda}^>(t, t')\Sigma_{\xi}^<(t', t) + \delta_{\sigma'\lambda}\Sigma_{\xi}^>(t, t')G_{\eta\sigma}^<(t', t)]. \tag{5.19}
\end{aligned}$$

Using Fourier transformations of the central-region Green's functions and self-energies in the wide-band limit, the correlations given by Eq. (5.19) can be further simplified. Detailed expression for correlations $S_{\xi\zeta}^{\sigma\sigma', \lambda\eta}(t, t')$ and their Fourier transforms can be found in Appendix B. Some correlation functions are not just functions of time difference $t - t'$. Thus, similarly as in [303] we used Wigner representation assuming that in experiments fluctuations are measured on timescales much larger than the driving period $\mathcal{T} = 2\pi/\omega_L$, which is the period of one molecular spin precession. The Wigner coordinates are given by $T' = (t + t')/2$ and $\tau = t - t'$, while the correlation functions are defined as

$$S_{\xi\zeta}^{\sigma\sigma', \lambda\eta}(\tau) = \frac{1}{\mathcal{T}} \int_0^{\mathcal{T}} dt \langle \delta \hat{I}_{\xi, \sigma\sigma'}(t + \tau) \delta \hat{I}_{\zeta, \lambda\eta}(t) \rangle. \tag{5.20}$$

The Fourier transform of $S_{\xi\zeta}^{\sigma\sigma', \lambda\eta}(\tau)$ can be written as

$$S_{\xi\zeta}^{\sigma\sigma', \lambda\eta}(\Omega, \Omega') = 2\pi\delta(\Omega - \Omega')S_{\xi\zeta}^{\sigma\sigma', \lambda\eta}(\Omega), \tag{5.21}$$

where

$$S_{\xi\zeta}^{\sigma\sigma', \lambda\eta}(\Omega) = \int d\tau e^{i\Omega\tau} S_{\xi\zeta}^{\sigma\sigma', \lambda\eta}(\tau). \tag{5.22}$$

For the correlations which depend only on $t - t'$, the Wigner representation is identical to the standard representation.

Finally, using Eqs. (5.11) and (5.19), the formal expression for the nonsymmetrized noise of charge and spin currents in standard coordinates t and t' can be obtained as

$$\begin{aligned}
S_{\xi\xi}^{\nu\mu}(t, t') = & -\frac{q_\nu q_\mu}{\hbar^2} \text{Tr} \left\{ \int dt_1 \int dt_2 \left\{ \hat{\sigma}_\nu [\hat{G}^r(t, t_1) \hat{\Sigma}_\xi^>(t_1, t') + \hat{G}^>(t, t_1) \hat{\Sigma}_\xi^a(t_1, t')] \right. \right. \\
& \times \hat{\sigma}_\mu [\hat{G}^r(t', t_2) \hat{\Sigma}_\xi^<(t_2, t) + \hat{G}^<(t', t_2) \hat{\Sigma}_\xi^a(t_2, t)] \\
& + \hat{\sigma}_\nu [\hat{\Sigma}_\xi^>(t, t_1) \hat{G}^a(t_1, t') + \hat{\Sigma}_\xi^r(t, t_1) \hat{G}^>(t_1, t')] \\
& \times \hat{\sigma}_\mu [\hat{\Sigma}_\xi^<(t', t_2) \hat{G}^a(t_2, t) + \hat{\Sigma}_\xi^r(t', t_2) \hat{G}^<(t_2, t)] \\
& - \hat{\sigma}_\nu \hat{G}^>(t, t') \hat{\sigma}_\mu [\hat{\Sigma}_\xi^r(t', t_1) \hat{G}^r(t_1, t_2) \hat{\Sigma}_\xi^<(t_2, t) + \hat{\Sigma}_\xi^<(t', t_1) \hat{G}^a(t_1, t_2) \hat{\Sigma}_\xi^a(t_2, t) \\
& + \hat{\Sigma}_\xi^r(t', t_1) \hat{G}^<(t_1, t_2) \hat{\Sigma}_\xi^a(t_2, t)] \\
& - \hat{\sigma}_\nu [\hat{\Sigma}_\xi^r(t, t_1) \hat{G}^r(t_1, t_2) \hat{\Sigma}_\xi^>(t_2, t') + \hat{\Sigma}_\xi^>(t, t_1) \hat{G}^a(t_1, t_2) \hat{\Sigma}_\xi^a(t_2, t')] \\
& + \hat{\Sigma}_\xi^r(t, t_1) \hat{G}^>(t_1, t_2) \hat{\Sigma}_\xi^a(t_2, t') \hat{\sigma}_\mu \hat{G}^<(t', t) \left. \right\} \\
& - \delta_{\xi\xi} \hat{\sigma}_\nu [\hat{G}^>(t, t') \hat{\sigma}_\mu \hat{\Sigma}_\xi^<(t', t) + \hat{\Sigma}_\xi^>(t, t') \hat{\sigma}_\mu \hat{G}^<(t', t)] \left. \right\}, \tag{5.23}
\end{aligned}$$

where Tr denotes the trace in the electronic spin space.

The symmetrized noise of charge and spin currents reads [46, 130]

$$S_{\xi\xi S}^{\nu\mu}(t, t') = \frac{1}{2} \langle \{ \delta \hat{I}_{\xi\nu}(t), \delta \hat{I}_{\xi\mu}(t') \} \rangle, \tag{5.24}$$

where $\{, \}$ denotes the anticommutator. According to Eqs. (5.11), (5.20), (5.22) and (5.24), in the Wigner representation the nonsymmetrized noise spectrum reads

$$\begin{aligned}
S_{\xi\xi}^{\nu\mu}(\Omega) &= \int d\tau e^{i\Omega\tau} S_{\xi\xi}^{\nu\mu}(\tau) \\
&= \int d\tau e^{i\Omega\tau} \frac{1}{\mathcal{T}} \int_0^{\mathcal{T}} dt \langle \delta \hat{I}_{\xi\nu}(t + \tau) \delta \hat{I}_{\xi\mu}(t) \rangle \\
&= -\frac{q_\nu q_\mu}{\hbar^2} \sum_{\sigma\sigma'} \sum_{\lambda\eta} (\sigma_\nu)_{\sigma\sigma'} (\sigma_\mu)_{\lambda\eta} S_{\xi\xi}^{\sigma\sigma', \lambda\eta}(\Omega), \tag{5.25}
\end{aligned}$$

while the symmetrized noise spectrum equals

$$\begin{aligned}
S_{\xi\xi S}^{\nu\mu}(\Omega) &= \frac{1}{2} [S_{\xi\xi}^{\nu\mu}(\Omega) + S_{\xi\xi}^{\mu\nu}(-\Omega)] \\
&= -\frac{q_\nu q_\mu}{2\hbar^2} \sum_{\sigma\sigma'} \sum_{\lambda\eta} (\sigma_\nu)_{\sigma\sigma'} (\sigma_\mu)_{\lambda\eta} S_{\xi\xi S}^{\sigma\sigma', \lambda\eta}(\Omega), \tag{5.26}
\end{aligned}$$

where $S_{\xi\xi S}^{\sigma\sigma', \lambda\eta}(\Omega) = [S_{\xi\xi}^{\sigma\sigma', \lambda\eta}(\Omega) + S_{\xi\xi}^{\lambda\eta, \sigma\sigma'}(-\Omega)]/2$. It is of experimental interest to investigate zero-frequency noise power. The expressions for the zero-frequency noise power of both charge and spin current components, $S_{\xi\xi S}^{\nu\mu}(\Omega = 0)$, can be found in Appendix B.

5.3 Shot noise of charge current

For the charge current noise it is convenient to drop superscripts $\nu = \mu = 0$. The charge current noise spectrum can be obtained as [294]

$$S_{\xi\xi}(\Omega) = -\frac{e^2}{\hbar^2} [S_{\xi\xi}^{11,11}(\Omega) + S_{\xi\xi}^{11,22}(\Omega) + S_{\xi\xi}^{22,11}(\Omega) + S_{\xi\xi}^{22,22}(\Omega)]. \quad (5.27)$$

In this section we analyze the zero-frequency noise power of the charge current $S_{\xi\xi} = S_{\xi\xi}(0) = S_{\xi\xi S}(0)$ at zero temperature. Taking into account that thermal noise disappears at zero temperature, the only contribution to the noise comes from the shot noise. We consider symmetric coupling between the molecular orbital and the leads in the wide-band limit $\Gamma_L = \Gamma_R = \Gamma/2$.

The charge current from lead ξ can be expressed as

$$I_\xi = \frac{e\Gamma_\xi\Gamma_\zeta}{\hbar} \int \frac{d\epsilon}{2\pi} [f_\xi(\epsilon) - f_\zeta(\epsilon)] \times [|G_{11}^{r\delta}(\epsilon)|^2 + |G_{12}^{r\delta}(\epsilon)|^2 + |G_{21}^{r\delta}(\epsilon)|^2 + |G_{22}^{r\delta}(\epsilon)|^2], \quad (5.28)$$

where $\xi \neq \zeta$, with complex functions $G_{11}^{r\delta}(\epsilon)$, $G_{12}^{r\delta}(\epsilon)$, $G_{21}^{r\delta}(\epsilon)$ and $G_{22}^{r\delta}(\epsilon)$ defined in Appendix B. The charge current conservation implies that the auto-correlation noise power $S_{LL}(0)$ and cross-correlation noise power $S_{LR}(0)$ satisfy the relation $S_{LL}(0) + S_{LR}(0) = 0$. Thus, it is sufficient to study only one correlation function.

Tuning the parameters in the system such as the tilt angle θ , the dc-bias voltage $eV = \mu_L - \mu_R$, where μ_L and μ_R are the chemical potentials of the leads, and \vec{B} , the shot noise can be controlled and minimized. In Fig. 5.1(a) we present the average charge current as a staircase function of bias voltage, where the bias is varied in four different ways. Each step corresponds to a new available transport channel. The transport channels are located at the Floquet quasienergies $\epsilon_1 = \epsilon_0 - (\omega_L/2) - (JS/2)$, $\epsilon_2 = \epsilon_0 + (\omega_L/2) - (JS/2)$, $\epsilon_3 = \epsilon_0 - (\omega_L/2) + (JS/2)$, and $\epsilon_4 = \epsilon_0 + (\omega_L/2) + (JS/2)$ (see Appendix A).

In the presence of the external magnetic field and the precessing molecular spin, the initially degenerate electronic level with energy ϵ_0 results in four nondegenerate transport channels, which has an important influence on the noise. The precessing molecular spin helps incoming electrons to jump into the higher levels, absorbing an energy quantum ω_L . Due to photon absorption and emission processes the shot noise can be nonzero even if the average charge current is zero. The correlated current fluctuations give nonzero noise power. The tunneling of electrons followed by photon absorption lead to the novel features in the noise. Elastic tunneling contributes to the sub-Poissonian Fano factor around resonances and competes with the spin-flip events caused by the molecular spin precession. The resulting noise is

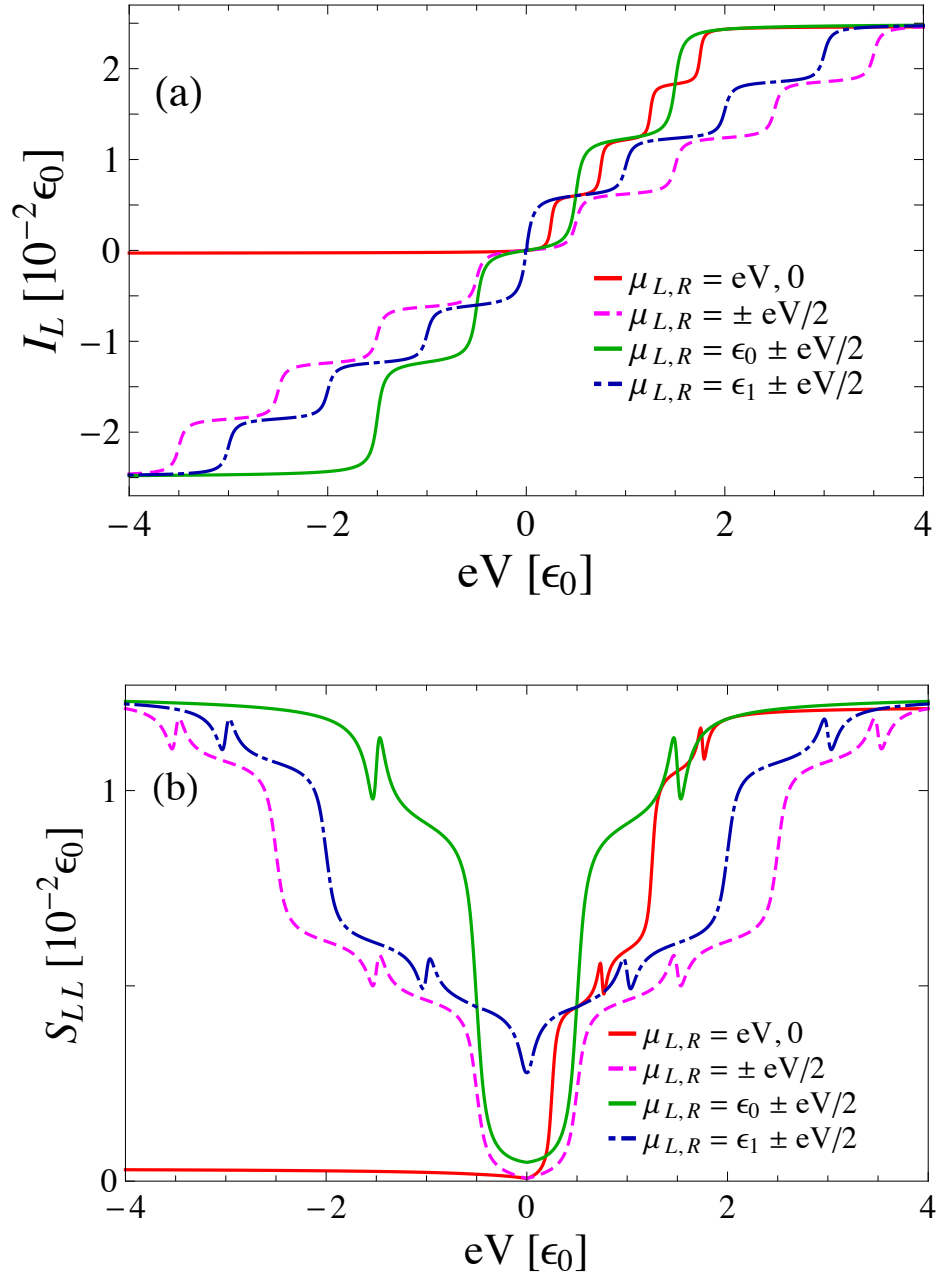


FIGURE 5.1: (a) Charge current I_L and (b) auto-correlation shot noise S_{LL} as functions of bias-voltage eV . All plots are obtained at zero temperature, with $\vec{B} = B\vec{e}_z$. The other parameters are: $\Gamma_L = \Gamma_R = \Gamma/2$, $\Gamma = 0.05 \epsilon_0$, $\omega_L = 0.5 \epsilon_0$, $J = 0.01 \epsilon_0$, $S = 100$, and $\theta = \pi/2$. The molecular quasienergy levels are located at: $\epsilon_1 = 0.25 \epsilon_0$, $\epsilon_2 = 0.75 \epsilon_0$, $\epsilon_3 = 1.25 \epsilon_0$, and $\epsilon_4 = 1.75 \epsilon_0$.

presented in Fig. 5.1(b). The noise power shows the molecular quasienergy spectrum and each step or dip-like feature in the noise denotes the energy of a new available transport channel. The noise has two steps and two dip-like features which correspond to these resonances. Charge current and noise power are saturated for large bias voltages. The Fano factor is depicted in Fig. 5.2. Due to the absorption (emission) processes [227] and quantum interference effect the Fano factor is a deformed step-like function, where each step corresponds to a resonance.

If the Fermi levels of the leads lie below the resonances, the shot noise approaches zero for $eV \rightarrow 0$ [red and dashed pink lines in Fig. 5.1(b)]. This is due to the fact that a small number of electron states can participate in transport inside this small bias window and both current and noise are close to 0. If the bias voltage is varied with respect to the resonant energy ϵ_1 such that $\mu_{L,R} = \epsilon_1 \pm eV/2$ [dot-dashed blue line in Fig. 5.1(b)], we observe a valley at zero bias, which corresponds to $\mu_L = \mu_R = \epsilon_1$. As $eV = 0$ the net tunneling current is zero, but the precession-assisted inelastic processes, involving absorption of an energy quantum ω_L give rise to the noise here. If the bias-voltage is varied with respect to ϵ_0 such that $\mu_{L,R} = \epsilon_0 \pm eV/2$ [green line in Fig. 5.1(b)], at $eV = 0$ the inelastic processes involving absorption of an energy quantum ω_L give nonzero noise power. Thus, for $eV \rightarrow 0$ the Fano factor $F \gg 1$ indicating that the noise is super Poissonian. In this regime electrons can absorb emitted energy quantum ω_L and occupy energy level with higher energy. As the bias voltage is increased, the noise is enhanced since the number of the correlated electron pairs increases with the increase of the Fermi level. For larger bias, due to the absorption and emission of an energy ω_L , electrons can jump to a level with higher energy or lower level during the transport, and the Fano factor $F < 1$ indicating the sub-Poissonian noise.

Around resonances $\mu_{L,R} = \epsilon_i$, $i = 1, 2, 3, 4$, the probability of transmission is very high, resulting in the small Fano factor. However, if the resonant quasienergy levels are much higher than the Fermi energy of the leads, the probability of transmission is very low and the Fano factor is close to 1 as shown in Fig. 5.2 (red line). This means that the stochastic processes are uncorrelated. If the two levels connected with the inelastic photon emission (absorption) tunnel processes, or all four levels, lie between the Fermi levels of the leads, the Fano factor approaches $1/2$, which is in agreement with [304]. For $eV = \epsilon_3$ [see Fig. 5.2 (red line)] a spin down electron can tunnel elastically, or inelastically in a spin-flip process leading to the increase of the Fano factor. Spin-flip processes increase electron traveling time, leading to sub-Poissonian noise. Pauli exclusion principle also leads to sub-Poissonian noise, since it prevents the double occupancy of a level.

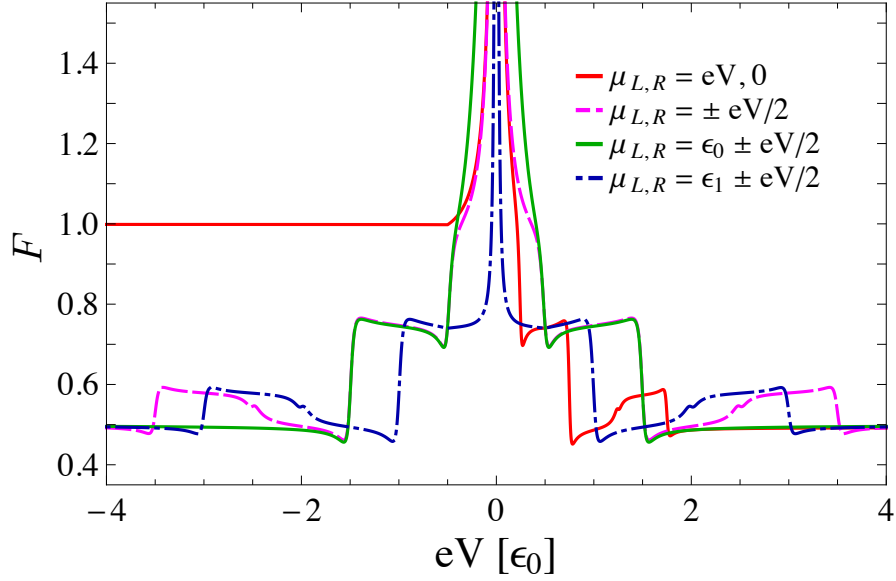


FIGURE 5.2: Fano factor F as a function of bias-voltage eV . All plots are obtained at zero temperature, with $\vec{B} = B\vec{e}_z$. The other parameters are set to: $\Gamma = 0.05 \epsilon_0$, $\Gamma_L = \Gamma_R = \Gamma/2$, $\omega_L = 0.5 \epsilon_0$, $J = 0.01 \epsilon_0$, $S = 100$, and $\theta = \pi/2$. The positions of the molecular quasienergy levels are: $\epsilon_1 = 0.25 \epsilon_0$, $\epsilon_2 = 0.75 \epsilon_0$, $\epsilon_3 = 1.25 \epsilon_0$, and $\epsilon_4 = 1.75 \epsilon_0$.

The precessing molecular spin induces interference between electron states connected with spin-flip processes. The dip-like features in the noise power are present due to the destructive interference effect between the transport channels connected with spin-flip events and the change of energy by one energy quantum ω_L , i.e., between levels with energies ϵ_1 and $\epsilon_2 = \epsilon_1 + \omega_L$, or ϵ_3 and $\epsilon_4 = \epsilon_3 + \omega_L$. When one or both pairs of the levels connected with spin-flip events enter the bias-voltage window, then an electron from the left lead can tunnel through both levels via elastic or inelastic spin-flip processes. Different tunneling pathways ending in the final state with the same energy, destructively interfere, similarly as in the Fano effect [277], leading to a dip in the noise power. Namely, the state with lower energy, ϵ_1 (or ϵ_3) mimics the discrete state in the Fano effect. An electron tunnels into the state ϵ_1 (or ϵ_3), undergoes a spin-flip and absorbs an energy quantum ω_L . The other state with energy ϵ_2 (or ϵ_4) is an analog of the continuum in the Fano effect, and the electron tunnels elastically through this level. These two tunneling processes, one elastic and the other inelastic interfere, leading to a dip in the noise power. This is presented in Fig. 5.3 where we observe a distinct dip due to the quantum interference effect for $\omega_L = 0.5 \epsilon_0$, which corresponds to $\mu_L = \epsilon_2$ and $\mu_R = \epsilon_1$. The other two steps occur when the Fermi energy of the right or left lead

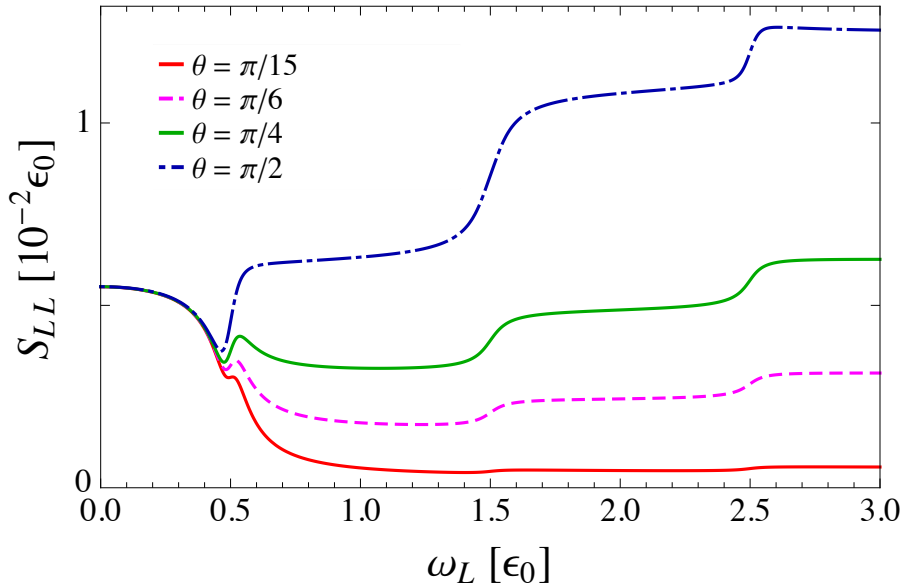


FIGURE 5.3: Shot noise of charge current S_{LL} as a function of the Larmor frequency ω_L , for different tilt angles θ , with $\vec{B} = B\vec{e}_z$, at zero temperature. The other parameters are: $\Gamma = 0.05 \epsilon_0$, $\Gamma_L = \Gamma_R = \Gamma/2$, $\mu_L = 0.75 \epsilon_0$, $\mu_R = 0.25 \epsilon_0$, $J = 0.01 \epsilon_0$, and $S = 100$. For $\omega_L = \mu_L - \mu_R$ we observe a dip due to destructive quantum interference.

is in resonance with one of the quasienergy levels. The magnitude of the precessing component of the molecular spin, which induces spin-flip processes between molecular quasienergy levels, equals $JS \sin(\theta)/2$. Therefore, the dip increases with the increase of the tilt angle θ , and is maximal for $\theta = \pi/2$. Quantum interference effects manifest themselves in the form of dip-like features in Fig. 5.1(b). If we vary, for instance, the bias-voltage as $eV = \mu_L$, where $\mu_R = 0$ (red line), we observe dip-like features for $eV = \epsilon_2$ and $eV = \epsilon_4$, i.e., when one or both pairs of the levels which are connected with spin-flip events enter the bias-voltage window.

Finally, in Fig. 5.4 we plotted the noise power of charge current S_{LL} as a function of $\mu = \mu_L = \mu_R$ at zero temperature. It shows nonmonotonic dependence on the tunneling rates Γ . Here, for small Γ (red line) the noise is increased if μ is positioned between levels connected with spin-flip events, and is contributed only by absorption processes of an energy quantum ω_L , as we vary the chemical potentials. For larger Γ (green line), the charge current noise is increased since levels broaden and overlap, and more electrons can tunnel through them. With further increase of Γ (dotted blue line) the noise starts to decrease, and it is finally suppressed for $\Gamma \gg \omega_L$, since a current-carrying electron sees the molecular spin as nearly static in this case, leading to the reduction of the inelastic spin-flip processes.

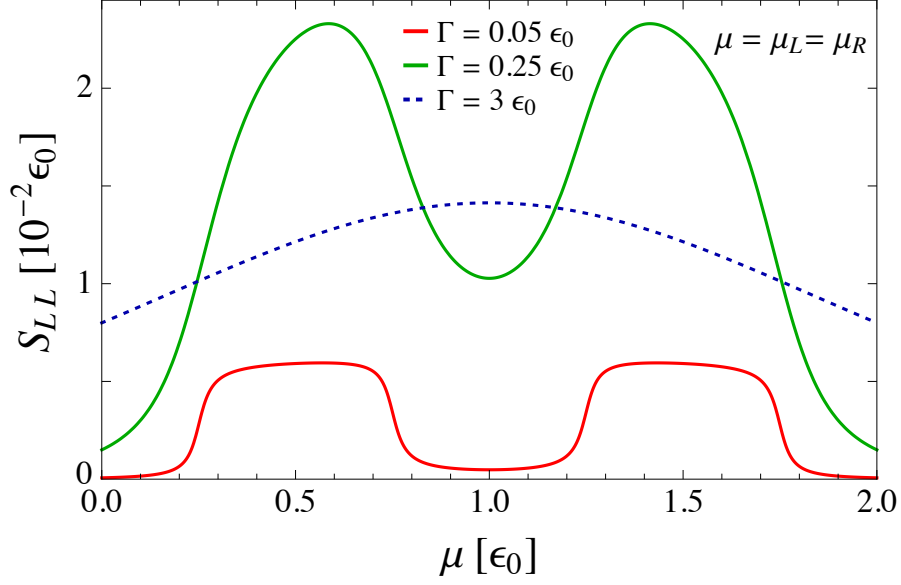


FIGURE 5.4: Shot noise of charge current S_{LL} as a function of the chemical potential of the leads $\mu = \mu_L = \mu_R$, with $\vec{B} = B\vec{e}_z$, for three different couplings Γ , where $\Gamma_L = \Gamma_R = \Gamma/2$, at zero temperature. The other parameters are: $\omega_L = 0.5\epsilon_0$, $J = 0.01\epsilon_0$, $S = 100$, and $\theta = \pi/2$. The molecular quasienergy levels are positioned at: $\epsilon_1 = 0.25\epsilon_0$, $\epsilon_2 = 0.75\epsilon_0$, $\epsilon_3 = 1.25\epsilon_0$, and $\epsilon_4 = 1.75\epsilon_0$.

5.4 Shot noise of spin current and spin-transfer torque

In this section we present the spin-current noise-spectrum components and relations between them. Later we introduce the noise of spin-transfer torque and investigate the zero-frequency spin-torque shot noise at zero temperature. The components of the nonsymmetrized spin-current noise spectrum read

$$S_{\xi\xi}^{xx}(\Omega) = -\frac{1}{4}[S_{\xi\xi}^{12,21}(\Omega) + S_{\xi\xi}^{21,12}(\Omega)], \quad (5.29)$$

$$S_{\xi\xi}^{xy}(\Omega) = -\frac{i}{4}[S_{\xi\xi}^{12,21}(\Omega) - S_{\xi\xi}^{21,12}(\Omega)], \quad (5.30)$$

$$S_{\xi\xi}^{zz}(\Omega) = -\frac{1}{4}[S_{\xi\xi}^{11,11}(\Omega) - S_{\xi\xi}^{11,22}(\Omega) - S_{\xi\xi}^{22,11}(\Omega) + S_{\xi\xi}^{22,22}(\Omega)], \quad (5.31)$$

where Eq. (5.31) denotes the noise of the z component of the spin current [292, 294]. Since the polarization of the spin current precesses in the xy plane, the remaining components of the spin-current noise spectrum satisfy the following

relations:

$$S_{\xi\zeta}^{yy}(\Omega) = S_{\xi\zeta}^{xx}(\Omega), \quad (5.32)$$

$$S_{\xi\zeta}^{yx}(\Omega) = -S_{\xi\zeta}^{xy}(\Omega), \quad (5.33)$$

$$S_{\xi\zeta}^{xz}(\Omega) = S_{\xi\zeta}^{zx}(\Omega) = S_{\xi\zeta}^{yz}(\Omega) = S_{\xi\zeta}^{zy}(\Omega) = 0. \quad (5.34)$$

Taking into account that the spin current is not a conserved quantity, it is important to notice that the complete information from the noise spectrum can be obtained by studying both auto-correlation noise spectrum $S_{\xi\xi}^{jk}(\Omega)$ and cross-correlation noise spectrum $S_{\xi\zeta}^{jk}(\Omega)$, $\zeta \neq \xi$. Therefore, it is more convenient to investigate the spin-torque noise spectrum, where both auto-correlation and cross-correlation noise components of spin currents are included. The spin-transfer torque operator can be defined as

$$\hat{T}_j = -(\hat{I}_{Lj} + \hat{I}_{Rj}), \quad j = x, y, z; \quad (5.35)$$

while its fluctuation reads

$$\delta\hat{T}_j(t) = -[\delta\hat{I}_{Lj}(t) + \delta\hat{I}_{Rj}(t)]. \quad (5.36)$$

Accordingly, the nonsymmetrized and symmetrized spin-torque noise can be obtained using the spin-current noise components as

$$\begin{aligned} S_T^{jk}(t, t') &= \langle \delta\hat{T}_j(t) \delta\hat{T}_k(t') \rangle \\ &= \sum_{\xi\zeta} S_{\xi\zeta}^{jk}(t, t'), \quad j, k = x, y, z; \end{aligned} \quad (5.37)$$

$$S_{TS}^{jk}(t, t') = \frac{1}{2}[S_T^{jk}(t, t') + S_T^{kj}(t', t)], \quad (5.38)$$

with the corresponding noise spectrums given by

$$S_T^{jk}(\Omega) = \sum_{\xi\zeta} S_{\xi\zeta}^{jk}(\Omega), \quad (5.39)$$

$$S_{TS}^{jk}(\Omega) = \sum_{\xi\zeta} S_{\xi\zeta S}^{jk}(\Omega). \quad (5.40)$$

According to Eqs. (5.32), (5.33), and (5.39), $S_T^{xx}(\Omega) = S_T^{yy}(\Omega)$ and $S_T^{yx}(\Omega) = -S_T^{xy}(\Omega)$.

In the remainder of the section we investigate the zero-frequency spin-torque shot noise $S_T^{jk} = S_T^{jk}(0)$ at zero temperature. The exact expressions for the zero-frequency noise components are given in Appendix B, where $S_T^{xx}(0) = S_{TS}^{xx}(0)$, $S_T^{yy}(0) = S_{TS}^{yy}(0)$, $S_T^{zz}(0) = S_{TS}^{zz}(0)$, while $S_T^{xy}(0)$ is a complex imaginary function, and $S_T^{xy}(0) = 0$ according to Eqs. (5.33) and (5.40). Since $S_T^{xx}(0) = S_T^{yy}(0)$, all results and discussions related to $S_T^{xx}(0)$ also refer to $S_T^{yy}(0)$.

In the absence of spin-flip events each spin-transport channel can be treated independently. The presence of the precessing molecular spin affects the spin current noise. This occurs due to the spin-flip processes which convert spin-up state into spin down state and vice versa. It has already been demonstrated that spin-flip processes contribute to the noise of spin current [292]. Since the number of particles with different spins changes and is not conserved, this generates additional spin-current fluctuations. Spin-flip processes induce correlations of currents with opposite spins. Superposition of opposite spin states and quantum interference effect can contribute to the spin-torque noise, and offers the possibility of molecular spin manipulation via these interference effects.

Spin currents $I_{\xi x}$ and $I_{\xi y}$ are periodic functions of time, with period $\mathcal{T} = 2\pi/\omega_L$, while $I_{\xi z}$ is time-independent. Spin currents are auto-correlated in the sense that two spin-currents polarized along the same direction are correlated, while $I_{\xi x}$ and $I_{\xi y}$ are also correlated between themselves. Due to the precessional motion of the molecular spin, inelastic spin currents with spin-flip events induce noise of spin currents even for $eV = 0$. Nonequilibrium precession-assisted noise of spin-transfer torque at zero temperature is the subject of our investigation here. Electrons with the same and different spin orientations are correlated during transport. The spin-current formula gives information on available transport channels and inelastic spin-flip processes. The correlations between the torques in the same direction induce spin-torque noise, which is nonzero even for $eV = 0$, due to the molecular spin precession. The noise component S_T^{xy} is induced by the molecular spin precession and vanishes for a static molecular spin. The noises of spin currents and spin-transfer torque are driven by the bias voltage and by the molecular spin precession. Hence, in the case when both the molecular spin is static (absence of inelastic spin-flip processes) and $eV = 0$ (no net contribution of elastic tunneling processes), they are all equal to zero.

In Fig. 5.5(a) we present zero-frequency spin-torque noise components S_T^{xx} , $\text{Im}\{S_T^{xy}\}$, and S_T^{zz} as functions of the bias voltage $eV = \mu_L - \mu_R$, for $\mu_R = 0$ at zero temperature. The magnitude of the noise at resonance energies ϵ_i , $i = 1, 2, 3, 4$, is determined by the angle θ between the molecular spin and \vec{e}_z . We plotted component S_T^{xx} for $\theta = 0$ [dotted purple line in Fig. 5.5(a)], $\theta = \pi$ [red line in Fig. 5.5(a)] and $\theta = \pi/2$ [dot-dashed pink line in Fig. 5.5(a)], while $\text{Im}\{S_T^{xy}\}$ and S_T^{zz} are plotted for $\theta = \pi/2$ [blue and green lines in Fig. 5.5(a)]. In cases $\theta = 0, \pi$, there are only two transport channels of opposite spins determined by the resulting Zeeman field $B \pm JS/g\mu_B$. The two steps of equal height are located at these resonances, where the only contribution to the spin-torque noise comes from elastic tunneling events. For $\theta = \pi/2$, the elastic tunneling contributes with four steps with equal heights located at resonances ϵ_i , but due to the contributions of the

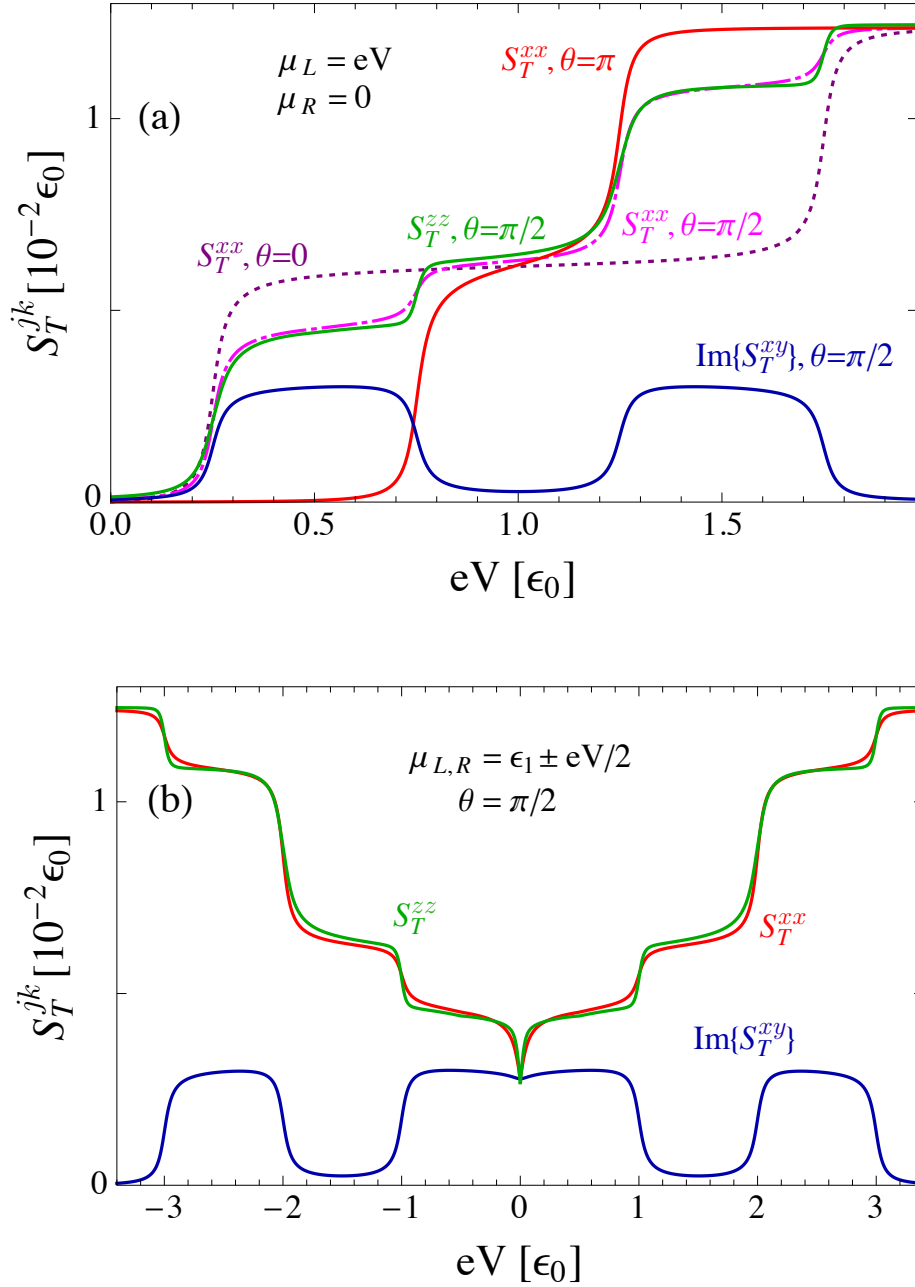


FIGURE 5.5: Spin-torque shot noise components S_T^{jk} as functions of the bias voltage eV for (a) $\mu_R = 0$, $\mu_L = eV$ and (b) $\mu_{L,R} = \epsilon_1 \pm (eV/2)$. All plots are obtained at zero temperature, with $\vec{B} = B\vec{e}_z$, and $\Gamma_L = \Gamma_R = \Gamma/2$, for $\Gamma = 0.05 \epsilon_0$. The other parameters are: $\omega_L = 0.5 \epsilon_0$, $J = 0.01 \epsilon_0$, and $S = 100$. The molecular quasienergy levels lie at: $\epsilon_1 = 0.25 \epsilon_0$, $\epsilon_2 = 0.75 \epsilon_0$, $\epsilon_3 = 1.25 \epsilon_0$, and $\epsilon_4 = 1.75 \epsilon_0$.

inelastic precession-assisted processes between quasienergy levels, the heights of the peaks in S_T^{xx} are not equal anymore (dot-dashed pink line). We observed that the contribution of the one quantum ω_L absorption tunneling processes to S_T^{xx} shows steps at spin-down levels ϵ_1 and ϵ_3 , while it is constant between and after the bias has passed these levels. The component S_T^{zz} shows similar behavior (green line). Similarly as in the case of the inelastic tunneling involving the absorption of one energy quantum ω_L , in S_T^{xx} we observed inelastic processes involving the absorption of two energy quanta $2\omega_L$, in the form of steps at spin-down levels ϵ_1 , ϵ_3 , $\epsilon_2 - 2\omega_L$ and $\epsilon_4 - 2\omega_L$, which have negligible contribution compared to the other terms. These processes are a result of correlations of two oscillating spin-currents. For large bias voltage the spin-torque noise components S_T^{xx} and S_T^{zz} become saturated.

The behavior of the component $\text{Im}\{S_T^{xy}\}$ is completely different in nature. It is contributed only by one energy quantum ω_L absorption (emission) processes. Interestingly, we obtained the following relation between the Gilbert damping parameter given by Eq. (4.47) and $\text{Im}\{S_T^{xy}\}$ at zero temperature

$$\text{Im}\{S_T^{xy}\} = \frac{\omega_L S \sin^2(\theta)}{2} \alpha. \quad (5.41)$$

Hence, the component $\text{Im}\{S_T^{xy}\}$ is nonzero for Fermi levels of the leads positioned in the regions where inelastic tunneling processes occur.

Fig. 5.5(b) shows bias-voltage dependence of S_T^{xx} , $\text{Im}\{S_T^{xy}\}$, and S_T^{zz} for chemical potentials $\mu_{L,R} = \epsilon_1 \pm eV/2$ at zero temperature. Similarly as in the case of charge current shot noise, we observe a valley at zero bias, which corresponds to $\mu_L = \mu_R = \epsilon_1$ in the case of S_T^{xx} and S_T^{zz} . For $eV = 0$ the contribution of elastic tunnel processes to the noise is 0, but the precession-assisted inelastic processes, involving absorption of an energy quantum ω_L , give rise to the spin-torque noise components S_T^{xx} and S_T^{zz} . The spin-torque noise is increased via precession-assisted inelastic processes. The steps correspond to the position of the chemical potentials $\mu_{L,R}$ at the other three resonances. Similarly as the Gilbert damping coefficient α , the torque noise component $\text{Im}\{S_T^{xy}\}$ approaches a constant value in the regions of the bias-voltage where inelastic spin-flip processes occur.

In Fig. 5.6 we plotted S_T^{xx} , $\text{Im}\{S_T^{xy}\}$ and S_T^{zz} components of the spin-torque noise as functions of the bias voltage $eV = \mu_L - \mu_R$ for $\mu_R = \epsilon_1$. Both S_T^{xx} and S_T^{zz} show a dip at $\mu_L = \epsilon_2$, i.e., $eV = \epsilon_2 - \epsilon_1 = \omega_L$. The dip is due to the quantum interference effect between the spin-tunneling paths through levels ϵ_1 and ϵ_2 , again in analogy with the Fano effect [277].

The spin-torque noise is influenced by the magnetic field \vec{B} , since it determines the spin-up and spin-down molecular quasienergy levels. The dependence

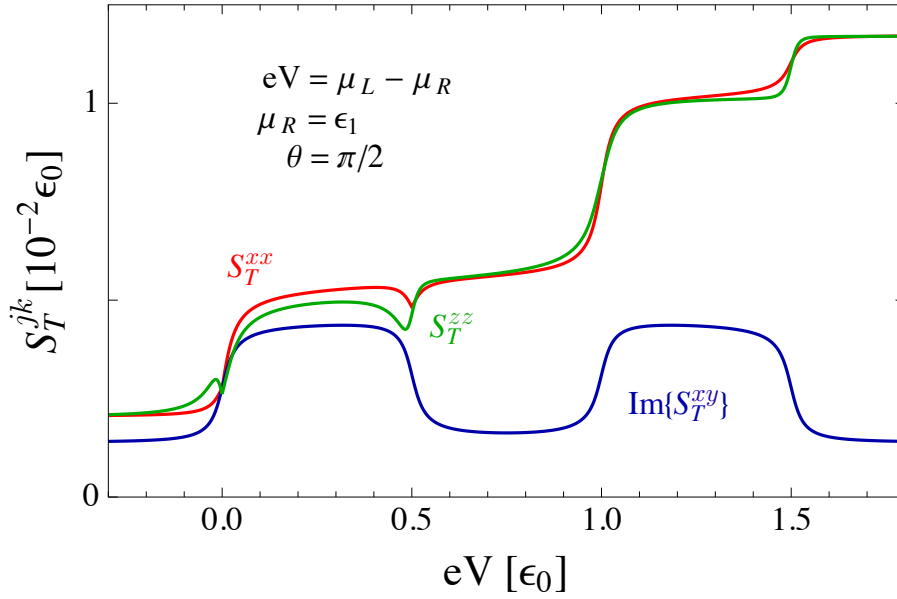


FIGURE 5.6: Spin-torque shot noise components S_T^{jk} as functions of the bias-voltage $eV = \mu_L - \mu_R$ with $\mu_R = (\epsilon_1 + \epsilon_2)/2$, $\theta = \pi/2$, and $\vec{B} = B\vec{e}_z$, at zero temperature. The other parameters are set to: $\Gamma = 0.05 \epsilon_0$, $\Gamma_L = \Gamma_R = \Gamma/2$, $\omega_L = 0.5 \epsilon_0$, $J = 0.01 \epsilon_0$, and $S = 100$. The molecular quasienergy levels are located at: $\epsilon_1 = 0.25 \epsilon_0$, $\epsilon_2 = 0.75 \epsilon_0$, $\epsilon_3 = 1.25 \epsilon_0$, and $\epsilon_4 = 1.75 \epsilon_0$.

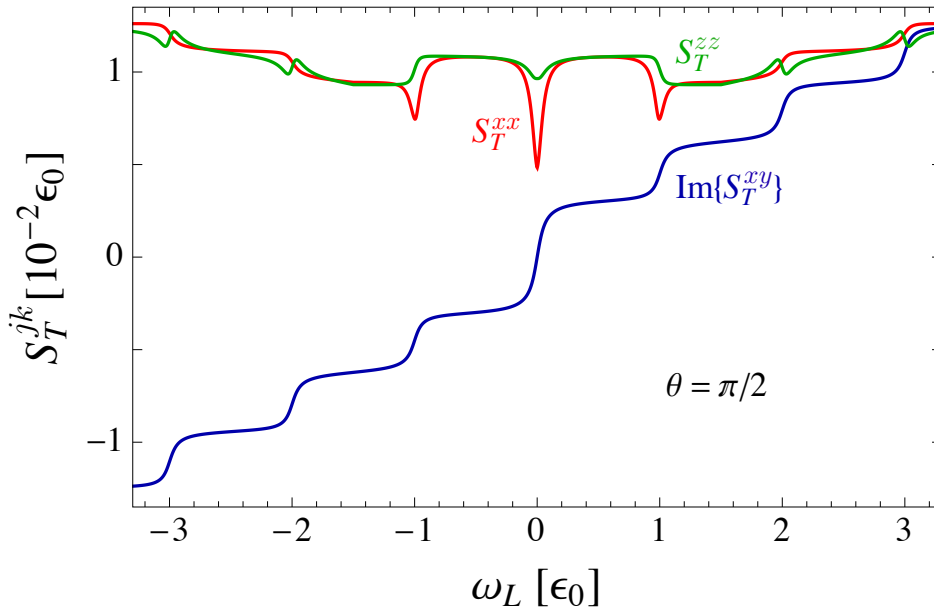


FIGURE 5.7: Spin-torque shot noise components S_T^{jk} as functions of the Larmor frequency ω_L for $\mu_L = 1.5 \epsilon_0$, $\mu_R = 0$, and $\theta = \pi/2$. All plots are obtained for $\vec{B} = B\vec{e}_z$ at zero temperature. The other parameters are set to: $\Gamma_L = \Gamma_R = \Gamma/2$, $\Gamma = 0.05 \epsilon_0$, $J = 0.01 \epsilon_0$, and $S = 100$.

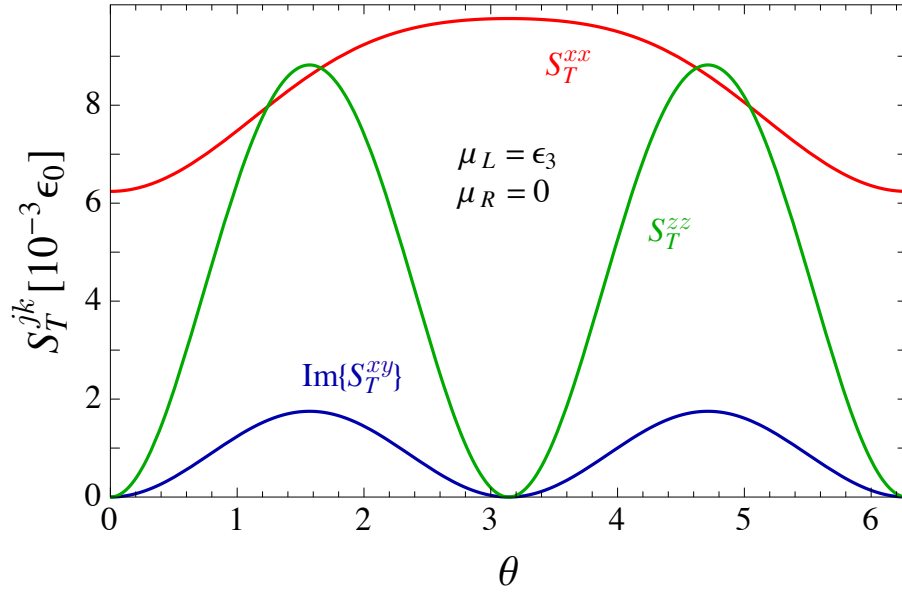


FIGURE 5.8: Spin-torque shot noise components as functions of the tilt angle θ for $\mu_L = \epsilon_3$, $\mu_R = 0$. All plots are obtained at zero temperature, with $\vec{B} = B\vec{e}_z$, $\Gamma = 0.05 \epsilon_0$, and $\Gamma_L = \Gamma_R = \Gamma/2$. The other parameters are set to: $\omega_L = 0.5 \epsilon_0$, $J = 0.01 \epsilon_0$, and $S = 100$.

of S_T^{xx} , $\text{Im}\{S_T^{xy}\}$, and S_T^{zz} on the Larmor frequency ω_L is depicted in Fig. 5.7. The steps, dips or peaks in the plots are located at resonant tunneling frequencies $\omega_L = \pm|2\mu_{L,R} - 2\epsilon_0 \pm JS|$. For $\omega_L = 0$ there are only two transport channels, one at energy $\epsilon_0 + JS/2$ which is equal to the Fermi energy of the left lead, and the other at $\epsilon_0 - JS/2$ located between μ_L and μ_R . The contributions of the elastic spin transport processes through these levels result in dips in the components S_T^{xx} and S_T^{zz} , while $\text{Im}\{S_T^{xy}\} = 0$. For $\omega = \epsilon_0$ corresponding to $\mu_R = \epsilon_1$ and $\mu_R = \epsilon_4 - 2\omega_L$, both the elastic and spin-flip tunneling events involving the absorption of energy of one quantum ω_L contribute with a dip, while the spin-flip processes involving the absorption of an energy equal to $2\omega_L$ contribute with a peak to the component S_T^{xx} . For $\omega_L = 2\epsilon_0$ and $\omega_L = 3\epsilon_0$ corresponding to $\mu_L = \epsilon_2$ and $\mu_R = \epsilon_3$, both elastic and spin-flip processes with the absorption of an energy equal to ω_L contribute with a step, while the inelastic processes involving the absorption of an energy $2\omega_L$ give negligible contribution to S_T^{xx} . The component S_T^{zz} shows dips at these two points, since here the dominant contribution comes from inelastic tunneling spin-flip events. The component S_T^{zz} is an even, while $\text{Im}\{S_T^{xy}\}$ is an odd function of ω_L . The spin-torque noise S_T^{xx} is an even function of ω_L for $\theta = \pi/2$.

The noise of spin-transfer torque can be modified by changing the tilt angle θ , bias-voltage eV , or the magnetic field \vec{B} , i.e., by adjusting these parameters. The spin-torque noise components as functions of θ for $\mu_L = \epsilon_3$ and $\mu_R = 0$ at

zero temperature are shown in Fig. 5.8. As already mentioned, the magnitudes and the appearance of the spin-torque noise components at resonance energies can be controlled by θ , since it influences the polarization of the spin currents. Here we see that both S_T^{zz} and $\text{Im}\{S_T^{xy}\}$ are zero for $\theta = 0, \pi$, as then the molecular spin is static and its magnitude is constant along z -direction. These torque noise components take their maximum values for $\theta = \pi/2$, where both elastic and inelastic tunneling contributions are maximal. The component S_T^{xx} takes its minimum value for $\theta = 0$, and its maximum value for $\theta = \pi$, with only elastic tunneling contributions in both cases. For $\theta = \pi/2$ the inelastic tunneling events give maximal contribution, while energy conserving processes give minimal contribution to S_T^{xx} .

5.5 Conclusions

In this chapter we have first theoretically studied noise of charge and spin transport through a small junction, consisting of a single molecular orbital in the presence of a molecular spin precession with Larmor frequency ω_L in a constant magnetic field. The orbital is connected to two Fermi leads. We used the Keldysh nonequilibrium Green's functions method to derive the noise components of charge and spin currents and spin-transfer torque.

Then we analyzed the shot noise of charge current and observed characteristics which differ from the ones in the current. In the noise power we observed dip-like features which we attribute to inelastic processes, due to the molecular spin precession, leading to the quantum interference effect between correlated transport channels.

Since the inelastic tunneling processes lead to a spin-transfer torque acting on the molecular spin, we have also investigated the spin-torque noise components contributed by these processes, involving the change of energy by an energy quantum ω_L . We observed quantum interference between spin-tunneling processes as well. The spin-torque noise components are driven by both the bias voltage and the molecular spin precession. The in-plane noise components S_T^{xx} and S_T^{yy} are also contributed by the processes involving the absorption of an energy equal to $2\omega_L$. We obtained the relation between $\text{Im}\{S_T^{xy}\}$ and the Gilbert damping coefficient α at zero temperature.

Taking into account that the noise of charge and spin transport can be controlled by the parameters such as bias voltage and external magnetic field, our results might be useful in molecular electronics and spintronics. Finding a way to control the spin states of single-molecule magnets in tunnel junctions could be one of the future tasks.

Chapter 6

Conclusions and outlook

In this thesis we have investigated the charge and spin transport through a molecular orbital connected to two leads, and coupled via exchange interaction with a precessing molecular spin in a magnetic field. The expressions for charge and spin currents and related noises have been derived using the Keldysh nonequilibrium Green's functions formalism. The exchange coupling between the electronic spins and the magnetization dynamics of the molecule leads to inelastic tunneling processes, which contribute to the spin currents. In turn, a spin-transfer torque is generated onto the molecular spin by the spin-currents. This torque includes a Gilbert damping and a field-like torque component that modifies the precession frequency. The related torque coefficients can be controlled by the bias and gate voltages, or via the external magnetic fields.

We have also theoretically studied the ac-transport through the molecular orbital in the presence of oscillating voltages in the leads treated as a perturbation. We have found that in the low ac-frequency regime the molecular junction behaves as a classical electric circuit, which can be tuned from capacitive-like to inductive-like response. For an ac frequency that matches the Larmor frequency we have observed two effects. First, around ac frequency matching the Larmor frequency, the components of the dynamic conductance associated with the resonant position of the chemical potentials with molecular quasienergy levels, both increase after going to a local minimum, allowing the detection of the internal precession time scale. Second, the setup can be employed to generate and manipulate dc-spin currents by adjusting the molecular spin direction and the phase difference between ac voltages in the leads and Larmor precession.

In the end, we have studied the fluctuations of charge and spin transport through the junction under a dc-bias voltage. We have observed dips in the shot noise of charge current due to precession-assisted inelastic tunneling processes,

leading to the destructive quantum interference effect between different tunneling pathways. The correlations between the spin-transfer torques in the same direction are driven by the bias voltage and the molecular spin precession. The spin-torque noise components in the plane of the molecular spin precession are contributed by spin-flip processes, involving the absorption of energy equal to one or two Larmor frequencies. The correlations between the perpendicular spin-transfer torques in the precession plane are related to the Gilbert damping coefficient. We observed quantum destructive interference effects between spin-tunneling processes as well.

Taking into account that spin-transport properties can be controlled by external parameters such as bias and gate voltages, as well as by external magnetic fields, our results might be useful in molecular spintronics. It may be possible to control the spin state of a single-molecule magnet via current-induced torques using e.g., ferromagnetic leads. One of the tasks for future research could be the quantum treatment of a single-molecule magnet in tunneling junctions, in view of its possible application in magnetic storage. This would have to be complemented by a theoretical study of the molecular magnetization dynamics in the presence of spin transport.

Appendix A

Floquet theorem

We consider a system with a time-periodic Hamiltonian $\hat{H}(t) = \hat{H}(t + \mathcal{T})$, where \mathcal{T} is the period, while $\omega = 2\pi/\mathcal{T}$ is the corresponding frequency. The Hamiltonian consists of a nonperturbed part \hat{H}_0 and a time-dependent periodic part $\hat{V}(t) = \hat{V}(t + \mathcal{T})$,

$$\hat{H}(t) = \hat{H}_0 + \hat{V}(t). \quad (\text{A.1})$$

The Hamiltonian $\hat{H}(t)$ can be expressed as a Fourier series

$$\hat{H}(t) = \sum_{n=-\infty}^{\infty} \hat{H}^{(n)} e^{in\omega t}. \quad (\text{A.2})$$

The **Floquet theorem** claims that the solutions of the Schrödinger equation

$$\hat{H}(t)|\psi(t)\rangle = i\hbar \frac{\partial}{\partial t} |\psi(t)\rangle, \quad (\text{A.3})$$

can be written as

$$|\psi_\alpha(t)\rangle = e^{-i\epsilon_\alpha t} |\phi_\alpha(t)\rangle, \quad (\text{A.4})$$

with $|\phi_\alpha(t)\rangle = |\phi_\alpha(t + \mathcal{T})\rangle$ [224–226]. The wave function $|\psi_\alpha(t)\rangle$ is the wave function of the system called the quasienergy state, while ϵ_α is called the quasienergy. Replacing Eq. (A.4) into Eq. (A.3) yields

$$\hat{\mathcal{H}}(t)|\phi_\alpha(t)\rangle = \epsilon_\alpha |\phi_\alpha(t)\rangle, \quad (\text{A.5})$$

where $\hat{\mathcal{H}}(t) = \hat{H}(t) - i\partial/\partial t$. The quasienergy state $|\psi_\alpha(t)\rangle$ can be expanded as a Fourier series, using the orthonormal set of eigenstates of the Hamiltonian \hat{H}_0

denoted as $\{|\beta\rangle\}$,

$$|\psi_\alpha(t)\rangle = e^{-i\epsilon_\alpha t} \sum_{n,\beta} F_{\alpha\beta}^{(n)} e^{-in\omega t} |\beta\rangle. \quad (\text{A.6})$$

Substituting Eqs. (A.2) and (A.6) into Eq. (A.3) one eliminates the time dependence and after some algebra obtains [225, 228]

$$\sum_{k,\gamma} \langle \alpha n | \hat{H}^F | \gamma k \rangle F_{\gamma\beta}^{(k)} = \epsilon_\beta F_{\alpha\beta}^{(n)}, \quad (\text{A.7})$$

with $|\alpha n\rangle = |\alpha\rangle \otimes |n\rangle$, where $\langle t | n \rangle = e^{in\omega t}$, $n \in \mathbb{Z}$, are the Fourier vectors, while index α characterize the system. In Eq. (A.7), \hat{H}^F is the Floquet Hamiltonian with matrix elements given by [225, 228]

$$\langle \alpha n | \hat{H}^F | \beta m \rangle = \langle \alpha | \hat{H}^{(n-m)} | \beta \rangle + n\omega \delta_{\alpha\beta} \delta_{nm}, \quad (\text{A.8})$$

which can be written in a shorter form as

$$H_{\alpha n, \beta m}^F = H_{\alpha\beta}^{(n-m)} + n\omega \delta_{\alpha\beta} \delta_{nm}, \quad (\text{A.9})$$

whereas the quasienergies ϵ_α can be obtained as the eigenvalues of the Floquet Hamiltonian \hat{H}^F ,

$$\det|\hat{H}^F - \epsilon \hat{I}| = 0. \quad (\text{A.10})$$

The number of quasienergies corresponding to the quasienergy state $|\psi_\alpha(t)\rangle$ is infinite, given by $\epsilon_\alpha + n\hbar\omega$. Thus, it is sufficient to consider, for instance, quasienergies within the interval $[-\omega/2, \omega/2)$.

Example: We consider Hamiltonian of the molecular orbital given by Eq. (4.4) in the Hilbert space spanned by the eigenvectors of electron spin operator \hat{s}_z , $|\downarrow\rangle = |1\rangle$ and $|\uparrow\rangle = |2\rangle$,

$$\hat{H}_{\text{MO}}(t) = \lambda_1 |1\rangle\langle 1| + \lambda_2 |2\rangle\langle 2| + \frac{JS_\perp}{2} e^{i\omega_L t} |1\rangle\langle 2| + \frac{JS_\perp}{2} e^{-i\omega_L t} |2\rangle\langle 1|, \quad (\text{A.11})$$

where $\lambda_1 = \epsilon_0 - (\omega_L + JS_z)/2$ and $\lambda_2 = \epsilon_0 + (\omega_L + JS_z)/2$. The only nonzero components of the $\hat{H}_{\text{MO}}(t)$ expressed as a Fourier series

$$\hat{H}_{\text{MO}}(t) = \sum_{n=-\infty}^{\infty} \hat{H}_{\text{MO}}^{(n)} e^{in\omega_L t}, \quad (\text{A.12})$$

are given by

$$\hat{H}_{\text{MO}}^{(0)} = \lambda_1|1\rangle\langle 1| + \lambda_2|2\rangle\langle 2|, \quad (\text{A.13})$$

$$\hat{H}_{\text{MO}}^{(1)} = \frac{JS_{\perp}}{2}e^{i\omega_L t}|1\rangle\langle 2|, \quad (\text{A.14})$$

$$\hat{H}_{\text{MO}}^{(-1)} = \frac{JS_{\perp}}{2}e^{-i\omega_L t}|2\rangle\langle 1|. \quad (\text{A.15})$$

Using Eq. (A.9) the matrix elements of the Floquet Hamiltonian can be obtained as

$$H_{1n,1m}^{\text{F}} = (\lambda_1 + n\hbar\omega_L)\delta_{nm}, \quad (\text{A.16})$$

$$H_{1n,2m}^{\text{F}} = \frac{JS_{\perp}}{2}\delta_{n,m+1}, \quad (\text{A.17})$$

$$H_{2n,1m}^{\text{F}} = \frac{JS_{\perp}}{2}\delta_{n,m-1}, \quad (\text{A.18})$$

$$H_{2n,2m}^{\text{F}} = (\lambda_2 + n\hbar\omega_L)\delta_{nm}. \quad (\text{A.19})$$

Similarly as in [227] the matrix of the Floquet Hamiltonian is block diagonal with a block given by

$$\begin{pmatrix} \lambda_2 + (n-1)\omega_L & JS_{\perp}/2 \\ JS_{\perp}/2 & \lambda_1 + n\omega_L \end{pmatrix}. \quad (\text{A.20})$$

Choosing $n = 0$, we obtain the corresponding quasienergies given by the eigenvalues of the block as

$$\epsilon_1 = \epsilon_0 - \frac{\omega_L}{2} - \frac{JS}{2}, \quad (\text{A.21})$$

$$\epsilon_3 = \epsilon_0 - \frac{\omega_L}{2} + \frac{JS}{2}. \quad (\text{A.22})$$

The states of the neighboring block are equal to

$$\epsilon_2 = \epsilon_1 + \omega_L = \epsilon_0 + \frac{\omega_L}{2} - \frac{JS}{2}, \quad (\text{A.23})$$

$$\epsilon_4 = \epsilon_2 + \omega_L = \epsilon_0 + \frac{\omega_L}{2} + \frac{JS}{2}. \quad (\text{A.24})$$

The precessing component of the molecular spin couples state with quasienergy ϵ_1 with the state with quasienergy ϵ_2 , and state with quasienergy ϵ_3 with the state with quasienergy ϵ_4 , where an electron can absorb or emit an energy ω_L accompanied with a spin-flip.

In the case when the time-dependent part of the Hamiltonian $\hat{H}_{\text{MO}}(t)$ given by Eq. (A.11) can be treated as a perturbation, as in Chapter 3, where $(JS_{\perp}/2)^2 \rightarrow 0$,

the quasienergies can be approximated as

$$\epsilon_{1,2} = \epsilon_0 \mp \frac{\omega_L}{2} - \frac{JS_z}{2}, \quad (\text{A.25})$$

$$\epsilon_{3,4} = \epsilon_0 \mp \frac{\omega_L}{2} + \frac{JS_z}{2}. \quad (\text{A.26})$$

Appendix B

Noise power of charge and spin transport

Here we present the expressions for the zero-frequency noise power components of the charge and spin currents and spin-transfer torque, starting from the general expression given below. In the wide-band limit, the retarded and advanced self-energies $\Sigma^{r,a}$ are energy independent, and $S_{\xi\xi}^{\sigma\sigma',\lambda\eta}(t, t')$ given by Eq. (5.19) can be expressed as

$$\begin{aligned}
S_{\xi\xi}^{\sigma\sigma',\lambda\eta}(t, t') &= \int \frac{d\epsilon_1}{2\pi} \int \frac{d\epsilon_2}{2\pi} \int \frac{d\epsilon_3}{2\pi} \int \frac{d\epsilon_4}{2\pi} e^{-i(\epsilon_1-\epsilon_2)t} e^{i(\epsilon_3-\epsilon_4)t'} \\
&\times \left\{ [G_{\sigma'\lambda}^r(\epsilon_1, \epsilon_3)\Sigma_{\zeta}^>(\epsilon_3) + 2G_{\sigma'\lambda}^>(\epsilon_1, \epsilon_3)\Sigma_{\zeta}^a] \right. \\
&\quad \times [G_{\eta\sigma}^r(\epsilon_4, \epsilon_2)\Sigma_{\xi}^<(\epsilon_2) + 2G_{\eta\sigma}^<(\epsilon_4, \epsilon_2)\Sigma_{\xi}^a] \\
&\quad + [\Sigma_{\xi}^>(\epsilon_1)G_{\sigma'\lambda}^a(\epsilon_1, \epsilon_3) + 2G_{\sigma'\lambda}^>(\epsilon_1, \epsilon_3)\Sigma_{\xi}^r] \\
&\quad \times [\Sigma_{\zeta}^<(\epsilon_4)G_{\eta\sigma}^a(\epsilon_4, \epsilon_2) + 2G_{\eta\sigma}^<(\epsilon_4, \epsilon_2)\Sigma_{\zeta}^r] \\
&\quad \left. + 4\Sigma_{\xi}^r\Sigma_{\zeta}^aG_{\eta\sigma}^<(\epsilon_4, \epsilon_2)G_{\sigma'\lambda}^>(\epsilon_1, \epsilon_3) \right\} \\
&- \delta_{\xi\zeta} \int \frac{d\epsilon_1}{2\pi} \int \frac{d\epsilon_2}{2\pi} \int \frac{d\epsilon_3}{2\pi} \\
&\quad \times \left\{ e^{-i(\epsilon_1-\epsilon_2)t} e^{i(\epsilon_3-\epsilon_2)t'} \delta_{\eta\sigma} G_{\sigma'\lambda}^>(\epsilon_1, \epsilon_3)\Sigma_{\xi}^<(\epsilon_2) \right. \\
&\quad \left. + e^{-i(\epsilon_1-\epsilon_2)t} e^{i(\epsilon_1-\epsilon_3)t'} \delta_{\sigma'\lambda}\Sigma_{\xi}^>(\epsilon_1)G_{\eta\sigma}^<(\epsilon_3, \epsilon_2) \right\}. \tag{B.1}
\end{aligned}$$

The Fourier transform of Eq. (B.1) in the Wigner representation is given by

$$\begin{aligned}
S_{\xi\xi}^{\sigma\sigma',\lambda\eta}(\Omega) = & \int \frac{d\epsilon}{2\pi} \{ [G_{\sigma'\lambda}^{r\delta}(\epsilon)\Sigma_{\zeta}^{>}(\epsilon) + 2G_{\sigma'\lambda}^{>\delta}(\epsilon)\Sigma_{\zeta}^a] \\
& \times [G_{\eta\sigma}^{r\delta}(\epsilon - \Omega)\Sigma_{\xi}^{<}(\epsilon - \Omega) + 2G_{\eta\sigma}^{<\delta}(\epsilon - \Omega)\Sigma_{\xi}^a] \\
& + [\Sigma_{\xi}^{>}(\epsilon)G_{\sigma'\lambda}^{a\delta}(\epsilon) + 2G_{\sigma'\lambda}^{>\delta}(\epsilon)\Sigma_{\xi}^r] \\
& \times [\Sigma_{\zeta}^{<}(\epsilon - \Omega)G_{\eta\sigma}^{a\delta}(\epsilon - \Omega) + 2G_{\eta\sigma}^{<\delta}(\epsilon - \Omega)\Sigma_{\zeta}^r] \\
& + 4\Sigma_{\xi}^r\Sigma_{\zeta}^a G_{\eta\sigma}^{<\delta}(\epsilon - \Omega)G_{\sigma'\lambda}^{>\delta}(\epsilon) \\
& - \delta_{\xi\zeta}[\delta_{\eta\sigma}G_{\sigma'\lambda}^{>\delta}(\epsilon)\Sigma_{\xi}^{<}(\epsilon - \Omega) + \delta_{\sigma'\lambda}\Sigma_{\xi}^{>}(\epsilon)G_{\eta\sigma}^{<\delta}(\epsilon - \Omega)] \}, \quad (\text{B.2})
\end{aligned}$$

where $\{\sigma\sigma', \lambda\eta\} = \{\{11, 11\}, \{12, 21\}, \{11, 22\}, \{22, 11\}, \{21, 12\}, \{22, 22\}\}$. For all other configurations of superscripts, Fourier transforms $S_{\xi\xi}^{\sigma\sigma',\lambda\eta}(\Omega)$ equal zero, i.e., $S_{\xi\xi}^{\sigma\sigma,12}(\Omega) = S_{\xi\xi}^{\sigma\sigma,21}(\Omega) = S_{\xi\xi}^{12,\sigma\sigma}(\Omega) = S_{\xi\xi}^{21,\sigma\sigma}(\Omega) = S_{\xi\xi}^{12,12}(\Omega) = S_{\xi\xi}^{21,21}(\Omega) = 0$. In the expression (B.2),

$$G_{11}^{r\delta}(\epsilon) = \frac{G_{11}^{0r}(\epsilon)}{1 - \gamma^2 G_{11}^{0r}(\epsilon)G_{22}^{0r}(\epsilon - \omega_L)} := A(\epsilon), \quad (\text{B.3})$$

$$G_{12}^{r\delta}(\epsilon) = \frac{\gamma G_{11}^{0r}(\epsilon)G_{22}^{0r}(\epsilon - \omega_L)}{1 - \gamma^2 G_{11}^{0r}(\epsilon)G_{22}^{0r}(\epsilon - \omega_L)} := B(\epsilon), \quad (\text{B.4})$$

$$G_{21}^{r\delta}(\epsilon) = \frac{\gamma G_{11}^{0r}(\epsilon + \omega_L)G_{22}^{0r}(\epsilon)}{1 - \gamma^2 G_{11}^{0r}(\epsilon + \omega_L)G_{22}^{0r}(\epsilon)} := B(\epsilon + \omega_L), \quad (\text{B.5})$$

$$G_{22}^{r\delta}(\epsilon) = \frac{G_{22}^{0r}(\epsilon)}{1 - \gamma^2 G_{22}^{0r}(\epsilon)G_{11}^{0r}(\epsilon + \omega_L)} := C(\epsilon), \quad (\text{B.6})$$

$$G_{11}^{<\delta,>\delta}(\epsilon) = \Sigma^{<,>}(\epsilon)|A(\epsilon)|^2 + \Sigma^{<,>}(\epsilon - \omega_L)|B(\epsilon)|^2, \quad (\text{B.7})$$

$$G_{12}^{<\delta,>\delta}(\epsilon) = \Sigma^{<,>}(\epsilon)A(\epsilon)B^*(\epsilon) + \Sigma^{<,>}(\epsilon - \omega_L)B(\epsilon)C^*(\epsilon - \omega_L), \quad (\text{B.8})$$

$$G_{21}^{<\delta,>\delta}(\epsilon) = \Sigma^{<,>}(\epsilon + \omega_L)B(\epsilon + \omega_L)A^*(\epsilon + \omega_L) + \Sigma^{<,>}(\epsilon)C(\epsilon)B^*(\epsilon + \omega_L), \quad (\text{B.9})$$

$$G_{22}^{<\delta,>\delta}(\epsilon) = \Sigma^{<,>}(\epsilon)|C(\epsilon)|^2 + \Sigma^{<,>}(\epsilon + \omega_L)|B(\epsilon + \omega_L)|^2. \quad (\text{B.10})$$

The auto-correlation zero-frequency noise power of the charge current, and the noise power of the spin current polarized along the z -direction are given by

$$\begin{aligned}
S_{LLS}^{00,zz}(0) &= q_{0,z}^2 \int \frac{d\epsilon}{2\pi} \\
&\times \{ \{ f_L(\epsilon)[1 - f_R(\epsilon)] + f_R(\epsilon)[1 - f_L(\epsilon)] \} \\
&\quad \times [2\Gamma_L^2 \Gamma_R \text{Im}\{A(\epsilon)\} |A(\epsilon)|^2 + \Gamma_L^3 \Gamma_R |A(\epsilon)|^4 \\
&\quad + \Gamma_L \Gamma_R |A(\epsilon)|^2 + \Gamma_L^3 \Gamma_R |B(\epsilon + \omega_L)|^4 \\
&\quad \pm (2\Gamma_L^2 \Gamma_R \text{Im}\{C(\epsilon)\} |B(\epsilon + \omega_L)|^2 + 2\Gamma_L^2 \Gamma_R \text{Im}\{A(\epsilon)\} |B(\epsilon)|^2 \\
&\quad + 2\Gamma_L^3 \Gamma_R |A(\epsilon)|^2 |B(\epsilon)|^2 + 2\Gamma_L^3 \Gamma_R |B(\epsilon + \omega_L)|^2 |C(\epsilon)|^2 \\
&\quad + 2\Gamma_L^2 \Gamma_R \text{Im}\{C(\epsilon)\} |C(\epsilon)|^2 + \Gamma_L^3 \Gamma_R |C(\epsilon)|^4 + \Gamma_L \Gamma_R |C(\epsilon)|^2 + \Gamma_L^3 \Gamma_R |B(\epsilon)|^4] \\
&+ \{ f_L(\epsilon)[1 - f_L(\epsilon - \omega_L)] + f_L(\epsilon - \omega_L)[1 - f_L(\epsilon)] \} \\
&\quad \times [2\Gamma_L^3 \text{Im}\{A(\epsilon)\} |B(\epsilon)|^2 + \Gamma_L^4 |A(\epsilon)|^2 |B(\epsilon)|^2 + \Gamma_L^2 |B(\epsilon)|^2 \\
&\quad \pm (2\Gamma_L^3 \text{Im}\{B^2(\epsilon)A^*(\epsilon)\} + 2\Gamma_L^3 \text{Im}\{B^2(\epsilon)C^*(\epsilon - \omega_L)\} \\
&\quad - 2\Gamma_L^2 \text{Re}\{B^2(\epsilon)\} + 2\Gamma_L^4 \text{Re}\{A(\epsilon)B^{*2}(\epsilon)C(\epsilon - \omega_L)\}) \\
&\quad + 2\Gamma_L^3 \text{Im}\{C(\epsilon - \omega_L)\} |B(\epsilon)|^2 + \Gamma_L^4 |B(\epsilon)|^2 |C(\epsilon - \omega_L)|^2 + \Gamma_L^2 |B(\epsilon)|^2] \\
&+ \{ f_L(\epsilon)[1 - f_R(\epsilon - \omega_L)] + f_R(\epsilon - \omega_L)[1 - f_L(\epsilon)] \} \\
&\quad \times [2\Gamma_L^2 \Gamma_R \text{Im}\{A(\epsilon)\} |B(\epsilon)|^2 + \Gamma_L^3 \Gamma_R |A(\epsilon)|^2 |B(\epsilon)|^2 + \Gamma_L \Gamma_R |B(\epsilon)|^2 \\
&\quad \pm (2\Gamma_L^2 \Gamma_R \text{Im}\{B^2(\epsilon)C^*(\epsilon - \omega_L)\} + 2\Gamma_L^3 \Gamma_R \text{Re}\{A(\epsilon)B^{*2}(\epsilon)C(\epsilon - \omega_L)\}) \\
&\quad + \Gamma_L^3 \Gamma_R |B(\epsilon)|^2 |C(\epsilon - \omega_L)|^2] \\
&+ \{ f_R(\epsilon)[1 - f_L(\epsilon - \omega_L)] + f_L(\epsilon - \omega_L)[1 - f_R(\epsilon)] \} \\
&\quad \times [\Gamma_L^3 \Gamma_R |A(\epsilon)|^2 |B(\epsilon)|^2 + 2\Gamma_L^2 \Gamma_R |B(\epsilon)|^2 \text{Im}\{C(\epsilon - \omega_L)\} \\
&\quad \pm (2\Gamma_L^2 \Gamma_R \text{Im}\{A^*(\epsilon)B^2(\epsilon)\} + 2\Gamma_L^3 \Gamma_R \text{Re}\{A(\epsilon)B^{*2}(\epsilon)C(\epsilon - \omega_L)\}) \\
&\quad + \Gamma_L^3 \Gamma_R |B(\epsilon)|^2 |C(\epsilon - \omega_L)|^2 + \Gamma_L \Gamma_R |B(\epsilon)|^2] \\
&+ \{ f_R(\epsilon)[1 - f_R(\epsilon - \omega_L)] + f_R(\epsilon - \omega_L)[1 - f_R(\epsilon)] \} \\
&\quad \times [\Gamma_L^2 \Gamma_R^2 |A(\epsilon)|^2 |B(\epsilon)|^2 + \Gamma_L^2 \Gamma_R^2 |B(\epsilon)|^2 |C(\epsilon - \omega_L)|^2 \\
&\quad \pm 2\Gamma_L^2 \Gamma_R^2 \text{Re}\{A(\epsilon)B^{*2}(\epsilon)C(\epsilon - \omega_L)\}]. \tag{B.11}
\end{aligned}$$

The cross-correlation zero-frequency noise power of the charge current, and the noise power of the spin current polarized along the z -direction read

$$\begin{aligned}
S_{LRS}^{00,zz}(0) &= q_{0,z}^2 \int \frac{d\epsilon}{2\pi} \\
&\times \{ \{ f_L(\epsilon)[1 - f_R(\epsilon)] + f_R(\epsilon)[1 - f_L(\epsilon)] \} \\
&\quad \times [\Gamma_L \Gamma_R \Gamma \text{Im}\{A(\epsilon)\}|A(\epsilon)|^2 - \Gamma_L \Gamma_R \text{Re}\{A^2(\epsilon)\} \\
&\quad + \Gamma_L^2 \Gamma_R^2 |A(\epsilon)|^4 + \Gamma_L^2 \Gamma_R^2 |B(\epsilon)|^4 + \Gamma_L^2 \Gamma_R^2 |B(\epsilon + \omega_L)|^4 \\
&\quad \pm (\Gamma_L \Gamma_R \Gamma \text{Im}\{A(\epsilon)\}|B(\epsilon)|^2 + 2\Gamma_L^2 \Gamma_R^2 |A(\epsilon)|^2 |B(\epsilon)|^2 \\
&\quad + 2\Gamma_L^2 \Gamma_R^2 |B(\epsilon + \omega_L)|^2 |C(\epsilon)|^2 + \Gamma_L \Gamma_R \Gamma \text{Im}\{C(\epsilon)\}|B(\epsilon + \omega_L)|^2) \\
&\quad + \Gamma_L \Gamma_R \Gamma \text{Im}\{C(\epsilon)\}|C(\epsilon)|^2 + \Gamma_L^2 \Gamma_R^2 |C(\epsilon)|^4 - \Gamma_L \Gamma_R \text{Re}\{C^2(\epsilon)\}] \\
&\quad + \{ f_L(\epsilon)[1 - f_L(\epsilon - \omega_L)] + f_L(\epsilon - \omega_L)[1 - f_L(\epsilon)] \} \\
&\quad \times [\Gamma_L^2 \Gamma_R \text{Im}\{A(\epsilon)\}|B(\epsilon)|^2 + \Gamma_L^3 \Gamma_R |A(\epsilon)|^2 |B(\epsilon)|^2 \\
&\quad \pm (\Gamma_L^2 \Gamma_R \text{Im}\{B^2(\epsilon)C^*(\epsilon - \omega_L)\} + \Gamma_L^2 \Gamma_R \text{Im}\{A^*(\epsilon)B^2(\epsilon)\} \\
&\quad + 2\Gamma_L^3 \Gamma_R \text{Re}\{A(\epsilon)B^{*2}(\epsilon)C(\epsilon - \omega_L)\}) \\
&\quad + \Gamma_L^2 \Gamma_R |B(\epsilon)|^2 \text{Im}\{C(\epsilon - \omega_L)\} + \Gamma_L^3 \Gamma_R |B(\epsilon)|^2 |C(\epsilon - \omega_L)|^2] \\
&\quad + \{ f_L(\epsilon)[1 - f_R(\epsilon - \omega_L)] + f_R(\epsilon - \omega_L)[1 - f_L(\epsilon)] \} \\
&\quad \times [\Gamma_L \Gamma_R^2 \text{Im}\{A(\epsilon)\}|B(\epsilon)|^2 + \Gamma_L^2 \Gamma_R^2 |A(\epsilon)|^2 |B(\epsilon)|^2 \\
&\quad \pm (\Gamma_L^2 \Gamma_R \text{Im}\{A^*(\epsilon)B^2(\epsilon)\} + \Gamma_L \Gamma_R^2 \text{Im}\{B^2(\epsilon)C^*(\epsilon - \omega_L)\} \\
&\quad + 2\Gamma_L^2 \Gamma_R^2 \text{Re}\{A(\epsilon)B^{*2}(\epsilon)C(\epsilon - \omega_L)\} - \Gamma_L \Gamma_R \text{Re}\{B^2(\epsilon)\}) \\
&\quad + \Gamma_L^2 \Gamma_R |B(\epsilon)|^2 \text{Im}\{C(\epsilon - \omega_L)\} + \Gamma_L^2 \Gamma_R^2 |B(\epsilon)|^2 |C(\epsilon - \omega_L)|^2] \\
&\quad + \{ f_R(\epsilon)[1 - f_L(\epsilon - \omega_L)] + f_L(\epsilon - \omega_L)[1 - f_R(\epsilon)] \} \\
&\quad \times [\Gamma_L^2 \Gamma_R^2 |A(\epsilon)|^2 |B(\epsilon)|^2 + \Gamma_L^2 \Gamma_R \text{Im}\{A(\epsilon)\}|B(\epsilon)|^2 \\
&\quad \pm (\Gamma_L \Gamma_R^2 \text{Im}\{A^*(\epsilon)B^2(\epsilon)\} + \Gamma_L^2 \Gamma_R \text{Im}\{B^2(\epsilon)C^*(\epsilon - \omega_L)\} \\
&\quad + 2\Gamma_L^2 \Gamma_R^2 \text{Re}\{A(\epsilon)B^{*2}(\epsilon)C(\epsilon - \omega_L)\} - \Gamma_L \Gamma_R \text{Re}\{B^2(\epsilon)\}) \\
&\quad + \Gamma_L^2 \Gamma_R^2 |B(\epsilon)|^2 |C(\epsilon - \omega_L)|^2 + \Gamma_L \Gamma_R^2 |B(\epsilon)|^2 \text{Im}\{C(\epsilon - \omega_L)\}] \\
&\quad + \{ f_R(\epsilon)[1 - f_R(\epsilon - \omega_L)] + f_R(\epsilon - \omega_L)[1 - f_R(\epsilon)] \} \\
&\quad \times [\Gamma_L \Gamma_R^3 |A(\epsilon)|^2 |B(\epsilon)|^2 + \Gamma_L \Gamma_R^2 \text{Im}\{A(\epsilon)\}|B(\epsilon)|^2 \\
&\quad \pm (\Gamma_L \Gamma_R^2 \text{Im}\{A^*(\epsilon)B^2(\epsilon)\} + \Gamma_L \Gamma_R^2 \text{Im}\{B^2(\epsilon)C^*(\epsilon - \omega_L)\} \\
&\quad + 2\Gamma_L \Gamma_R^3 \text{Re}\{A(\epsilon)B^{*2}(\epsilon)C(\epsilon - \omega_L)\}) \\
&\quad + \Gamma_L \Gamma_R^3 |B(\epsilon)|^2 |C(\epsilon - \omega_L)|^2 + \Gamma_L \Gamma_R^2 |B(\epsilon)|^2 \text{Im}\{C(\epsilon - \omega_L)\}] \}. \quad (\text{B.12})
\end{aligned}$$

The auto-correlation zero-frequency noise power of the spin current polarized along the x -direction can be expressed as

$$\begin{aligned}
S_{LLS}^{xx}(0) = & \int \frac{d\epsilon}{8\pi} \\
& \times \{ \{ f_L(\epsilon)[1 - f_R(\epsilon)] + f_R(\epsilon)[1 - f_L(\epsilon)] \} \\
& \quad \times [2\Gamma_L^2\Gamma_R|A(\epsilon)|^2\text{Im}\{C(\epsilon)\} + 2\Gamma_L^2\Gamma_R\text{Im}\{A(\epsilon)\}|C(\epsilon)|^2 \\
& \quad + 2\Gamma_L^3\Gamma_R|A(\epsilon)|^2|C(\epsilon)|^2 + \Gamma_L\Gamma_R|A(\epsilon)|^2 + \Gamma_L\Gamma_R|C(\epsilon)|^2] \\
& + \{ f_L(\epsilon)[1 - f_L(\epsilon - \omega_L)] + f_L(\epsilon - \omega_L)[1 - f_L(\epsilon)] \} \\
& \quad \times [2\Gamma_L^3|B(\epsilon)|^2\text{Im}\{C(\epsilon)\} + 2\Gamma_L^3\text{Im}\{A(\epsilon - \omega_L)\}|B(\epsilon)|^2 \\
& \quad + \Gamma_L^4|A(\epsilon - \omega_L)|^2|B(\epsilon)|^2 + \Gamma_L^4|B(\epsilon)|^2|C(\epsilon)|^2 + 2\Gamma_L^2|B(\epsilon)|^2] \\
& + \{ f_L(\epsilon)[1 - f_R(\epsilon - \omega_L)] + f_R(\epsilon - \omega_L)[1 - f_L(\epsilon)] \} \\
& \quad \times [2\Gamma_L^2\Gamma_R|B(\epsilon)|^2\text{Im}\{C(\epsilon)\} + \Gamma_L^3\Gamma_R|A(\epsilon - \omega_L)|^2|B(\epsilon)|^2 \\
& \quad + \Gamma_L^3\Gamma_R|B(\epsilon)|^2|C(\epsilon)|^2 + \Gamma_L\Gamma_R|B(\epsilon)|^2] \\
& + \{ f_R(\epsilon)[1 - f_L(\epsilon - \omega_L)] + f_L(\epsilon - \omega_L)[1 - f_R(\epsilon)] \} \\
& \quad \times [2\Gamma_L^2\Gamma_R\text{Im}\{A(\epsilon - \omega_L)\}|B(\epsilon)|^2 + \Gamma_L^3\Gamma_R|A(\epsilon - \omega_L)|^2|B(\epsilon)|^2 \\
& \quad + \Gamma_L^3\Gamma_R|B(\epsilon)|^2|C(\epsilon)|^2 + \Gamma_L\Gamma_R|B(\epsilon)|^2] \\
& + \{ f_R(\epsilon)[1 - f_R(\epsilon - \omega_L)] + f_R(\epsilon - \omega_L)[1 - f_R(\epsilon)] \} \\
& \quad \times [\Gamma_L^2\Gamma_R^2|A(\epsilon - \omega_L)|^2|B(\epsilon)|^2 + \Gamma_L^2\Gamma_R^2|B(\epsilon)|^2|C(\epsilon)|^2] \\
& + \{ \Gamma_L^4 f_L(\epsilon - 2\omega_L)[1 - f_L(\epsilon)] + \Gamma_L^3\Gamma_R f_L(\epsilon - 2\omega_L)[1 - f_R(\epsilon)] \\
& + \Gamma_L^3\Gamma_R f_R(\epsilon - 2\omega_L)[1 - f_L(\epsilon)] + \Gamma_L^2\Gamma_R^2 f_R(\epsilon - 2\omega_L)[1 - f_R(\epsilon)] \\
& + \Gamma_L^4 f_L(\epsilon)[1 - f_L(\epsilon - 2\omega_L)] + \Gamma_L^3\Gamma_R f_L(\epsilon)[1 - f_R(\epsilon - 2\omega_L)] \\
& + \Gamma_L^3\Gamma_R f_R(\epsilon)[1 - f_L(\epsilon - 2\omega_L)] + \Gamma_L^2\Gamma_R^2 f_R(\epsilon)[1 - f_R(\epsilon - 2\omega_L)] \} \\
& \quad \times |B(\epsilon)|^2|B(\epsilon - \omega_L)|^2 \}, \tag{B.13}
\end{aligned}$$

and

$$S_{LLS}^{yy}(0) = S_{LLS}^{xx}(0). \tag{B.14}$$

The cross-correlation zero-frequency noise power of the spin current polarized along the x -direction can be written as

$$\begin{aligned}
S_{LRS}^{xx}(0) = & \int \frac{d\epsilon}{8\pi} \\
& \times \{ \{ f_L(\epsilon)[1 - f_R(\epsilon)] + f_R(\epsilon)[1 - f_L(\epsilon)] \} \\
& \quad \times [\Gamma_L \Gamma_R \Gamma |A(\epsilon)|^2 \text{Im}\{C(\epsilon)\} + \Gamma_L \Gamma_R \Gamma \text{Im}\{A(\epsilon)\} |C(\epsilon)|^2 \\
& \quad + 2\Gamma_L^2 \Gamma_R^2 |A(\epsilon)|^2 |C(\epsilon)|^2 - 2\Gamma_L \Gamma_R \text{Re}\{A(\epsilon)C(\epsilon)\}] \\
& + \{ f_L(\epsilon)[1 - f_L(\epsilon - \omega_L)] + f_L(\epsilon - \omega_L)[1 - f_L(\epsilon)] \} \\
& \quad \times [\Gamma_L^2 \Gamma_R |B(\epsilon)|^2 \text{Im}\{C(\epsilon)\} + \Gamma_L^2 \Gamma_R \text{Im}\{A(\epsilon - \omega_L)\} |B(\epsilon)|^2 \\
& \quad + \Gamma_L^3 \Gamma_R |A(\epsilon - \omega_L)|^2 |B(\epsilon)|^2 + \Gamma_L^3 \Gamma_R |B(\epsilon)|^2 |C(\epsilon)|^2] \\
& + \{ f_L(\epsilon)[1 - f_R(\epsilon - \omega_L)] + f_R(\epsilon - \omega_L)[1 - f_L(\epsilon)] \} \\
& \quad \times [\Gamma_L \Gamma_R^2 |B(\epsilon)|^2 \text{Im}\{C(\epsilon)\} + \Gamma_L^2 \Gamma_R \text{Im}\{A(\epsilon - \omega_L)\} |B(\epsilon)|^2 \\
& \quad + \Gamma_L^2 \Gamma_R^2 |A(\epsilon - \omega_L)|^2 |B(\epsilon)|^2 + \Gamma_L^2 \Gamma_R^2 |B(\epsilon)|^2 |C(\epsilon)|^2] \\
& + \{ f_R(\epsilon)[1 - f_L(\epsilon - \omega_L)] + f_L(\epsilon - \omega_L)[1 - f_R(\epsilon)] \} \\
& \quad \times [\Gamma_L^2 \Gamma_R |B(\epsilon)|^2 \text{Im}\{C(\epsilon)\} + \Gamma_L \Gamma_R^2 \text{Im}\{A(\epsilon - \omega_L)\} |B(\epsilon)|^2 \\
& \quad + \Gamma_L^2 \Gamma_R^2 |A(\epsilon - \omega_L)|^2 |B(\epsilon)|^2 + \Gamma_L^2 \Gamma_R^2 |B(\epsilon)|^2 |C(\epsilon)|^2] \\
& + \{ f_R(\epsilon)[1 - f_R(\epsilon - \omega_L)] + f_R(\epsilon - \omega_L)[1 - f_R(\epsilon)] \} \\
& \quad \times [\Gamma_L \Gamma_R^2 |B(\epsilon)|^2 \text{Im}\{C(\epsilon)\} + \Gamma_L \Gamma_R^2 \text{Im}\{A(\epsilon - \omega_L)\} |B(\epsilon)|^2 \\
& \quad + \Gamma_L \Gamma_R^3 |A(\epsilon - \omega_L)|^2 |B(\epsilon)|^2 + \Gamma_L \Gamma_R^3 |B(\epsilon)|^2 |C(\epsilon)|^2] \\
& + \{ \Gamma_L^3 \Gamma_R f_L(\epsilon - 2\omega_L)[1 - f_L(\epsilon)] + \Gamma_L^2 \Gamma_R^2 f_L(\epsilon - 2\omega_L)[1 - f_R(\epsilon)] \\
& \quad + \Gamma_L^2 \Gamma_R^2 f_R(\epsilon - 2\omega_L)[1 - f_L(\epsilon)] + \Gamma_L \Gamma_R^3 f_R(\epsilon - 2\omega_L)[1 - f_R(\epsilon)] \\
& \quad + \Gamma_L^3 \Gamma_R f_L(\epsilon)[1 - f_L(\epsilon - 2\omega_L)] + \Gamma_L^2 \Gamma_R^2 f_L(\epsilon)[1 - f_R(\epsilon - 2\omega_L)] \\
& \quad + \Gamma_L^2 \Gamma_R^2 f_R(\epsilon)[1 - f_L(\epsilon - 2\omega_L)] + \Gamma_L \Gamma_R^3 f_R(\epsilon)[1 - f_R(\epsilon - 2\omega_L)] \} \\
& \quad \times |B(\epsilon)|^2 |B(\epsilon - \omega_L)|^2 \}, \tag{B.15}
\end{aligned}$$

and

$$S_{LRS}^{yy}(0) = S_{LRS}^{xx}(0). \tag{B.16}$$

The symmetrized auto-correlation zero-frequency noise, correlating the spin currents polarized along the x - and y -directions is equal to zero,

$$S_{LLS}^{xy}(0) = 0. \quad (\text{B.17})$$

The cross-correlation zero-frequency noise, correlating the spin currents polarized along the x - and y -directions is given by

$$\begin{aligned}
S_{LRS}^{xy}(0) = & \int \frac{d\epsilon}{8\pi} \\
& \times \{ \{ f_L(\epsilon)[1 - f_R(\epsilon)] + f_R(\epsilon)[1 - f_L(\epsilon)] \} \\
& \quad \times [(\Gamma_L \Gamma_R^2 - \Gamma_L^2 \Gamma_R) |A(\epsilon)|^2 \text{Re}\{C(\epsilon)\} + (\Gamma_L^2 \Gamma_R - \Gamma_L \Gamma_R^2) \text{Re}\{A(\epsilon)\} |C(\epsilon)|^2] \\
& \quad + \{ f_L(\epsilon)[1 - f_L(\epsilon - \omega_L)] + f_L(\epsilon - \omega_L)[1 - f_L(\epsilon)] \} \\
& \quad \times [\Gamma_L^2 \Gamma_R |B(\epsilon)|^2 \text{Re}\{C(\epsilon)\} - \Gamma_L^2 \Gamma_R \text{Re}\{A(\epsilon - \omega_L)\} |B(\epsilon)|^2] \\
& \quad + \{ f_L(\epsilon)[1 - f_R(\epsilon - \omega_L)] + f_R(\epsilon - \omega_L)[1 - f_L(\epsilon)] \} \\
& \quad \times [\Gamma_L \Gamma_R^2 |B(\epsilon)|^2 \text{Re}\{C(\epsilon)\} + \Gamma_L^2 \Gamma_R \text{Re}\{A(\epsilon - \omega_L)\} |B(\epsilon)|^2] \\
& \quad + \{ f_L(\epsilon - \omega_L)[1 - f_R(\epsilon)] + f_R(\epsilon)[1 - f_L(\epsilon - \omega_L)] \} \\
& \quad \times [-\Gamma_L^2 \Gamma_R |B(\epsilon)|^2 \text{Re}\{C(\epsilon)\} - \Gamma_L \Gamma_R^2 \text{Re}\{A(\epsilon - \omega_L)\} |B(\epsilon)|^2] \\
& \quad + \{ f_R(\epsilon)[1 - f_R(\epsilon - \omega_L)] + f_R(\epsilon - \omega_L)[1 - f_R(\epsilon)] \} \\
& \quad \times [-\Gamma_L \Gamma_R^2 |B(\epsilon)|^2 \text{Re}\{C(\epsilon)\} + \Gamma_L \Gamma_R^2 \text{Re}\{A(\epsilon - \omega_L)\} |B(\epsilon)|^2] \}. \quad (\text{B.18})
\end{aligned}$$

The zero-frequency spin-torque noise power of the spin-torque component along the x -direction can be expressed as

$$\begin{aligned}
S_T^{xx}(0) = & \int \frac{d\epsilon}{8\pi} \\
& \times \{ \{ f_L(\epsilon)[1 - f_R(\epsilon)] + f_R(\epsilon)[1 - f_L(\epsilon)] \} \\
& \quad \times [4\Gamma_L\Gamma_R\Gamma|A(\epsilon)|^2\text{Im}\{C(\epsilon)\} + 4\Gamma_L\Gamma_R\Gamma\text{Im}\{A(\epsilon)\}|C(\epsilon)|^2 \\
& \quad + 2\Gamma_L\Gamma_R\Gamma^2|A(\epsilon)|^2|C(\epsilon)|^2 + 2\Gamma_L\Gamma_R|A(\epsilon)|^2 + 2\Gamma_L\Gamma_R|C(\epsilon)|^2 \\
& \quad - 4\Gamma_L\Gamma_R\text{Re}\{A(\epsilon)C(\epsilon)\}] \\
& + \{ f_L(\epsilon)[1 - f_L(\epsilon - \omega_L)] + f_L(\epsilon - \omega_L)[1 - f_L(\epsilon)] \} \\
& \quad \times [2\Gamma_L^2\Gamma|B(\epsilon)|^2\text{Im}\{C(\epsilon)\} + 2\Gamma_L^2\Gamma\text{Im}\{A(\epsilon - \omega_L)\}|B(\epsilon)|^2 \\
& \quad + \Gamma_L^2\Gamma^2|A(\epsilon - \omega_L)|^2|B(\epsilon)|^2 + \Gamma_L^2\Gamma^2|B(\epsilon)|^2|C(\epsilon)|^2 + 2\Gamma_L^2|B(\epsilon)|^2] \\
& + \{ f_L(\epsilon)[1 - f_R(\epsilon - \omega_L)] + f_R(\epsilon - \omega_L)[1 - f_L(\epsilon)] \} \\
& \quad \times [2\Gamma_L\Gamma_R\Gamma|B(\epsilon)|^2\text{Im}\{C(\epsilon)\} + 2\Gamma_L\Gamma_R\Gamma\text{Im}\{A(\epsilon - \omega_L)\}|B(\epsilon)|^2 \\
& \quad + \Gamma_L\Gamma_R\Gamma^2|A(\epsilon - \omega_L)|^2|B(\epsilon)|^2 + \Gamma_L\Gamma_R\Gamma^2|B(\epsilon)|^2|C(\epsilon)|^2 + 2\Gamma_L\Gamma_R|B(\epsilon)|^2] \\
& + \{ f_R(\epsilon)[1 - f_L(\epsilon - \omega_L)] + f_L(\epsilon - \omega_L)[1 - f_R(\epsilon)] \} \\
& \quad \times [2\Gamma_L\Gamma_R\Gamma|B(\epsilon)|^2\text{Im}\{C(\epsilon)\} + 2\Gamma_L\Gamma_R\Gamma\text{Im}\{A(\epsilon - \omega_L)\}|B(\epsilon)|^2 \\
& \quad + \Gamma_L\Gamma_R\Gamma^2|A(\epsilon - \omega_L)|^2|B(\epsilon)|^2 + \Gamma_L\Gamma_R\Gamma^2|B(\epsilon)|^2|C(\epsilon)|^2 + 2\Gamma_L\Gamma_R|B(\epsilon)|^2] \\
& + \{ f_R(\epsilon)[1 - f_R(\epsilon - \omega_L)] + f_R(\epsilon - \omega_L)[1 - f_R(\epsilon)] \} \\
& \quad \times [2\Gamma_R^2\Gamma|B(\epsilon)|^2\text{Im}\{C(\epsilon)\} + 2\Gamma_R^2\Gamma\text{Im}\{A(\epsilon - \omega_L)\}|B(\epsilon)|^2 \\
& \quad + \Gamma_R^2\Gamma^2|A(\epsilon - \omega_L)|^2|B(\epsilon)|^2 + \Gamma_R^2\Gamma^2|B(\epsilon)|^2|C(\epsilon)|^2 + 2\Gamma_R^2|B(\epsilon)|^2] \\
& + \{ \Gamma_L^2\Gamma^2 f_L(\epsilon - 2\omega_L)[1 - f_L(\epsilon)] + \Gamma_L\Gamma_R\Gamma^2 f_L(\epsilon - 2\omega_L)[1 - f_R(\epsilon)] \\
& \quad + \Gamma_L\Gamma_R\Gamma^2 f_R(\epsilon - 2\omega_L)[1 - f_L(\epsilon)] + \Gamma_R^2\Gamma^2 f_R(\epsilon - 2\omega_L)[1 - f_R(\epsilon)] \\
& \quad + \Gamma_L^2\Gamma^2 f_L(\epsilon)[1 - f_L(\epsilon - 2\omega_L)] + \Gamma_L\Gamma_R\Gamma^2 f_L(\epsilon)[1 - f_R(\epsilon - 2\omega_L)] \\
& \quad + \Gamma_L\Gamma_R\Gamma^2 f_R(\epsilon)[1 - f_L(\epsilon - 2\omega_L)] + \Gamma_R^2\Gamma^2 f_R(\epsilon)[1 - f_R(\epsilon - 2\omega_L)] \} \\
& \quad \times |B(\epsilon)|^2|B(\epsilon - \omega_L)|^2, \tag{B.19}
\end{aligned}$$

and

$$S_T^{yy}(0) = S_T^{xx}(0). \tag{B.20}$$

The nonsymmetrized zero-frequency spin-torque noise, correlating spin-torque components along the x - and y -directions, reads

$$\begin{aligned}
S_T^{xy}(0) = & i \int \frac{d\epsilon}{8\pi} \\
& \times \{ [f_L(\epsilon - \omega_L) - f_L(\epsilon)] \\
& \quad \times [2\Gamma_L^2 \Gamma \text{Im}\{A(\epsilon - \omega_L)\} |B(\epsilon)|^2 + 2\Gamma_L^2 \Gamma |B(\epsilon)|^2 \text{Im}\{C(\epsilon)\} \\
& \quad + \Gamma_L^2 \Gamma^2 |A(\epsilon - \omega_L)|^2 |B(\epsilon)|^2 + \Gamma_L^2 \Gamma^2 |B(\epsilon)|^2 |C(\epsilon)|^2 + 2\Gamma_L^2 |B(\epsilon)|^2 \\
& \quad + \Gamma_L^2 \Gamma^2 |B(\epsilon)|^2 |B(\epsilon + \omega_L)|^2 + \Gamma_L^2 \Gamma^2 |B(\epsilon)|^2 |B(\epsilon - \omega_L)|^2] \\
& + [f_R(\epsilon - \omega_L) - f_L(\epsilon)] \\
& \quad \times [2\Gamma_L \Gamma_R \Gamma \text{Im}\{A(\epsilon - \omega_L)\} |B(\epsilon)|^2 + 2\Gamma_L \Gamma_R \Gamma |B(\epsilon)|^2 \text{Im}\{C(\epsilon)\} \\
& \quad + \Gamma_L \Gamma_R \Gamma^2 |A(\epsilon - \omega_L)|^2 |B(\epsilon)|^2 + \Gamma_L \Gamma_R \Gamma^2 |B(\epsilon)|^2 |C(\epsilon)|^2 + 2\Gamma_L \Gamma_R |B(\epsilon)|^2 \\
& \quad + \Gamma_L \Gamma_R \Gamma^2 |B(\epsilon)|^2 |B(\epsilon + \omega_L)|^2 + \Gamma_L \Gamma_R \Gamma^2 |B(\epsilon)|^2 |B(\epsilon - \omega_L)|^2] \\
& + [f_L(\epsilon - \omega_L) - f_R(\epsilon)] \\
& \quad \times [2\Gamma_L \Gamma_R \Gamma \text{Im}\{A(\epsilon - \omega_L)\} |B(\epsilon)|^2 + 2\Gamma_L \Gamma_R \Gamma |B(\epsilon)|^2 \text{Im}\{C(\epsilon)\} \\
& \quad + \Gamma_L \Gamma_R \Gamma^2 |A(\epsilon - \omega_L)|^2 |B(\epsilon)|^2 + \Gamma_L \Gamma_R \Gamma^2 |B(\epsilon)|^2 |C(\epsilon)|^2 + 2\Gamma_L \Gamma_R |B(\epsilon)|^2 \\
& \quad + \Gamma_L \Gamma_R \Gamma^2 |B(\epsilon)|^2 |B(\epsilon + \omega_L)|^2 + \Gamma_L \Gamma_R \Gamma^2 |B(\epsilon)|^2 |B(\epsilon - \omega_L)|^2] \\
& + [f_R(\epsilon - \omega_L) - f_R(\epsilon)] \\
& \quad \times [2\Gamma_R^2 \Gamma \text{Im}\{A(\epsilon - \omega_L)\} |B(\epsilon)|^2 + 2\Gamma_R^2 \Gamma |B(\epsilon)|^2 \text{Im}\{C(\epsilon)\} \\
& \quad + \Gamma_R^2 \Gamma^2 |A(\epsilon - \omega_L)|^2 |B(\epsilon)|^2 + \Gamma_R^2 \Gamma^2 |B(\epsilon)|^2 |C(\epsilon)|^2 + 2\Gamma_R^2 |B(\epsilon)|^2 \\
& \quad + \Gamma_R^2 \Gamma^2 |B(\epsilon)|^2 |B(\epsilon + \omega_L)|^2 + \Gamma_R^2 \Gamma^2 |B(\epsilon)|^2 |B(\epsilon - \omega_L)|^2] \}. \tag{B.21}
\end{aligned}$$

The symmetrized zero-frequency spin-torque noise, correlating spin-torque components along the x - and y -directions, is equal to zero,

$$S_{TS}^{xy}(0) = 0. \tag{B.22}$$

The zero-frequency spin-torque noise power of the spin-torque component along the z -direction can be written as

$$\begin{aligned}
S_T^{zz}(0) = & \int \frac{d\epsilon}{8\pi} \\
& \times \{ \{ f_L(\epsilon)[1 - f_R(\epsilon)] + f_R(\epsilon)[1 - f_L(\epsilon)] \} \\
& \quad \times [4\Gamma_L\Gamma_R\Gamma\text{Im}\{A(\epsilon)\}|A(\epsilon)|^2 - 2\Gamma_L\Gamma_R\text{Re}\{A^2(\epsilon)\} \\
& \quad + \Gamma_L\Gamma_R\Gamma^2|A(\epsilon)|^4 + \Gamma_L\Gamma_R\Gamma^2|B(\epsilon)|^4 + \Gamma_L\Gamma_R\Gamma^2|B(\epsilon + \omega_L)|^4 \\
& \quad - 4\Gamma_L\Gamma_R\Gamma\text{Im}\{A(\epsilon)\}|B(\epsilon)|^2 - 2\Gamma_L\Gamma_R\Gamma^2|A(\epsilon)|^2|B(\epsilon)|^2 \\
& \quad - 2\Gamma_L\Gamma_R\Gamma^2|B(\epsilon + \omega_L)|^2|C(\epsilon)|^2 - 4\Gamma_L\Gamma_R\Gamma\text{Im}\{C(\epsilon)\}|B(\epsilon + \omega_L)|^2 \\
& \quad + 4\Gamma_L\Gamma_R\Gamma\text{Im}\{C(\epsilon)\}|C(\epsilon)|^2 + \Gamma_L\Gamma_R\Gamma^2|C(\epsilon)|^4 + 2\Gamma_L\Gamma_R|A(\epsilon)|^2 \\
& \quad + 2\Gamma_L\Gamma_R|C(\epsilon)|^2 - 2\Gamma_L\Gamma_R\text{Re}\{C^2(\epsilon)\}] \\
& + \{ f_L(\epsilon)[1 - f_L(\epsilon - \omega_L)] + f_L(\epsilon - \omega_L)[1 - f_L(\epsilon)] \} \\
& \quad \times [2\Gamma_L^2\Gamma\text{Im}\{A(\epsilon)\}|B(\epsilon)|^2 + \Gamma_L^2\Gamma^2|A(\epsilon)|^2|B(\epsilon)|^2 \\
& \quad - 2\Gamma_L^2\Gamma\text{Im}\{B^2(\epsilon)C^*(\epsilon - \omega_L)\} - 2\Gamma_L^2\Gamma\text{Im}\{A^*(\epsilon)B^2(\epsilon)\} \\
& \quad - 2\Gamma_L^2\Gamma^2\text{Re}\{A(\epsilon)B^{*2}(\epsilon)C(\epsilon - \omega_L)\}] \\
& \quad + 2\Gamma_L^2\Gamma|B(\epsilon)|^2\text{Im}\{C(\epsilon - \omega_L)\} + \Gamma_L^2\Gamma^2|B(\epsilon)|^2|C(\epsilon - \omega_L)|^2 \\
& \quad + 2\Gamma_L^2|B(\epsilon)|^2 + 2\Gamma_L^2\text{Re}\{B^2(\epsilon)\}] \\
& + \{ f_L(\epsilon)[1 - f_R(\epsilon - \omega_L)] + f_R(\epsilon - \omega_L)[1 - f_L(\epsilon)] \} \\
& \quad \times [2\Gamma_L\Gamma_R\Gamma\text{Im}\{A(\epsilon)\}|B(\epsilon)|^2 + \Gamma_L\Gamma_R\Gamma^2|A(\epsilon)|^2|B(\epsilon)|^2 \\
& \quad - 2\Gamma_L\Gamma_R\Gamma\text{Im}\{B^2(\epsilon)C^*(\epsilon - \omega_L)\} - 2\Gamma_L\Gamma_R\Gamma\text{Im}\{A^*(\epsilon)B^2(\epsilon)\} \\
& \quad - 2\Gamma_L\Gamma_R\Gamma^2\text{Re}\{A(\epsilon)B^{*2}(\epsilon)C(\epsilon - \omega_L)\}] \\
& \quad + 2\Gamma_L\Gamma_R\Gamma|B(\epsilon)|^2\text{Im}\{C(\epsilon - \omega_L)\} + \Gamma_L\Gamma_R\Gamma^2|B(\epsilon)|^2|C(\epsilon - \omega_L)|^2 \\
& \quad + 2\Gamma_L\Gamma_R|B(\epsilon)|^2 + 2\Gamma_L\Gamma_R\text{Re}\{B^2(\epsilon)\}] \\
& + \{ f_R(\epsilon)[1 - f_L(\epsilon - \omega_L)] + f_L(\epsilon - \omega_L)[1 - f_R(\epsilon)] \} \\
& \quad \times [2\Gamma_L\Gamma_R\Gamma\text{Im}\{A(\epsilon)\}|B(\epsilon)|^2 + \Gamma_L\Gamma_R\Gamma^2|A(\epsilon)|^2|B(\epsilon)|^2 \\
& \quad - 2\Gamma_L\Gamma_R\Gamma\text{Im}\{B^2(\epsilon)C^*(\epsilon - \omega_L)\} - 2\Gamma_L\Gamma_R\Gamma\text{Im}\{A^*(\epsilon)B^2(\epsilon)\} \\
& \quad - 2\Gamma_L\Gamma_R\Gamma^2\text{Re}\{A(\epsilon)B^{*2}(\epsilon)C(\epsilon - \omega_L)\}] \\
& \quad + 2\Gamma_L\Gamma_R\Gamma|B(\epsilon)|^2\text{Im}\{C(\epsilon - \omega_L)\} + \Gamma_L\Gamma_R\Gamma^2|B(\epsilon)|^2|C(\epsilon - \omega_L)|^2 \\
& \quad + 2\Gamma_L\Gamma_R|B(\epsilon)|^2 + 2\Gamma_L\Gamma_R\text{Re}\{B^2(\epsilon)\}] \\
& + \{ f_R(\epsilon)[1 - f_R(\epsilon - \omega_L)] + f_R(\epsilon - \omega_L)[1 - f_R(\epsilon)] \} \\
& \quad \times [2\Gamma_R^2\Gamma\text{Im}\{A(\epsilon)\}|B(\epsilon)|^2 + \Gamma_R^2\Gamma^2|A(\epsilon)|^2|B(\epsilon)|^2 \\
& \quad - 2\Gamma_R^2\Gamma\text{Im}\{B^2(\epsilon)C^*(\epsilon - \omega_L)\} - 2\Gamma_R^2\Gamma\text{Im}\{A^*(\epsilon)B^2(\epsilon)\} \\
& \quad - 2\Gamma_R^2\Gamma^2\text{Re}\{A(\epsilon)B^{*2}(\epsilon)C(\epsilon - \omega_L)\}] \\
& \quad + 2\Gamma_R^2\Gamma|B(\epsilon)|^2\text{Im}\{C(\epsilon - \omega_L)\} + \Gamma_R^2\Gamma^2|B(\epsilon)|^2|C(\epsilon - \omega_L)|^2 \\
& \quad + 2\Gamma_R^2|B(\epsilon)|^2 + 2\Gamma_R^2\text{Re}\{B^2(\epsilon)\}]. \tag{B.23}
\end{aligned}$$

Bibliography

- [1] A. Aviram and M. Ratner, Chem. Phys. Lett. **29**, 277 (1974).
- [2] A. Nitzan and M. A. Ratner, Science **300**, 1384 (2003).
- [3] J. C. Cuevas, E. Scheer, *Molecular Electronics: An Introduction to Theory and Experiment* (Word Scientific, Singapore, 2010).
- [4] G. E. Moore, Electronics **38**, 114 (1965).
- [5] C. Joachim, J. K. Gimzewski, and A. Aviram, Nature **408**, 541 (2000).
- [6] A. Aviram and M. A. Ratner, *Molecular electronics I*, Vol. 852 of Annals of the New York Academy of Sciences (New York Academy of Sciences, 1998).
- [7] M. A. Reed, C. Zhou, C. J. Muller, T. P. Burgin, and J. M. Tour, Science, **278**, 252 (1997).
- [8] C. P. Collier, G. Mattersteig, E. W. Wong, Y. Luo, K. Beverly, J. Sampario, F. M. Raymo, J. F. Stoddart, J. R. Heath, Science **289**, 1172 (2000).
- [9] E. Braun, Y. Eichen, U. Sivan, and G. Ben-Yoseph, Nature **391**, 775 (1998).
- [10] Y. Benenson, T. Paz-Elizur, R. Adar, E. Keinan, Z. Livneh, and E. Shapiro, Nature **414**, 330 (2001).
- [11] K. Keren, M. Krueger, R. Gilard, G. Ben-Yoseph, U. Sivan, and E. Braun, Science **297**, 72 (2002).
- [12] S. Lijima, Nature **354**, 56 (1991).
- [13] D. Porath and J. Millo, J. Appl. Phys. **81**, 2241 (1997).
- [14] M. Thorwart, M. Grifoni, G. Cuniberti, H. W. Ch. Postma, and C. Dekker, Phys. Rev. Lett. **89**, 196402 (2002).
- [15] H. Park, J. Park, A. K. L. Lim, E. H. Anderson, A. P. Alivisatos, and P. L. McEuen, Nature **407**, 57 (2000).

- [16] T. K. Ng and P. A. Lee, *Phys. Rev. Lett.* **61**, 1768 (1988).
- [17] S. M. Cronenwett, T. H. Osterkamp, and L. P. Kouwenhoven, *Science* **281**, 540 (1998).
- [18] W. Liang, M. P. Shores, M. Bockrath, J. R. Long, and H. Park, *Nature* **417**, 725 (2002).
- [19] J. J. Parks, A. R. Champagne, G. R. Hutchison, S. Flores-Tores, H. D. Urbina, and D. C. Ralph, *Phys. Rev. Lett.* **99**, 026601 (2007).
- [20] J. Chen, M. A. Reed, A. M. Rawlett, and J. M. Tour, *Science* **286**, 1550 (1999).
- [21] E. Pop, D. Mann, J. Cao, Q. Wang, K. Goodson, and H. Dai, *Phys. Rev. Lett.* **95**, 155505 (2005).
- [22] T. Frederiksen, M. Brandbyge, N. Lorente, and A. P. Jauho, *Phys. Rev. Lett.* **93**, 256601 (2004).
- [23] T. Böhler, A. Edtbauer, and E. Scheer, *Phys. Rev. B* **76**, 125432 (2007).
- [24] M. Galperin, M. A. Ratner, and A. Nitzan, *J. Phys.: Condens. Matter* **19**, 103201 (2007).
- [25] M. Galperin, M. A. Ratner, A. Nitzan, and A. Troisi, *Science* **319**, 1056 (2008).
- [26] F. Haupt, T. Novotný, and W. Belzig, *Phys. Rev. Lett.* **103**, 136601 (2009).
- [27] J. Repp, P. Liljeroth, and G. Meyer, *Nature Physics* **6**, 975 (2010).
- [28] H. B. Heersche, Z. de Groot, J. A. Folk, H. S. J. van der Zant, C. Romeike, M. R. Wegewijs, L. Zobbi, D. Barreca, E. Tondello, and A. Cornia, *Phys. Rev. Lett.* **96**, 206801 (2006).
- [29] M.-H. Jo, J. E. Grose, K. Baheti, M. M. Deshmukh, J. J. Sokol, E. M. Rumberger, D. N. Hendrickson, J. R. Long, H. Park, and D. C. Ralph, *Nano Lett.* **6**, 2014 (2006).
- [30] A. Mugarza, C. Krull, R. Robles, S. Stepanow, G. Ceballos, and P. Gambardella, *Nature Communications* **2**, 490 (2011).
- [31] D. D. Dunlap, R. Garcia, E. Schabtach, and C. Bustamante, *Proc. Natl. Acad. Sci. (USA)* **90**, 7652 (1993).

-
- [32] A. Y. Kasumov, M. Kociak, S. Gueron, B. Reulet, V. T. Volkov, D. V. Klinov, and H. Bouchiat, *Science* **291**, 280 (2001).
- [33] S. Kohler, J. Lehmann, and P. Hänggi, *Phys. Rep.* **406**, 379 (2005).
- [34] B. D. Fainberg, M. Jouravlev, and A. Nitzan, *Phys. Rev. B* **76**, 245329 (2007).
- [35] M. Galperin and S. Tretiak, *J. Chem. Phys.* **128**, 124705 (2008).
- [36] J. Lehmann, S. Kohler, P. Hänggi, and A. Nitzan, *J. Chem. Phys.* **118**, 3283 (2003).
- [37] D. Dulić, S. J. van der Molen, T. Kudernac, H. T. Jonkman, J. J. D. de Jong, T. N. Bowden, J. van Esch, B. L. Feringa, and B. J. van Wees, *Phys. Rev. Lett.* **91**, 207402 (2003).
- [38] S. van der Molen, J. Liao, T. Kudernac, J. Agustsson, L. Bernard, M. Calame, B. van Wees, B. Feringa, and C. Schönenberger, *Nano Lett.* **9**, 76 (2009).
- [39] Y. Kim, T. J. Hellmuth, D. Sysoiev, F. Pauly, T. Pietsch, J. Wolf, A. Erbe, T. Huhn, U. Groth, U. E. Steiner, and E. Scheer, *Nano Lett.* **12**(7), 3736 (2012).
- [40] L. Bogani and W. Wernsdorfer, *Nature Mater.* **7**, 179 (2008).
- [41] L. Zhu, K. L. Yao, Z. L. Liu, *Appl. Phys. Lett.* **97**, 202101 (2010).
- [42] C. Timm, *Phys. Rev. B* **76**, 014421 (2007).
- [43] N. J. Tao, *Nature Nanotechnology* **1**, 173 (2006).
- [44] C. A. Martin, J. M. van Ruitenbeek, and H. S. J. van der Zant, *Nanotechnology* **21**, 265201 (2010).
- [45] A.-P. Jauho, N. S. Wingreen, and Y. Meir, *Phys. Rev. B* **50**, 5528 (1994).
- [46] A.-P. Jauho and H. Haug, *Quantum Kinetics in Transport and Optics of Semiconductors* (Springer, Berlin, 2008).
- [47] J. Taylor, H. Guo, and J. Wang, *Phys. Rev. B* **63**, 245407 (2001).
- [48] Y. Zhu, J. Maciejko, T. Ji, H. Guo, and J. Wang, *Phys. Rev. B* **71**, 075317 (2005).
- [49] Z. Feng, J. Maciejko, J. Wang, and H. Guo, *Phys. Rev. B* **77**, 075302 (2008).
- [50] J. Koch and F. von Oppen, *Phys. Rev. Lett.* **94**, 206804 (2005).

-
- [51] O. Entin-Wohlman, Y. Imry, and A. Aharony, Phys. Rev. B **81**, 113408 (2010).
- [52] M. Galperin, A. Nitzan, and M. A. Ratner, Phys. Rev. B **76**, 035301 (2007).
- [53] R. Landauer, Phys. Lett. **85**, 91 (1981).
- [54] S. Datta, *Electronic Transport in Mesoscopic Systems* (Cambridge University Press, Cambridge, England, 1995).
- [55] E. G. Emberly and G. Kirczenow, Phys. Rev. B **61**, 5740 (2000).
- [56] A. Troisi and M. A. Ratner, Phys. Rev. B **72**, 033408 (2005).
- [57] W. Kohn and L. J. Sham, Phys. Rev. **140**, A1133 (1965).
- [58] J. C. Cuevas, J. Henrich, F. Pauly, W. Wenzel, and G. Schön, Nanotechnology **14**, 29 (2003).
- [59] E. Runge and E. K. U. Gross, Phys. Rev. Lett. **52**, 997 (1984).
- [60] N. Sai, N. Bushong, R. Hatcher, and M. D. Ventra, Phys. Rev. B **75**, 115410 (2007).
- [61] E. Khosravi, S. Kurth, G. Stefanucci, and E. K. U. Gross, Appl. Phys. A **93**, 355 (2008).
- [62] K. Blum, *Density Matrix Theory and Applications* (Plenum Press, New York, 1981).
- [63] V. May and O. Kühn, *Charge and Energy Transfer Dynamics in Molecular Systems* (Wiley-VCH, Weinheim, 2004).
- [64] J. Lehmann, S. Kohler, V. May, and P. Hänggi, J. Chem. Phys. **121**, 2278 (2004).
- [65] C. Timm, Phys. Rev. B **77**, 195416 (2008).
- [66] M. Esposito and M. Galperin, Phys. Rev. B **79**, 205303 (2009).
- [67] Y. Chen, A. Prociuk, T. Perrine, and B. D. Dunietz, Phys. Rev. B **74**, 245320 (2006).
- [68] T. Frederiksen, N. Lorente, M. Paulsson, and M. Brandbyge, Phys. Rev. B **75**, 235441 (2007).
- [69] K. G. Wilson, Rev. Mod. Phys. **47**, 773 (1975).

- [70] T. Korb, F. Reininghaus, H. Schoeller, and J. König, *Phys. Rev. B* **76**, 165316 (2007).
- [71] F. B. Anders, *Phys. Rev. Lett.* **101**, 066804 (2008).
- [72] L. A. Bumm, J. J. Arnold, M. T. Cygan, T. D. Dunbar, T. P. Burgin, L. Jones, D. L. Allara, J. M. Tour, and P. S. Weiss, *Science*, **271**, 1705 (1996).
- [73] B. C. Stipe, M. A. Rezaei, and W. Ho, *Science* **280**, 1732 (1998).
- [74] J. Gaudio, L. J. Lauhon, and W. Ho, *Phys. Rev. Lett.* **85**, 1918 (2000).
- [75] N. Ogawa, G. Mikaelian, and W. Ho, *Phys. Rev. Lett.* **98**, 166103 (2007).
- [76] T. Böhler, J. Grebing, A. Mayer-Gindner, H. Löhneysen, and E. Scheer, *Nanotechnology* **15**, 465 (2004).
- [77] D. Secker, S. Wagner, S. Ballmann, R. Härtle, M. Toss, and H. B. Weber, *Phys. Rev. Lett.* **106**, 136807 (2011).
- [78] S. Sampaz, P. Jarillo-Herrero, Y. M. Blanter, C. Dekker, and H. S. J. van der Zant, *Phys. Rev. Lett.* **96**, 026801 (2006).
- [79] A. K. Hüttel, B. Witkamp, M. Leijnse, M. R. Wegewijs, and H. S. J. van der Zant, *Phys. Rev. Lett.* **102**, 225501 (2009).
- [80] H. Song, Y. Kim, Y. H. Jang, H. Jeong, M. A. Reed, and T. Lee, *Nature (London)* **462**, 1039 (2009).
- [81] X. D. Cui, A. Primak, X. Zarate, J. Tomfohr, O. F. Sankey, A. L. Moore, T. A. Moore, D. Gust, G. Harris, and S. M. Lindsay, *Science* **294**, 571 (2001).
- [82] S. H. Choi, B. Kim, and C. Daniel Frisbie, *Science* **320**, 1482 (2008).
- [83] W. Ho, *J. Chem. Phys.* **117**, 11033 (2002).
- [84] M. Kula, J. Jiang, and Y. Luo, *Nano Lett.* **6**, 1693 (2006).
- [85] Y. Kim, H. Song, F. Strigl, H.-F. Pernau, T. Lee, and E. Scheer, *Phys. Rev. Lett.* **106**, 196804 (2011).
- [86] I. Žutić, J. Fabian, and S. Das Sarma, *Rev. Mod. Phys.* **76**, 323 (2004).
- [87] P. Grünberg, R. Schreiber, Y. Pang, M. B. Brodsky, and H. Sowers, *Phys. Rev. Lett.* **57**, 2442 (1986).

- [88] M. N. Baibich, J. M. Broto, A. Fert, F. Nguyen Van Dau, F. Petroff, P. Etienne, G. Creuzet, A. Friederich, and J. Chazelas, *Phys. Rev. Lett.* **61**, 2472 (1988).
- [89] A. N. Pasupathy, R. C. Bialczak, J. Martinek, J. E. Grose, L. A. K. Donev, P. L. McEuen, and D. C. Ralph, *Science* **306**, 86 (2004).
- [90] M. Misiorny and J. Barnaś, *Phys. Rev. B* **75**, 134425 (2007).
- [91] A. Caneschi, D. Gatteschi, R. Sessoli, A. L. Barra, L. C. Brunel, and M. Guillot, *J. Am. Chem. Soc.* **113**, 5873 (1991).
- [92] W. Wernsdorfer and R. Sessoli, *Science* **284**, 133 (1999).
- [93] J. R. Friedman, M. P. Sarachik, J. Tejada, and R. Ziolo, *Phys. Rev. Lett.* **76**, 3830 (1996).
- [94] L. Thomas, F. Lioni, R. Ballou, D. Gatteschi, R. Sessoli, and B. Barbara, *Nature (London)* **383**, 145-147 (1996).
- [95] C. Sangregorio, T. Ohm, C. Paulsen, R. Sessoli, and D. Gatteschi, *Phys. Rev. Lett.* **78**, 4645 (1997).
- [96] W. Wernsdorfer, M. Murugesu, and G. Christou, *Phys. Rev. Lett.* **96**, 057208 (2006).
- [97] A. Ardavan, O. Rival, J. J. L. Morton, S. J. Blundell, A. M. Tyryshkin, G. A. Timco, and R. E. P. Winpenny, *Phys. Rev. Lett.* **98**, 057201 (2007).
- [98] S. Carretta, P. Santini, G. Amoretti, T. Guidi, J. R. D. Copley, Y. Qiu, R. Caciuffo, G. A. Timco, and R. E. P. Winpenny, *Phys. Rev. Lett.* **98**, 167401 (2007).
- [99] S. Bertaina, S. Gambarelli, T. Mitra, B. Tsukerblat, A. Muller, and B. Barbara, *Nature (London)* **453**, 203 (2008).
- [100] A. Garg, *EuroPhys. Lett.* **22**, 205 (1993).
- [101] W. Wernsdorfer, N. E. Chakov, and G. Christou, *Phys. Rev. Lett.* **95**, 037203 (2005).
- [102] M. N. Leuenberger and D. Loss, *Nature (London)* **410**, 789 (2001).
- [103] W. Wernsdorfer, N. Aliaga-Alcalde, D. N. Hendrickson, and G. Christou, *Nature* **416**, 406 (2002).

- [104] M. R. Cheeseman, V. S. Oganessian, R. Sessoli, D. Gatteschi, and A. J. Thomson, *Chem. Commun.* **17**, 1677 (1997).
- [105] C. Timm and M. Di Ventura, *Phys. Rev. B* **86**, 104427 (2012).
- [106] S. A. Wolf, D. D. Awschalom, R. A. Buhrman, J. M. Daughton, S. von Molnár, M. L. Roukes, A. Y. Chtchelkanova, and D. M. Treger, *Science* **294**, 1488 (2001).
- [107] D. D. Awschalom, M. E. Flatte, and N. Samarth, *Spintronics*, *Scientific American* **286**, 67-73 (2002).
- [108] J.C. Slonczewski, *J. Magn. Magn. Mater.* **159**, L1 (1996).
- [109] L. Berger, *Phys. Rev. B* **54**, 9353 (1996).
- [110] Y. Tserkovnyak, A. Brataas, G. E. W. Bauer, and B. I. Halperin, *Rev. Mod. Phys.* **77**, 1375 (2005).
- [111] D. C. Ralph and M. D. Stiles, *J. Magn. Magn. Mater.* **320**, 1190 (2008).
- [112] M. Misiorny and J. Barnaś, *Phys. Rev. B* **76**, 054448 (2007).
- [113] M. Misiorny and J. Barnaś, *Phys. Rev. B* **77**, 172414 (2008).
- [114] H-Z. Lu, B. Zhou, and S-Q. Shen, *Phys. Rev. B* **79**, 174419 (2009).
- [115] L. P. Kadanoff and G. Baym, *Quantum Statistical Mechanics* (Benjamin, New York, 1962).
- [116] L. P. Keldysh, *Sov. Phys. JETP* **20**, 1018 (1965).
- [117] A. Fetter and J. D. Walecka, *Quantum Theory of Many-Particle Systems* (Dover Publications, Inc., Mineola, N. Y., 2003).
- [118] H. Bruus and K. Flensberg, *Many-Body Quantum Theory in Condensed Matter Physics* (Oxford University Press, 2004).
- [119] J. Rammer, *Quantum Field Theory of Non-equilibrium States* (Cambridge University Press, Cambridge, UK, 2011).
- [120] T. Frederiksen, MSc. Thesis, Technical University of Denmark (2004).
- [121] A. Abrikosov, L. P. Gorkov, I. E. Dzyaloshinski, *Methods of Quantum Field Theory in Statistical physics* (Dover, New York, 1975).
- [122] G. D. Mahan, *Many-Particle Physics* (Plenum, New York, 1990).

- [123] M. Gell-Mann and F. Low, Phys. Rev. **84**, 350 (1951).
- [124] J. Schwinger, Proc. Natl. Acad. Sci. U.S.A. **37**, 452 (1951).
- [125] J. Rammer and H. Smith, Rev. Mod. Phys. **58**, 323 (1986).
- [126] D. C. Langreth, in *Linear and Nonlinear Electron Transport in Solids*, edited by J. T. Devreese and E. Van Doren (Plenum, New York, 1976).
- [127] Y. Meir and N. S. Wingreen, Phys. Rev. Lett. **68**, 2512 (1992).
- [128] R. Landauer, IBM J. Res. Dev. **1**, 223 (1957).
- [129] R. Landauer, IBM J. Res. Dev. **32**, 306 (1988).
- [130] Y. M. Blanter and M. Büttiker, Physics Reports, **336**, 2 (2000).
- [131] W. Schottky, Ann. Phys. (Leipzig) **57**, 541 (1918).
- [132] L. Y. Chen and C. S. Ting, Phys. Rev. B **43**, 4534 (1991).
- [133] O. L. Bø and Y. Galperin, J. Phys.: Condens. Matter **8** 3033 (1996).
- [134] B. Dong and X. L. Lei, J. Phys.: Condens. Matter **14**, 4963 (2002).
- [135] J.-X. Zhu and A. V. Balatsky, Phys. Rev. B **67**, 165326 (2003).
- [136] M. Galperin, A. Nitzan, and M. A. Ratner, Phys. Rev. B **74**, 075326 (2007).
- [137] A. Morello and L. J. de Jongh Phys. Rev. B **76**, 184425 (2007).
- [138] F. M. Souza, A. P. Jauho, and J. C. Egues, Phys. Rev. B **78**, 155303 (2008).
- [139] G.-H. Ding and T.-K. Ng, Phys. Rev. B **56**, 15521 (1997).
- [140] M. Büttiker, Phys. Rev. Lett. **65**, 2901 (1990).
- [141] T. Martin and R. Landauer, Phys. Rev. B **45**, 1742 (1992).
- [142] J. B. Johnson, Phys. Rev. **32**, 97 (1928).
- [143] H. Nyquist, Phys. Rev. **32**, 110 (1928).
- [144] H. B. Callen and T. W. Welton, Phys. Rev. **83**, 34 (1951).
- [145] L. D. Landau and E. M. Lifshitz *Statistical Physics, Part 1, Course of Theoretical Physics Vol. 5* (Pergamon Press, Oxford, 1980).
- [146] R. Sessoli, D. Gatteschi, A. Caneschi, and M. A. Novak, Nature (London) **365**, 141 (1993).

-
- [147] W. Wernsdorfer, *Nature Mater.* **6**, 174 (2007).
- [148] G. Christou, D. Gatteschi, D. Hendrickson, and R. Sessoli, *MRS Bulletin* **25**, 66 (2000).
- [149] D. Gatteschi, R. Sessoli, and J. Villain, *Molecular Nanomagnets* (Oxford University Press, New York, 2006).
- [150] C. Romeike, M. R. Wegewijs, W. Hofstetter, and H. Schoeller, *Phys. Rev. Lett.* **96**, 196601 (2006).
- [151] C. Romeike, M. R. Wegewijs, W. Hofstetter, and H. Schoeller, *Phys. Rev. Lett.* **97**, 206601 (2006).
- [152] D. Roosen, M. R. Wegewijs, and W. Hofstetter, *Phys. Rev. Lett.* **100**, 087201 (2008).
- [153] D. Gatteschi and R. Sessoli, *Angew. Chem. Int. Ed.* **42**, 268 (2003).
- [154] T. Lis, *Acta Crystallogr. Sect. B* **36**, 2042 (1980).
- [155] M. Novak, R. Sessoli, A. Caneschi, and D. Gatteschi, *J. Magn. Magn. Matter.* **146**, 211 (1995).
- [156] A. L. Barra, D. Gatteschi, and R. Sessoli, *Phys. Rev. B* **56**, 8192 (1997).
- [157] M. Misiorny, I. Weymann, J. Barnas, *Phys. Rev. B* **79**, 224420 (2009).
- [158] F. Elste and C. Timm, *Phys. Rev. B* **81**, 024421 (2010).
- [159] R. Skomski, *Simple Models of Magnetism* (Oxford University Press, 2008).
- [160] R. Boca, *Theoretical Foundations of Molecular Magnetism* (Elsevier, Amsterdam, 1999).
- [161] R. Sessoli, H. L. Tsai, A. R. Schake, Sh. Wang, J. B. Vincent, K. Folting, D. Gatteschi, G. Christou, and D. N. Hendrickson, *J. Am. Chem. Soc.* **115**, 1804 (1993).
- [162] D. A. Garanin and E. M. Chudnovsky, *Phys. Rev. B* **56**, 11102 (1997).
- [163] J. R. Friedman, *Phys. Rev. B* **57**, 10291 (1998).
- [164] L. Landau, *Phys. Z. Sowjetunion* **2**, 46 (1932).
- [165] C. Zener, *Proc. R. Soc. London, Ser. A* **137**, 696 (1932).
- [166] M. N. Leuenberger and D. Loss, *Phys. Rev. B* **61**, 12200 (2000).

- [167] W. Wernsdorfer, *Int. J. Nanotechnology* **7**, 497 (2010).
- [168] C. Hicke and M. I. Dykman, *Phys. Rev. B* **78**, 024401 (2008).
- [169] K. Xia, P. J. Kelly, G. E. W. Bauer, A. Brataas, and I. Turek, *Phys. Rev. B* **65**, 220401 (2002).
- [170] E. B. Myers, D. C. Ralph, J. A. Katine, R. N. Louie, and R. A. Buhrman, *Science* **285**, 867 (1999).
- [171] S. I. Kiselev, J. C. Sankey, I. N. Krivotov, N. C. Emley, R. J. Schoelkopf, R. A. Buhrman, and D. C. Ralph, *Nature* **425**, 380 (2003).
- [172] Y. T. Cui, G. Finocchio, C. Wang, J. A. Katine, R. A. Buhrman, and D. C. Ralph, *Phys. Rev. Lett.* **104**, 097201 (2010).
- [173] J. Z. Sun, *Phys. Rev. B* **62**, 570 (2000).
- [174] L. Landau and E. M. Lifshitz, *Phys. Z. Sowjetunion* **8**, 153 (1935).
- [175] T. L. Gilbert, *Phys. Rev.* **100**, 1243 (1955); T. Gilbert, *IEEE Trans. Magn.* **40**, 3443 (2004).
- [176] L. Landau, E. M. Lifshitz, and L. P. Pitaevski, *Statistical Physics, part 2*, 3rd edition (Pergamon, Oxford, 1980).
- [177] X. Waintal, E. B. Myers, P. W. Brouwer, and D. C. Ralph, *Phys. Rev. B* **62**, 12317 (2000).
- [178] M. D. Stiles and A. Zangwill, *Phys. Rev. B* **66**, 014407 (2002).
- [179] Y. Tserkovnyak, A. Brataas, and G. E. W. Bauer, *Phys. Rev. Lett.* **88**, 117601 (2002).
- [180] I. N. Krivorotov, N. C. Emley, J. C. Sankey, S. I. Kiselev, D. C. Ralph, and R. A. Buhrman, *Science* **307**, 228 (2005).
- [181] J. A. Katine, F. J. Albert, R. A. Buhrman, E. B. Myers, and D. C. Ralph, *Phys. Rev. Lett.* **84**, 3149 (2000).
- [182] A. Brataas, A. D. Kent, and H. Ohno, *Nature Materials* **11**, 372 (2012).
- [183] D. D. Awschalom, D. Loss, and N. Samarth, *Semiconductor Spintronics and Quantum Computation* (Springer, Berlin, 2002).
- [184] G.-H. Kim and T.-S. Kim, *Phys. Rev. Lett.* **92**, 137203 (2004).

- [185] M. N. Leuenberger and E. R. Mucciolo, *Phys. Rev. Lett.* **97**, 126601 (2006).
- [186] S. Teber, C. Holmqvist, and M. Fogelström, *Phys. Rev. B* **81**, 174503 (2010).
- [187] C. Holmqvist, S. Teber, and M. Fogelström, *Phys. Rev. B* **83**, 104521 (2011).
- [188] C. Holmqvist, W. Belzig, and M. Fogelström, *Phys. Rev. B* **86**, 054519 (2012).
- [189] N. Bode, L. Arrachea, G. S. Lozano, T. S. Nunner, and F. von Oppen, *Phys. Rev. B* **85**, 115440 (2012).
- [190] J. -X. Zhu, Z. Nussinov, A. Shnirman, and A. V. Balatsky, *Phys. Rev. Lett.* **92**, 107001 (2004).
- [191] Z. Nussinov, A. Shnirman, D. P. Arovas, A. V. Balatsky, and J. -X. Zhu, *Phys. Rev. B* **71**, 214520 (2005).
- [192] J. Michelsen, V. S. Shumeiko, and G. Wendin, *Phys. Rev. B* **77**, 184506 (2008).
- [193] K. Mosshammer, G. Kiesslich, and T. Brandes, *Phys. Rev. B* **86**, 165447 (2012).
- [194] C. Timm and F. Elste, *Phys. Rev. B* **73**, 235304 (2006).
- [195] F. Elste and C. Timm, *Phys. Rev. B* **73**, 235305 (2006).
- [196] S. Voss, M. Fonin, U. Rüdiger, M. Burgert, and U. Groth, *Appl. Phys. Lett.* **90**, 133104 (2007).
- [197] B. Y. Choi, S. J. Kahng, S. Kim, H. Kim, H. W. Kim, Y. J. Song, J. Ihm, and Y. Kuk, *Phys. Rev. Lett.* **96**, 156106 (2006).
- [198] E. Lörtscher, J. W. Ciszek, J. Tour, and H. Riel, *Small* **2**, 973 (2006).
- [199] C. Benesch, M. F. Rode, M. Cizek, R. Härtle, O. Rubio-Pons, M. Thoss, and A. L. Sobolewski, *J. Phys. Chem. C* **113**, 10315 (2009).
- [200] A. S. Zyazin, J. W. G. van den Berg, E. A. Osorio, H. S. J. van der Zant, N. P. Konstantinidis, M. Leijnse, M. R. Wegewijs, F. May, W. Hofstetter, C. Danieli, and A. Cornia, *Nano Lett.* **10**, 3307 (2010).
- [201] N. Roch, R. Vincent, F. Elste, W. Harneit, W. Wernsdorfer, C. Timm, and F. Balestro, *Phys. Rev. B* **83**, 081407(R) (2011).

- [202] C. Hirjibehedin, C.-Y. Lin, A. Otte, M. Ternes, C. P. Lutz, B. A. Jones, and A. J. Heinrich, *Science* **317**, 1199 (2007).
- [203] L. Zhou, J. Wiebe, S. Lounis, E. Vedmedenko, F. Meier, S. Blügel, P. H. Dederichs, and R. Wiesendanger, *Nat. Phys.* **6**, 187 (2010).
- [204] S. Kahle, Z. Deng, N. Malinowski, C. Tonnoir, A. Forment-Aliaga, N. Thon-tasen, G. Rinke, D. Le, V. Turkowski, T. S. Rahman, S. Rauschenbach, M. Ternes, and K. Kern, *Nano Lett.* **12**, 518-521 (2012).
- [205] R. Smit, Y. Noat, C. Untiedt, N. Lang, M. van Hemert, and J. van Ruitenbeek, *Nature (London)* **419**, 906 (2002).
- [206] A.F. Otte, M. Ternes, K. von Bergmann, S. Loth, H. Brune, C.P. Lutz, C.F. Hirjibehedin, A.J. Heinrich, *Nat. Phys.* **4**, 847 (2008).
- [207] J. Parks, A. Champagne, T. Costi, W. Shum, A. Pasupathy, E. Neuscamman, S. Flores-Torres, P. Cornaglia, A. Aligia, C. Balseiro, G.-L. Chan, H. Abrunña, and D. Ralph, *Science* **328**, 1370 (2010).
- [208] F. Delgado, J. J. Palacios, and J. Fernández-Rossier, *Phys. Rev. Lett.* **104**, 026601 (2010).
- [209] S. Loth, K. von Bergmann, M. Ternes, A. F. Otte, C. P. Lutz, and A. J. Heinrich, *Nat. Phys.* **6**, 340 (2010).
- [210] J. Fransson, *Phys. Rev. B* **77**, 205316 (2008).
- [211] C. López-Monís, C. Emary, G. Kiesslich, G. Platero, and T. Brandes, *Phys. Rev. B* **85**, 045301 (2012).
- [212] J. Xiao, G. E. W. Bauer, and A. Brataas, *Phys. Rev. B* **77**, 224419 (2008).
- [213] J. C. Slonczewski, *Phys. Rev. B* **71**, 024411 (2005).
- [214] J. C. Sankey, Y-T. Cui, J. Z. Sun, J. C. Slonczweski, R. A. Buhrman, and D. C. Ralph, *Nat. Phys.* **4**, 67 (2008).
- [215] A. L. Chudnovskiy, J. Swiebodzinski, and A. Kamenev, *Phys. Rev. Lett.* **101**, 066601 (2008).
- [216] S. Krause, G. Berbil-Bautista, G. Herzog, M. Bode, and R. Wiesendanger, *Science* **317**, 1537 (2007).
- [217] S. Krause, G. Herzog, A. Schlenhoff, A. Sonntag, and R. Wiesendanger, *Phys. Rev. Lett.* **107**, 186601 (2011).

- [218] C. Kittel, Phys. Rev. **73**, 155 (1948).
- [219] M. Filipović, C. Holmqvist, F. Haupt, and W. Belzig, Phys. Rev. B **87**, 045426 (2013); **88**, 119901(E) (2013).
- [220] N. S. Wingreen, A.-P. Jauho, and Y. Meir, Phys. Rev. B **48**, 8487 (1993).
- [221] B. Wang, J. Wang, and H. Guo, Phys. Rev. B **67**, 092408 (2003).
- [222] However, z -polarized dc spin currents appear in higher-order approximations [221, 223].
- [223] M. Filipović and W. Belzig, arXiv:1412.3994.
- [224] G. Floquet, Ann. Sci. Ecole Normale Supérieure **12**, 47 (1883).
- [225] Jon H. Shirley, PhD Thesis, California Institute of Technology, (1963).
- [226] M. Grifoni and P. Hänggi, Phys. Rep. **304**, 229 (1998).
- [227] B. H. Wu and C. Timm, Phys. Rev. B **81**, 075309 (2010).
- [228] S.-I. Chu and D. A. Telnov, Phys. Rep. **390**, 1 (2004).
- [229] M. V. Costache, M. Sladkov, S. M. Watts, C. H. van der Wal, and B. J. van Wees, Phys. Rev. Lett. **97**, 216603 (2006).
- [230] C. Bell, S. Milikisyants, M. Huber, and J. Aarts, Phys. Rev. Lett. **100**, 047002 (2008).
- [231] M. Harder, Z. X. Cao, Y. S. Gui, X. L. Fan, and C.-M. Hu, Phys. Rev. B **84**, 054423 (2011).
- [232] K. Ando, S. Takahashi, J. Ieda, H. Kurebayashi, T. Trypiniotis, C. H. W. Barnes, S. Maekawa, and E. Saitoh, Nature Mater. **10**, 655 (2011).
- [233] B. Dong, H. L. Cui, and X. L. Lei, Phys. Rev. B **69**, 205315 (2004).
- [234] G. Stefanucci and C. O. Almbladh, Europhys. Lett **67**, 14 (2004).
- [235] K. Burke, R. Car, and R. Gebauer Phys. Rev. Lett **94**, 146803 (2005).
- [236] S. Kurth, G. Stefanucci, C. O. Almbladh, A. Rubio, and E. K. U. Gross, Phys. Rev. B **72**, 035308 (2005).
- [237] G. Q. Li, S. Welack, M. Schreiber, and U. Kleinekathöfer, Phys. Rev. B **77**, 075321 (2008).

- [238] A. H. L. Dayem and R. J. Martin, *Phys. Rev. Lett.* **8**, 246 (1962).
- [239] P. K. Tien and J. P. Gordon, *Phys. Rev.* **129**, 647 (1963).
- [240] G. Platero and R. Aguado, *Phys. Rep.* **395**, 1 (2004).
- [241] W. Zheng, Y. Wei, J. Wang and H. Guo, *Phys. Rev. B* **61**, 13121 (2000).
- [242] J. Wu, B. Wang, J. Wang, and H. Guo, *Phys. Rev. B* **72**, 195324 (2005).
- [243] A. Tikhonov, R. D. Coalson, and Y. Dahnovsky, *J. Chem. Phys.* **116**, 10909 (2002).
- [244] U. Kleinekathöfer, G.-Q. Li, S. Welack, and M. Schreiber, *Europhys. Lett.* **75**, 139 (2006).
- [245] G.-Q. Li, M. Schreiber, and U. Kleinekathöfer, *Europhys. Lett.* **79**, 27006 (2007).
- [246] J. K. Viljas and J. C. Cuevas, *Phys. Rev. B* **75**, 075406 (2007).
- [247] J. K. Viljas, F. Pauly, and J. C. Cuevas, *Phys. Rev. B* **76**, 033403 (2007).
- [248] J. K. Viljas, F. Pauly, and J. C. Cuevas, *Phys. Rev. B* **77**, 155119 (2008).
- [249] L.-Y. Hsu and H. Rabitz, *Phys. Rev. Lett.* **109**, 186801 (2012).
- [250] B. D. Fainberg, *Phys. Rev. B* **88**, 245435 (2013).
- [251] M. Chauvin, P. vomStein, H. Pothier, P. Joyez, M. E. Huber, D. Esteve, and C. Urbina, *Phys. Rev. Lett.* **97**, 067006 (2006).
- [252] D. C. Guhr, D. Rettinger, J. Boneberg, A. Erbe, P. Leiderer, and E. Scheer, *Phys. Rev. Lett.* **99**, 086801 (2007).
- [253] N. Ittah, G. Noy, I. Yutsis, and Y. Selzer, *Nano Lett.* **9**, 1615 (2009).
- [254] G. Noy, A. Ophir, and Y. Selzer, *Angew. Chem. Int. Ed.* **49**, 5734 (2010).
- [255] M. A. Mangold, M. Calame, M. Mayor, and A. W. Holleitner, *J. Am. Chem. Soc.* **133**, 12185 (2011).
- [256] M. Büttiker, H. Thomas, and A. Prêtre, *Phys. Lett. A* **180**, 364 (1993).
- [257] M. Büttiker, A. Prêtre, and H. Thomas, *Phys. Rev. Lett.* **70**, 4114 (1993).
- [258] M. Büttiker, *J. Phys. Cond. Mat.* **5**, 9361 (1993).
- [259] Y. Wei and J. Wang, *Phys. Rev. B* **79**, 195315 (2009).

- [260] B. G. Wang, J. Wang, and H. Guo, Phys. Rev. Lett. **82**, 398 (1999).
- [261] P. Stadler, W. Belzig, and G. Rastelli, Phys. Rev. Lett. **113**, 047201 (2014).
- [262] A. Prêtre, H. Thomas, and M. Büttiker, Phys. Rev. B **54**, 8130 (1996).
- [263] M. Büttiker and T. Christen, in *Quantum Transport in Semiconductor Sub-micron Structures*, edited by B. Kramer (Kluwer Academic Publishers, Dordrecht, 1996).
- [264] M. Büttiker, A. Prêtre, and H. Thomas, Z. Phys. B: Conens. Matter **94**, 133 (1994).
- [265] V. Gasparian, T. Christen, and M. Büttiker, Phys. Rev. A **54**, 4022 (1996).
- [266] A. Kumar, L. Saminadayar, D. C. Glattli, Y. Jin, and B. Etienne, Phys. Rev. Lett. **76**, 2778 (1996).
- [267] V. V. Kuznetsov, E. E. Mendez, X. Zuo, G. L. Snider, and E. T. Croke, Phys. Rev. Lett. **85**, 397 (2000).
- [268] O. M. Bulashenko and J. M. Rubí, Phys. Rev. B **64**, 045307 (2001).
- [269] O. M. Bulashenko and J. M. Rubí, Phys. Rev. B **67**, 115322 (2003).
- [270] E. Onac, F. Balestro, B. Trauzettel, C. F. J. Lodewijk, and L. P. Kouwenhoven, Phys. Rev. Lett. **96**, 026803 (2006).
- [271] A. E. Miroschnichenko, S. Flach, and Y. S. Kivshar, Rev. Mod. Phys. **82**, 2257 (2010).
- [272] C. M. Guédon, H. Valkenier, T. Markussen, K. S. Thygesen, J. C. Hummel, and S. J. van der Molen, Nature Nanotech. **7**, 305 (2012).
- [273] H. Vázquez, R. Skouta, S. Schneebeli, M. Kamenetska, R. Beslov, L. Venkataraman, and M. S. Hybertsen, Nature Nanotech. **7**, 663 (2012).
- [274] R. Stadler, Phys. Rev. B **80**, 125401 (2009).
- [275] M. A. Ratner, J. Phys. Chem. **94**, 4877 (1990).
- [276] T. Hansen, G. C. Solomon, D. Q. Andrews, and M. A. Ratner, J. Chem. Phys. **131**, 194704 (2009).
- [277] U. Fano, Phys. Rev. **124**, 1866 (1961).
- [278] J. Faist, F. Capasso, C. Sirtori, K. W. West, and L. N. Pfeiffer, Nature **390**, 589 (1997).

- [279] O. Entin-Wohlman, Y. Imry, S. A. Gurvitz, and A. Aharony, *Phys. Rev. B* **75**, 193308 (2007).
- [280] D. Sánchez and L. Serra, *Phys. Rev. B* **74**, 153313 (2006).
- [281] Piotr Stefański, *J. Phys.: Cond. Matter* **22**, 505303 (2010).
- [282] S. A. Gurvitz, D. Mozyrsky, and G. P. Berman, *Phys. Rev. B* **72**, 205341 (2005).
- [283] S. A. Gurvitz, *IEEE Trans. Nanotechnology* **4**, 45 (2005).
- [284] D. Mozyrsky, L. Fedichkin, S. A. Gurvitz, and G. P. Berman, *Phys. Rev. B* **66**, 161313 (2002).
- [285] E. G. Mishchenko, *Phys. Rev. B* **68**, 100409(R) (2003).
- [286] T. Gramespacher and M. Büttiker, *Phys. Rev. Lett.* **81**, 2763 (1998).
- [287] R. Landauer, *Nature* **392**, 658 (1998).
- [288] M. Büttiker, *Phys. Rev. B* **46**, 12485 (1992).
- [289] X. Y. Shen, B. Dong, X. L. Lei, N. J. M. Horing, *Phys. Rev. B* **76**, 115308 (2007).
- [290] A. Lamacraft, *Phys. Rev. B* **69**, 081301(R) (2004).
- [291] M. Zareyan and W. Belzig, *Europhys. Lett.* **70**, 817 (2005).
- [292] B. Wang, J. Wang, and H. Guo, *Phys. Rev. B* **69**, 153301 (2004).
- [293] S. H. Ouyang, C. H. Lam, and J. Q. You, *Euro. Phys. J. B* **64**, 67 (2008).
- [294] O. Sauret and D. Feinberg, *Phys. Rev. Lett.* **92**, 106601 (2004).
- [295] M. J. Stevens, A. L. Smirl, R. D. R. Bhat, A. Najmale, J. E. Sipe, and H. M. van Driel, *Phys. Rev. Lett.* **90**, 136603 (2003).
- [296] A. Brataas, Y. Tserkovnyak, G. E. W. Bauer, and B. I. Halperin, *Phys. Rev. B* **66**, 060404(R) (2002).
- [297] R. L. Dragomirova and B. K. Nikolić, *Phys. Rev. B* **75**, 085328 (2007).
- [298] Y. He, D. Hou, and R. Han, *J. Appl. Phys.* **101**, 023710 (2007).
- [299] Y. Yu, H. Zhan, L. Wan, B. Wang, Y. Wei, Q. Sun and J. Wang, *Nanotechnology* **24**, 155202 (2013).

-
- [300] J. Foros, A. Brataas, Y. Tserkovnyak, and G. E. W. Bauer, Phys. Rev. Lett. **95**, 016601 (2005).
- [301] Y. Wang and L. J. Sham, Phys. Rev. B **85**, 092403 (2012).
- [302] Y. Wang and L. J. Sham, Phys. Rev. B **87**, 174433 (2013).
- [303] M. H. Pedersen and M. Büttiker, Phys. Rev. B **58**, 12993 (1998).
- [304] A. Thielmann, M. H. Hettler, J. König, and G. Schön, Phys. Rev. B **68**, 115105 (2003).

